



January 2022

## Exploring [2+2] Photoreaction To Synthesize Cyclobutane Di- And Tetracarboxylic Acid Building Blocks From Biomass-Derived Precursors

Dominic Nkafu Nkemngong

[How does access to this work benefit you? Let us know!](#)

Follow this and additional works at: <https://commons.und.edu/theses>

---

### Recommended Citation

Nkemngong, Dominic Nkafu, "Exploring [2+2] Photoreaction To Synthesize Cyclobutane Di- And Tetracarboxylic Acid Building Blocks From Biomass-Derived Precursors" (2022). *Theses and Dissertations*. 4364.

<https://commons.und.edu/theses/4364>

This Dissertation is brought to you for free and open access by the Theses, Dissertations, and Senior Projects at UND Scholarly Commons. It has been accepted for inclusion in Theses and Dissertations by an authorized administrator of UND Scholarly Commons. For more information, please contact [und.common@library.und.edu](mailto:und.common@library.und.edu).

EXPLORING [2+2] PHOTOREACTION TO SYNTHESIZE CYCLOBUTANE DI-  
AND TETRACARBOXYLIC ACID BUILDING BLOCKS FROM BIOMASS-  
DERIVED PRECURSORS

by

Dominic Nkafu Nkemngong

Bachelor of Science, University of Buea, 2012

Master of Science, University of Buea, 2015

A Dissertation

Submitted to the Graduate Faculty

of the

University of North Dakota

in partial fulfillment of the requirements

for the degree of

Doctor of Philosophy

Grand Forks, North Dakota

August

2022



Name: Dominic Nkafu Nkemngong  
Degree: Doctor of Philosophy

This document, submitted in partial fulfillment of the requirements for the degree from the University of North Dakota, has been read by the Faculty Advisory Committee under whom the work has been done and is hereby approved.

DocuSigned by:  
Dr. Qianli (Rick) Chu  
Qianli (Rick) Chu, Ph.D. (Chairperson)

DocuSigned by:  
Evguenii Kozliak  
Evguenii Kozliak, Ph.D. (Committee Member)

DocuSigned by:  
Guodong Du  
Guodong Du, Ph.D. (Committee Member)

DocuSigned by:  
Binglin Sui, Ph.D.  
Binglin Sui, Ph.D. (Committee Member)

DocuSigned by:  
Frank Bowman  
Frank Bowman, Ph.D. (Committee Member)

This document is being submitted by the appointed advisory committee as having met all the requirements of the School of Graduate Studies at the University of North Dakota and is hereby approved.

DocuSigned by:  
Chris Nelson  
Chris Nelson  
Dean of the School of Graduate Studies  
7/27/2022  
Date

## PERMISSION

Title            Exploring [2+2] Photoreaction to Synthesize Cyclobutane Di- and  
                      Tetracarboxylic Acid Building Blocks from Biomass-derived  
                      Precursors

Department    Chemistry

Degree         Doctor of Philosophy

In presenting this dissertation in partial fulfillment of the requirements for a graduate degree from the University of North Dakota, I agree that the library of this University shall make it freely available for inspection. I further agree that permission for extensive copying for scholarly purposes may be granted by the professor who supervised my dissertation work or, in her (or his) absence, by the Chairperson of the department or the dean of the School of Graduate Studies. It is understood that any copying or publication or other use of this dissertation or part thereof for financial gain shall not be allowed without my written permission. It is also understood that due recognition shall be given to me and to the University of North Dakota in any scholarly use which may be made of any material in my dissertation.

Dominic Nkafu Nkemngong

July 22, 2022

## TABLE OF CONTENTS

LIST OF FIGURES .....	x
LIST OF TABLES .....	xvii
LIST OF ABBREVIATION .....	xix
ACKNOWLEDGEMENTS .....	xxi
ABSTRACT .....	xxii

### CHAPTER ONE

#### **An Efficient and Concise Synthesis of Cyclobutane-1,2,3,4-dianhydride from Maleic Anhydride, Maleic and Fumaric Acids Using ECO-UV**

1.0. Introduction .....	1
1.1. Synthesis and Applications of Maleic Anhydride, Fumaric and Maleic Acids 4	
1.2. Results and Discussion .....	7
1.2.1 Synthesis of CBDAN-1 from CBTA-1 and Maleic Anhydride .....	7
1.2.2. Synthesis of CBTA-1 from Maleic Anhydride, Fumaric and Maleic Acids	9
1.2.3. Initial thermal studies on the stability of CBDAN-1 and CBTA-1 .....	14
1.3. Photoreaction of Maleic Anhydride Derivatives .....	17
1.3.1. Synthesis of CBDAN-3, CBDAN-4, CBTA-3, and CBTA-4 .....	17
1.3.2. Synthesis of CBDAN-5 .....	18
1.3.3. Thermal Studies on CBDANs .....	19
1.4. Conclusion .....	22
1.5. Experimental Section .....	23
1.5.1. Materials and Procedures .....	23
1.5.2. Synthesis of Cyclobutane-1,2,3,4-tetracarboxylic Dianhydride (CBDAN-1) from Maleic Anhydride .....	23

1.5.3. Synthesis of Cyclobutane-1,2,3,4-tetracarboxylic acid (CBTA-1) from Maleic Acid (MA) .....	24
1.5.4. Synthesis of Cyclobutane-1,2,3,4-tetracarboxylic acid (CBTA-1) from Fumaric Acid .....	26
1.5.7. Synthesis of 1,2 and 1,3-dimethyl-cyclobutane-1,2,3,4-tetracarboxylic acid (CBTA-3 and CBTA-4) from CBDAN-3 and CBDAN-4.....	29
1.5.8. Synthesis of 1,2,3,4-tetramethyl-cyclobutane-1,2,3,4-tetracarboxylic anhydride (CBDAN-5) from 2,3-dimethylmaleic anhydride (DMMAAn).....	30

## CHAPTER TWO

### **Cyclobutane-1,2,3,4-carboxylic Dianhydride: A Platform for the Synthesis of Biomass Derived Dicarboxylic Acids for Polymeric Applications**

2.0. Introduction .....	31
2.1. Results and Discussion.....	34
2.1.1. Synthesis of CBDAs from CBDAN-1 .....	34
2.1.2. Description of the Structures of CBDAx.....	36
2.1.2.1. CBDAx-1 Structure .....	36
2.1.2.2. CBDAx-2 1,2-diacid Structure .....	38
2.1.2.3. CBDAx-3 Structure .....	39
2.1.2.4. CBDAx-4 Structure .....	40
2.1.3. Initial thermal studies on the stability of CBDAxs.....	41
2.1.4. Synthesis of CBDExs from CBDAxs .....	45
2.1.5. Initial thermal studies on the stability of CBDExs .....	46
2.2. Conclusion.....	48
2.3. Experimental Section .....	48
2.3.1. Materials and Procedures.....	48

2.3.2. Synthesis of CBDAx-1 from CBDAN-1 .....	49
2.3.3. Synthesis of CBDAx-2 from CBDAN-1 .....	50
2.3.4. Synthesis of CBDAx-3 from CBDAN-1 .....	51
2.3.5. Synthesis of CBDAx-4 from CBDAN-1 .....	52
2.3.6. Synthesis of CBDAx-5 from CBDAN-1 .....	53
2.3.7. Synthesis of CBDAx-6 from CBDAN-1 .....	54
2.3.8. Synthesis of CBDAx-7 from CBDAN-1 .....	55
2.3.9. Synthesis of CBDAx-8 from CBDAN-1 .....	56
2.3.10. General Methods of Ester Synthesis.....	57

### **CHAPTER THREE**

#### **A Cyclobutane Carboxylic Dianhydride (CBDAN-2) as a Building Block for Metal-Organic and Polymeric Materials Introduction**

3.0. Introduction.....	61
3.1. Results and Discussion.....	63
3.1.1. Description of CBDAN-2.....	66
3.1.2. Initial thermal studies on CBDAN-2 and CBTA-2 .....	67
3.1.3. Synthesis of Imide and Polyimides .....	68
3.1.4. Thermal Stability of Polyimides.....	73
3.1.5. Synthesis of CBTA-2.....	75
3.1.6. Synthesis of a Cobalt - CBTA-2 Coordination Complex .....	75
3.1.7. Description of Co-CBTA-2 Complex.....	77
3.1.8. Thermochromic Properties .....	79
3.1.9. Initial Thermal Properties of Co-CBTA-2 Complex.....	80
3.1.10. Synthesis of Cyclobutane-containing Diacids from CBDAN-2.....	82
3.2. Conclusion.....	83



3.3. Experimental Section .....	84
3.3.1 Chemicals and measurements.....	84
3.3.2. Synthesis of tricyclo[4.2.2.0 <sup>2,5</sup> ]dec-7-ene-3,4,9,10-tetracarboxylic dianhydride (CBDAN-2) from benzene and maleic anhydride.....	85
3.3.3. Synthesis of 5,12-Dibutyl-5,12-diazapentacyclo[7.5.2.0 <sup>2,8</sup> ,0 <sup>3,7</sup> ,0 <sup>10,14</sup> ]hexadec-15-ene-4,6,11,13-tetrone (CBTIM-2) from CBDAN-2. ....	86
3.3.4. General synthesis of polyimides from CBDAN-2.....	87
3.3.5. Synthesis of tricyclo[4.2.2.0 <sup>2,5</sup> ]dec-7-ene-3,4,9,10-tetracarboxylic acid (CBTA-2) from CBDAN-2 .....	88
3.3.6. Synthesis of Co-CBTA-2 Complex.....	89
3.3.7. Synthesis of Cyclobutane-containing Diacids from CBDAN-2.....	90

## CHAPTER FOUR

### Preliminary Exploration of the Photoreactivity and Applications of some 2(5H)-Furanones

4.0. Introduction .....	92
4.0.1. Background, Hypothesis and Concept.....	93
4.0.2. Study Design.....	96
4.1. Results and Discussion.....	98
4.1.1. Synthesis of Cyclobutane Dilactone-1&2 (CBDL-1&2) from 2(5H)-Furanone .....	98
4.1.2. Description of CBDL-1 and CBDL-2 Structure.....	99
4.1.3. Synthesis of Cyclobutane Dilactone-3 (CBDL-3) from 5-Hydroxy-2(5H)-Furanone .....	100
4.1.4. Synthesis of Cyclobutane Dilactone-4&5 (CBDL-4&5) from 3-methyl-2(5H)-Furanone .....	101

4.1.5. Initial Thermal Studies on CBLAC-1, CBDL-2, and CBLAC-3 .....	101
4.2. Conclusion.....	103
4.3. Experimental Section .....	104
4.3.1. Materials and Procedures.....	104
4.3.2. Synthesis of Cyclobutane Dilactone-1&2 from 2(5H)-Furanone.....	104
4.3.3. Synthesis of Cyclobutane Dilactone-3 from 5-Hydroxy-2(5H)-Furanone .....	106
4.3.4. Synthesis of Cyclobutane Dilactone- 4 and 5 from 3-Methyl-2(5H)-furanone .....	106

## **CHAPTER FIVE**

### **Conclusions and Perspectives**

Appendix A: Crystal Data.....	111
Appendix B .....	114
Selected NMR and FT-IR Spectra of Synthesized Compounds .....	114
Appendix C .....	191
High Resolution Mass Spectrometry Data of Synthesized Compounds .....	191
Appendix D.....	197
Selected GPC traces .....	197
REFERENCES .....	199

## LIST OF FIGURES

Figure 1: UV-Vis absorbance of maleic and fumaric acids in solid state.....	3
Figure 2: Crystal structure of maleic acid showing: Right: Oak Ridge Thermal Ellipsoid Plot (ORTEP). Left: the distance between adjacent maleic acid molecules .....	3
Figure 3: Crystal structure of fumaric acid showing: (a) Oak Ridge Thermal Ellipsoid Plot (ORTEP) representing 50% electron density. (b) the distance between adjacent fumaric acid molecules in the commercialized form. (c) the distance between adjacent fumaric acid molecules in the sublime form. The molecules become more organized, parrallel and closely packed. ....	4
Figure 4: The $^1\text{H}$ NMR spectra (DMSO- $d_6$ ) as the reaction proceeds at times, 0, 12 and 24 hours, respectively. The maleic acid characteristic olefin peak at 6.27 ppm completely disappears while the characteristic methine peak of the cyclobutane ring of the CBTA-1 at 3.44 ppm emerges. ....	13
Figure 5: The $^1\text{H}$ NMR spectra (DMSO- $d_6$ ) as the reaction proceeds at times, 0, 12 and 24 hours, respectively. The fumaric acid characteristic olefin peak at 6.68 ppm completely disappears while the characteristic methine peak of the cyclobutane ring of the CBTA-1 at 3.44 ppm emerges. ....	14
Figure 6: TGA and DTG curves of CBDAN-1 and CBTA-1 a) TGA curves of CBDAN-1 and CBTA-1 recorded from 50 °C to 600 °C with a heating rate of 20 °C·min $^{-1}$ under N $_2$ atmosphere, b) DTG curves of CBDAN-1 and CBTA-1 recorded from 50 °C to 600 °C with a heating rate of 20 °C·min $^{-1}$ under N $_2$ atmosphere.....	16
Figure 7: The first heating DSC curve of CBTA-1 recorded from 50 °C to 280 °C with a heating rate of 10 °C·min $^{-1}$ under N $_2$ . ....	17
Figure 8: TGA and DTG curves of CBDAN-1, CBDAN-3 and CBDAN-5 a) TGA curves of CBDAN-1, CBDAN-3 and CBDAN-5 recorded from 50 °C to 600 °C with a heating rate of 20 °C·min $^{-1}$ under N $_2$ atmosphere, b) DTG curves of CBDAN-1 CBDAN-3 and CBDAN-5 recorded from 50 °C to 600 °C with a heating rate of 20 °C·min $^{-1}$ under N $_2$ atmosphere .....	21

Figure 9: Chemical and x-ray single-crystal structure of CBDAx-1: (a) chemical structure (b) One molecule shown as Oak Ridge Thermal Ellipsoid Plot (ORTEP) representing 50% electron density; (b) The planar conformation adopted by cyclobutane rings (the two methylene phenyl groups are omitted for clarity). ....38

Figure 10: Chemical and x-ray single-crystal structure of CBDAx- 2 1,2-diacid: (a) chemical structure (b) One molecule shown as Oak Ridge Thermal Ellipsoid Plot (ORTEP) representing 50% electron density; (b) The planar conformation adopted by cyclobutane rings (the two phenyl groups are omitted for clarity).....39

Figure 11: Chemical and x-ray single-crystal structure of CBDAx-3: (a) chemical structure (b) One molecule shown as Oak Ridge Thermal Ellipsoid Plot (ORTEP) representing 50% electron density; (b) The planar conformation adopted by cyclobutane rings (the two cyclohexyl groups are omitted for clarity).....40

Figure 12: Chemical and x-ray single-crystal structure of CBDAx-4: (a) chemical structure (b) One molecule shown as Oak Ridge Thermal Ellipsoid Plot (ORTEP) representing 50% electron density; (b) The planar conformation adopted by cyclobutane rings (the two tert-butyl groups are omitted for clarity).....41

Figure 13: TGA and DTG curves of CBDAx-1 via CBDAx-5 a) TGA curves of CBDAx-1 via CBDAx-5 recorded from 50 °C to 600 °C with a heating rate of 20 °C·min<sup>-1</sup> under N<sub>2</sub> atmosphere, b) DTG curves of CBDAx-1 via CBDAx-5 recorded from 50 °C to 600 °C with a heating rate of 20 °C·min<sup>-1</sup> under N<sub>2</sub> atmosphere.....43

Figure 14: TGA and DTG curves of CBDAx-6 and CBDAx-7 recorded from 50 °C to 600 °C with a heating rate of 20 °C·min<sup>-1</sup> under N<sub>2</sub> atmosphere.....44

Figure 15: TGA and DTG curves of CBDAx-8 recorded from 50 °C to 600 °C with a heating rate of 20 °C·min<sup>-1</sup> under N<sub>2</sub> atmosphere.....45

Figure 16: TGA curves of CBDEx-1 through CBDAx-5 recorded from 0 °C to 600 °C with a heating rate of 20 °C·min<sup>-1</sup> under N<sub>2</sub> atmosphere, b) DTG curves of CBDEx-1 through CBDAx-5 recorded from 50 °C to 600 °C with a heating rate of 20 °C·min<sup>-1</sup> under N<sub>2</sub> atmosphere.....47

Figure 17: Chemical and crystal structure of CBDAN-2 represented in black and red, b) crystal structure of CBDAN-2 in Oak Ridge Thermal Ellipsoid Plot (ORTEP) at the 50% probability level except for the hydrogen atoms, c) CBDAN-2 shown in capped sticks style to highlight the flat nature of the molecule .....	66
Figure 18: TGA and DTG curves of CBDAN-2 and CBTA-2; (a) TGA curves recorded from 50 °C to 600 °C with a heating rate of 20 °C·min <sup>-1</sup> under N <sub>2</sub> atmosphere. (b) DTG curves recorded from 50 °C to 600 °C with a heating rate of 20 °C·min <sup>-1</sup> under N <sub>2</sub> atmosphere.....	68
Figure 19: FT-IR spectra of P-I, P-II, and P-III for comparison with CBDAN-2 and the model compound (CBDAN-2_n-butylimide).....	72
Figure 20: Images of the synthesized P-I and P-III respectively. ....	73
Figure 21: TGA and DTG curves of polymers made from CBDAN-2; (a) TGA curves recorded from 50 °C to 600 °C with a heating rate of 20 °C·min <sup>-1</sup> under N <sub>2</sub> atmosphere. (b) DTG curves recorded from 50 °C to 600 °C with a heating rate of 20 °C·min <sup>-1</sup> under N <sub>2</sub> atmosphere.....	74
Figure 22: FT-IR spectra of CBTA-2 and Co-CBTA-2 complex (heated and unheated) .....	77
Figure 23: Symmetric unit of Co-CBTA-2 Complex in Oak Ridge Thermal Ellipsoid Plot (ORTEP) at the 50% probability level except for the hydrogen atoms; the octahedral Co <sup>2+</sup> center interacts with two CBTA-2 molecules, and three H <sub>2</sub> O molecules. Top, face, and side view of a single unit of Co-CBTA-2 complex shown.....	78
Figure 24: Side view of the Co-CBTA-2 complex shown in polyhedral style; b) Side view of the 2D Co-CBTA-2 complex shown in capped sticks style.....	79
Figure 25: Thermochromic behavior of Co-CBTA-2 complex .....	80
Figure 26: TGA and DTG curves of Co-CBTA-2 complex (heated and unheated); (a) TGA curves recorded from 50 °C to 600 °C with a heating rate of 20 °C·min <sup>-1</sup> under N <sub>2</sub> atmosphere. (b) DTG curves recorded from 50 °C to 600 °C with a heating rate of 20 °C·min <sup>-1</sup> under N <sub>2</sub> atmosphere. ....	82

Figure 27: UV-Vis absorbance of 5-hydroxy-2(5H)-furanone, 2(5H)-furanone, 3-methyl-2(5H)-furanone, and 4-methyl-2(5H)-furanone in ethanol. ....	97
Figure 28: Chemical and x-ray single-crystal structure of CBDL-1 and CBDL-2: One molecule shown as Oak Ridge Thermal Ellipsoid Plot (ORTEP) representing 50% electron density. ....	100
Figure 29: TGA and DTG curves of CBDL-1 and CBDL-2 recorded from 0 °C to 600 °C with a heating rate of 20 °C·min <sup>-1</sup> under N <sub>2</sub> atmosphere, b) DTG curves of CBDL-1 and CBDL-2 recorded from 0 °C to 600 °C with a heating rate of 20 °C·min <sup>-1</sup> under N <sub>2</sub> atmosphere. ....	103
Figure 30: Comparison of Kapton and polyimides synthesized from CBDAN-2. ....	109
Figure 31: Project summary, emphasizing the biomass origin of starting material. ....	110
Figure 32: <sup>1</sup> H NMR spectrum of CBDAN-1 in DMSO-d <sub>6</sub> at room temperature. ....	115
Figure 33: <sup>13</sup> C NMR spectrum of CBDAN-1 in Acetone-d <sub>6</sub> at room temperature. ....	116
Figure 34: FT-IR spectrum of CBDAN-1. ....	117
Figure 35: <sup>1</sup> H NMR spectrum of CBTA-1 in DMSO-d <sub>6</sub> at room temperature. ....	118
Figure 36: <sup>13</sup> C NMR spectrum of CBTA-1 in DMSO-d <sub>6</sub> at room temperature. ....	119
Figure 37: FT-IR spectrum of CBTA-1. ....	120
Figure 38: <sup>1</sup> H NMR spectrum of CBTE-1 in DMSO-d <sub>6</sub> at room temperature. ....	121
Figure 39: <sup>13</sup> C NMR spectrum of CBTE-1 in DMSO-d <sub>6</sub> at room temperature. ....	122
Figure 40: FT-IR spectrum of CBTE-1. ....	123
Figure 41: <sup>1</sup> H NMR spectrum of CBDAN-4 in DMSO-d <sub>6</sub> at room temperature. ....	124
Figure 42: <sup>13</sup> C NMR spectrum of CBDAN-4 in DMSO-d <sub>6</sub> at room temperature. ....	125
Figure 43: FT-IR spectrum of CBDAN-4. ....	126
Figure 44: <sup>1</sup> H NMR spectrum of CBTA-4 in DMSO-d <sub>6</sub> at room temperature. ....	127
Figure 45: <sup>13</sup> C NMR spectrum of CBTA-4 in DMSO-d <sub>6</sub> at room temperature. ....	128
Figure 46: FT-IR spectrum of CBTA-4. ....	129
Figure 47: <sup>1</sup> H NMR spectrum of CBDAN-5 in DMSO-d <sub>6</sub> at room temperature. ....	130
Figure 48: <sup>13</sup> C NMR spectrum of CBDAN-5 in DMSO-d <sub>6</sub> at room temperature. ....	131
Figure 49: FT-IR spectrum of CBDAN-5. ....	132
Figure 50: <sup>1</sup> H NMR spectrum of CBDAx-1 in DMSO-d <sub>6</sub> at room temperature. ....	133

Figure 51: $^{13}\text{C}$ NMR spectrum of CBDAx-1 in $\text{DSMO-d}_6$ at room temperature .....	134
Figure 52: FT-IR spectrum of CBDAx-1.....	135
Figure 53: $^1\text{H}$ NMR spectrum of CBDAx-2 in $\text{DSMO-d}_6$ at room temperature .....	136
Figure 54: $^{13}\text{C}$ NMR spectrum of CBDAx-2 in $\text{DSMO-d}_6$ at room temperature .....	137
Figure 55: FT-IR spectrum of CBDAx-2.....	138
Figure 56: $^1\text{H}$ NMR spectrum of CBDAx-3 in $\text{DSMO-d}_6$ at room temperature .....	139
Figure 57: $^{13}\text{C}$ NMR spectrum of CBDAx-3 in $\text{DSMO-d}_6$ at room temperature .....	140
Figure 58: FT-IR spectrum of CBDAx-3.....	141
Figure 59: $^1\text{H}$ NMR spectrum of CBDAx-4 in $\text{DSMO-d}_6$ at room temperature .....	142
Figure 60: $^{13}\text{C}$ NMR spectrum of CBDAx-4 in $\text{DSMO-d}_6$ at room temperature .....	143
Figure 61: FT-IR spectrum of CBDAx-4.....	144
Figure 62: $^1\text{H}$ NMR spectrum of CBDAx-5 in $\text{DSMO-d}_6$ at room temperature .....	145
Figure 63: $^1\text{H}$ NMR spectrum of CBDAx-5 in $\text{DSMO-d}_6$ at room temperature .....	146
Figure 64: FT-IR spectrum of CBDAx-5.....	147
Figure 65: $^1\text{H}$ NMR spectrum of CBDAx-6 in $\text{DSMO-d}_6$ at room temperature .....	148
Figure 66: $^{13}\text{C}$ NMR spectrum of CBDAx-6 in $\text{DSMO-d}_6$ at room temperature .....	149
Figure 67: FT-IR NMR spectrum of CBDAx-6 .....	150
Figure 68: $^1\text{H}$ NMR spectrum of CBDAx-7 in $\text{DSMO-d}_6$ at room temperature .....	151
Figure 69: $^{13}\text{C}$ NMR spectrum of CBDAx-7 in $\text{DSMO-d}_6$ at room temperature .....	152
Figure 70: FT-IR NMR spectrum of CBDAx-7 .....	153
Figure 71: $^1\text{H}$ NMR spectrum of CBDAx-8 in $\text{DSMO-d}_6$ at room temperature .....	154
Figure 72: $^{13}\text{C}$ NMR spectrum of CBDAx-8 in $\text{DSMO-d}_6$ at room temperature .....	156
Figure 73: FT-IR NMR spectrum of CBDAx-8 .....	156
Figure 74: $^1\text{H}$ NMR spectrum of CBDEx-1 in $\text{DSMO-d}_6$ at room temperature.....	157
Figure 75: $^{13}\text{C}$ NMR spectrum of CBDEx-1 in $\text{DSMO-d}_6$ at room temperature.....	158
Figure 76: FT-IR NMR spectrum of CBDEx-1 .....	159
Figure 77: $^1\text{H}$ NMR spectrum of CBDEx-2 in $\text{DSMO-d}_6$ at room temperature.....	160
Figure 78: $^{13}\text{C}$ NMR spectrum of CBDEx-2 in $\text{DSMO-d}_6$ at room temperature.....	161
Figure 79: FT-IR NMR spectrum of CBDEx-2.....	162
Figure 80: $^1\text{H}$ NMR spectrum of CBDEx-3 in $\text{DSMO-d}_6$ at room temperature.....	163

Figure 81: $^{13}\text{C}$ NMR spectrum of CBDEx-3 in DMSO- $d_6$ at room temperature.....	164
Figure 82: FT-IR NMR spectrum of CBDEx-3.....	164
Figure 83: $^1\text{H}$ NMR spectrum of CBDEx-4 in DMSO- $d_6$ at room temperature.....	165
Figure 84: $^{13}\text{C}$ NMR spectrum of CBDEx-4 in DMSO- $d_6$ at room temperature.....	166
Figure 85: FT-IR NMR spectrum of CBDEx-4.....	167
Figure 86: $^1\text{H}$ NMR spectrum of CBDEx-5 in DMSO- $d_6$ at room temperature.....	168
Figure 87: $^{13}\text{C}$ NMR spectrum of CBDEx-5 in DMSO- $d_6$ at room temperature.....	169
Figure 88: FT-IR NMR spectrum of CBDEx-5.....	169
Figure 89: $^1\text{H}$ NMR spectrum of CBDAN-2 in DMSO- $d_6$ at room temperature.....	170
Figure 90: $^{13}\text{C}$ NMR spectrum of CBDAN-2 in DMSO- $d_6$ at room temperature.....	171
Figure 91: FT-IR NMR spectrum of CBDAN-2.....	172
Figure 92: $^1\text{H}$ NMR spectrum of CBTA-2 in DMSO- $d_6$ at room temperature.....	173
Figure 93: $^{13}\text{C}$ NMR spectrum of CBTA-2 in DMSO- $d_6$ at room temperature.....	174
Figure 94: FT-IR NMR spectrum of CBTA-2.....	175
Figure 95: $^1\text{H}$ NMR spectrum of CBDIM-2 in DMSO- $d_6$ at room temperature.....	176
Figure 96: $^{13}\text{C}$ NMR spectrum of CBDIM-2 in DMSO- $d_6$ at room temperature.....	177
Figure 97: FT-IR NMR spectrum of CBDIM-2.....	178
Figure 98: $^1\text{H}$ NMR spectrum of Polyimide-I in $\text{CDCl}_3/\text{TFA}$ at room temperature..	179
Figure 99: $^{13}\text{C}$ NMR spectrum of Polyimide-I in $\text{CDCl}_3/\text{TFA}$ at room temperature.	180
Figure 100: FT-IR spectrum of Polyimide-I.....	181
Figure 101: $^1\text{H}$ NMR spectrum of CBDAxx-1 in DMSO- $d_6$ at room temperature ...	182
Figure 102: $^1\text{H}$ NMR spectrum of CBDAxx-2 in DMSO- $d_6$ at room temperature ...	183
Figure 103: $^1\text{H}$ NMR spectrum of mixture of CBDL-1&2 in DMSO- $d_6$ at r.t. ....	184
Figure 104: $^{13}\text{C}$ NMR spectrum of mixture of CBDL-1&2 in DMSO- $d_6$ at r.t. ....	185
Figure 105: FT-IR NMR spectrum of mixture of CBDL-1&2 in DMSO- $d_6$ at r.t. ...	185
Figure 106: $^1\text{H}$ NMR spectrum of CBDL-1 in DMSO- $d_6$ at room temperature.....	186
Figure 107: $^{13}\text{C}$ NMR spectrum of CBDL-1 in DMSO- $d_6$ at room temperature.....	187
Figure 108: $^1\text{H}$ NMR spectrum of CBDL-3 in DMSO- $d_6$ at room temperature.....	187
Figure 109: $^{13}\text{C}$ NMR spectrum of CBDL-3 in DMSO- $d_6$ at room temperature.....	188
Figure 110: FT-IR NMR spectrum of CBDL-3.....	189



Figure 111: <sup>1</sup> H NMR spectrum of CBDL-4&5 in DMSO-d <sub>6</sub> at room temperature .	190
Figure 112: HRMS spectrum of CBDAx-1 .....	192
Figure 113: HRMS spectrum of CBDAx-2. ....	193
Figure 114: HRMS spectrum of CBDAx-3. ....	194
Figure 115: HRMS spectrum of CBDAx-4. ....	195
Figure 116: HRMS spectrum of CBDAx-5. ....	196
Figure 117: GPC chromatogram report of polyimide I (P-1). ....	198

## LIST OF TABLES

Table 1: Optimization of the synthesis of CBDAN-1 from MAn .....	8
Table 2: Optimization of reaction conditions of photodimerization of maleic acid ....	11
Table 3: Thermogravimetric analysis data for CBDAN-1, CBDAN-3, and CBDAN-5 .....	20
Table 4: Summary of CBDAx Synthesis .....	36
Table 5: Melting point data for CBDAx-1 through CBDAx-8.....	42
Table 6: Thermogravimetric analysis data for CBDAx-1 through CBDAx-8.....	42
Table 7: Thermogravimetric analysis data for CBDEx-1 through CBDEx-5.....	46
Table 8: Thermogravimetric analysis of polymers .....	75
Table 9: Molecular weight distribution of polyimides from GPC.....	75
Table 10: Thermogravimetric analysis of CBLAC-1 and CBDL-2 and CBLAC-3 ..	102
Table 11: Table A-1: Crystal data of CBDAN-1, CBTA-1, sublime FA .....	111
Table 12: Crystal data of CBDAx-1 through CBDAx-4 .....	112
Table 13: Crystal data of CBDAN-2, CBTA-2_Co Complex and model compound	113
Table 14: Crystal data of CBDLs.....	114

## LIST OF SCHEMES

Scheme 1: Dimerization of maleic anhydride.....	24
Scheme 2: Dimerization of maleic acid .....	24
Scheme 3: Dimerization of fumaric acid .....	26
Scheme 4: Dehydration of CBTA-1 to CBDAN-1 .....	27
Scheme 5: Dimerization of citraconic anhydride.....	28
Scheme 6: Hydrolysis of CBDAN-3 and CBDAN-4 .....	29
Scheme 7: Dimerization of 2,3-dimethylmaleic anhydride .....	30
Scheme 8: Synthesis of CBDAXs from Biomass precursors via CBDAN-1 .....	33
Scheme 9: Synthesis of CBDAX-1.....	50
Scheme 10: Synthesis of CBDAX-2.....	50
Scheme 11: Synthesis of CBDAX-3.....	51
Scheme 12: Synthesis of CBDAX-4.....	52
Scheme 13: Synthesis of CBDAX-5.....	54
Scheme 14: Synthesis of CBDAX-6.....	55
Scheme 15: Synthesis of CBDAX-7.....	56
Scheme 16: Synthesis of CBDAX-8.....	57
Scheme 17: General methods to the synthesis of CBDExs .....	59
Scheme 19: Synthesis and Applications of CBDAN-2 and its Derivatives.....	64
Scheme 20: Synthesis and crystal structure of CBDIM-2 .....	71
Scheme 21: Synthesis of CBDAN-2.....	86
Scheme 22: Synthesis of CBDIM-2.....	86
Scheme 23: General method for synthesis of polyimides.....	88
Scheme 24: Synthesis of CBTA-2 .....	88
Scheme 25: Synthesis of Co-CBTA-2 complex .....	90
Scheme 26: General method for synthesis of CBDAXs.....	91
Scheme 27: Project concept .....	95
Scheme 28: Synthesis of CBDL-1&2 .....	105
Scheme 29: Synthesis of CBDL-3 .....	106
Scheme 30: Synthesis of CBDL-4&5 .....	107

## LIST OF ABBREVIATION

2D:	Two-dimensional
CBDA:	Cyclobutane diacid
CBDAN:	Cyclobutane dianhydride
CBDAx:	Cyclobutane diacid of the x series
CBDEx:	Cyclobutane diester of the x series
CBDIM:	Cyclobutane di-imide
CBDL:	Cyclobutane dilactone
CBTA:	Cyclobutane-tetracarboxylic acid
CBTE:	Cyclobutane-tetracarboxylic ester
DCM:	Dichloromethane
DMF:	N,N-dimethylformamide
DMSO:	Dimethyl sulfoxide
DSC:	Differential scanning calorimetry
DTG:	Derivative temperature
ECO-UV:	Energy-efficient, Cost-effective, and Operator-friendly
FT-IR:	Fourier transform infrared spectroscopy
GPC:	Gel permeation chromatography
HRMS:	High resolution mass spectrometer
MOMs:	Metal-organic materials
NMR:	Nuclear magnetic resonance
ORTEP:	Oak ridge thermal ellipsoid plot
SC-XRD:	Single crystal X-ray diffraction
SEM:	Scanning electron microscopy
T5%:	Temperature at onset of decomposition
Td:	Temperature at maximum decomposition
TFA:	Trifluoroacetic acid
Tg:	Glass transition temperature

TGA: Thermogravimetric analysis  
TMS: Tetramethylsilane  
UV-C: Ultraviolet-C Radiation  
UV-Vis: Ultraviolet-visible spectroscopy

## ACKNOWLEDGEMENTS

I would like to gratefully acknowledge my advisor Dr. Chu, for the enthusiastic supervision and the support that he provided me at each step of my work. I also gratefully acknowledge all those that serve on my committee, Drs. Guodong Du, Binglin Sui, Evguenii Kozliak, Frank Bowman, and previous members Drs. Lothar Stahl (retired), Irina Smoliakova (retired), Thomasson Kathryn (RIP), and Tao Yu (RIP). Your objective criticism and guidance were the thrust in this work.

I thank the chair of the Department Dr. Alena Kubatova and the chemistry department at UND for the facilities placed at my disposal for the conduct of this study. This work would not have been possible without the funds provided by ND ESPCoR and CSMS.

Thanks to Drs. Zhihan Wang and Rahul Shahni for assistant in the laboratory during the conduct of this study. I would also like to thank my friends and colleagues; Cheo Akongnwi, Lengwe Habrine, Houssein Amjaour, Joseph Robertson, Tiffany Shiu, and Brent Kastern whom we worked together.

Special thanks go to my parents Mr. and Mrs. Nkemngong, my siblings; Valery, Laura, Blaise, Noella, Lorena (RIP), Mara and my girlfriend Ethel Doh for moral support. Your prayers and support were priceless, I love you all.

To those whose names have not been mentioned, I say, “thank you” and may God bless you.

Above all I thank God for his grace and blessings.

To my family

## ABSTRACT

Materials are a vital part of human life, as such it is important that the precursors to these materials are sustainable. Currently, these precursors are synthesized by the oxidation of petroleum derived hydrocarbons. Petroleum is not sustainable and is feared to deplete soon. Derivatizing the currently available biomass-based building blocks will diversify and increase the number of precursors for materials and gradually reduce our reliance on petrochemicals.

The carboxylic dianhydride, CBDAN-1, a potential biomass-derived precursor for material synthesis, was synthesized from the photodimerization of maleic anhydride or the dehydration of CBTA-1. CBTA-1 was synthesized from the photodimerization of maleic and fumaric acids using UV-C (254 nm). Other carboxylic dianhydrides; CBDAN-3, CBDAN-4, and CBDAN-5, were synthesized from the photodimerization of citraconic anhydride and 2,3-dimethylmaleic anhydride respectively using black light. The CBDANs showed good thermal stability, making them desirable to be used as precursors for material synthesis.

To demonstrate the versatility of CBDANs, CBDAN-1 was used to synthesize eight cyclobutane containing diacids using an amine, alcohol, or Grignard reagent as nucleophiles. The TGA of the synthesized diacids showed that these molecules were thermally stable enough to be incorporated as precursors in polymer synthesis. A carboxylic dianhydride (CBDAN-2), synthesized from maleic anhydride and benzene was



used to synthesize polyimides with 2,2-bis[4-(4-aminophenoxy)phenyl]hexafluoropropane, 2,2-bis(3-amino-4-hydroxyphenyl)hexafluoropropane and hexane-1,6-diamine. The polyimides showed desirable properties such as high  $T_d$ . Metal-organic materials synthesized from the polytopic ligand CBTA-2, a derivative of CBDAN-2, showed good thermal and interesting thermochromic behavior. CBDAN-2 was also used to synthesize two dicarboxylic acids which can be used in the synthesis of polyesters.

Furanones share several features in common with the furanediones. The latter has been shown to be a versatile precursor in material synthesis. We therefore hypothesized that dimers of furanones could also be explored in the synthesis of precursors to materials. Cyclobutane-containing dilactones (CBDL) were obtained from the photodimerization of 2(5H)-furanone, 3-methyl-2(5H)-furanone, and 5-hydroxy-2(5H)-furanone under UV-C (254 nm). The thermal stability of these dilactones showed that they are stable enough to be incorporated into polymers.

In conclusion, in this dissertation, the synthesis and characterization of several cyclobutane-containing diacids, dianhydrides and dilactones have been shown. Also, one of the synthesized dianhydride was used to synthesize polyimides and MOMs. All these monomers and materials were synthesized from potential biomass-derived precursors using simple, efficient, and ecofriendly methods.

## CHAPTER ONE

### **An Efficient and Concise Synthesis of Cyclobutane-1,2,3,4-dianhydride from Maleic Anhydride, Maleic and Fumaric Acids Using ECO-UV**

#### **1.0.Introduction**

Cyclobutane-1,2,3,4-dianhydride (CBDAN-1) is a versatile building block that can be used in the synthesis of polyimides, metal-organic materials, diacids, etc. Little attention has been paid to the synthesis of CBDAN-1 from biomass derived precursors. Deriving this important building block from renewable sources would go a long way to help in the quest to phaseout petrochemicals. CBDAN-1 can be synthesized by the direct dimerization of maleic anhydride or the dehydration of cyclobutane-1,2,3,4-tetracarboxylic acid (CBTA-1). CBTA-1 can be obtained from the direct dimerization of fumaric and maleic acids.

Direct sensitization-excitation photochemical reactions in solid state are governed by the molecule's topochemical crystal lattice packing and the absorption properties of reacting species.<sup>1-3</sup> In this regard, reaction in solid-state will only occur if the conformation of the reacting molecules and distance from the closest molecule in the crystal lattice agree with the Schmidt principles.<sup>2,3</sup> Moreover, the reacting species must have absorbance in the wavelength of the exciting photons. Also, the photons must have the right amount of energy to excite reacting species.<sup>4</sup> Designing these experiments not only require finding olefins that have the appropriate crystal packing but also sorting the photon source which will excite reacting species.<sup>5, 6, 7</sup>

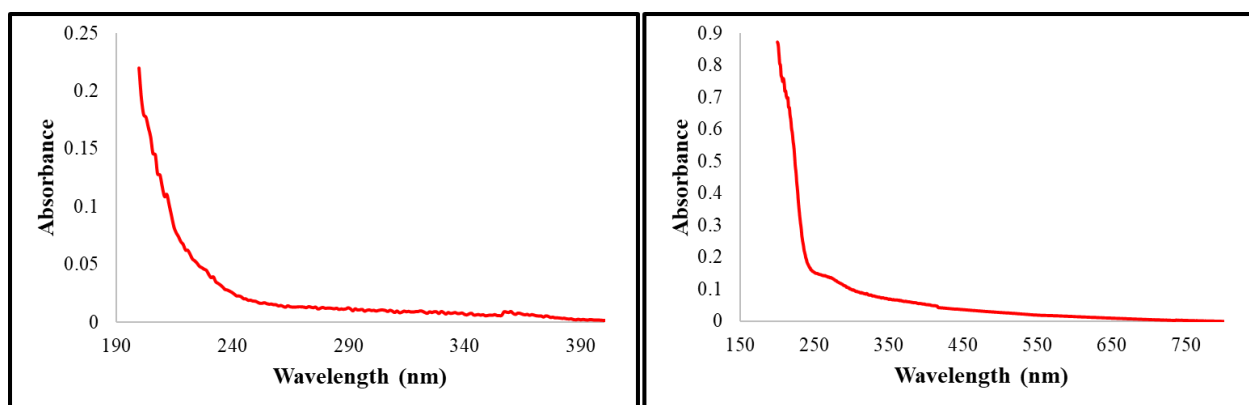
Several light sources providing appropriate energy for molecular activation in photochemistry have been described in literature with each having their unique advantages.<sup>8,9, 10</sup> Research in our group has largely been carried out using UV lamps, which is nontraditional. These lamps, termed ECO-UV (Energy-efficient, Cost-effective, and Operator-friendly) have been shown to be cost effective and environmentally friendly. The goal of using ECO-UV is to efficiently manage energy while reducing cost in the production process.

To find the appropriate lamps to use, the UV-Vis absorptions of maleic and fumaric acids were explored to understand their absorption pattern in solid state. The data obtained showed that maleic and fumaric acids have a high absorbance between 200 nm - 260 nm and 380 nm, respectively (Figure 1). In this regard, it was hypothesized that low pressure mercury monochromatic lamps producing UV-C (254 nm) could produce enough energy to excite both maleic and fumaric acid molecules, and upon excitation, they would dimerize to CBTA-1.

Interestingly, individual maleic acid molecules in the crystal lattice packing are parallel and 3.7 Å apart, and therefore follow the Schmidt principle (Figure 2).<sup>2, 11, 12</sup> On the other hand, individual fumaric acid molecules are unparallel, and the distance between the olefins are 3.6 Å and 4.7 Å, respectively (Figure 3).<sup>7, 13</sup> This packing limits clean photodimerization of fumaric acid in solid state. To achieve photo reactivity in this case, the crystal lattice packing must be altered.

The crystal packing of commercially available FA is incongruence with the Schmidt's principles governing photoreaction in solid state.<sup>13</sup> Based on previous work in our

laboratory, we hypothesized that there should be a crystalline form of fumaric acid that would dimerize. To find this crystalline form, FA was melted and immediately subjected to recrystallization at low or high temperatures to force recrystallization in extreme conditions. This way we hypothesized that a new, less unfavorable, crystalline form might be formed which could be photoreactive. It was found out that FA molecules in sublime crystals were parallel and closely packed (Figure 3).



*UV-Vis absorbance of maleic acid in solid state*

*UV-Vis absorbance of fumaric acid in solid state*

**Figure 1:** UV-Vis absorbance of maleic and fumaric acids in solid state

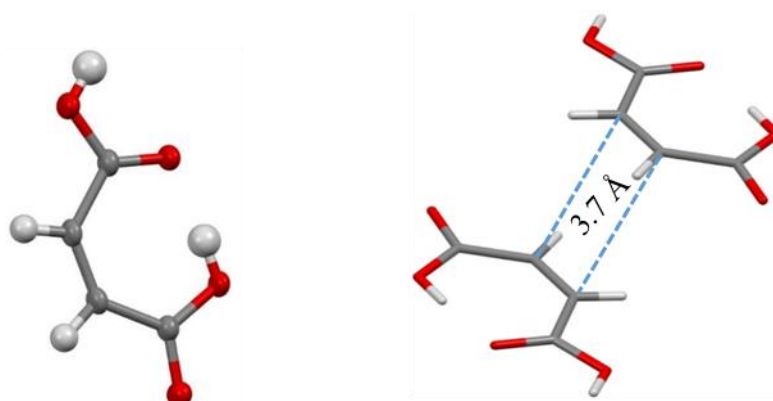


**Figure 2:** Crystal structure of maleic acid showing: Right: Oak Ridge Thermal Ellipsoid Plot (ORTEP). Left: the distance between adjacent maleic acid molecules

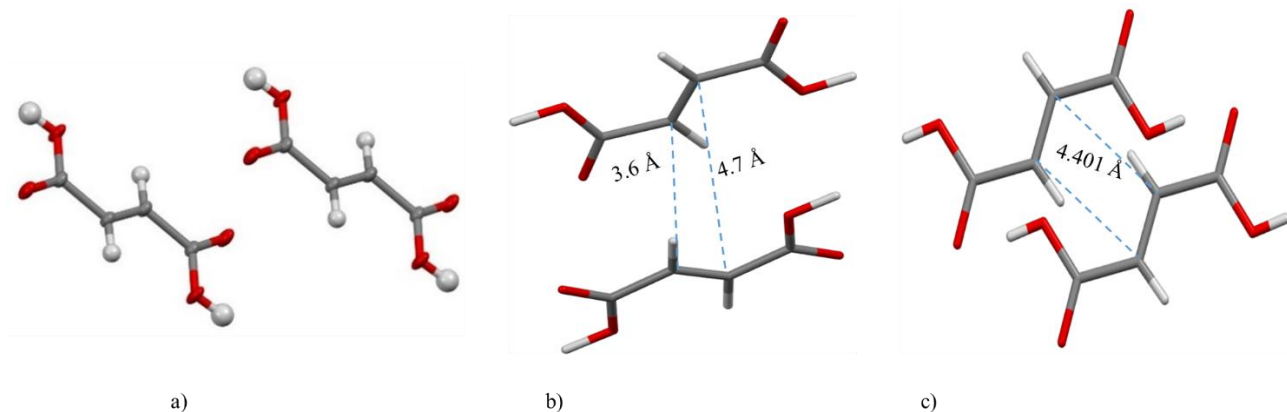


**Figure 3:** Crystal structure of fumaric acid showing: **(a)** Oak Ridge Thermal Ellipsoid Plot (ORTEP) representing 50% electron density. **(b)** the distance between adjacent fumaric acid molecules in the commercialized form. **(c)** the distance between adjacent fumaric acid molecules in the sublime form. The molecules become more organized, parallel and closely packed.

### 1.1.Synthesis and Applications of Maleic Anhydride, Fumaric and Maleic Acids

Maleic acid is widely synthesized from the hydrolysis of maleic anhydride, the latter is obtained from the catalytic oxidation of butane or benzene. Recently, attention has been paid to the synthesis of maleic acid from biomass-based precursors. Maleic acid is a versatile precursor used in the making of unsaturated polyester resins, lubricant additives, surface coatings, textiles, photographic chemicals, plasticizers, pharmaceutical products, and agricultural chemicals.<sup>14</sup> It is also used industrially as an adhesion promoter for different substrates such as nylon and zinc coated metals, as a corrosion inhibitor and anti-scaling agent. Both liquid and vapor phase oxidation routes are currently being studied and improved for the synthesis of MA from furan, furfural and 5-hydroxymethylfurfural.<sup>15, 16</sup>

Initial studies in this area began using O<sub>2</sub> or H<sub>2</sub>O<sub>2</sub> as oxidants over widely available catalysts.<sup>17</sup> Later studies to improve MA selectivity were conducted in liquid phase using homogeneous H<sub>3</sub>PMo<sub>12</sub>O<sub>40</sub> and VO(acac)<sub>2</sub> catalysts.<sup>15, 18, 19</sup> Heterogeneous catalysis has also been reported with the vapor phase oxidation of furfural and 5-hydroxymethylfurfural using vanadium oxide or vanadium-molybdenum mixed oxides supported on Al<sub>2</sub>O<sub>3</sub>. Recent studies have focused on the improvement of yield and selectivity via solvent and catalytic system optimizations.<sup>20</sup> Shi and co-workers exploited a liquid phase oxidation of furfural using combination of the copper nitrate with phosphomolybdic acid as a catalyst to selectively convert furfural to maleic acid with a 49.2% yield and 51.7% selectivity respectively.<sup>21</sup>

Yu and co-workers reported the direct synthesis of maleic acid from xylose based on the use of deep eutectic solvents following a standard H<sub>2</sub>O<sub>2</sub> dehydration of xylose. They obtained a maleic acid yield of 20.8%, along with 5.0% of fumaric acid.<sup>22</sup> Yang and co-workers developed a method for the synthesis of MA from furfural using a combination of H<sub>2</sub>O<sub>2</sub> and KBr/graphitic carbon nitride (g-C<sub>3</sub>N<sub>4</sub>) as a catalyst in an aqueous phase reaction system. They obtained optimal yields of 70% with good selectivity.<sup>19</sup> Recently, Thiagarajan and co-workers reported an efficient way to combine photochemistry and electro- or biochemistry to oxidize furfural to MA.<sup>23</sup> The optimal overall yield obtained in their study was 97% with almost 100% conversion in certain conditions.

Maleic anhydride is the third most important anhydride for industrial uses trailing phthalic and acetic anhydrides.<sup>24</sup> It has a wide variety of industrial applications such as it is used in the synthesis of fumaric, malic, tartaric, maleic acids, succinic acid, and its

anhydride. It is used in the polymer industry, for making coatings, polyesters, alkyd resins, BDO, manufacturing of paints, varnishes, and lube oil additives. It is also used as a feedstock in the production of tetrahydrophthalic anhydride, THF and butyrolactone.<sup>25</sup> Recently, there has been increasing reports on the production of MAN from biomass-derived feedstocks as concerns on the exploitation of fossil fuels looms.<sup>26-28</sup>

The earliest proposals in this area came from Yedur and co-workers who reported the production of MAN from biomass-derived succinic acid via succinic anhydride. In their work, molybdenum oxide-based catalysts were used for the dehydration reactions.<sup>25</sup> In recent years many successes have been achieved with the gas or liquid phase oxidation of furfural and levulinic acid. Chatzidimitriou and Bond, recently reported a catalytic pathway for the synthesis of maleic anhydride (MAN) via oxidative cleavage of the methyl carbon in levulinic acid over supported various vanadates with MAN yields as high as 71 %.<sup>29</sup> Agirre and co-workers reported an industrial scale production route in the synthesis of MAN from furfural. They demonstrated the production of MAN from furfural via aqueous phase oxidation, using H<sub>2</sub>O<sub>2</sub> as oxidant, and via gas phase oxidation, using molecular oxygen.<sup>24</sup>

Fumaric acid (FA) has wide applications in food additives, food acidulants, unsaturated polyester resins (UPR), alkyd resins, paper resins, plasticizers, lubricating oils, oil field fluids, inks, dermatological formulations, local therapeutics, and other pharmaceuticals.<sup>14, 30</sup> The FA market share is expected to reach USD 974.4 million by 2027. FA production began in 1932 using an acid-catalyzed isomerization of maleic

acid. It is currently produced from fermentation.<sup>30, 31</sup> The deprotonated form of fumaric acid, fumarate, is an intermediate metabolite in the citric acid and urea cycles used by living organisms, making this molecule very attractive as a fermentation product.<sup>32</sup> Xu and co-workers reported on the synthesis of FA by the direct fermentation of biomass feedstock using metabolically engineered *Saccharomyces cerevisiae*.<sup>32</sup> The final engineered *S. cerevisiae* strain could produce FA up to a concentration of 1675±52 mg L<sup>-1</sup> without a change in microbial growth at optimal output in fed-batch culture.

Swart and co-workers developed a method of producing fumarate from *Rhizopus oryzae* using the Crabtree effect to reduce ethanol by-product formation. They reported a fumarate production rate of 0.150 g L<sup>-1</sup> h<sup>-1</sup> per glucose addition at a rate of 0.197 g L<sup>-1</sup> h<sup>-1</sup> with a resulting yield of 0.802 g g<sup>-1</sup> fumarate.<sup>33</sup> Recent studies have focused on the improvement of the microbial strain, elimination of by-product and production cost reduction. Recombinant strains of the microorganisms, *Rhizopus oryzae*, *Escherichia coli*, *Saccharomyces cerevisiae*, and *Torulopsis glabrata* and their mutants are currently used in the production of fumarate.<sup>34</sup>

## **1.2. Results and Discussion**

### **1.2.1 Synthesis of CBDAN-1 from CBTA-1 and Maleic Anhydride**

CBDAN-1 was synthesized from either the dimerization of maleic anhydride (MAn) or the dehydration of CBTA-1. X-ray crystallography revealed the structure of CBDAN-1 to be consistent with the cis, trans, cis conformation.<sup>6, 35, 36</sup> In the synthesis of CBDAN-1 from maleic anhydride, crystals started precipitating from solution at about



3 hours and reached a 70 % reaction yield at about 72 hours. Higher yield was not attained since the reaction takes place in the solution phase.

After 72 hours, the solvent was evaporated, and the residue dried. <sup>1</sup>H NMR analysis of the residue showed it contained maleic acid from hydrolysis of maleic anhydride, residual CBDAN-1, and residual maleic anhydride. This residue was dissolved in ethyl acetate and irradiated with blacklight, and more CBDAN-1 was formed from unhydrolyzed maleic anhydride increasing yield by 5 %. In the solution phase, some of the MAn is hydrolyzed to maleic acid (MA) and fumaric acid (FA), which do not dimerize under these conditions (Table 1). The reaction was faster when the solvent was dried with molecular sieves and ran under nitrogen. Saturation of the ethyl acetate solution with MAn does not increase the yield under these conditions probably because more photons are needed to drive the reaction, which could not be provided by the four bulbs used.

**Table 1:** Optimization of the synthesis of CBDAN-1 from MAn

S/N	Solvent	Condition	Time (hours)	Yield (%)	Component of Residue
1	Ethyl acetate	Under N <sub>2</sub>	72	68	MAn, MA, FA, + impurities
2	Ethyl acetate (Dried with molecular sieves)	n/a	60	70	MAn + impurities
3	Ethyl acetate (Dried with molecular sieves)	Under N <sub>2</sub>	72	75	MAn + impurities
4	Chloroform	n/a	72	40	MAn, MA, FA, + impurities
5	Acetone	n/a	72	n/a	MAn, MA, FA, + impurities
6	Acetonitrile	n/a	72	n/a	MAn, MA, FA, + impurities

Dehydration of CBTA-1 in acetic anhydride also yielded CBDAN-1. Acetic anhydride was used as both a solvent and as a component in the reaction. The water released from CBTA-1 hydrolyzes acetic anhydride to acetic acid thereby promoting the formation of product. The product was obtained with a greater than 93 % yield. CBDAN-1 was also synthesized from CBTA-1 by heating CBTA-1 to 230 °C in an oven for 24 hours. From the TGA analysis of CBTA-1, we observed a 7.3 % loss in weight around 250 °C and no further weight drop until around 300 °C (Figure 6). This loss in weight is consistent with the loss of a water molecule. The sample was then analyzed by heating CBTA-1 to between 220 °C (with an increment of 5 °C) and 250 °C, holding for a few minutes at each temperature to observe the chemical transformation in the molecule. This change was monitored through <sup>1</sup>H NMR spectroscopy. <sup>1</sup>H NMR spectroscopy showed that there was the conversion of CBTA-1 to CBDAN-1 at temperatures between 225 °C and 230 °C. Further work showed that heating CBTA-1 to 230 °C and holding at this temperature for 24 hours was optimal for the reaction. Therefore, this method offers a simple and solvent free method of synthesizing CBDAN-1 from CBTA-1. Moreover, given the fact that CBTA-1 can be synthesized from maleic and fumaric acids, which are easily obtained from the biomass, this solvent free route of synthesizing CBDAN-1 could offer a competitive advantage to synthesis from maleic anhydride.

### **1.2.2. Synthesis of CBTA-1 from Maleic Anhydride, Fumaric and Maleic Acids**

CBTA-1 was synthesized from the dimerization of MA or FA. X-ray crystallography revealed the structure of the product to be consistent with the cis, trans, cis conformation.<sup>6, 36</sup> The crystal packing and hydrogen bonding interactions of CBTA

have been well studied and they present incredible features in building MOFs.<sup>37</sup> CBTA-1 was readily synthesized from commercially available MA through a [2+2] photodimerization in the solid-state under UV-C. The UV-Vis absorption spectra of MA showed high absorption between 200 to 260 nm (Figure 1) explaining why lamps producing UV-C were the most appropriate to drive the reaction. This solvent-free photocycloaddition is possible because the distance between complementary  $\pi$ - $\pi$  interactions in adjacent MA molecules is less than 4.2 Å (Figure 2), which agrees with the Schmidt principle and hence should dimerize. The reaction begins at about 2 hours of exposure and completes within 24 hours with > 98 % conversion of MA to CBTA-1 (Figure 3). The current procedure to dimerize MA was established after several reaction conditions were tried and optimized for the synthesis of CBTA-1 (Table 1).

**Table 2:** Optimization of reaction conditions of photodimerization of maleic acid

SN	Irradiation Source	Method of Irradiation	Solvent	Temp	Time (hours)	Outcome
1	UV-B	Solution	Acetonitrile	rt	72	FA <sup>a</sup>
2	UV-B	Solution	Acetone	rt	72	FA <sup>a</sup>
3	UV-B	Solution	CHCl <sub>3</sub>	rt	72	FA <sup>a</sup>
4	UV-B	Solution	Benzene	rt	72	FA <sup>a</sup>
5	UV-B	Solution	Water	rt	72	FA <sup>a</sup>
6	UV-B	Solution	HCl (aq)	rt	72	MA
7	UV-B	Solution	NaCl (aq)	rt	72	FA <sup>a</sup>
8	UV-B	Solid-state	na	rt	72	MA
9	UV-C	Solution	Acetonitrile	rt	72	MA
10	UV-C	Solution	Acetone	rt	72	MA
11	UV-C	Solution	CHCl <sub>3</sub>	rt	72	MA
12	UV-C	Solution	Benzene	rt	72	MA
13	UV-C	Solution	Water	rt	72	MA
14	UV-C	Solution	HCl (aq)	rt	72	MA
15	UV-C	Solid-state	NaCl (aq)	rt	24	MA
16	UV-C	Solid-state	na	rt	24	CBTA-1
17	Hg	Solid-state	na	rt	72	CBTA-1 + FA + impurities
18	Hg	Solid-state	KBr	rt	72	CBTA-1 + FA + impurities
19	Hg	Solid-state	NaCl	rt	72	CBTA-1 + FA + impurities

<sup>a</sup> FA is fumaric acid; UV-A, UV-B and Hg isomerizes MA to FA

CBTA-1 was also readily synthesized from FA through a [2+2] photodimerization in the solid-state under UV-C. The crystal packing of the commercially available form of FA shows that individual FA molecules are unparallel, and the distance between the olefins are 3.6 Å and 4.7 Å respectively (Figure 5).<sup>7, 13</sup> This form, though photoreactive, produces multiple products. However, when the commercial form of FA is heated to its sublimation temperature at about 220 °C, crystals are formed on the sides of the reaction

vessel. These crystals called sublime crystals can dimerize to CBTA-1 upon irradiation with germicidal lamps producing UV-C. The dimerization of sublime crystals of FA also occurred after the crystals had been subjected to grinding. This suggests that the photo reactive crystalline form created by heating is stable upon grinding. Intriguingly, the crystal packing of FA molecules in the sublime form has individual FA molecules that are parallel, but the distance between the olefins is 4.4 Å (Figure 3).

Contrary to the Schmidt principle, this crystalline form dimerized upon photo irradiation in solid state. The UV-Vis absorption spectra of FA showed high absorption between 200 to 380 nm (Figure 1) explaining why lamps producing UV-C were the most appropriate to drive the reaction. The reaction begins at about 2 hours of exposure and completes within 24 hours with > 98 % conversion of FA to CBTA-1 (Figure 5). The reaction product was characterized using  $^1\text{H}$ ,  $^{13}\text{C}$ , NMR, FT-IR spectroscopy, and X-ray crystallography.

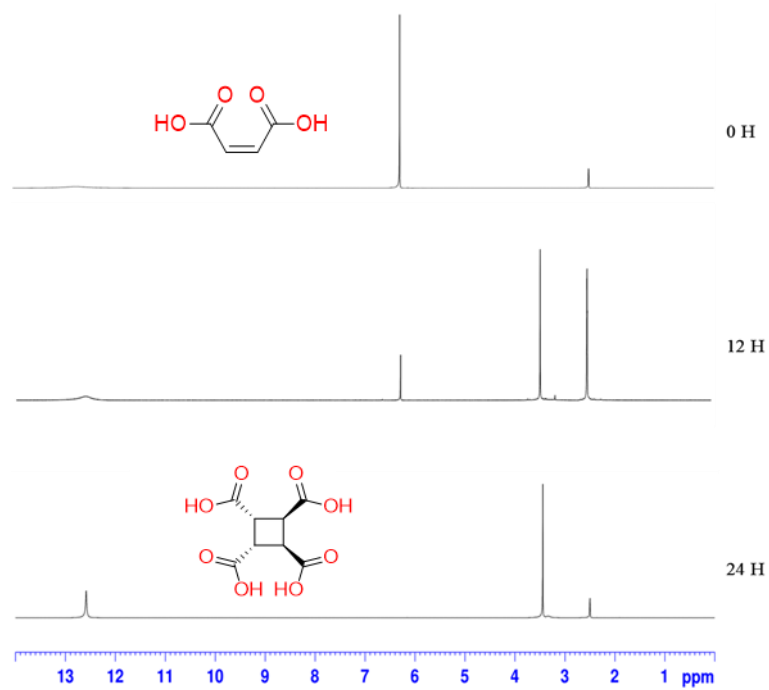


**Figure 4:** The <sup>1</sup>H NMR spectra (DMSO-d<sub>6</sub>) as the reaction proceeds at times, 0, 12 and 24 hours, respectively. The maleic acid characteristic olefin peak at 6.27 ppm completely disappears while the characteristic methine peak of the cyclobutane ring of the CBTA-1 at 3.44 ppm emerges.

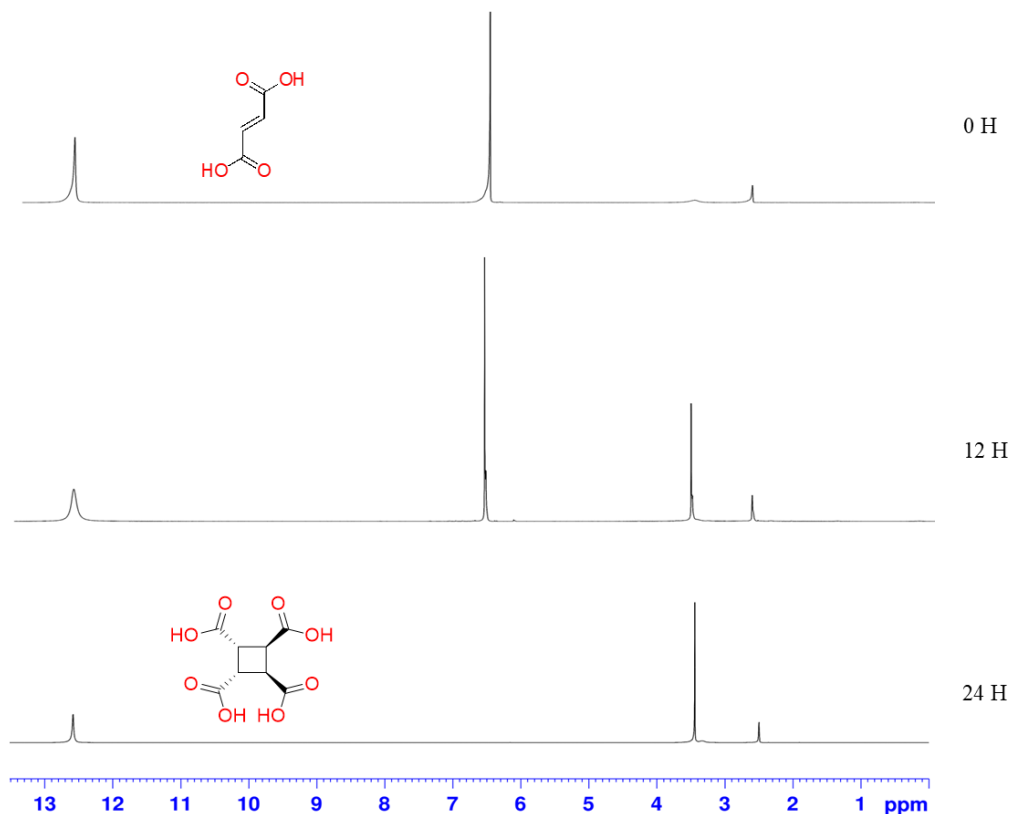


**Figure 5:** The <sup>1</sup>H NMR spectra (DMSO-d<sub>6</sub>) as the reaction proceeds at times, 0, 12 and 24 hours, respectively. The fumaric acid characteristic olefin peak at 6.68 ppm completely disappears while the characteristic methine peak of the cyclobutane ring of the CBTA-1 at 3.44 ppm emerges.

### 1.2.3. Initial thermal studies on the stability of CBDAN-1 and CBTA-1

Though CBDAN-1 and CBTA-1 were first synthesized long time ago, there have been limited studies on their thermal properties. These thermal property studies provide data which give insight into the applicability of these intermediates in the synthesis of polymeric materials. TGA showed that CBTA-1 had its T<sub>5</sub>, T<sub>10</sub> and T<sub>d</sub> at 259 °C, 306 °C and 330 °C, respectively. CBTA-1 starts rapidly losing weight at 242 °C and at 330 °C, 50 % of its weight was lost (Figure 6). On the other hand, CBDAN-1 had its T<sub>5</sub>, T<sub>10</sub> and T<sub>d</sub> at 315 °C, 342 °C and 368 °C, respectively. CBDAN-1 starts rapidly losing

weight at 290 °C and at 368 °C, 50 % of its weight was lost. This shows that CBDAN-1 and CBTA-1 are thermally stable, and the DSC data confirms the results (Figure 7). This comes as no surprise since the cyclobutane ring has previously been shown to possess good thermal, physical and chemical properties.<sup>38-42</sup> This explains why CBTA-1 has been used in the synthesis of MOFs and CBDAN-1 in the synthesis of polyimides.<sup>43-45</sup> In both applications, the precursors must be thermally stable. This initial thermal and physical evaluation shows that the cyclobutane ring in these monomers has stability comparable to other existing CBDA monomers.<sup>41, 46</sup> It also shows that CBDAN-1 is thermally stable enough and could therefore serve as a precursor in material synthesis.<sup>43, 47</sup>



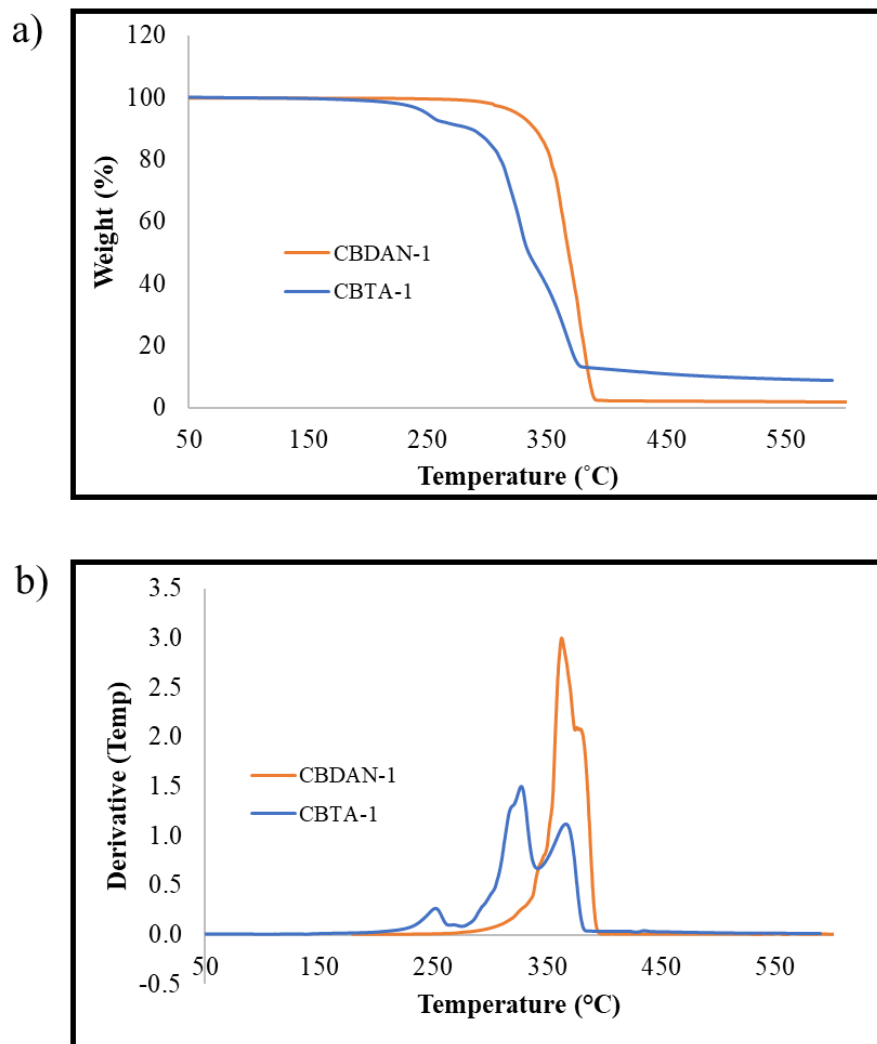


**Figure 6:** TGA and DTG curves of CBDAN-1 and CBTA-1 **a)** TGA curves of CBDAN-1 and CBTA-1 recorded from 50 °C to 600 °C with a heating rate of 20 °C·min<sup>-1</sup> under N<sub>2</sub> atmosphere, **b)** DTG curves of CBDAN-1 and CBTA-1 recorded from 50 °C to 600 °C with a heating rate of 20 °C·min<sup>-1</sup> under N<sub>2</sub> atmosphere

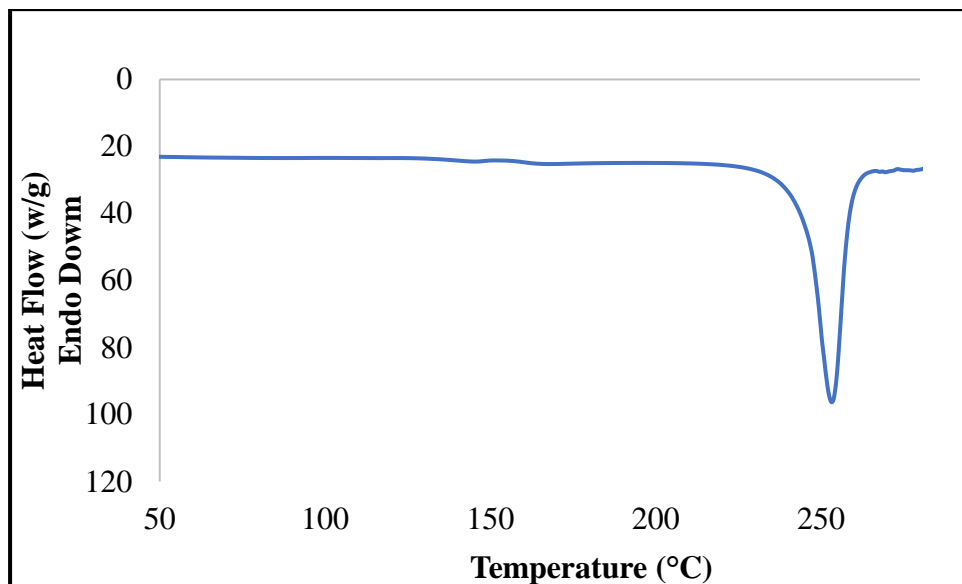


**Figure 7:** The first heating DSC curve of CBTA-1 recorded from 50 °C to 280 °C with a heating rate of 10 °C·min<sup>-1</sup> under N<sub>2</sub>.

### 1.3. Photoreaction of Maleic Anhydride Derivatives

#### 1.3.1. Synthesis of CBDAN-3, CBDAN-4, CBTA-3, and CBTA-4

CBDAN-3 and CBDAN-4 were synthesized from citraconic anhydride using low energy black light. Citraconic anhydride can be obtained from the distillation of fermentation derived itaconic acid. The photodimerization of citraconic anhydride occurred in solution phase and no visible crystals or precipitate was formed. However, after 72 hours, when the solvent was evaporated using a rotavapor, CBDAN-3 and CBDAN-4 separated out as a mixture with a greater than 98% yield for the combined product. <sup>1</sup>H NMR shows that the two products are formed with a 1:1 ratio. No other side products were observed for this reaction. It is possible that there are two ways in which CiAn dimerization can be achieved, giving rise to the two products vis-à-vis head-to-tail and head-to-head products. However, after the reaction is complete, if the

vial is set opened for solvent to evaporate gradually, one isomer crystalizes and the other remains as an oil.

<sup>1</sup>H NMR showed that the crystal is a single product, CBDAN-4, while the oil contains two products, CBDAN-3, and CBDAN-4. Saturation of the ethyl acetate solution with MAN does not increase the yield under this setup, probably because more photons are needed to drive the reaction, which could not be provided by the four bulbs used. Synthesis of CBTA-3 and CBTA-4 was conducted by hydrolyzing CBDAN-3 and CBDAN-4 in a like manner like CBDAN-1. Hydrolysis of the mixture of CBDAN-3 and CBDAN-4 to CBTA-3 and CBTA-4 completed within 2 hours when the mixture was heated to reflux in a solution of water/ethyl acetate (3:1) to give a mixture of CBTA-3 and CBTA-4.

### **1.3.2. Synthesis of CBDAN-5**

CBDAN-5 was readily synthesized from 2,3-dimethylmaleic anhydride using low energy black light. 2,3-Dimethylmaleic anhydride can be isolated from the roots of the plant species *Colocasia esculenta*.<sup>48</sup> CBDAN-5 crystals started precipitating from solution in about 3 hours and reached a 95 % reaction yield in about 4 days. After 4 days, the solvent was evaporated and the residue dried. Analysis of the residue using <sup>1</sup>H NMR showed that the only compound found in the residue is unreacted 2,3-dimethylmaleic anhydride. This showed that no side products were produced in this reaction. This analysis also showed that residual water in the solvent did not hydrolyze 2,3-dimethylmaleic anhydride to 2,3-dimethylmaleic acid as was the case in the synthesis of CBDAN-1. This is probably because the two methyl substituents make it

difficult for the ring to open. Also, with only one product formed, it indicates there is only one possible way for this molecule to react in the solution. This is in contrast with the photodimerization of citraconic anhydride whereby an almost equal amount of two isomers is formed. This result is, however, consistent with the photodimerization of MAn, which forms only one product in solution.

Conclusion can also be drawn that a substitution of the proton with a methyl group in the cyclobutane ring makes it difficult for the molecule to be hydrolyzed, presumably due to the steric hinderance or electron donation from the methyl groups. This might explain why no hydrolyzed products are found in the case of citraconic anhydride photodimerization. Saturation of the ethyl acetate solution with 2,3-dimethylmaleic anhydride does not increase the yield under these experimental conditions probably because more photons are needed to drive the reaction, which could not be provided by the four bulbs used.

### **1.3.3. Thermal Studies on CBDANs**

Like CBDAN-1, the carboxylic dianhydrides showed good thermal stabilities establishing the potential of these precursors to be used as monomers for materials synthesis. The  $T_5$ ,  $T_{10}$  and  $T_d$  of the various CBDANs have been summarized in Table 2. For comparison, the data for CBDAN-1 has been included in the table. None of the CBDANs lost weight until about 200 °C (Figure 8). This initial study shows that the cyclobutane ring in the CBDANs is stable and they could therefore serve as a precursor in material synthesis.<sup>38, 39</sup> Since the CBDANs have already been used in the synthesis of polyimides, they can however be converted into their CBTAs and exploited in the

synthesis of MOMs, or they can be hydrolyzed with various nucleophiles to make diacids, which can be used in material synthesis.<sup>40, 46</sup> It was interesting to know that CBDAN-1 is the most thermally stable. Attempts to hydrolyze CBDAN-5 were unsuccessful.

**Table 3:** Thermogravimetric analysis data for CBDAN-1, CBDAN-3, and CBDAN-5

**Thermogravimetric analysis (TGA)**

<b>Sample</b>	<b>T<sub>5</sub></b>	<b>T<sub>10</sub></b>	<b>T<sub>d</sub></b>
CBDAN-1	316	340	365
CBDAN-3	240	261	410
CBDAN-5	281	300	345

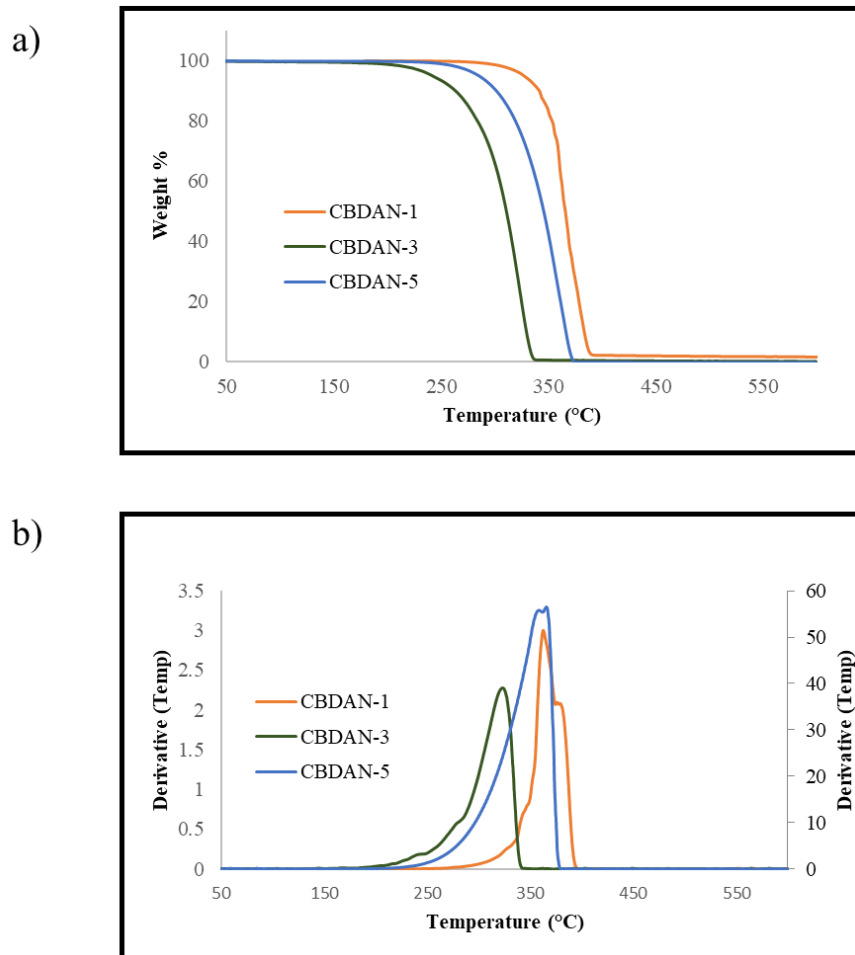


**Figure 8:** TGA and DTG curves of CBDAN-1, CBDAN-3 and CBDAN-5 **a)** TGA curves of CBDAN-1, CBDAN-3 and CBDAN-5 recorded from 50 °C to 600 °C with a heating rate of 20 °C·min<sup>-1</sup> under N<sub>2</sub> atmosphere, **b)** DTG curves of CBDAN-1, CBDAN-3 and CBDAN-5 recorded from 50 °C to 600 °C with a heating rate of 20 °C·min<sup>-1</sup> under N<sub>2</sub> atmosphere

#### **1.4. Conclusion**

This work showed simple, efficient, and ecofriendly methods to synthesize CBDAN-1, a molecule with potential to become a platform for the synthesis of several cyclobutane-containing diacids (CBDAs). CBDAN-1 was synthesized through direct dimerization of maleic anhydride or dehydration of CBTA-1. CBTA-1 was synthesized by direct dimerization of fumaric and maleic acids in the solid state using germicidal lamps. CBTA-1 was converted to CBDAN-1 by heating for 24 hours at 230 °C or through acetic anhydride assisted dehydration. Initial thermal studies on CBDAN-1 and CBTA-1 showed that these molecules were thermally stable to be incorporated into polymers or MOMs. Based on these promising results, the photoreaction of derivatives of maleic acid were studied. Citraconic anhydride and 1,2-dimethyl maleic anhydride also dimerized under irradiation with blacklights. However, photodimerization of citraconic acid resulted in the formation of two isomers. The derivatives also showed the desired thermal stability. These dianhydrides could be exploited further to synthesize MOMs, polyimides or undergo ring opening reactions with various amine, alcohol, or Grignard bases via nucleophilic reactions to make diacids.

## **1.5. Experimental Section**

### **1.5.1. Materials and Procedures**

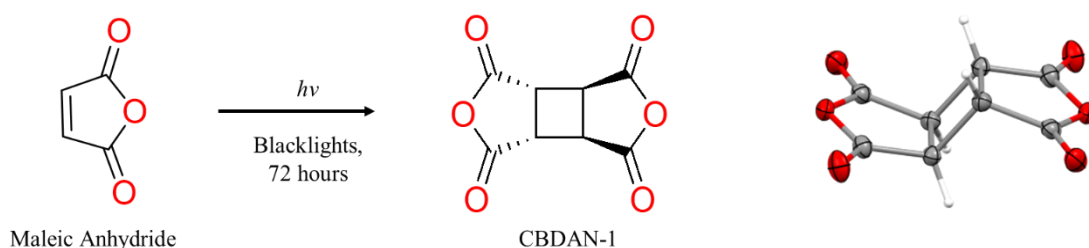
All chemicals were purchased from Alfa Aesar, Sigma-Aldrich, or Acros, and used without further purification. Blacklight used in the photoreaction was Fiet Electric 7-watt LED bulb or 15W Eiko EK15526 F15T8/BL. Germicidal lamps used in the photoreaction was Germicidal lamp T5 G5 39/ 41W ozone free Sankyo Denki Co., Ltd. The solution phase nuclear magnetic resonance spectra (NMR) were recorded with Bruker AVANCE ( $^1\text{H}$ : 500 MHz,  $^{13}\text{C}$ : 125 MHz). Proton and carbon chemical shifts were reported in ppm downfield from tetramethylsilane (TMS). Spectra were recorded in DMSO- $d_6$  unless otherwise stated. Single crystal X-ray data were collected on a Bruker Kappa Apex II Duo X-Ray Diffractometer with Cu  $K\alpha$  ( $\lambda = 1.54178 \text{ \AA}$ ). Infrared spectroscopy (IR) was recorded on Thermo Scientific Nicolet iS5 FT-IR spectrometer. Differential scanning calorimetry (DSC) was recorded with a Perkin Elmer Jade DSC with a ramping rate of  $20 \text{ }^\circ\text{C} \cdot \text{min}^{-1}$  under nitrogen protection. Heat flow was recorded from both the first heating and cooling curve. Thermogravimetric analysis (TGA) was carried out with a Hi-Res TGA Q500 from TA Instruments using alumina pans at a heating rate of  $20 \text{ }^\circ\text{C} \cdot \text{min}^{-1}$  under nitrogen with a sample weight of about 10.0 mg. UV-Vis spectra were recorded on a Beckman DU400 UV-Vis spectrometer.

### **1.5.2. Synthesis of Cyclobutane-1,2,3,4-tetracarboxylic Dianhydride (CBDAN-1) from Maleic Anhydride**

Cyclobutane-1,2,3,4-tetracarboxylic dianhydride was prepared by dissolving 1.02 g (10.0 mmol) of maleic anhydride (MAN) in 20.0 mL of ethyl acetate (EtOAc) in a 20

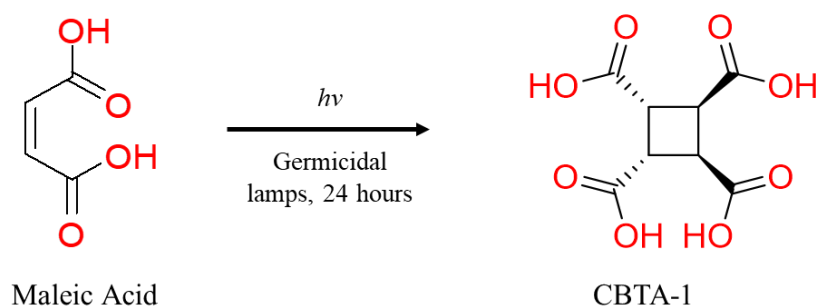


mL cornil vial and irradiated between four black lights, two on each side, for 72 hours. Crystals of the product precipitated to the bottom of the vial as the reaction proceeded. After 72 hours, the crystals were filtered out, washed with ethyl acetate, and dried at room temperature for residual solvent to evaporate. About 0.71 g of CBDAN-1 (71 %) was obtained. The product was analyzed using  $^1\text{H}$  and  $^{13}\text{C}$  NMR, FT-IR spectroscopy, and X-ray crystallography. The melting point was shown to be  $398^\circ\text{C}$ .  $^1\text{H}$  NMR  $\delta$  (ppm): 4.11 (s, 4H,  $\underline{\text{C}}\text{H}$ -cyclobutane);  $^{13}\text{C}$  NMR (Acetone- $\text{d}_6$ , 125 MHz)  $\delta$  (ppm): 171 ( $\underline{\text{C}}=\text{O}$ ), 41 ( $\underline{\text{C}}\text{H}$ -cyclobutane). FT-IR (solid)  $\bar{\nu}_{\text{max}}$  ( $\text{cm}^{-1}$ ): 3011 ( $\text{C}\text{aliph}\text{-H}$ ), 1845/1776/1715 (acid anhydride  $\text{C}=\text{O}$ ).



**Scheme 1:** Dimerization of maleic anhydride

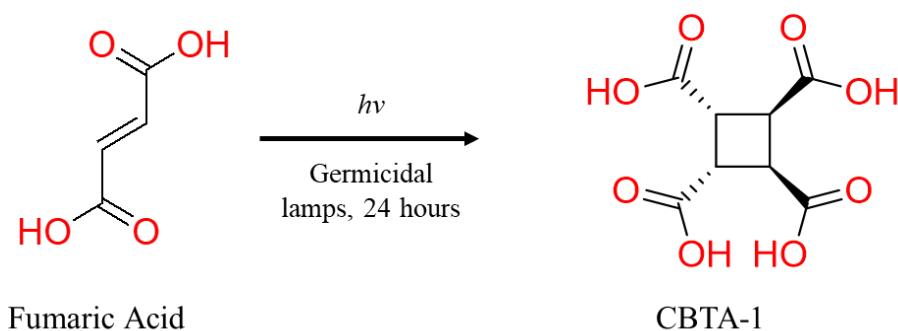
### 1.5.3. Synthesis of Cyclobutane-1,2,3,4-tetracarboxylic acid (CBTA-1) from Maleic Acid (MA)



**Scheme 2:** Dimerization of maleic acid

Ground MA powder (102 mg, 0.86 mmol) was placed on a quartz glass slide and evenly distributed to form a thin layer. The sample on the quartz slide was irradiated with two germicidal lamps (UV-C) placed at about 2.0 mm from the sample. The reaction proceeded in the solid state and the powder was mixed every two hours to ensure that all powder is exposed to the light source. The reaction was completed after 24 hours with a greater than 99 % conversion rate. The product was analyzed using  $^1\text{H}$  and  $^{13}\text{C}$  NMR, FT-IR spectroscopy, and crystallography. To scale up the reaction, 1.01 g (8.60 mmol) of ground MA powder was placed on a 12.0 cm x 12.0 cm quartz glass slide and evenly distributed to form a thin layer. The quartz slide was placed between four germicidal lamps (UV-C) with the lower back part touching one lamp, the upper one being at about 2.0 mm from the second lamp. The MA powder was irradiated with stirring every five hours for 3 days. After 3 days, the MA was completely converted to CBTA-1. The melting point was shown to be 239.4 – 241.6 °C.  $^1\text{H}$  NMR  $\delta$  (ppm): 12.59 (s, 4H, COOH) 3.44 (s, 4H, CH-cyclobutane).  $^{13}\text{C}$  NMR  $\delta$  (ppm): 172 (COOH), 41 (CH-cyclobutane). FT-IR (solid)  $\bar{\nu}_{\text{max}}$  ( $\text{cm}^{-1}$ ): 3330/2840 (carboxylic acid OH), 2974 (Caliph-H), 1708/1664 (carboxylic acid C=O).

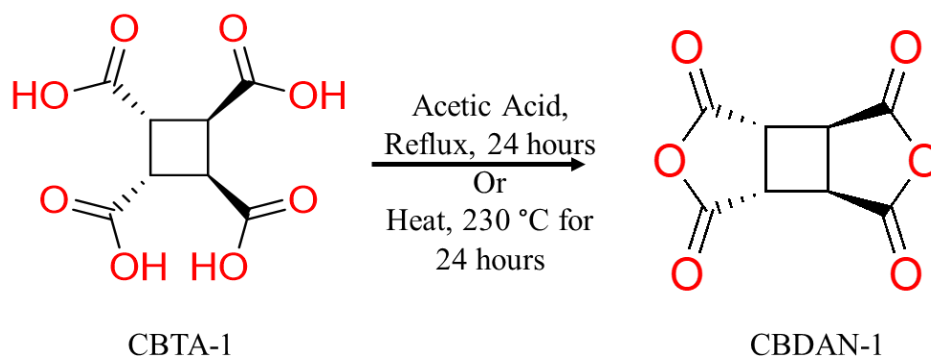
#### 1.5.4. Synthesis of Cyclobutane-1,2,3,4-tetracarboxylic acid (CBTA-1) from Fumaric Acid



**Scheme 3:** Dimerization of fumaric acid

Fumaric acid was heated in a 20 mL scintillation vial to about 200 °C, which caused recrystallization via sublimation. Sublimed crystals of FA (1.01 g, 8.60 mmol) were measured and placed on a 12.0 cm x 12.0 cm quartz glass slide and evenly distributed to form a thin layer. The quartz slide was placed between four germicidal lamps (UV-C) with the lower back part touching one lamp, the upper one being at about 2.0 mm from the second lamp. The reaction proceeded in the solid state and the crystals were mixed every five hours to ensure complete exposure to the light source. The reaction was completed after 24 hours with a greater than 99 % conversion rate. The product was characterized using  $^1\text{H}$  and  $^{13}\text{C}$  NMR, FT-IR spectroscopy, and X-ray crystallography. The melting point was shown to be 239.4 – 241.6 °C.  $^1\text{H}$  NMR  $\delta$  (ppm): 12.59 (s, 4H,  $\text{COOH}$ ) 3.44 (s, 4H,  $\text{CH}$ -cyclobutane).  $^{13}\text{C}$  NMR  $\delta$  (ppm): 172 ( $\text{COOH}$ ), 41 ( $\text{CH}$ -cyclobutane). FT-IR (solid)  $\bar{\nu}_{\text{max}}$  ( $\text{cm}^{-1}$ ): 3330/2840 (carboxylic acid OH), 2974 (C-H), 1708/1664 (carboxylic acid C=O).

**1.5.5. Synthesis of Cyclobutane-1,2,3,4-tetracarboxylic Dianhydride from (CBTA-1)**



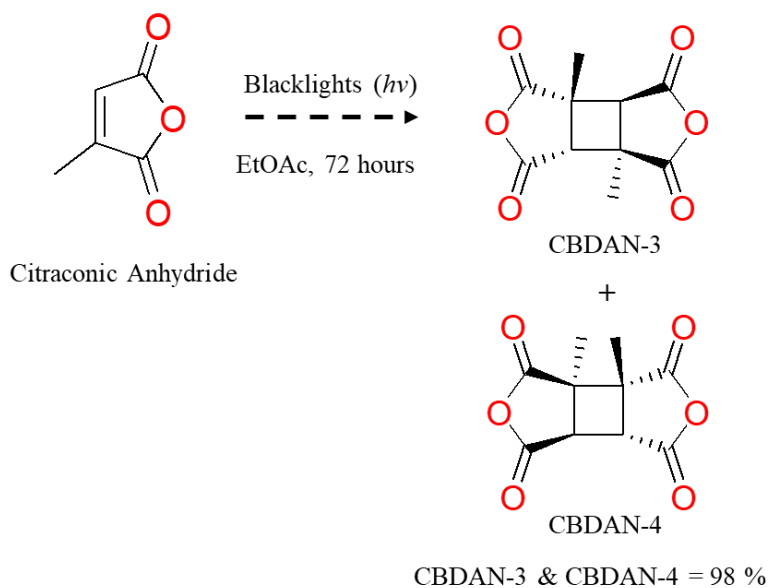
**Scheme 4:** Dehydration of CBTA-1 to CBDAN-1

CBTA-1 (1.02g, 4.30 mmol) powder was dissolved in 30.0 mL of acetic anhydride. The mixture was refluxed for 12 hours. After 12 hours, the acetic anhydride was evaporated out under vacuum in a rotavapor. The resulting oil left in the round bottom flask was washed by adding 40.0 mL of a 1:1 mixture of hexane and anhydrous diethyl ether to the flask and stirred overnight. The following day, a brown precipitate was formed at the bottom of the flask. This precipitate was washed three times, (4 hours each) with a 1:1 mixture of hexane and anhydrous diethyl ether resulting in a white precipitate. The precipitate was ascertained to be CBDAN-1 and was essentially pure, requiring no further purification. The product was characterized using  $^1\text{H}$  and  $^{13}\text{C}$  NMR, FT-IR spectroscopy, and X-ray crystallography. The melting point was shown to be 398°C.  $^1\text{H}$  NMR  $\delta$  (ppm): 4.11 (s, 4H,  $\underline{\text{C}}\underline{\text{H}}$ -cyclobutane).  $^{13}\text{C}$  NMR (Acetone- $d_6$ , 125 MHz)  $\delta$  (ppm): 171 ( $\underline{\text{C}}=\text{O}$ ), 41 ( $\underline{\text{C}}\underline{\text{H}}$ -cyclobutane). FT-IR (solid)  $\bar{\nu}_{\text{max}}$  ( $\text{cm}^{-1}$ ): 3011 ( $\underline{\text{C}}\underline{\text{H}}$ -H), 1845/1776/1715 (acid anhydride  $\text{C}=\text{O}$ ).

### 1.5.6. Synthesis of 1,2 and 1,3-dimethyl-cyclobutane-1,2,3,4-tetracarboxylic dianhydride (CBDAN-3, and CBDAN-4) from citraconic anhydride CiAn

CBDAN-3 was prepared by dissolving 1.01 g (8.90 mmol) of CiAn in 20.0 mL of ethyl acetate in a 20 mL cornil vial and irradiated between four blacklights, two on each side, for 72 hours. After 72 hours, ethyl acetate was slowly evaporated in the fume hood and CBDAN-3 crystallized out. The crystals were washed with chloroform and residual solvent was evaporated. About 1.00 g of CBDAN-3 (> 98 %) was obtained. The product was characterized using  $^1\text{H}$  and  $^{13}\text{C}$  NMR, FT-IR spectroscopy, and X-ray crystallography. The melting point of CBDAN-4 was measured to be 307 °C.

**CBDAN-4:**  $^1\text{H}$  NMR  $\delta$  (ppm): 3.89 (s, 4H,  $\text{CH}$ -cyclobutane), 1.37 (s, 6H,  $\text{CH}_3$ ).  $^{13}\text{C}$  NMR: 168 ( $\text{C}=\text{O}$ ), 44 ( $\text{CH}$ -cyclobutane), 16 ( $\text{CH}_3$ ). FT-IR (solid)  $\bar{\nu}_{\text{max}}$  ( $\text{cm}^{-1}$ ): 3013 ( $\text{C}-\text{H}$ ), 1834/1774 (acid anhydride  $\text{C}=\text{O}$ )

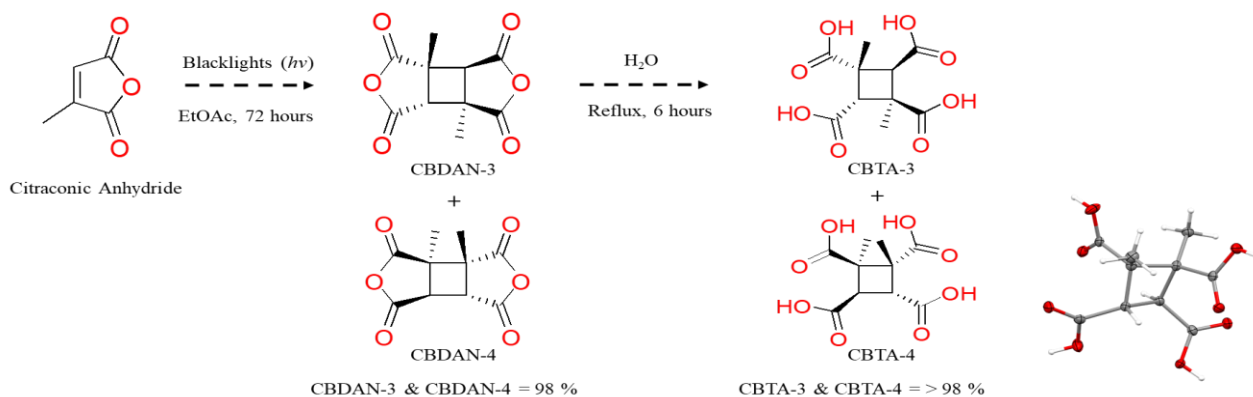


**Scheme 5:** Dimerization of citraconic anhydride

### 1.5.7. Synthesis of 1,2 and 1,3-dimethyl-cyclobutane-1,2,3,4-tetracarboxylic acid (CBTA-3 and CBTA-4) from CBDAN-3 and CBDAN-4

CBDAN-3 (1.02 g, 3.80 mmol) was added to a 50.0 mL mixture of water and ethyl acetate (3:1) in a round bottom flask. The mixture was stirred under reflux for 6 hours. CBDAN-2 dissolved in the water and was converted to CBTA-2. After 6 hours, the solution was filtered, and the water/ ethyl acetate was evaporated using a rotavapor leaving the white product which is essentially pure. About 1.09 g of CBTA-4 (> 98 %) was obtained. The product was characterized using  $^1\text{H}$  and  $^{13}\text{C}$  NMR, FT-IR spectroscopy, and X-ray crystallography. The melting point was measured to be 249.8 – 251.2 °C.

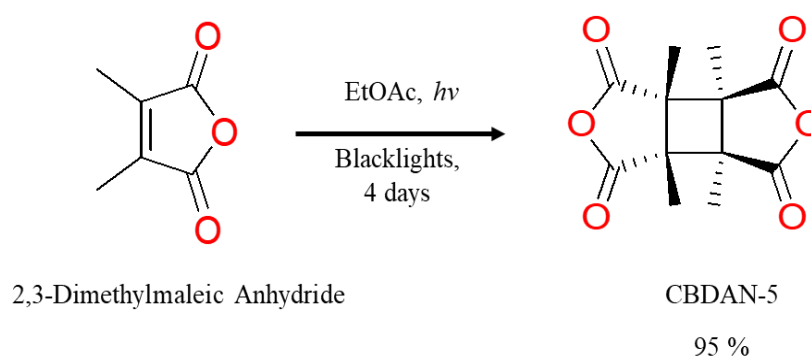
**CBTA-4:**  $^1\text{H}$  NMR  $\delta$  (ppm): 12.50 (s, 4H,  $\text{COOH}$ ), 3.74 (s, 4H,  $\text{CH}$ -cyclobutane), 1.37 (s, 6H,  $2\times\text{CH}_3$ ).  $^{13}\text{C}$  NMR  $\delta$  (ppm): 168 ( $\text{COOH}$ ), 44 ( $\text{CH}$ -cyclobutane), 16 ( $\text{CH}_3$ ). FTIR (solid)  $\bar{\nu}_{\text{max}}$  ( $\text{cm}^{-1}$ ): 3330/2840 (carboxylic acid OH), 3010 (C- $\text{H}$ ), 1840/1772 (acid anhydride  $\text{C}=\text{O}$ ).



**Scheme 6:** Hydrolysis of CBDAN-3 and CBDAN-4

**1.5.8. Synthesis of 1,2,3,4-tetramethyl-cyclobutane-1,2,3,4-tetracarboxylic anhydride (CBDAN-5) from 2,3-dimethylmaleic anhydride (DMMAAn)**

CBDAN-5 was prepared by dissolving 2.00 g (7.90 mmol) of DMMAAn in 20.0 mL of ethyl acetate in a 20 mL cornil vial and irradiated between four black lights for 4 days. The bulbs were placed two on each side of the cornil flask. Crystals of the product precipitated to the bottom of the vial as the reaction proceeded. After 4 days hours, the crystals were filtered out, washed with ethyl acetate, and dried at room temperature for residual solvent to evaporate. About 1.91 g of CBDAN-5 (95%) was obtained. The product was characterized using  $^1\text{H}$  and  $^{13}\text{C}$  NMR, FT-IR spectroscopy, and X-ray crystallography. The melting point was shown to be 388 °C.  $^1\text{H}$  NMR  $\delta$  (ppm): 1.26 (s, 12H, 4x $\text{CH}_3$ ).  $^{13}\text{C}$  NMR  $\delta$  (ppm): 171 ( $\text{C}=\text{O}$ ), 50 ( $\text{CH}$ -cyclobutane), 12 ( $\text{CH}_3$ ). FTIR (solid)  $\bar{\nu}_{\text{max}}$  ( $\text{cm}^{-1}$ ): 2990 (Caliph-H), 1843/1783 (acid anhydride  $\text{C}=\text{O}$ ).



**Scheme 7:** Dimerization of 2,3-dimethylmaleic anhydride

## CHAPTER TWO

### **Cyclobutane-1,2,3,4-carboxylic Dianhydride: A Platform for the Synthesis of Biomass Derived Dicarboxylic Acids for Polymeric Applications**

#### **2.0. Introduction**

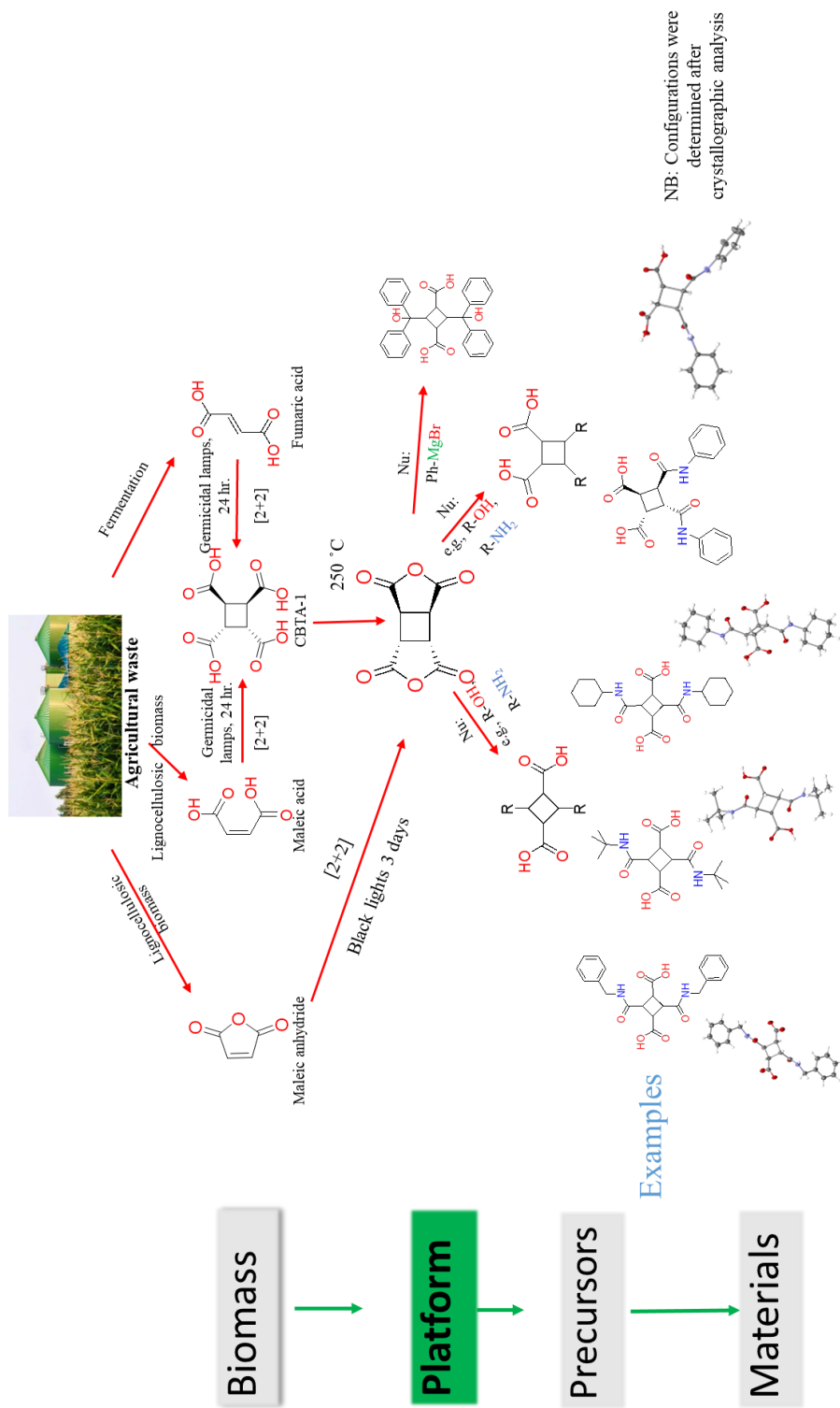
Biobased materials are increasingly becoming widely available due to their advantages of being sustainable and renewable.<sup>49, 50, 50</sup> Fossil fuels are gradually being alienated as a source to obtain precursors for material synthesis. This is because of the environmental concerns associated with their exploration and the huge fluctuations in the price to obtain them.<sup>51, 52</sup> Petroleum-based precursors to materials are cheap, versatile, and already overwhelm the materials industry.<sup>53, 54</sup> For there to be competition, materials synthesized from renewable precursors must provide advantageous attributes. Materials synthesized from building blocks containing cyclobutane have already been reported to be stable, with good glass transition temperatures and exhibiting semi-rigidity.<sup>38-42</sup>

This study was designed to evaluate CBDAN-1 as a platform in which a library of cyclobutane-containing dicarboxylic acid precursor with several different backbones could be made. These precursors with varying backbones could offer great material properties to compete with their counterparts in the non-renewables. Cyclobutane-1,2,3,4-tetracarboxylic dianhydride CBDAN-1, is a dianhydride that can be synthesized from the dimerization of maleic anhydride or from the dehydration of cyclobutane-1,2,3,4-tetracarboxylic acid (CBTA-1).<sup>55</sup> CBDAN-1 can be readily derivatized via reactions with nucleophiles. Upon nucleophilic reactions with various nucleophiles containing the alcohol, amine functional groups or Grignard reagent, several



dicarboxylic acids could be synthesized from CBDAN-1. For example, a completely biobased cyclobutane diacid can be synthesized from furfural (one of the top value-added chemicals per DOE)<sup>56</sup> derived molecules.<sup>20, 28</sup> This diacid can be synthesized from the reaction between CBDAN-1 and furfuryl amine, the latter is also obtained from furfural.<sup>51, 57</sup>

Maleic anhydride, fumaric and maleic acid are biobased molecules that are the precursors to CBDAN-1 and can be obtained directly from lignocellulosic biomass via furfural.<sup>16, 17, 20, 24, 27, 29, 51, 57-59</sup> Fumaric acid offers another advantage in that it can be obtained through fermentation.<sup>30, 60</sup> These molecules can be used in the synthesis of CBDAN-1. The goal of this study is to demonstrate that CBDAN-1 can be used to synthesize a library of cyclobutane containing diacids. CBDAN-1 will be reacted with various amine, alcohol, or Grignard reagent to generate a library of cyclobutane containing dicarboxylic acids through nucleophilic reactions (Scheme 1). The synthesized diacids will then be subjected to thermal studies to evaluate their suitability for applications in polymeric synthesis.



**Scheme 8:** Synthesis of CBDAXs from Biomass precursors via CBDAN-1

## 2.1. Results and Discussion

### 2.1.1. Synthesis of CBDAs from CBDAN-1

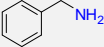
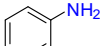
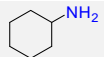
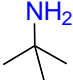
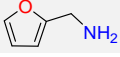
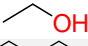
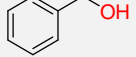
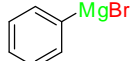
The synthesis of CBDAs from CBDAN-1 followed a general pattern. Briefly, nucleophiles readily reacted with the dianhydride yielding the diacid with amines being more reactive than alcohols. The order of reactivity of amines was  $1^\circ > 2^\circ > 3^\circ$ . The  $1^\circ$  amines reacted upon addition to the mixture and the reaction was completed within minutes. For alcohols, the reaction occurred only with primary aliphatic ones when reacted in large excess. No reactivity was observed with any other class of alcohols. Cyclohexanol, *tert*-butanol and phenol had no reactivity. The product of reaction of CBDAN-1 with amines yielded both the 1,2- and 1,3- substituted product, the 1,3-product formed in a larger proportion in all cases.

It was observed that the reaction is controlled by the solvent type such that solvents where CBDAN-1 had lower solubility favored the 1,3-product. As such it was thought that if the reaction process can be slowed, one of the products can be isolated. A solvent in which CBDAN-1 had low solubility was selected for the reactions. The goal was to reduce solubility and slow the reaction so that as soon as CBDAN-1 dissolves in the solvent, the nucleophile reacts instantaneously and forms just the more favored 1,3-product. There would be little time for the less favored 1,2-product to be formed. The starting materials were added then the solvent added, and the reaction was stirred for reaction to proceed. The 1,3-product was more favored, while the 1,2-product was not observed in the precipitate formed. The reaction with isopropyl amine was difficult to optimize to obtain a single product. However, when the temperature of the reaction

mixture was dropped to zero, using an ice bath, more of the 1,3-product was formed. The reaction was then washed with methylene chloride to wash away all the 1,2-product.

It is worth noting that the 1,2-product has a higher solubility in organic solvents than the 1,3-product. With piperidine, both 1,2- and 1,3-products were obtained in equal proportion. Even at temperatures about 0 °C, both products were still formed in almost equal proportions. When an ice bath made of dry ice and acetone was used to achieve temperatures of - 80 °C, more of the 1,2-product was obtained. Still there was the 1,3-product formed. Piperidine being a cyclic 2° amine, its reactivity was somewhat different from that of isobutyl amine. The product with piperidine was soluble in most organic solvents. Several attempts to recrystallize the reaction product still could not achieve the separation of both products. Reaction of CBDAN-1 with benzylamine and furfuryl amine were similar albeit the ratio of 1,2- and 1,3-product formed with the latter was higher. However, running the reaction in an ice bath yielded mostly the 1,3-product. The trace amounts of 1,2-product were removed when the isolated product was washed with methanol. The CBDA were successfully isolated, and the results are summarized below (Table 4).

**Table 4:** Summary of CBDAx Synthesis

Monomer	Substrate Structure	Molecular Formula	Molar Mass (g mol <sup>-1</sup> )	Yield (%)
CBDAx-1		C <sub>22</sub> H <sub>22</sub> N <sub>2</sub> O <sub>6</sub>	410.42	91
CBDAx-2		C <sub>20</sub> H <sub>18</sub> N <sub>2</sub> O <sub>6</sub>	382.37	81.5
CBDAx-3		C <sub>20</sub> H <sub>30</sub> N <sub>2</sub> O <sub>6</sub>	394.46	89.5
CBDAx-4		C <sub>16</sub> H <sub>26</sub> N <sub>2</sub> O <sub>6</sub>	342.18	86.7
CBDAx-5		C <sub>18</sub> H <sub>18</sub> N <sub>2</sub> O <sub>8</sub>	390.34	86.0
CBDAx-6		C <sub>12</sub> H <sub>16</sub> O <sub>8</sub>	288.25	82.0
CBDAx-7		C <sub>22</sub> H <sub>20</sub> O <sub>8</sub>	412.39	81.0
CBDAx-8		C <sub>26</sub> H <sub>28</sub> O <sub>6</sub>	508.56	12.2

### 2.1.2. Description of the Structures of CBDAx

The spatial orientation of molecules is very crucial to determine their suitability in polymeric applications.<sup>61</sup> Syntheses of longer chain heavy molecular weight polymers often occurs when the diacids are farther apart.<sup>62, 63</sup> Also, if cross-linking is the desired outcome, orientation and short distances are important. The crystal structures of CBDAx-1 through CBDAx-4 were obtained. From these, inferences can be made to the other diacids from their NMR spectra.

#### 2.1.2.1. CBDAx-1 Structure

Single crystals of CBDAx-1 were unable to be grown directly probably because the hydrogen bonds formed between individual molecules would not let it. However, an *n*-butylamine salt of CBDAx-1 was able to form single crystals, this is probably because of disruption of the hydrogen bonds formed between CBDAx-1 molecules by the butylamine. The short-chain flexible cation, butylammonium, does not destroy the

structure of CBDA-1, but can be used to fill spaces in the crystal lattice reducing the chance of disorder. CBDAx-1 crystals were monoclinic with a P21/c space group. The two cyclobutane rings in each asymmetric unit are planar (Figure 9), indicating less flexibility of the four-membered ring structure.<sup>64</sup>

The single crystal of the CBDAx-1 salt showed that the four carbon atoms on the cyclobutane ring adopted a coplanar conformation and had carbon-carbon bond distances of around 1.55 Å (Figure 9). The two carboxylic groups on the opposite sides of the cyclobutane ring have a 180° angle between them. The distance between the two carboxylic groups is 4.776 Å. This distance is similar to the distance between two carboxylic groups on furan-based building block 2,5-furandicarboxylic acid.<sup>65</sup> The spatial orientation and distance between the two carboxylic acid groups makes it suitable for polymer synthesis.<sup>63</sup> The cyclobutane ring has been shown to have two exchangeable conformations, planar and puckered, with about 23° difference between them.<sup>66, 67</sup> The limited conformational flexibility of the cyclobutane ring is expected to give CBDAx-1 a unique semi-rigid character.<sup>67, 68</sup>

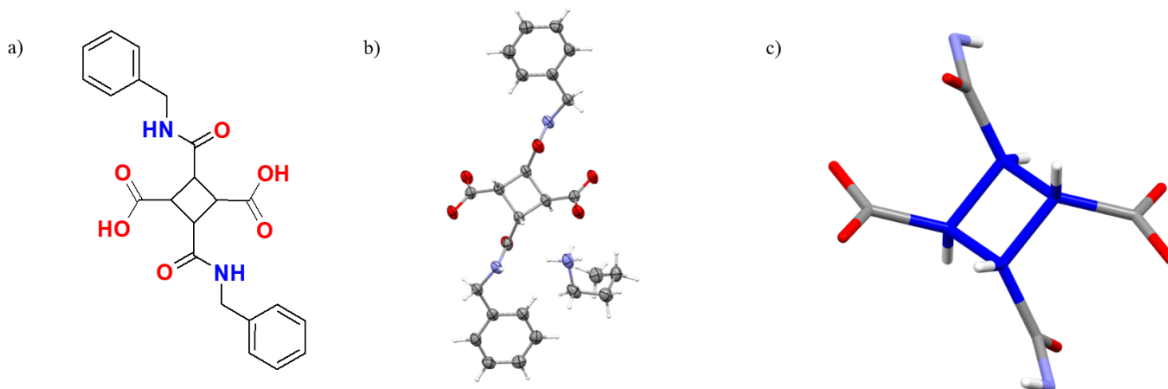


**Figure 9:** Chemical and x-ray single-crystal structure of CBDAx-1: (a) chemical structure (b) One molecule shown as Oak Ridge Thermal Ellipsoid Plot (ORTEP) representing 50% electron density; (b) The planar conformation adopted by cyclobutane rings (the two methylene phenyl groups are omitted for clarity).

#### 2.1.2.2. CBDAx-2 1,2-diacid Structure

In the case of CBDAx-2, in addition to the 1,3- diacid, the 1,2-diacid was also isolated and the crystal structure reported. The 1,2-diacid product was isolated by evaporating the solvent that resulted from the reaction pot. This solvent contained a mixture of both the 1,2- and 1,3-diacids. Their difference in solubility in methanol was exploited to isolate the 1,2-diacid. The 1,2-diacid is very soluble in methanol, thus the powder obtained from the filtrate was washed with methanol. Methanol was eventually evaporated giving the pure 1,2-diacid. Single crystals of CBDAx-2 1,2 diacid were grown by slow evaporation in methanol. The crystal showed that methanol fills up spaces in the crystal lattice reducing the chance of disorder. The crystals were triclinic with a P-1 space group. The single crystal of the CBDAx-2 1,2 diacid also showed that the four carbon atoms on the cyclobutane ring adopted a coplanar conformation and have carbon-carbon bond distances of around 1.55 Å (Figure 10). The two carboxylic groups on the opposite sides of the cyclobutane ring have a 180 ° angle between them.

The distance between the two carboxylic groups is 3.75 Å. This distance is shorter than the distance between two carboxylic groups on furan-based building block 2,5-furandicarboxylic acid<sup>65</sup> and longer than that in phthalic acid.<sup>69</sup> This makes CBDAx-2 a promising molecule to explore in polymer synthesis. The limited conformational flexibility of the cyclobutane ring is expected to give CBDAx-2 a unique semi-rigid character.<sup>67 68</sup>

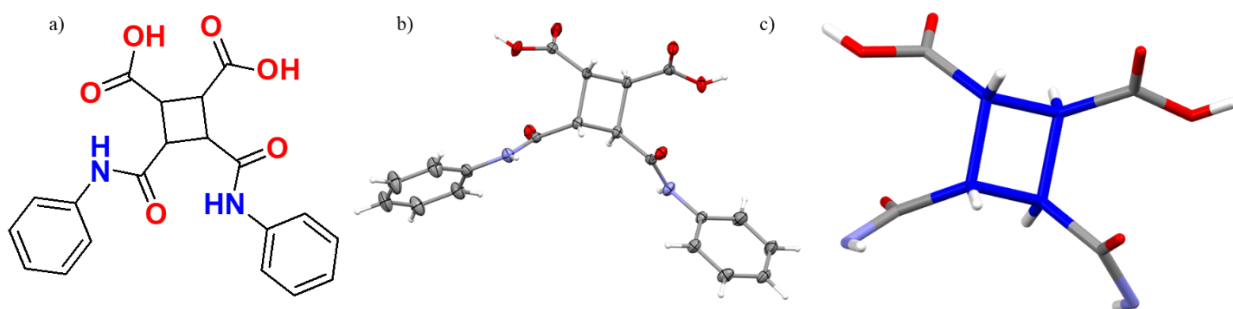


**Figure 10:** Chemical and x-ray single-crystal structure of CBDAx- 2 1,2-diacid: (a) chemical structure (b) One molecule shown as Oak Ridge Thermal Ellipsoid Plot (ORTEP) representing 50% electron density; (b) The planar conformation adopted by cyclobutane rings (the two phenyl groups are omitted for clarity).

### 2.1.2.3. CBDAx-3 Structure

Single crystals of CBDAx-3 were obtained by slow evaporation in methanol. The crystals were monoclinic with a P21/c space group. The crystal showed that methanol fills up spaces in the crystal lattice reducing the chance of disorder. The two cyclobutane rings in each asymmetric unit adopted a planar conformation (Figure 11), indicating less flexibility of the four-membered ring structure. The carbon-carbon bond distances of the cyclobutane ring were around 1.55 Å. The two carboxylic groups on the opposite sides of the cyclobutane ring have a 180° angle between them. The distance



between the two carboxylic groups is 4.74 Å. This distance is like the distance between two carboxylic groups on furan-based building block 2,5-furandicarboxylic acid.<sup>65</sup> The spatial orientation and distance of the two carboxylic acid groups makes it suitable for polymer construction.

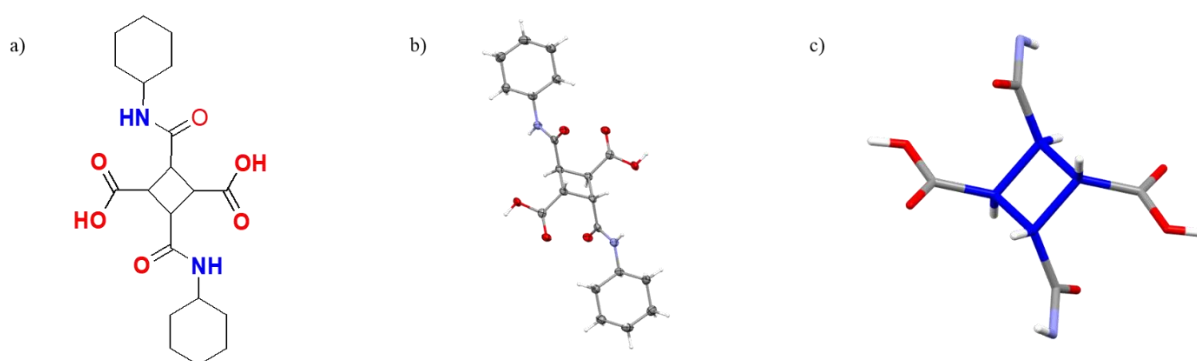


**Figure 11:** Chemical and x-ray single-crystal structure of CBDAx-3: (a) chemical structure (b) One molecule shown as Oak Ridge Thermal Ellipsoid Plot (ORTEP) representing 50% electron density; (b) The planar conformation adopted by cyclobutane rings (the two cyclohexyl groups are omitted for clarity).

#### 2.1.2.4. CBDAx-4 Structure

Single crystals of CBDAx-4 were grown by slow evaporation in methanol. The crystal showed that methanol fills up spaces in the crystal lattice reducing the chance of disorder. The crystals were triclinic with a P-1 space group. The two cyclobutane rings in each asymmetric unit adopted a planar configuration, indicating less flexibility of the four-membered ring structure. The single crystal structure of the CBDAx-4 shows that the four carbon atoms on the cyclobutane ring adopted a coplanar conformation and have carbon-carbon bond distances of around 1.55 Å (Figure 12). The two carboxylic groups on opposite sides of the cyclobutane ring have a 180° angle between them. The distance between the two carboxylic groups is 4.72 Å. This distance is like the distance

between two carboxylic groups on furan-based building block 2,5-furandicarboxylic acid.<sup>65</sup> This makes this molecule a promising feedstock to be explored in polymer synthesis.

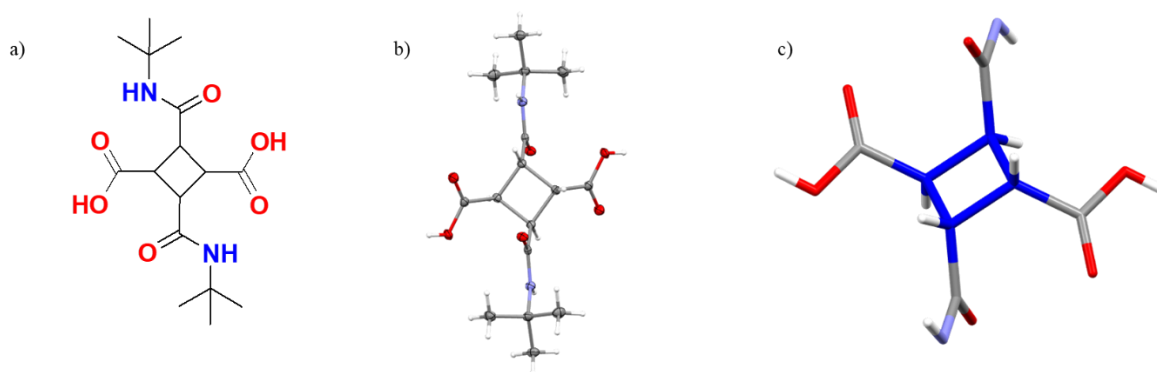


**Figure 12:** Chemical and x-ray single-crystal structure of CBDAx-4: (a) chemical structure (b) One molecule shown as Oak Ridge Thermal Ellipsoid Plot (ORTEP) representing 50% electron density; (b) The planar conformation adopted by cyclobutane rings (the two *tert*-butyl groups are omitted for clarity).

### 2.1.3. Initial thermal studies on the stability of CBDAx

Thermal studies on potential monomers are important because they provide data which give a suitable insight to the applicability of this intermediate in the synthesis of polymeric materials. Polymer syntheses requires stable monomers to be effective, therefore it is imperative that the initial thermal properties of the CBDAx monomers are studied (Figures 13, 14 and 15). Table 5 summarizes the melting points of various CBDAx. Table 6 summaries the  $T_5$ ,  $T_{10}$  and  $T_d$  data for CBDAx-1 through CBDAx-8. This initial thermal evaluation showed that the cyclobutane ring in these monomers has stability similar to other existing CBDA monomers. It also showed that these monomers are thermally stable enough and could therefore serve as precursors in material synthesis.

**Table 5:** Melting point data for CBDAx-1 through CBDAx-8

<b>SN</b>	<b>Compound</b>	<b>Melting point (°C)</b>
<b>1</b>	CBDAx-1	287.1 – 289.2
<b>2</b>	CBDAx-2	> 380 (decomposes)
<b>3</b>	CBDAx-3	248.8 – 252.1
<b>4</b>	CBDAx-4	256.8 – 258.0
<b>5</b>	CBDAx-5	262.8 – 264.0
<b>6</b>	CBDAx-6	n/a
<b>7</b>	CBDAx-7	115.6 – 117.1
<b>8</b>	CBDAx-8	318.5 – 320.2

**Table 6:** Thermogravimetric analysis data for CBDAx-1 through CBDAx-8**Thermogravimetric analysis (TGA)**

<b>Sample</b>	<b>T<sub>5</sub></b>	<b>T<sub>10</sub></b>	<b>T<sub>d</sub></b>
CBDAx-1	262	262	379
CBDAx-2	261	296	438
CBDAx-3	279	298	378
CBDAx-4	278	297	368
CBDAx-5	248	256	357
CBDAx-6	240	271	330
CBDAx-7	301	329	390
CBDAx-8	306	326	368

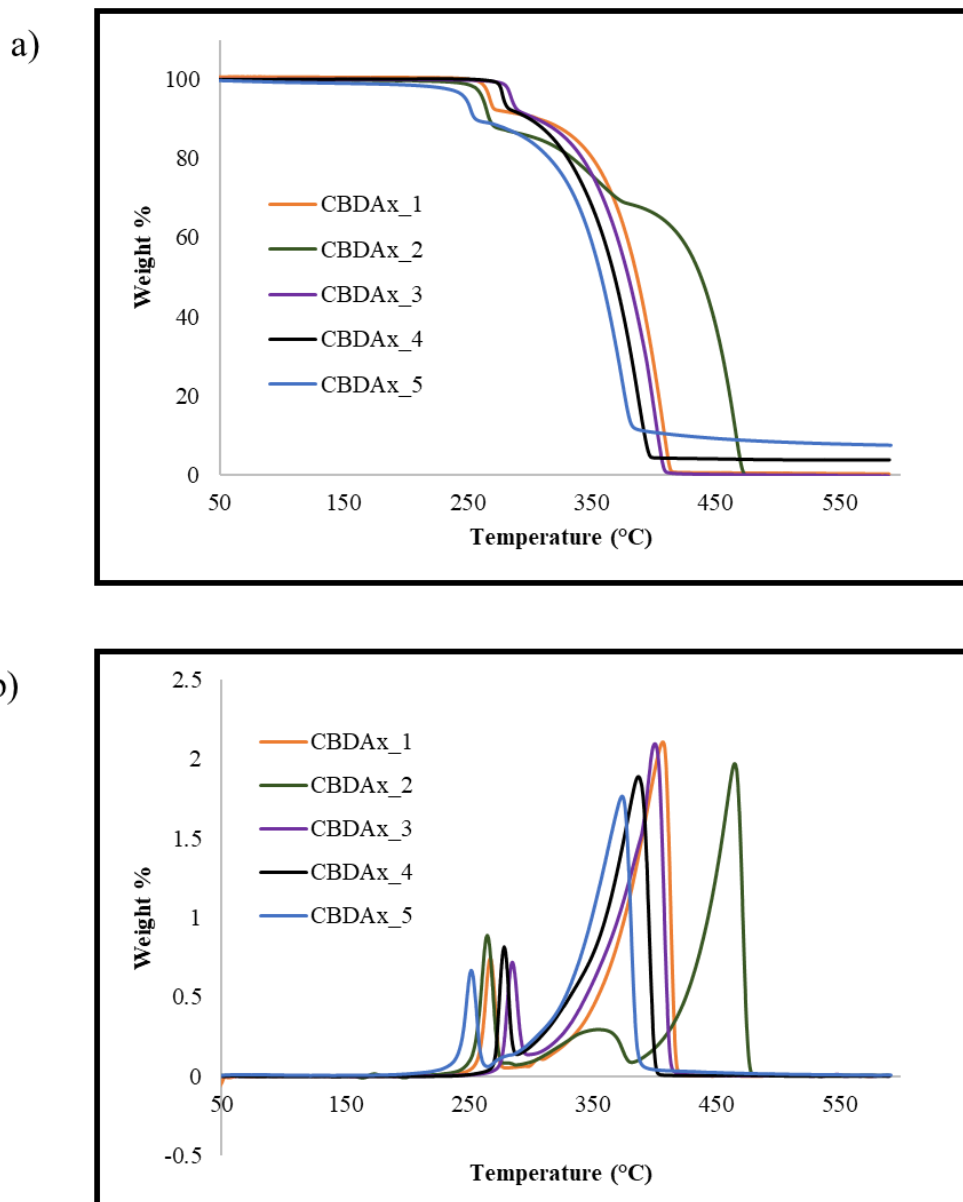


**Figure 13:** TGA and DTG curves of CBDAx-1 via CBDAx-5 **a)** TGA curves of CBDAx-1 via CBDAx-5 recorded from 50 °C to 600 °C with a heating rate of 20 °C·min<sup>-1</sup> under N<sub>2</sub> atmosphere, **b)** DTG curves of CBDAx-1 via CBDAx-5 recorded from 50 °C to 600 °C with a heating rate of 20 °C·min<sup>-1</sup> under N<sub>2</sub> atmosphere

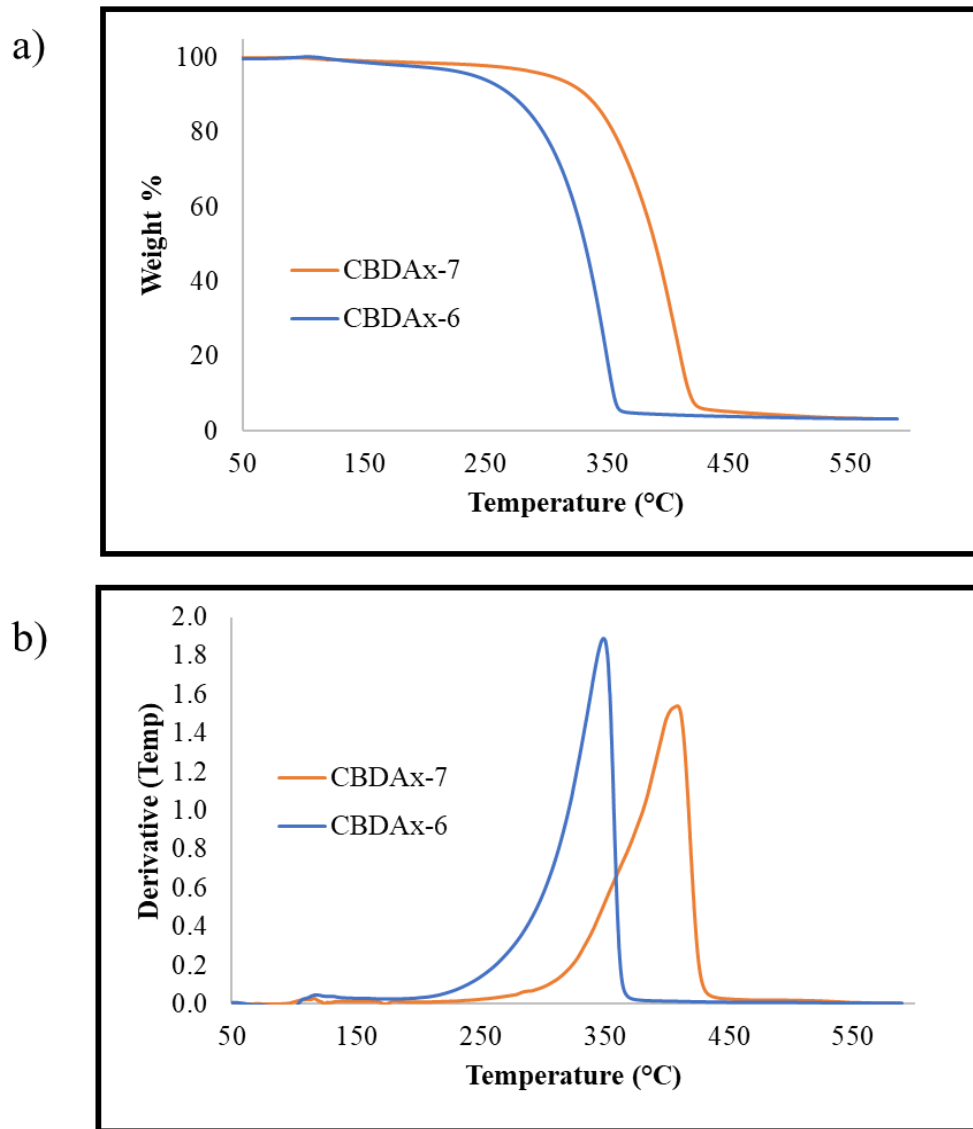


**Figure 14:** TGA and DTG curves of CBDAx-6 and CBDAx-7 recorded from 50 °C to 600 °C with a heating rate of 20 °C·min<sup>-1</sup> under N<sub>2</sub> atmosphere.

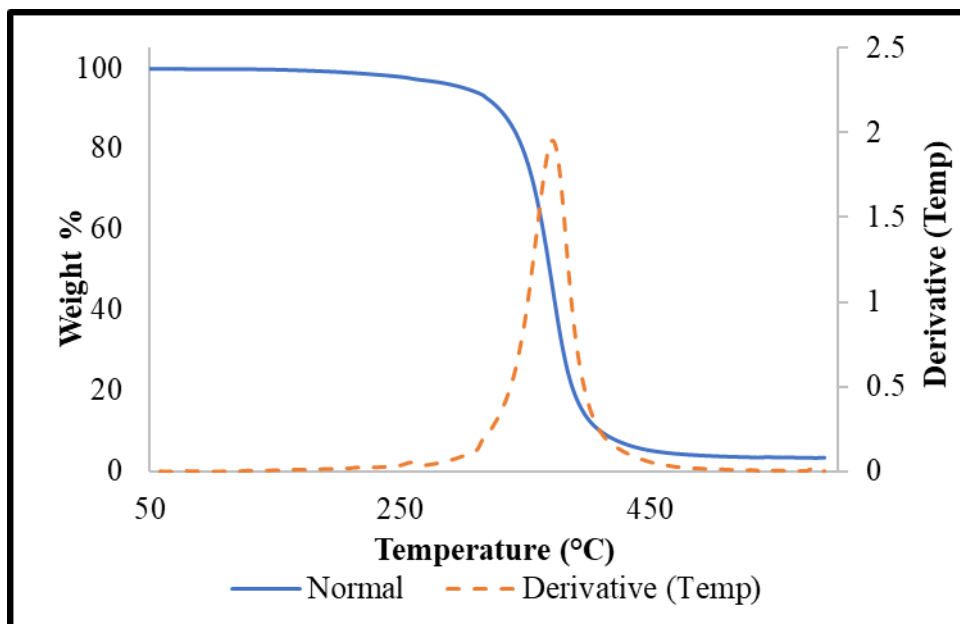


**Figure 15:** TGA and DTG curves of CBDAx-8 recorded from 50 °C to 600 °C with a heating rate of 20 °C·min<sup>-1</sup> under N<sub>2</sub> atmosphere.

#### 2.1.4. Synthesis of CBDExs from CBDAxS

Polyesters are synthesized via condensation reactions between a diacid and a diol. Initial studies to evaluate if the CBDAxS are suitable for polyester synthesis were hindered by the high melting points of the compounds and the ability of the compound to cyclize to form an imide. Melt polymerization is the industrial method of choice in polyester synthesis. This property of these diacids will pose a huge challenge to material synthesis. To circumvent this barrier, esters were synthesized from the diacids. CBDAx-1 through 5 were subjected to methyl ester synthesis. Syntheses of all methyl esters were successful using two methods. The esters were synthesized either via Fischer esterification or through their corresponding acyl chloride synthesized by means of thionyl chloride. The methyl esters had melting temperatures similar to those of the diacids making it challenging for them to be used in melt polymerization.

### 2.1.5. Initial thermal studies on the stability of CBDExs

Thermal studies on potential monomers are important because they provide data which give insights into their applicability in the synthesis of polymeric materials. Polymer syntheses requires stable monomers, therefore it is imperative that the initial thermal properties of the CBDEx monomers are studied. Table 7 summaries the  $T_5$ ,  $T_{10}$  and  $T_d$  data for CBDEx-1 through CBDEx-5 respectively. This initial thermal evaluation showed that the cyclobutane ring in these monomers has stability comparable to other existing CBDA monomers (Figure 16). It also shows that these monomers are thermally stable enough and could therefore serve as precursors in material synthesis.

**Table 7:** Thermogravimetric analysis data for CBDEx-1 through CBDEx-5

<b>Thermogravimetric analysis (TGA)</b>			
<b>Sample</b>	<b><math>T_5</math></b>	<b><math>T_{10}</math></b>	<b><math>T_d</math></b>
CBDEx-1	285	311	353
CBDEx-2	304	316	442
CBDEx-3	304	316	353
CBDEx-4	233	242	279
CBDEx-5	216	230	365

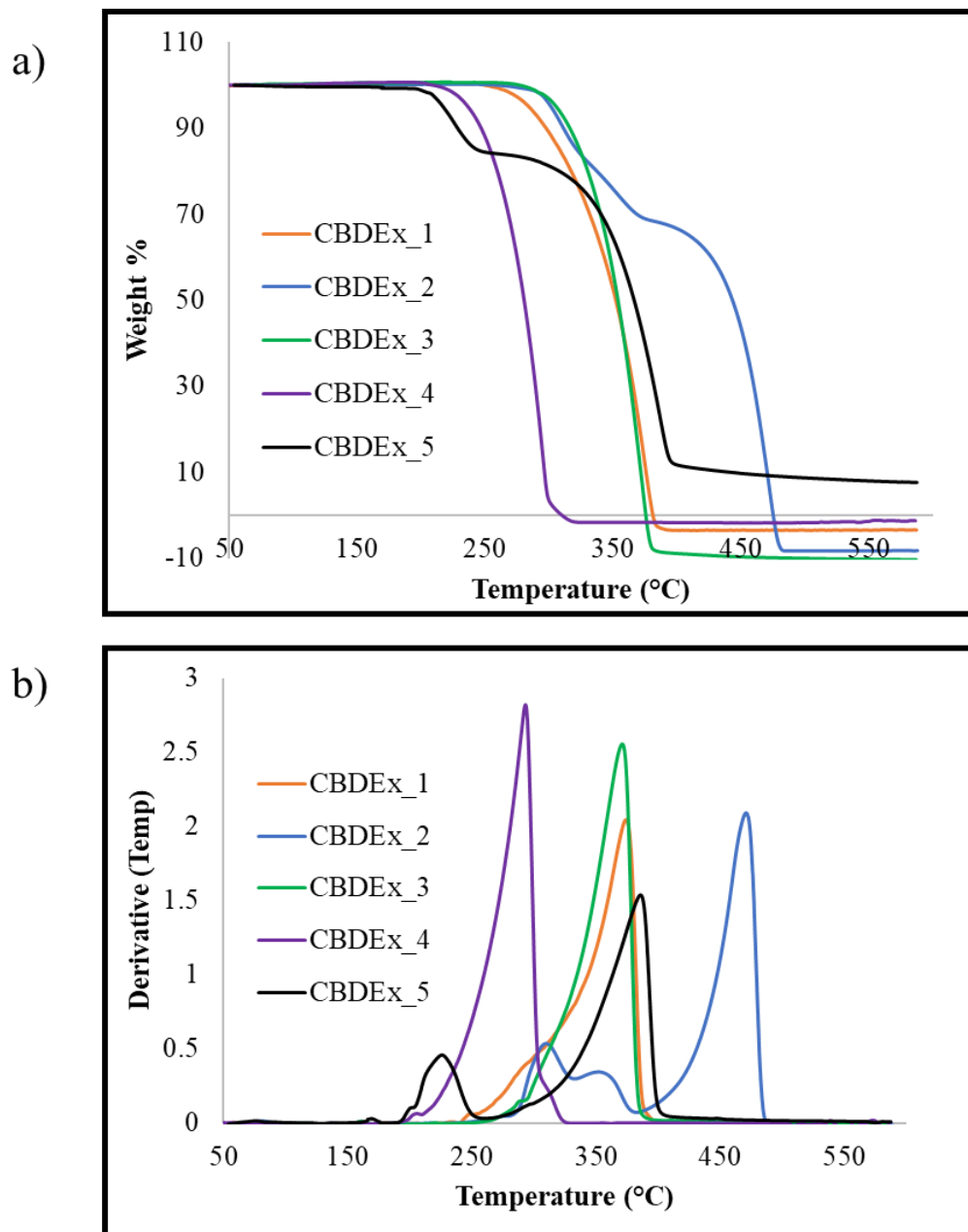


**Figure 16:** TGA curves of CBDEx-1 through CBDAx-5 recorded from 0 °C to 600 °C with a heating rate of 20 °C·min<sup>-1</sup> under N<sub>2</sub> atmosphere, **b)** DTG curves of CBDEx-1 through CBDAx-5 recorded from 50 °C to 600 °C with a heating rate of 20 °C·min<sup>-1</sup> under N<sub>2</sub> atmosphere



## **2.2. Conclusion**

A platform molecule for the synthesis of several CBDAs was introduced in this work. This work showed a simple, efficient, and ecofriendly novel method to add up to the library of cyclobutane containing dicarboxylic acids precursors for polymer synthesis. CBDAN-1 was used to synthesize a library of cyclobutane containing diacids. CBDAN-1 was synthesized via direct dimerization of maleic anhydride or dehydration of CBTA-1. A library of eight CBDAx was synthesized from CBDAN-1 by reaction with various amine, alcohol, or Grignard bases via nucleophilic reactions. CBDAx-1 through CBDAx-8 had high decomposition temperatures comparable to other monomers used in polymer synthesis. This initial thermal evaluation shows that these diacids are thermally stable enough and could therefore be exploited in the synthesis of desired polymeric materials.

## **2.3. Experimental Section**

### **2.3.1. Materials and Procedures**

All chemicals were purchased from Alfa Aesar, Sigma-Aldrich, or Acros, and used without further purification. Blacklight used in the photoreaction was Fiet Electric 7-watt LED bulb or 15W Eiko EK15526 F15T8/BL. Germicidal lamps used in the photoreaction was Germicidal lamp T5 G5 39/ 41W ozone free Sankyo Denki Co., Ltd. The solution phase nuclear magnetic resonance spectra (NMR) were recorded with Bruker AVANCE ( $^1\text{H}$ : 500 MHz,  $^{13}\text{C}$ : 125 MHz). Proton and carbon chemical shifts were reported in ppm downfield from tetramethylsilane (TMS). Spin-spin coupling

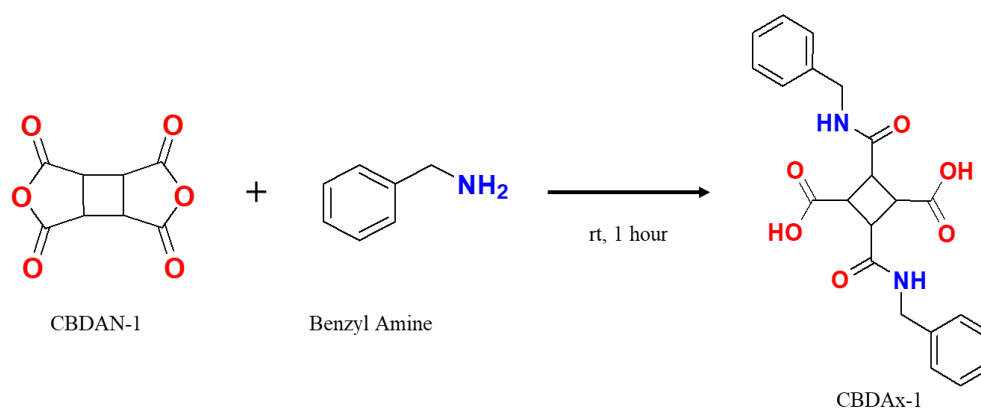
constants,  $J$ , are given in Hz. Spectra were recorded in DMSO- $d_6$  unless otherwise stated. Single crystal X-ray data were collected on a Bruker Kappa Apex II Duo X-Ray Diffractometer with Cu  $K\alpha$  ( $\lambda = 1.54178 \text{ \AA}$ ). Infrared spectroscopy (IR) was recorded on Thermo Scientific Nicolet iS5 FT-IR spectrometer. Thermogravimetric analysis (TGA) was carried out with a Hi-Res TGA Q500 from TA Instruments using alumina pans at a heating rate of  $20 \text{ }^\circ\text{C}\cdot\text{min}^{-1}$  under nitrogen with a sample weight of about 10 mg. UV-Vis spectra were recorded on a Beckman DU400 UV-Vis spectrometer.

### 2.3.2. Synthesis of CBDAx-1 from CBDAN-1

In an oven-dried round-bottom flask, cyclobutane-1,2,3,4-tetracarboxylic dianhydride (2.02 g, 10.20 mmol) was added to 100 mL acetone. Benzylamine (2100  $\mu\text{L}$ , 19.20 mmol), was dropwise added to the flask. The reaction mixture was stirred at room temperature for one hour. The product precipitated out of solution as the reaction proceeded and completion of reaction was checked by NMR of the solution. The pure product was filtered out of the solvent and dried before characterization. The product was characterized using  $^1\text{H}$  NMR,  $^{13}\text{C}$  NMR, FT-IR spectroscopy, and X-ray crystallography.

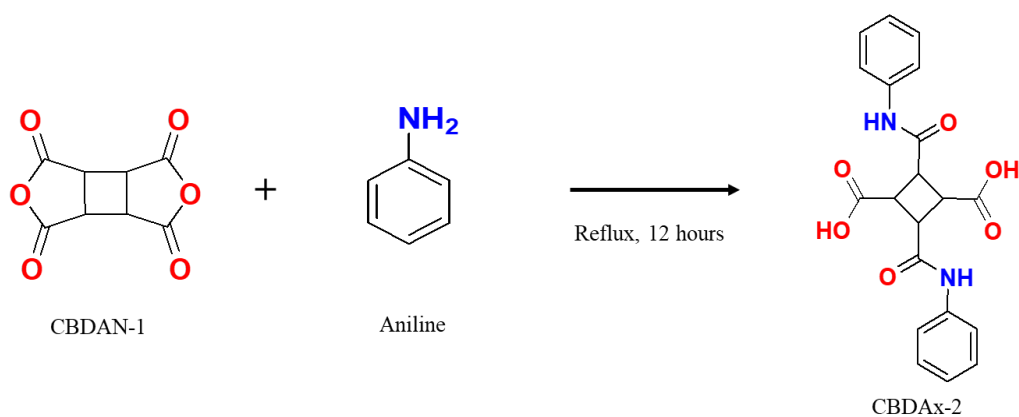
**CBDAx-1:**  $^1\text{H}$  NMR  $\delta$  (ppm): 12.40 (s, 2H, COOH) 8.50 - 8.52 (t,  $J = 5$ , 2H, CONH) 7.21 - 7.32 (m, 10H, Ar-H) (dd,  $J = 10$ , 5, 2H, CONH-CH<sub>2</sub>-Ar), 4.21 (dd,  $J = 10$ , 5, 2H, CONH-CH<sub>2</sub>-Ar) 3.66 (dd,  $J = 5$ , 10, 2H, cyclobutane-CH-CONH) 3.39 (dd,  $J = 5$ , 10, 2H, cyclobutane-CH-COOH);  $^{13}\text{C}$  NMR  $\delta$  (ppm): 173 (CONH) 170 (COOH) 139 128 127 127 (Ar) 42 (cyclobutane-CHCO) 42 (CO-CH<sub>2</sub>-Ar); FT-IR (solid)  $\bar{\nu}_{\text{max}}$  ( $\text{cm}^{-1}$ ): 3284 (CONH), 2917 (carboxylic acid OH/aliphatic  $\text{sp}^2$  C-H) 1691/1642 (carbonyl

C=O). HRMS (ESI/TOF): Calculated for  $[M + Na]^+$ ,  $C_{18}H_{20}O_2Na^+$ : 433.13; Found: 433.1375.



**Scheme 9:** Synthesis of CBDAx-1

### 2.3.3. Synthesis of CBDAx-2 from CBDAN-1



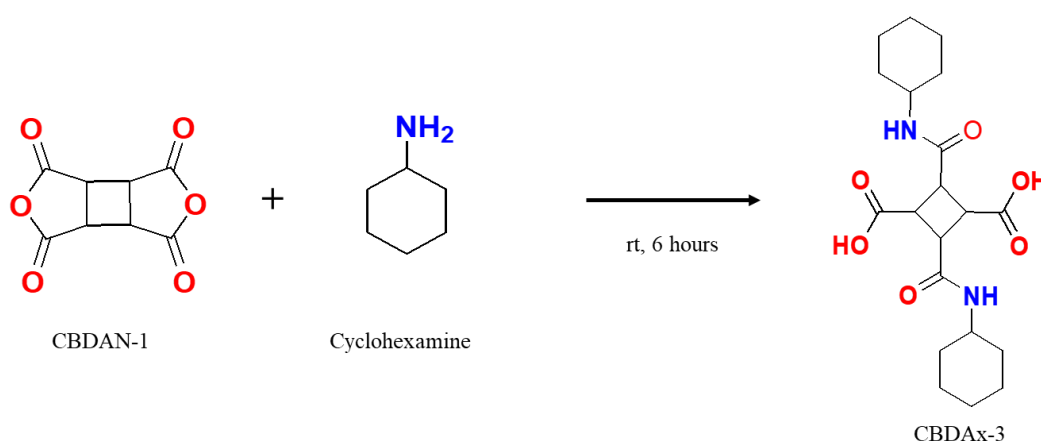
**Scheme 10:** Synthesis of CBDAx-2

In an oven-dried round-bottom flask, cyclobutane-1,2,3,4-tetracarboxylic dianhydride (2.01 g, 10.20 mmol), was placed in 100 mL acetone. Aniline (1800  $\mu$ L, 19.20 mmol) was dropwise added to the flask. The reaction mixture was stirred at reflux temperature for 12 hours. The product precipitated out of solution as the reaction proceeded and

completion of reaction was checked by  $^1\text{H}$  NMR of the solution. The pure product was filtered out of the solvent and dried before characterization. The product was characterized using  $^1\text{H}$  NMR,  $^{13}\text{C}$  NMR, FT-IR spectroscopy, and X-ray crystallography.

**CBDAx-2:**  $^1\text{H}$  NMR  $\delta$  (ppm): 12.49 (s, 2H, COOH) 10.16 (s, 2H, CONH) 7.06 - 7.61 (m, 10H, Ar-H) 3.86 (dd,  $J = 5, 10$ , 2H, CONH-CH-cyclobutane), 3.56 (dd,  $J = 5, 10$ , 2H, COOH-CH-cyclobutane);  $^{13}\text{C}$  NMR  $\delta$  (ppm): 171 (CONH), 169 (COOH), 119 - 139 (Ar), 52 (cyclobutane-CH-COOH), 42 (cyclobutane-CH-CONH); FT-IR (solid)  $\bar{\nu}_{\text{max}}$  ( $\text{cm}^{-1}$ ): 3308 (CONH) 2929 (carboxylic acid OH/aliphatic  $\text{sp}^2$  C-H) 1702/1655 (carbonyl C=O). HRMS (ESI/TOF): Calculated for  $[\text{M} + \text{Na}]^+$ ,  $\text{C}_{18}\text{H}_{20}\text{O}_2\text{Na}^+$ : 405.10; Found: 405.1063.

#### 2.3.4. Synthesis of CBDAx-3 from CBDAN-1



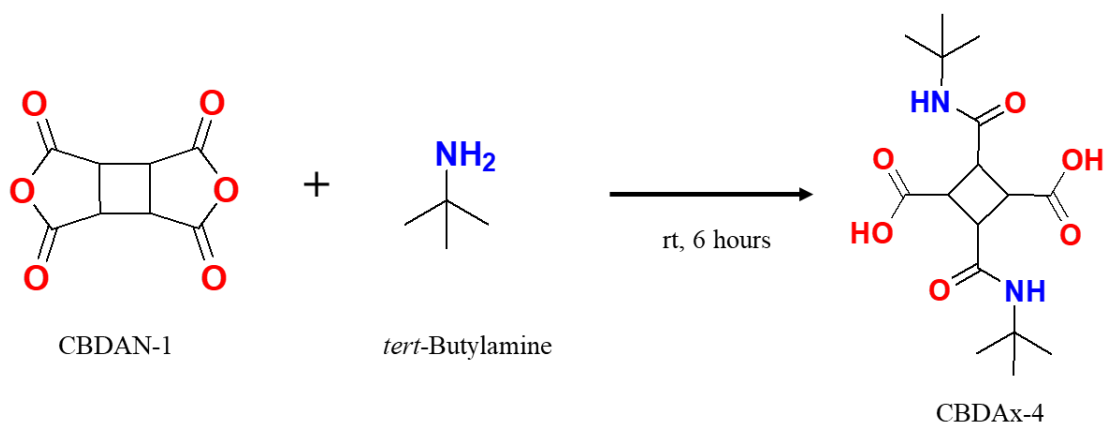
**Scheme 11:** Synthesis of CBDAx-3

In an oven-dried round-bottom flask, cyclobutane-1,2,3,4-tetracarboxylic dianhydride (2.01 g, 10.20 mmol) was placed in 100 mL acetone. Cyclohexylamine (2200  $\mu\text{L}$ , 19.20

mmol) was dropwise added to the flask. The reaction mixture was stirred at room temperature for six hours. The product precipitated out of solution as the reaction proceeded and completion of reaction was checked by NMR of the solution. The pure product was filtered out of the solvent and dried before characterization. The product was characterized using  $^1\text{H}$  NMR,  $^{13}\text{C}$  NMR, FT-IR spectroscopy, and X-ray crystallography.

**CBDAx-3:**  $^1\text{H}$  NMR  $\delta$  (ppm): 12.19 (s, 2H, COOH) 7.82 (d,  $J = 10$ , 2H) 3.49 (dd,  $J = 10$ , 20 2H, CONH-CH-cyclobutane), 3.31 (dd,  $J = 10$ , 10, 2H, COOH-CH-cyclobutane), 1.04 - 1.71 (m, 22H, 2xcyclohexane);  $^{13}\text{C}$  NMR  $\delta$  (ppm): 172 (CONH), 169 (COOH) 47 (CONH-CH-cyclobutane), 41 (COOH-CH-cyclobutane), 24 - 32 (cyclohexane); FT-IR (solid)  $\bar{\nu}_{\text{max}}$  ( $\text{cm}^{-1}$ ): 3375 (CONH), 2922 (carboxylic OH), 2856 (aliphatic  $\text{sp}^2\text{-C-H}$ ), 1728/1604 (carbonyl  $\text{C=O}$ ). HRMS (ESI/TOF): Calculated for  $[\text{M} + \text{Na}]^+$ ,  $\text{C}_{18}\text{H}_{20}\text{O}_2\text{Na}^+$ : 417.21; Found: 395.2128.

### 2.3.5. Synthesis of CBDAx-4 from CBDAN-1



**Scheme 12:** Synthesis of CBDAx-4

In an oven-dried round-bottom flask, cyclobutane-1,2,3,4-tetracarboxylic dianhydride (2.00 g, 10.20 mmol) was placed in 100 mL acetone. Tert-butylamine (2020  $\mu$ L, 19.20 mmol) was dropwise added to the flask. The reaction mixture was stirred at room temperature for 6 hours. The product precipitated out of solution as the reaction proceeded and completion of reaction was checked by NMR of the solution. The pure product was filtered out of the solvent and dried in an oven before characterization. The product was characterized using  $^1\text{H}$  NMR,  $^{13}\text{C}$  NMR, FT-IR spectroscopy, and X-ray crystallography.

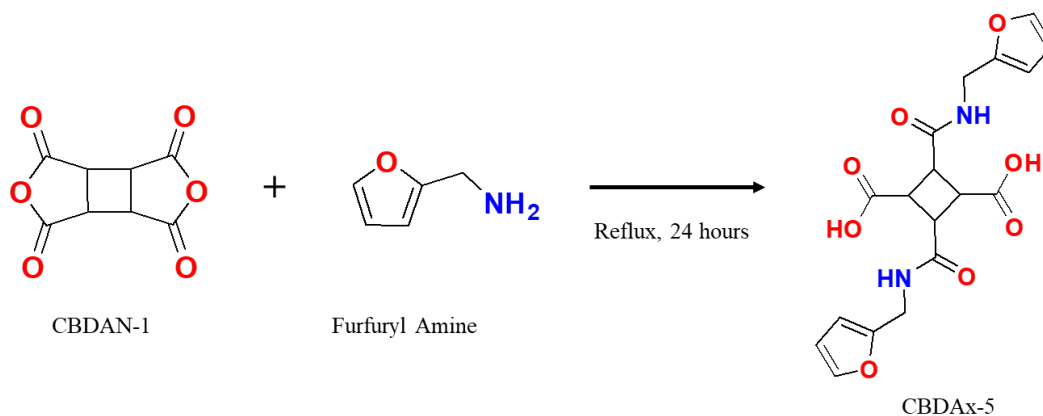
**CBDAx-4:**  $^1\text{H}$  NMR  $\delta$  (ppm): 12.19 (s, 2H, COOH) 7.50 (s, 2H, CONH) 3.49 (dd,  $J = 5, 10$ , 2H, CONH-CH-cyclobutane) 3.27 (dd,  $J = 5, 10$ , 2H, COOH-CH-cyclobutane) 1.20 (s, 18H,  $2 \times 3\{\text{CH}_3\}$ );  $^{13}\text{C}$  NMR  $\delta$  (ppm): 172 (CONH), 169 (COOH), 49 (CONH-CH-cyclobutane), 41 (COOH-CH-cyclobutane), 28 ( $3\{\text{CH}_3\}$ ); FT-IR (solid)  $\bar{\nu}_{\text{max}}$  ( $\text{cm}^{-1}$ ): 3418 (CONH), 2976 (carboxylic acid/aliphatic  $\text{sp}^2\text{-C-H}$ ), 1736/1721 (carbonyl C=O). HRMS (ESI/TOF): Calculated for  $[\text{M} + \text{Na}]^+$ ,  $\text{C}_{18}\text{H}_{20}\text{O}_2\text{Na}^+$ : 365.16; Found: 365.1689.

### 2.3.6. Synthesis of CBDAx-5 from CBDAN-1

In an oven-dried round-bottom flask, cyclobutane-1,2,3,4-tetracarboxylic dianhydride (2.00 g, 10.20 mmol) was placed in 100 mL acetone. A solution of 1800  $\mu$ L furfuryl amine (19.20 mmol) was dropwise added to the flask. The reaction mixture was stirred at room temperature for four hours. The product precipitated out of solution as the reaction proceeded and completion of reaction was checked by NMR of the solution. The product was washed with methanol, filtered out of the solvent and dried before

characterization. The product was characterized using  $^1\text{H}$  NMR,  $^{13}\text{C}$  NMR, and FT-IR spectroscopy.

**CBDAx-5:**  $^1\text{H}$  NMR  $\delta$  (ppm): 12.35 (s, 2H, COOH) 8.47 (t,  $J = 5$ , 2H, CONH) 6.22-7.56 (m, 6H, furan) 4.26 (dd,  $J = 10, 15$ , 2H, CONH-CH<sub>2</sub>-furan), 4.19 (dd, dd,  $J = 5, 10$ , 2H, CONH-CH<sub>2</sub>-furan) 3.60 (q, 2H,  $J = 5, 10$ , CONH-CH-cyclobutane) 3.34 (q,  $J = 5, 10$ , 2H, COOH-CH-cyclobutane);  $^{13}\text{C}$  NMR  $\delta$  (ppm): 172 (CONH), 170 (COOH), 106 – 152 (furan), 41 (COONH-CH<sub>2</sub>-furan), 35 (CH-cyclobutane); FT-IR (solid)  $\bar{\nu}_{\text{max}}$  (cm<sup>-1</sup>): 3288 (CONH), 2940 (carboxylic acid OH/aliphatic sp<sup>2</sup>-C-H), 1698/1640 (carbonyl C=O). HRMS (ESI/TOF): Calculated for  $[\text{M} + \text{Na}]^+$ , C<sub>18</sub>H<sub>20</sub>O<sub>2</sub>Na<sup>+</sup>: 413.09; Found: 413.0961.



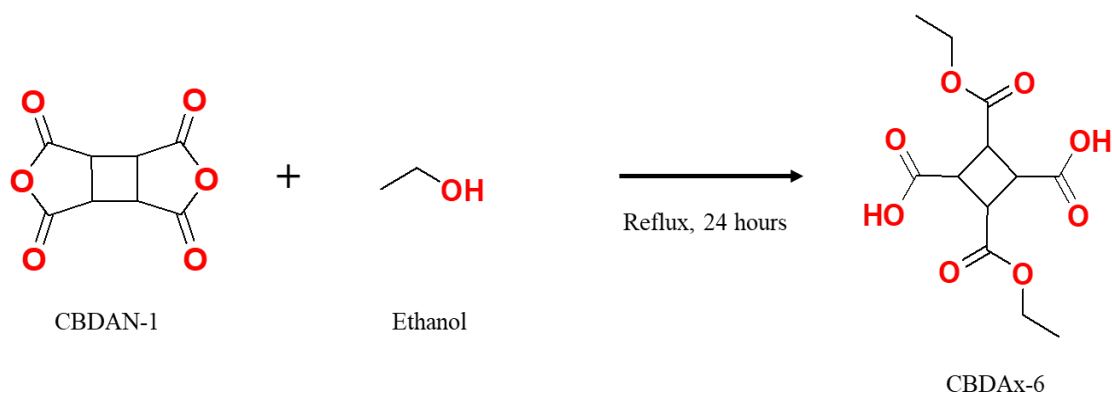
**Scheme 13:** Synthesis of CBDAx-5

### 2.3.7. Synthesis of CBDAx-6 from CBDAN-1

In an oven-dried round-bottom flask, cyclobutane-1,2,3,4-tetracarboxylic dianhydride (2.02 g, 10.20 mmol), was refluxed in 50 mL of ethanol (0.90 mol). The reaction mixture was stirred at room temperature for 8 hours. Completion of reaction was

checked by TLC. The solvent was evaporated out. The solid formed was the pure product which was washed and dried in an oven before characterization. The product was characterized using  $^1\text{H}$  NMR,  $^{13}\text{C}$  NMR, and FT-IR spectroscopy.

**CBDAx-6:**  $^1\text{H}$  NMR  $\delta$  (ppm): 12.79 (s, 2H, COOH) 4.01 - 4.07 (m, 4H, 2xCH<sub>2</sub>), 3.48 - 3.57 (m, 4H, CH-cyclobutane), 1.16 (t,  $J = 10$ , 6H, 2xCH<sub>3</sub>);  $^{13}\text{C}$  NMR  $\delta$  (ppm): 172 (COOEt), 171 (COOH), 60 (CH<sub>3</sub>-CH<sub>2</sub>-COO), 41 (CH-cyclobutane), 14 (CH<sub>3</sub>); FT-IR (solid)  $\bar{\nu}_{\text{max}}$  (cm<sup>-1</sup>): 2981 (carboxylic acid OH), 1700 (carbonyl C=O).



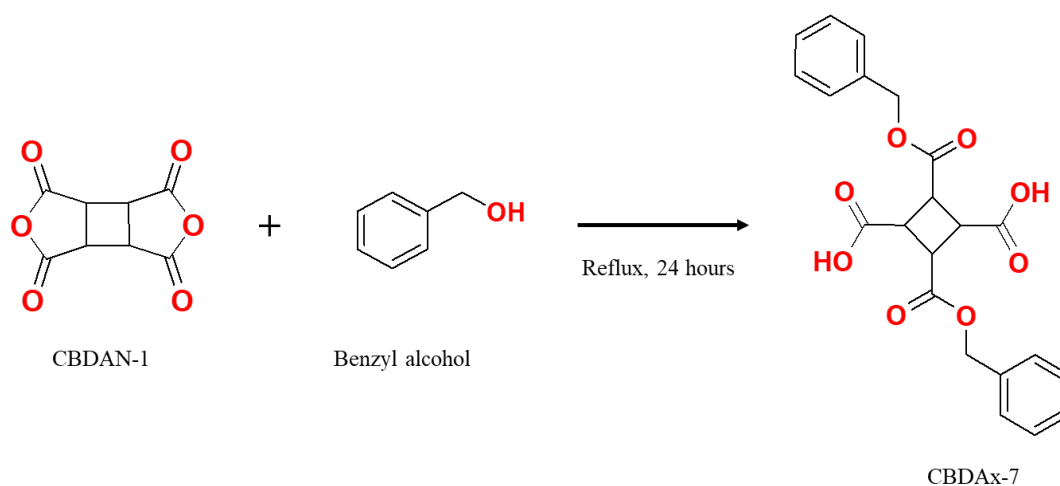
**Scheme 14:** Synthesis of CBDAx-6

### 2.3.8. Synthesis of CBDAx-7 from CBDAN-1

In an oven-dried round-bottom flask, cyclobutane-1,2,3,4-tetracarboxylic dianhydride (2.02 g, 10.20 mmol), was refluxed in 50 mL of benzyl alcohol (0.50 mol). The reaction mixture was stirred at room temperature for 8 hours. Completion of reaction was checked by TLC. The solvent was evaporated out. The solid formed was the pure product, which was washed and dried in an oven before characterization. The product characterized using  $^1\text{H}$  NMR,  $^{13}\text{C}$  NMR, and FT-IR spectroscopy.



**CBDAx-7:**  $^1\text{H}$  NMR  $\delta$  (ppm): 12.87 (s, 2H, COOH), 7.35 (m, 10H, Ar-H), 5.05 – 5.11 (m, 4H,  $\text{CH}_2\text{-Bz}$ ), 3.71 (d,  $J = 10$ , 2H,  $\text{BzOOC-CH-cyclobutane}$ ), 3.52 (d,  $J = 10$ , 2H,  $\text{HOOC-CH-cyclobutane}$ );  $^{13}\text{C}$  NMR  $\delta$  (ppm): 171 ( $\text{COOBz}$ ), 171 ( $\text{COOH}$ ), 128 – 136 (Ar), 66 (Ar- $\text{CH}_2$ ), 40 ( $\text{CH-cyclobutane}$ ); FT-IR (solid)  $\bar{\nu}_{\text{max}}$  ( $\text{cm}^{-1}$ ): 3316 (carboxylic acid OH), 2887 (aliphatic  $\text{sp}^2\text{-C-H}$ ), 1751/1725 (carbonyl  $\text{C=O}$ ).



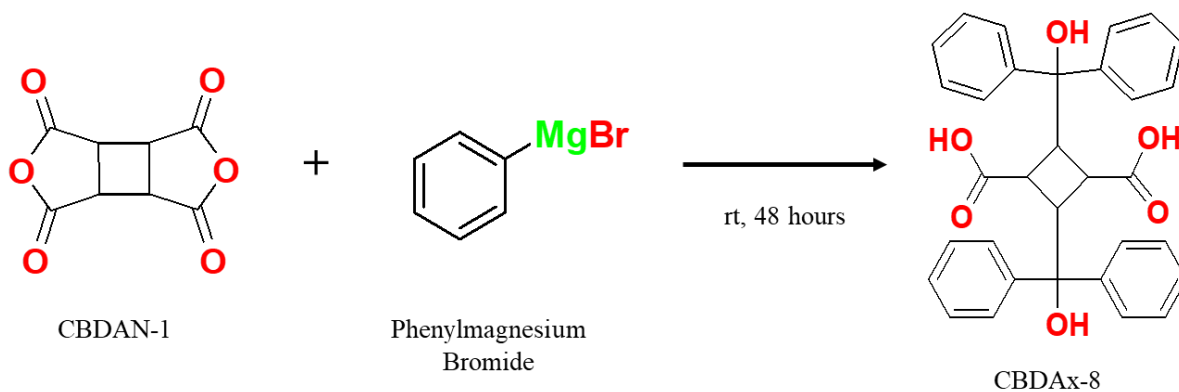
**Scheme 15:** Synthesis of CBDAx-7

### 2.3.9. Synthesis of CBDAx-8 from CBDAN-1

Magnesium turnings (2.00 g, 83.33 mmol) and 10.0 mL of anhydrous diethyl ether were added to a 100 mL round bottom flask. Then 8.0 mL of bromobenzene was added to the mixture. The flask was shaken until it started to form a cloudy solution. Once refluxing began, another 25.0 mL of anhydrous diethyl ether was slowly added. When most of the magnesium had been consumed and refluxing ceased, the next step of the reaction began. CBDAN-1 (1.02g, 5.20 mmol) was added directly into the flask. The content was refluxed for 48 hours and then left at room temperature for another 24 hours. A 50% aqueous HCl solution was used to dissolve the salt formed. The organic

layer was extracted twice with diethyl ether. The combined organic layer was washed with brine and dried over anhydrous sodium sulfate. The solvent was evaporated, and the crude product was recrystallized in ethanol. The product was characterized using  $^1\text{H}$  NMR,  $^{13}\text{C}$  NMR, and FT-IR spectroscopy.

**CBDAx-8:**  $^1\text{H}$  NMR  $\delta$  (ppm): 11.88 (s, 2H, COOH), 7.04 – 7.46 (m, 20H, Ar-H), 6.11 (s, 2H, OH), 4.05 (dd,  $J = 5, 15$ , 2H, CH-cyclobutane) 3.63 (dd,  $J = 5, 15$ , 2H, COOH-CH-cyclobutane);  $^{13}\text{C}$  NMR  $\delta$  (ppm): 175 (COOH), 125 - 140 (Ar), 90 (2{Ar}-C-OH), 45 (CH-cyclobutane), 41 (COOH-CH-cyclobutane); FT-IR (solid)  $\bar{\nu}_{\text{max}}$  ( $\text{cm}^{-1}$ ): 3468 (alcohol OH), 3051 (carboxylic acid OH), 2999 (aliphatic  $\text{sp}^2$  C-H), 1670 (carbonyl C=O).



**Scheme 16:** Synthesis of CBDAx-8

### 2.3.10. General Methods of Ester Synthesis

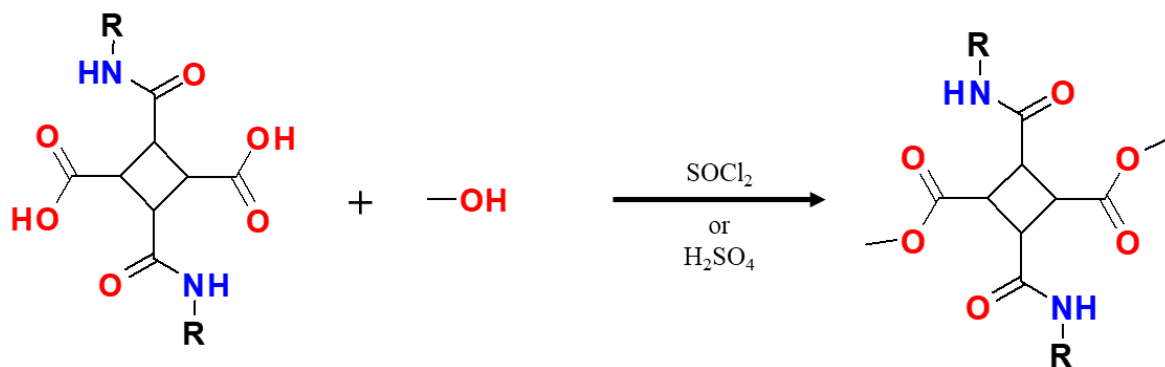
Esters were synthesized using two methods.

#### Method I:

CBDAx (1.0 mol) was added to 20.0 mL of methanol. Then 4.0 mol equivalent of thionyl chloride was added to the mixture dropwise. The mixture was stirred at room temperature for 4 hours. In all cases no obvious dissolution of the CBDAx was observed. After 4 hours the precipitate was diluted with more methanol and vacuum filtered. The filtrate was the product, which was essentially pure. The product was oven dried overnight before characterization. The product was characterized using  $^1\text{H}$  NMR,  $^{13}\text{C}$  NMR, FT-IR spectroscopy, and X-ray crystallography.

#### Method II:

Fischer esterification was also used to synthesize the CBDEx. Briefly, 1.0 mol of CBDAx was added to 20.0 mL of methanol. Large excess of  $\text{H}_2\text{SO}_4$  (10.0 mL) was dropwise added to the mixture. The mixture was stirred under heating at  $80\text{ }^\circ\text{C}$  for 12 hours. In all cases no obvious dissolution of the CBDAx was observed. After 12 hours the precipitate was vacuum filtered. The filtrate was the product, which was essentially pure. The product was oven dried over night before characterization. The product was characterized using  $^1\text{H}$  NMR,  $^{13}\text{C}$  NMR, FT-IR spectroscopy, and X-ray crystallography.



**Scheme 17:** General methods to the synthesis of CBDExs

**CBDEx-1:** Melting point: 244.5 °C.  $^1\text{H}$  NMR  $\delta$  (ppm): 8.53 (t,  $J = 5, 10$ , 2H, CONH) 7.21 - 7.32 (m, 10H, Ar-H) 4.31 (dd,  $J = 10, 15$ , 2H, CONH-CH<sub>2</sub>-Ar), 4.22 (dd,  $J = 5, 10$ , 2H, CONH-CH<sub>2</sub>-Ar) 3.67 3.66 3.65 3.63 (q, 1H) 3.41 3.38 3.37 3.36 (q, 1H) 3.35 (s, 1H);  $^{13}\text{C}$  NMR  $\delta$  (ppm): 171 (CONH), 170 (COOMe), 127 – 139 (Ar) 51 (OMe), 42 (CONH-CH<sub>2</sub>-Ar), 41 (CONH-CH-cyclobutane), 41 (COOMe-CH-cyclobutane); FT-IR (solid)  $\bar{\nu}_{\text{max}}$  (cm<sup>-1</sup>): 3294 (CONH), 2952 (aliphatic sp<sup>2</sup>-C-H), 1728 (carbonyl C=O).

**CBDEx-2:** Melting point: 279.3 °C  $^1\text{H}$  NMR  $\delta$  (ppm): 10.23 (s, 2H, CONH), 7.35 - 7.39 (m, 4H, Ar) 7.29 - 7.33 (m, 4H, Ar) 7.04 - 7.07 (m, 4H, Ar) 3.96 (dd,  $J = 5, 10$ , 2H, CONH-CH-cyclobutane) 3.66 (dd,  $J = 0, 10$ , 2H, MeCOO-CH-cyclobutane) 3.51 (s, 6H, OCH<sub>3</sub>);  $^{13}\text{C}$  NMR  $\delta$  (ppm): 171 (CONH), 168 (COOMe) 138 (Ar), 128 (Ar), 123 (Ar), 119 (Ar), 51 (OCH<sub>3</sub>), 42 (CH-cyclobutane); FT-IR (solid)  $\bar{\nu}_{\text{max}}$  (cm<sup>-1</sup>): 3293 (CONH), 2947 (aliphatic sp<sup>2</sup> C-H), 1733 (carbonyl C=O).

**CBDEx-3:** Melting point: 238.6 °C  $^1\text{H}$  NMR  $\delta$  (ppm): 7.94 (s, 2H, CONH), 3.34 - 3.59 (m, 4H, CH-cyclobutane), 3.5 (s, 6H, OMe), 1.11 - 1.66 (m, 22H, CH<sub>2</sub>-cyclohexane);  $^{13}\text{C}$  NMR  $\delta$  (ppm): 171 (CONH), 169 (COOMe) 51 (OMe) 49 (NH-CH-cyclohexane), 41 (CH-cyclobutane), 28 (cyclohexane); FT-IR (solid)  $\bar{\nu}_{\text{max}}$  (cm<sup>-1</sup>): 3283 (CONH), 2925 (aliphatic sp<sup>2</sup> C-H), 1728 (carbonyl C=O).

**CBDEx-4:** Melting point: 232.8 °C  $^1\text{H}$  NMR  $\delta$  (ppm): 7.68 (s, 2H, CONH) 3.62 (dd,  $J = 5, 10$  2H, NHOC-CH-cyclobutane) 3.52 (s, 3H, OMe) 3.34 (dd,  $J = 10, 15$ , 2H, MeOOC-CH-cyclobutane) 1.20 (s, 18H, *tert*-butyl);  $^{13}\text{C}$  NMR  $\delta$  (ppm): 171 (CONH),

169 (COOMe) 51 (OMe) 49 (C-*tert*-butyl), 41 (CH-cyclobutane), 28 (*tert*-butyl); FT-IR (solid)  $\bar{\nu}_{\max}$  (cm<sup>-1</sup>): 3370 (CONH), 2967 (aliphatic sp<sup>2</sup> C-H), 1715/1651 (carbonyl C=O).

**CBDEx-5:** Melting point: 206.2 °C <sup>1</sup>H NMR  $\delta$  (ppm): 8.57 (t,  $J = 5$ , 15, 2H, CONH), 7.58 (s, 2H, furan), 6.38 (d,  $J = 5$ , 2H, furan) 6.22 (d,  $J = 0$ , 2H, furan) 4.26 (dd,  $J = 10$ , 20, 2H, NHOC-CH<sub>2</sub>-furan), 4.18 (dd,  $J = 5$ , 20, 2H, NHOC-CH<sub>2</sub>-furan) 3.68 (dd,  $J = 5$ , 10 2H, NHOC-CH-cyclobutane) 3.45 (s, 6H, OMe) 3.42 (dd,  $J = 10$ , 10 2H, MeOOC-CH-cyclobutane); <sup>13</sup>C NMR  $\delta$  (ppm): ; FT-IR (solid)  $\bar{\nu}_{\max}$  (cm<sup>-1</sup>): 3295 (CONH), 2955 aliphatic sp<sup>2</sup> C-H () 1723/1634 (carbonyl C=O).

## CHAPTER THREE

### A Cyclobutane Carboxylic Dianhydride (CBDAN-2) as a Building Block for Metal-Organic and Polymeric Materials Introduction

#### 3.0. Introduction

Cyclobutane-containing carboxylic dianhydrides (CBDANs) are versatile building blocks that have a wide variety of applications.<sup>38, 70-75</sup> They are used in making polyimide resins, metal-organic materials (MOMs), as capping ligands in the preparation of gold colloids, and in the synthesis of energetic materials.<sup>37, 43, 47, 70, 75-78</sup> Carboxylic dianhydrides are best known for their wide variety of material applications in the fields of aerospace, high-performance engineering materials, cosmonautics, microelectronics, and medical devices.<sup>72, 74</sup> Their applications come from their characteristic attributes such as extreme thermal stability, excellent mechanical properties, good chemical and irradiation resistance.<sup>71, 75</sup>

Tetracarboxylic and dicarboxylic acids are a group of organic compounds with applications where strong hydrogen bonding is involved, such as capillary electrophoresis. They are widely used in the chiral separation of primary amines and synthesis of polyesters.<sup>44, 79, 80</sup> Recently, there has been increased interest in the use of tetracarboxylic acids in the synthesis of coordination materials.

In this study, we introduce a cyclobutane containing carboxylic dianhydride with no aromatic moieties. CBDAN-2 was synthesized from the direct photoreaction between maleic anhydride and benzene using inexpensive and safe commercially available blacklights. From previous works in our laboratory, it was realized that maleic

anhydride can be activated by both UV-A and B lights. It was therefore hypothesized that activated maleic anhydride could react with other olefin systems to form a carboxylic dianhydride.

Benzene is produced by both natural processes such as volcanic eruptions and forest fires and is a natural part of crude oil. It is widely used in the United States and ranks in the top 20 chemicals by production volume. Benzene can be synthesized from long chain fatty acids.<sup>81</sup> It can also be synthesized from lignin using RuW/HY30 as the multifunctional catalyst and water as the reaction medium.<sup>82</sup> Maleic anhydride is currently produced from the oxidation of benzene or butane. However, there has been increased interest in its production from the biomass with great success.<sup>24-27, 29, 59</sup> CBDAN-2 is potentially biomass derived. Phasing out nonrenewable sources for materials is farfetched, therefore, to reduce our reliance on nonrenewable sources of materials, we could begin with hybrid precursors consisting of both renewable and nonrenewable components.

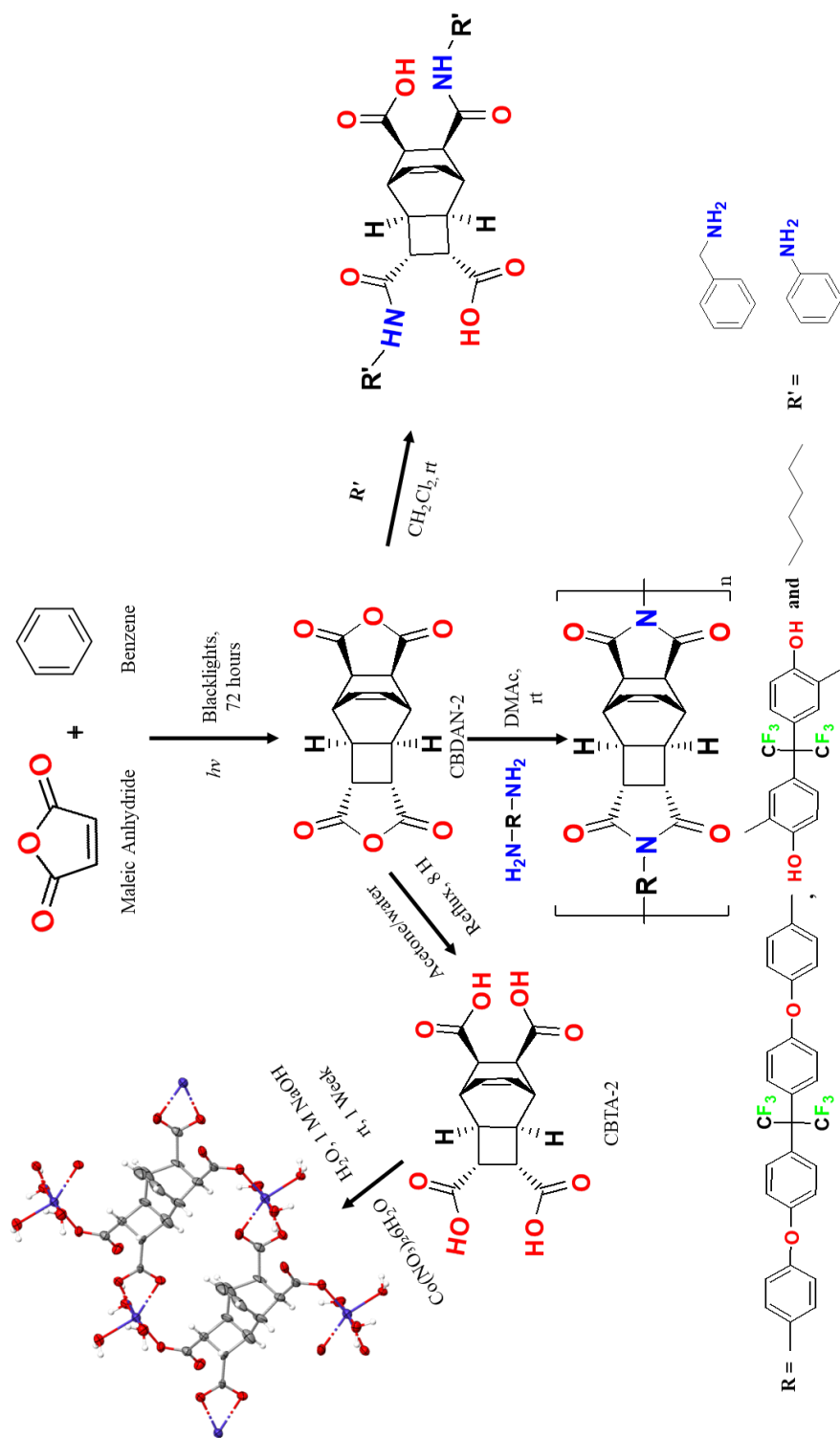
This aliphatic carboxylic dianhydride, CBDAN-2, presents a flexible molecule which could be used to synthesize polyimides with increased solubility and processibility.<sup>83,84</sup> Moreover, polyimides synthesized from aromatic carboxylic dianhydrides usually are colored, which has been attributed to the aromatic system.<sup>72, 73</sup> This limits their transparency and so they have limited uses in optical applications. CBDAN-2 has the possibility to reduce this coloration and might serve as an important precursor in optical materials applications.

CBDAN-2 can also be used as a polytopic ligand to synthesize a 2D metal-organic material using cobalt as the inorganic node. The metal-organic material synthesized from  $\text{Co}^{2+}$  and CBTA-2 could open a pathway for eventual utilization in the synthesis of metal-organic frameworks.<sup>46, 85, 86</sup> Moreover, CBDAN-2 can be converted to its dicarboxylic acid derivatives, which are important precursors in the synthesis of polyesters and other materials. CBDAN-2 has the potential to be a versatile building block in the synthesis of various materials. The goal of this study was to improve the synthetic procedure, investigate the stability and evaluate CBDAN-2 as a versatile precursor in material synthesis.

### **3.1. Results and Discussion**

CBDAN-2 was synthesized from maleic anhydride and benzene using low energy blacklights (Scheme 2). CBDAN-2 crystallized out from the solution reaching a 90 % reaction yield within 72 hours. Multiple groups have reported the synthesis of this molecule in literature, however, the previous methods have involved the use of high power lamps or photosensitizers.<sup>87, 88</sup> For example, Bryce-Smith used a Hanovia quartz immersion reactor with a 450-watt lamp and acetophenone, acetone or benzophenone as photosensitizers to synthesize photoreaction products using benzene or its derivatives with maleic anhydride.<sup>89</sup> Grovenstein and co-worker used a 1000-watt Hanovia mercury-arc lamp with or without acetone as a photosensitizer and achieved 10 – 15 % yields.<sup>90</sup>





**Scheme 18:** Synthesis and Applications of CBDAN-2 and its Derivatives

Photochemical reactions are not uncommon with aromatic systems, in fact several cases have been reported in literature such as in the production of photo dimer of anthracene and the transannular additions of oxygen to anthracene and higher polycyclic aromatic hydrocarbons to give e.g., photo-oxides.<sup>91, 92, 92, 93</sup> Photoaddition of maleic anhydride to anthracene promoted by ultraviolet irradiation has also been reported.<sup>94</sup> However, the photoaddition of maleic anhydride to benzene has no close parallel in thermal chemistry.<sup>95</sup> The product is a very stable 2:1-adduct. One would think it is possible to reverse the reaction via a reverse Diels-Alder. This is, however, not the case. As would be shown shortly, this adduct is very thermally and chemically stable.<sup>89, 93</sup>

The mechanism involved in the reaction between maleic anhydride and benzene is believed to occur via a two-step reaction.<sup>88, 90</sup> The first [2+2] photoaddition forms the cyclobutane ring and is followed by a Diels-Alder reaction forming the six-membered ring. It is widely known that benzene isomerizes to fulvene via the first optical transition, but it is believed that this isomerization is not associated with the mechanism of this reaction. Hypothetically, the reactions of benzene here would tie more with cyclohexatriene rather than a typical resonance stabilized benzene.<sup>88, 90</sup>

No photocyclization reaction was observed in the reaction between MAn and hexafluorobenzene. It is known that the substituents in olefins do not affect their [2+2] cycloaddition reactions.<sup>96</sup> Therefore, reaction between MAn and hexafluorobenzene would be possible. Nonetheless, the highly electronegative fluorine groups on the benzene, which forms a dienophile, would hinder a Diels-Alder reaction and so the product formation would be hindered. This experiment shed some light to confirm that

DA reaction is a possible mechanism for this reaction as has been previously thought. From previous research it is known that MAN can be sensitized using blacklights, and it was hypothesized that it would dimerize with benzene upon irradiation. Upon MAN sensitization, there would be a charge transfer to benzene, which in turn becomes activated and completes the reaction. Though this CBDAN-2 has been reported in literature, no application or further studies have been conducted on the molecule.

### 3.1.1. Description of CBDAN-2

Single crystal X-ray diffraction show that CBDAN-2 is monoclinic with the P 21/c space group. The oxygen on the furan rings on the CBDAN-2 dianhydride lie trans on the opposite site of the molecule and are 7.79 Å apart. This molecule planar giving it the potential to form linear chains of molecules, an attribute which makes it advantageous in synthesizing long chain high molecular weight polymers. Figure 17 shows the crystal structures of CBDAN in Oak Ridge Thermal Ellipsoid Plot (ORTEP) at the 50% probability level except for the hydrogen atoms and capped sticks style.

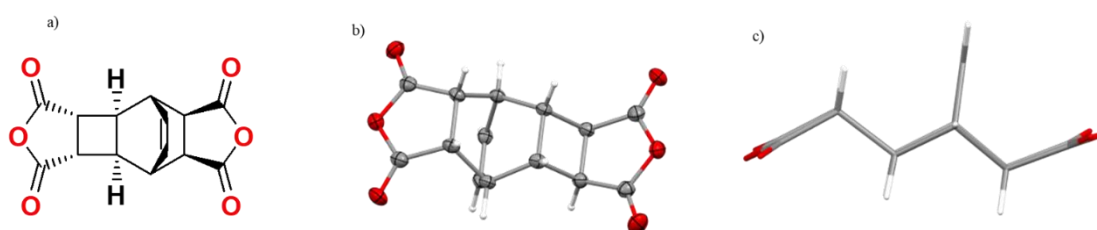


**Figure 17:** Chemical and crystal structure of CBDAN-2 represented in black and red, b) crystal structure of CBDAN-2 in Oak Ridge Thermal Ellipsoid Plot (ORTEP) at the 50% probability level except for the hydrogen atoms, c) CBDAN-2 shown in capped sticks style to highlight the flat nature of the molecule

### 3.1.2. Initial thermal studies on CBDAN-2 and CBTA-2

CBDAN-2 was stable on the laboratory bench for over a year. TGA showed that CBDAN-2 had its  $T_5$ ,  $T_{10}$  and  $T_d$  at 349 °C, 365 °C and 388 °C, respectively. CBDAN-2 starts losing weight at 308 °C and at 388 °C just 50 % of its weight was lost. TGA showed that CBTA-2 had its  $T_5$ ,  $T_{10}$  and  $T_d$  at 231 °C, 254, °C and 363 °C (Figure 18). CBTA-2 decomposes in two steps, the first decomposition corresponds to the loss of water while the second results from the decomposition of the resulting dianhydride. CBTA-2 starts showing a weight loss of about 218 °C due to removal of two molecules of H<sub>2</sub>O (calcd.: 11.6 %). This shows that the cyclobutane ring in both CBDAN-2 and CBTA-2 is thermally stable. These initial thermal studies show that both precursors are thermally stable enough and could therefore, serve as precursors in synthesis polymers and materials.<sup>97</sup>

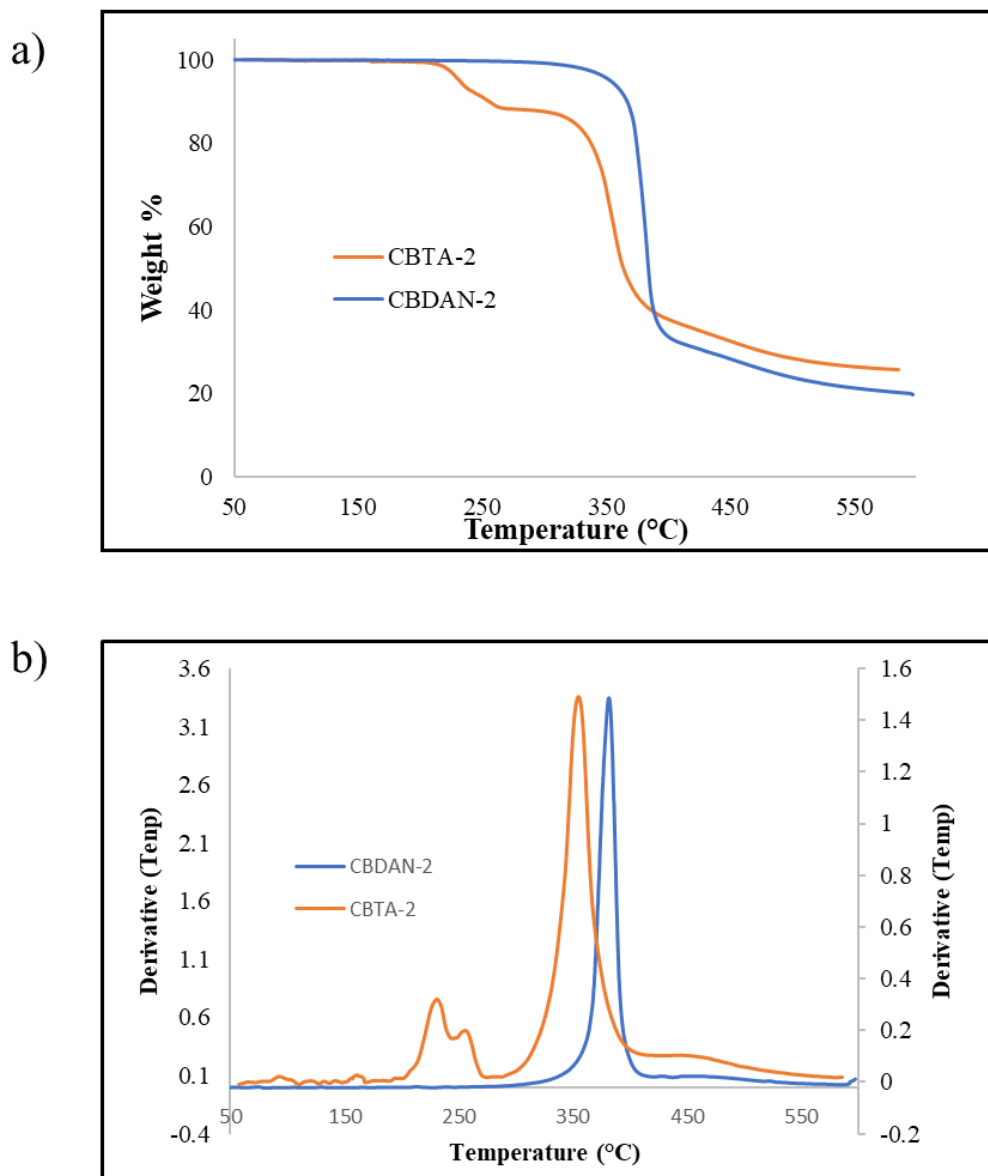


**Figure 18:** TGA and DTG curves of CBDAN-2 and CBTA-2; **(a)** TGA curves recorded from 50 °C to 600 °C with a heating rate of 20 °C·min<sup>-1</sup> under N<sub>2</sub> atmosphere. **(b)** DTG curves recorded from 50 °C to 600 °C with a heating rate of 20 °C·min<sup>-1</sup> under N<sub>2</sub> atmosphere.

### 3.1.3. Synthesis of Imide and Polyimides

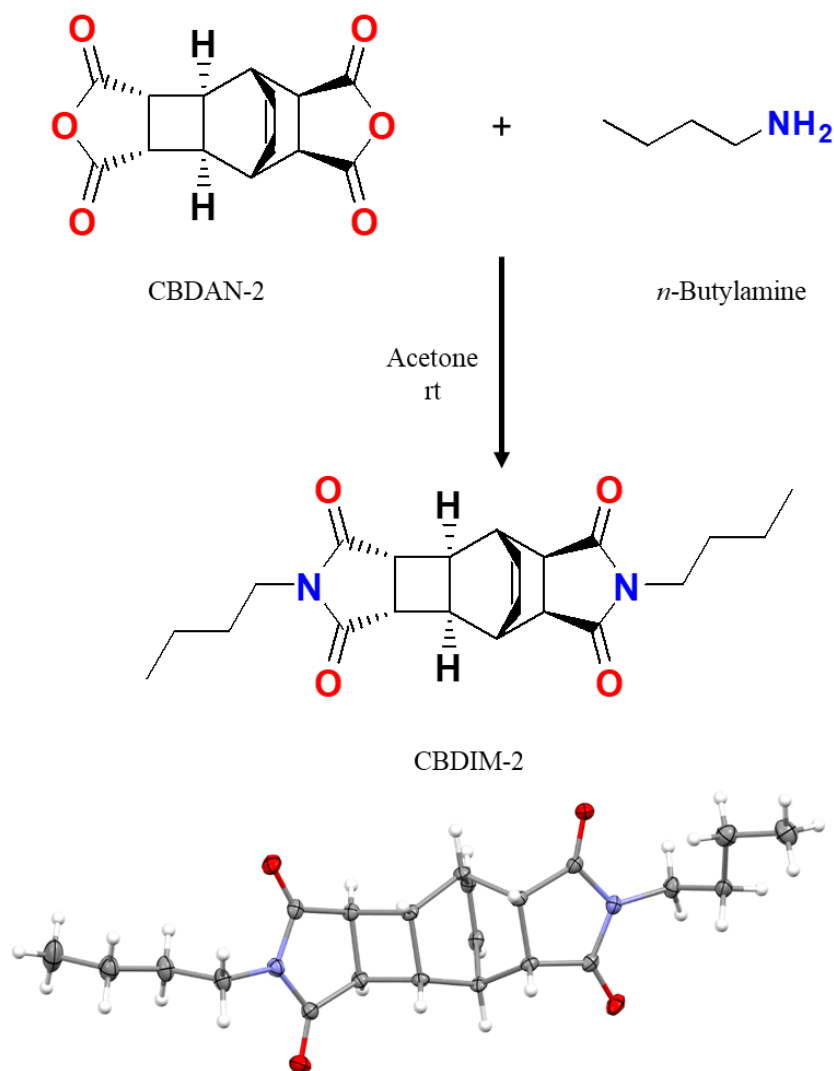
The imide and polyimides were synthesized using the two-step traditional polyimide synthesis method.<sup>71</sup> The first step involves the synthesis of the -amic (or -polyamic)

acid (AA or PAA respectively) and the second step is the thermal cyclocondensation.<sup>45,</sup>  
<sup>98</sup> Upon reaction with the diamine, the anhydride carbonyl is attacked and the ring opening occurs.<sup>77</sup> A linear chain polymer is formed from the link between a diamine and a dianhydride. The polyamic acid formed is usually a mixture of products, however, upon ring closing in the cyclocondensation step, a single polymer product is formed.<sup>78</sup> The polyamic acids are usually more soluble and easily processible, nonetheless when the ring is closed to form the polyimide, the solubility of the resulting polymer decreases significantly.<sup>78</sup>

The reaction between CBDAN-2 and *n*-butylamine was used as a model reaction to understand the reaction to form the polyamic acid and subsequent cyclocondensation (Scheme 3). Reaction of CBDAN-2 and *n*-butylamine formed a mixture of products as shown by the <sup>1</sup>H NMR spectra. However, after this imide was cyclized by heating in an oven first at 80 °C for 1 hour, then at 120 °C for 1 hour and finally 200 °C for 3 hours, <sup>1</sup>H NMR spectra showed a single product of the imide formed. X-ray crystals of the imide were grown in methanol and the structure revealed a single product, imide, as hypothesized. The rationale for developing this model compound was to show the formation of the imide. The FT-IR absorption of the imide in the model compound will be similar to that in polyimides synthesized from CBDAN-2. This can then be used to compare to the synthesized insoluble polyimides thus helping in their characterization. Also, the model reaction showed that CBDAN-2 could be used as a monomer for polymer synthesis. This model reaction was also used to confirm the two-step

polyimides synthesis. The IR spectra of synthesized polyimides with CBDAN-2 were then compared to those of the model

The chemical structures of the polyimides were confirmed by FT-IR spectra (Figure 19). All the polyimides exhibited absorptions around 1712 and 1687  $\text{cm}^{-1}$  (imide C=O asymmetric and symmetric stretching), 1765  $\text{cm}^{-1}$  ( $\text{sp}^2$  C=C stretching) and 2931  $\text{cm}^{-1}$  ( $\text{sp}^3$  C-H stretching). Moreover, the trifluoromethyl C-F stretching appeared at 1243 and 1248  $\text{cm}^{-1}$  in the FT-IR spectra of polymers PI and PII, respectively. The results demonstrated that the polyimides have the expected chemical structures. Molecular weights of polyimides could not be obtained because of their insolubility in common organic solvents. However, an oligomer of P-I was isolated, and the molecular weight was measured to be 5127  $\text{g mol}^{-1}$  (Table 9). Figure 20 shows a thin film synthesized from P-I and P-III.





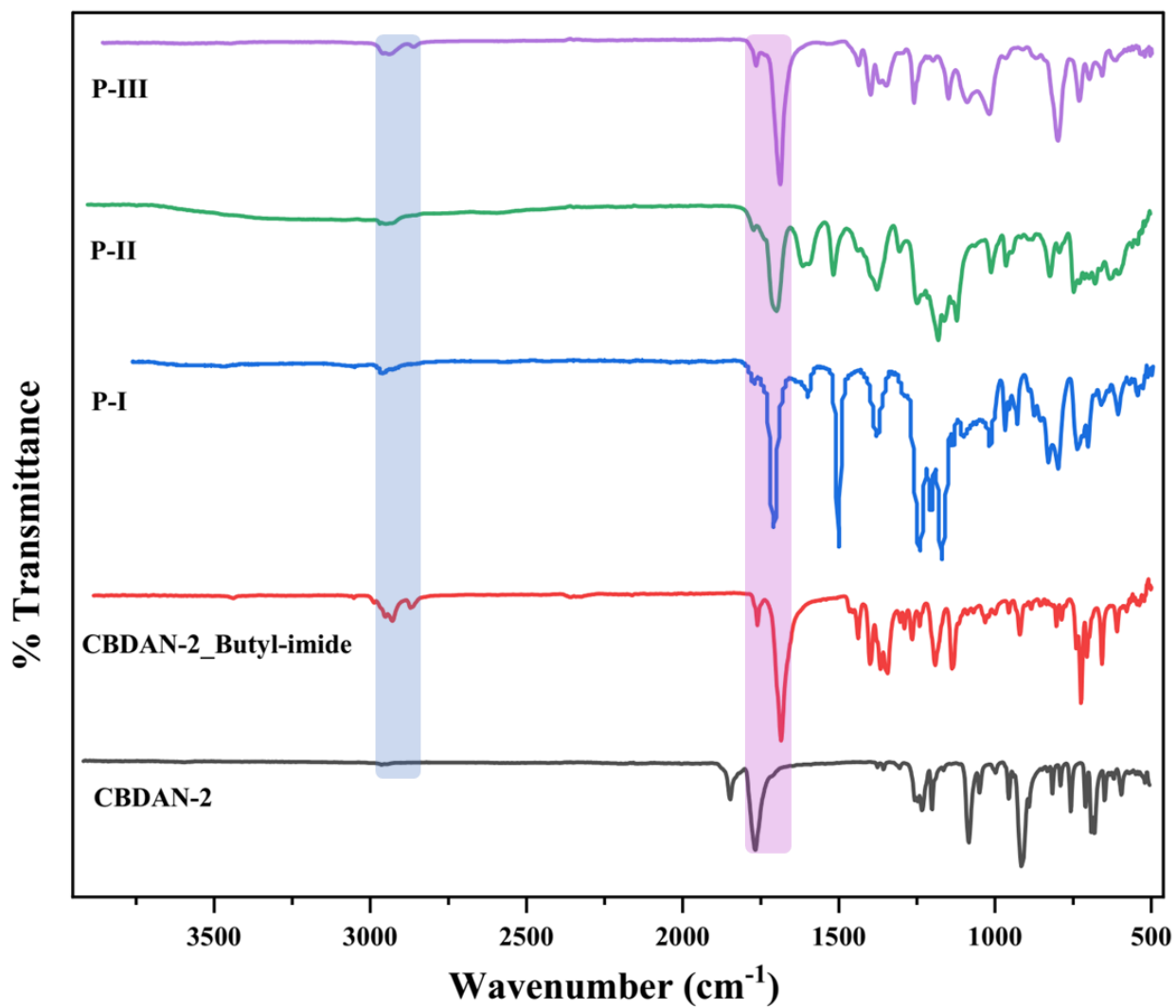


**Figure 19:** FT-IR spectra of P-I, P-II, and P-III for comparison with CBDAN-2 and the model compound (CBDAN-2\_*n*-butylimide).



Polyimide -I



Polyimide -III

**Figure 20:** Images of the synthesized P-I and P-III respectively.

### 3.1.4. Thermal Stability of Polyimides

The thermal properties of the polyimides were evaluated by TGA. The polyimides exhibited excellent thermal stability with the onset decomposition temperatures,  $T_5$  and the temperatures at 10 % of weight loss  $T_d$  in a range of 136 - 179 °C and 262 - 300 °C in nitrogen, respectively (Figure 21). The polyimides did not show obvious weight loss before the scanning temperature reached up to 400 °C in nitrogen, indicating that no thermal decomposition occurred (Table 8). The residual weight retentions at 700 °C for all but one of the polyimides were higher than 40 %. P-II exhibited much higher decomposition temperature than the other polyimides. The higher thermal stability of P-II can be explained by its high rigidity.

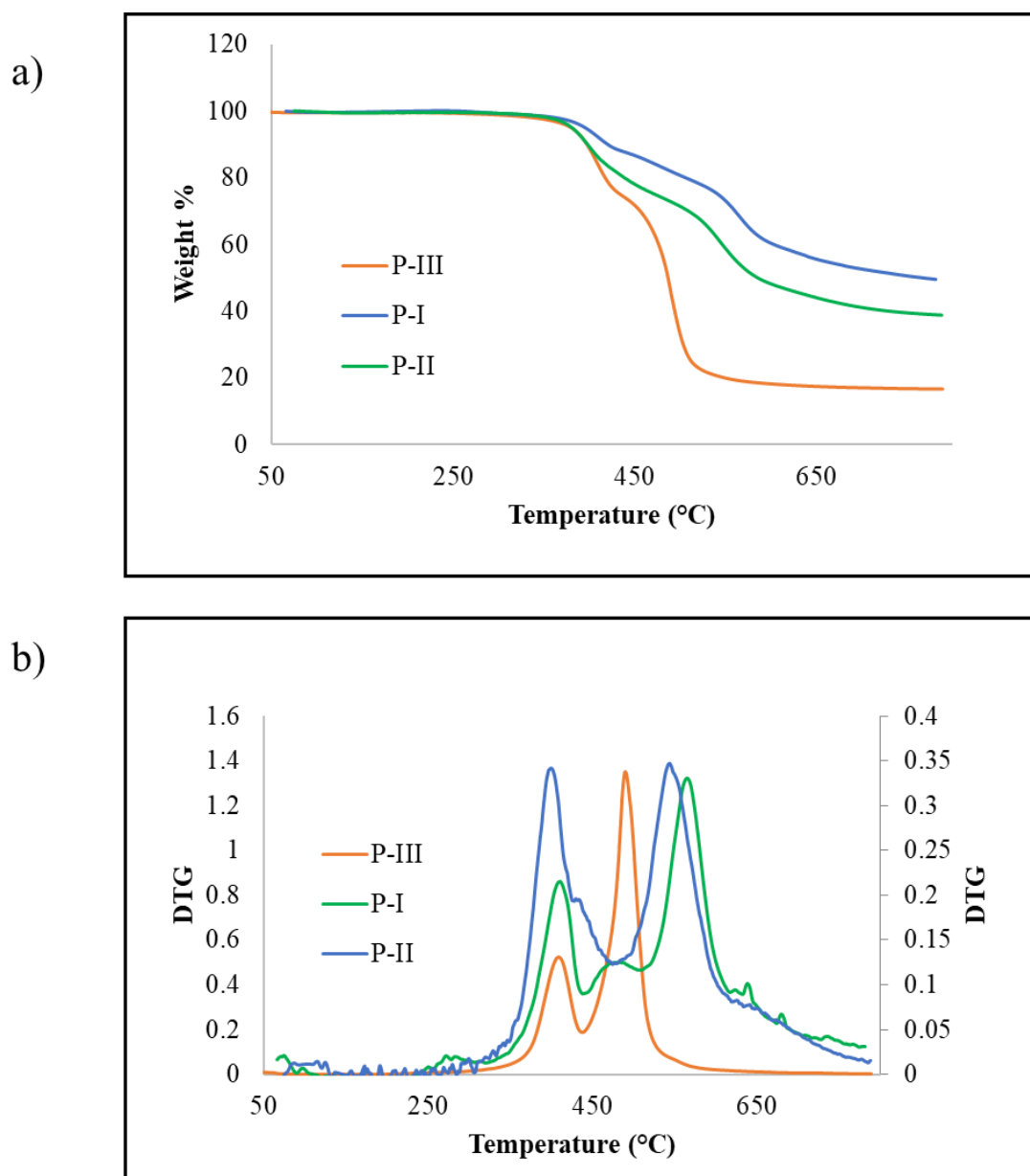


**Figure 21:** TGA and DTG curves of polymers made from CBDAN-2; (a) TGA curves recorded from 50 °C to 600 °C with a heating rate of 20 °C·min<sup>-1</sup> under N<sub>2</sub> atmosphere. (b) DTG curves recorded from 50 °C to 600 °C with a heating rate of 20 °C·min<sup>-1</sup> under N<sub>2</sub> atmosphere.

**Table 8:** Thermogravimetric analysis of polymers

<b>Thermogravimetric analysis (TGA)</b>			
<b>Sample</b>	<b>T<sub>5</sub></b>	<b>T<sub>10</sub></b>	<b>T<sub>d</sub></b>
<b>P-I</b>	384	397	740
<b>P-II</b>	380	397	591
<b>P-III</b>	380	397	486

**Table 9:** Molecular weight distribution of polyimides from GPC

<b>Molecular Weight Distribution (GPC)</b>			
<b>Sample</b>	<b>Mn (g mol<sup>-1</sup>)</b>	<b>Mw (g mol<sup>-1</sup>)</b>	<b>Polydispersity Index (Mw/Mn)</b>
P-I	2,858	5,127	1.794

### 3.1.5. Synthesis of CBTA-2

CBTA-2, the tetracarboxylic acid derivative of CBDAN-2 was synthesized to make metal-organic materials thereof. The synthesis of CBTA-2 was carried out by hydrolyzing CBDAN-2. Hydrolysis of CBDAN-2 to CBTA-2 was completed after 6 hours when CBDAN-2 was refluxed in a mixture of 3:1 water/ethyl acetate to give pure CBTA-2 with a yield of > 96 %. The synthesis was also completed under reflux in a 1.0 M aqueous solution of NaOH after precipitation from the solution using HCl.

### 3.1.6. Synthesis of a Cobalt - CBTA-2 Coordination Complex

The several electron rich oxygen moieties on tetracarboxylic acids makes them suitable multidentate ligands in coordination chemistry.<sup>97, 99, 100, 44, 76, 79, 101</sup> Metal-organic frameworks (MOFs) are a class of functional coordination nano-porous materials with well-structured frameworks, large surface area, and high stability.<sup>102</sup> Attention in MOF

synthesis have increased in recent years due to the increased interest in gas capture and storage, heterogeneous catalysis, proton conductivity, energy storage, and environmental protection.<sup>101, 80, 103</sup> The multiple electron rich oxygens in CBTA-2 make it attractive as a polytopic ligand in MOF synthesis.

To evaluate the potential of CBTA-2 for MOF synthesis, a metal-organic material was synthesized with  $\text{Co}(\text{NO}_3)_2 \cdot 6\text{H}_2\text{O}$ . The synthesized complex was characterized by FT-IR and crystallography. The FT-IR spectra of CBTA-2 and Co-CBTA-2 complex is shown in Figure 22. The spectra showed strong bands at  $1575 \text{ cm}^{-1}$  and  $1721 \text{ cm}^{-1}$  in the spectra of the complex and CBTA-2, respectively. This signal is characteristic to the carbonyl stretching of the carboxylic acid in both molecules. The signals could be explained by the fact that each of the two carbonyls trans to each other on CBTA-2, coordinate with different metal centers while the other does not. The other two acid groups in CBTA-2 ligand are deprotonated in the complex. The peaks at  $1345$  and  $1437 \text{ cm}^{-1}$  in the spectrum of the complex are attributed to symmetric and asymmetric stretching of the carboxylate anion, respectively, since both carboxylic acid groups of CBTA-2 are deprotonated in the complex.

In comparison, the signals at  $1721$  and  $1406 \text{ cm}^{-1}$  in the CBTA-2 spectrum represent the carbonyl and carboxylate stretching, respectively. The absorption at  $1770$  and  $1738 \text{ cm}^{-1}$  in CBTA-2 and the complex, respectively, represents the olefin bridge on the cyclohexane ring. Meanwhile, the absorption at  $3508 \text{ cm}^{-1}$  indicates the presence of coordinated  $\text{H}_2\text{O}$  molecules in the complex, which is consistent with its single crystal

X-ray structure. Also, the broad absorption between 3300 and 2500  $\text{cm}^{-1}$  on CBTA-2 represents the carboxylic acid hydroxyl stretching.

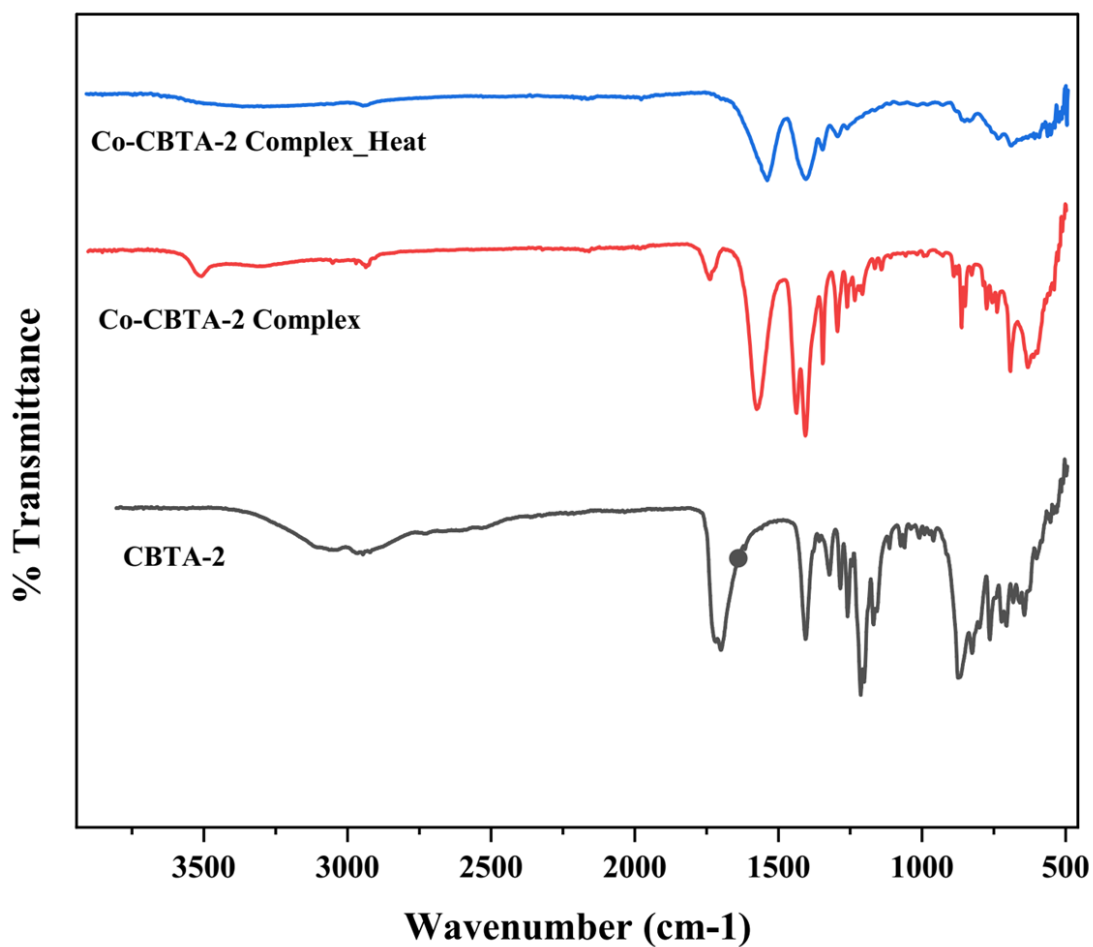


**Figure 22:** FT-IR spectra of CBTA-2 and Co-CBTA-2 complex (heated and unheated)

### 3.1.7. Description of Co-CBTA-2 Complex

The pink crystals of Co-CBTA-2 are monoclinic with the Pn space group. Single crystal X-ray diffraction analysis revealed that the ratio of Co: CBTA-2:  $\text{H}_2\text{O}$  in the Co-CBTA-2 complex is 2:1:6. Figures 23 and 24 show the asymmetric unit of Co-CBTA-2 complex in Oak Ridge Thermal Ellipsoid Plot (ORTEP). It can be observed that a

double stranded 2D coordination complex is formed between the  $\text{Co}^{2+}$  and CBTA-2. The  $\text{Co}^{2+}$  forms the backbone of the complex while the CBTA-2 forms the connections between two backbones. CBTA-2 links one backbone to the next and so the series continues. The  $\text{Co}^{2+}$  adopts an octahedral geometry with two CBTA-2 molecules interacting with the metal cation in the equatorial basal plane while the three  $\text{H}_2\text{O}$  molecules occupy the two opposite axial and one equatorial positions. The  $\text{O}-\text{Co}^{2+}-\text{O}$  angle of  $\text{Co}^{2+}$ , and  $\text{H}_2\text{O}$  is  $165.41(10)^\circ$  and the  $\text{O}-\text{Co}^{2+}$  distances are  $2.058(8)$  and  $2.146(7)$  Å, respectively.

The two carbonyls trans to each other, coordinate with the metal occupying the equatorial basal plane of the octahedral while the other does not. The two acid groups in CBTA-2 ligand are deprotonated in the complex balancing the charges and occupy the equatorial basal plane of the octahedral. The  $\text{O}^--\text{Co}^{2+}-\text{O}^-$  angle is  $45.32(10)^\circ$  and the two  $\text{O}^--\text{Co}^{2+}$  bond distances are  $2.058(8)$  and  $2.146(9)$  Å, respectively.

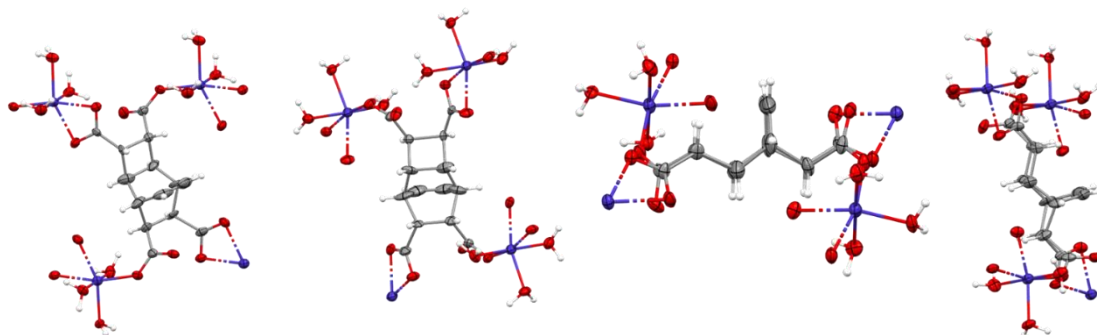


**Figure 23:** Symmetric unit of Co-CBTA-2 Complex in Oak Ridge Thermal Ellipsoid Plot (ORTEP) at the 50% probability level except for the hydrogen atoms; the octahedral  $\text{Co}^{2+}$  center interacts with two CBTA-2 molecules, and three  $\text{H}_2\text{O}$  molecules. Top, face, and side view of a single unit of Co-CBTA-2 complex shown.

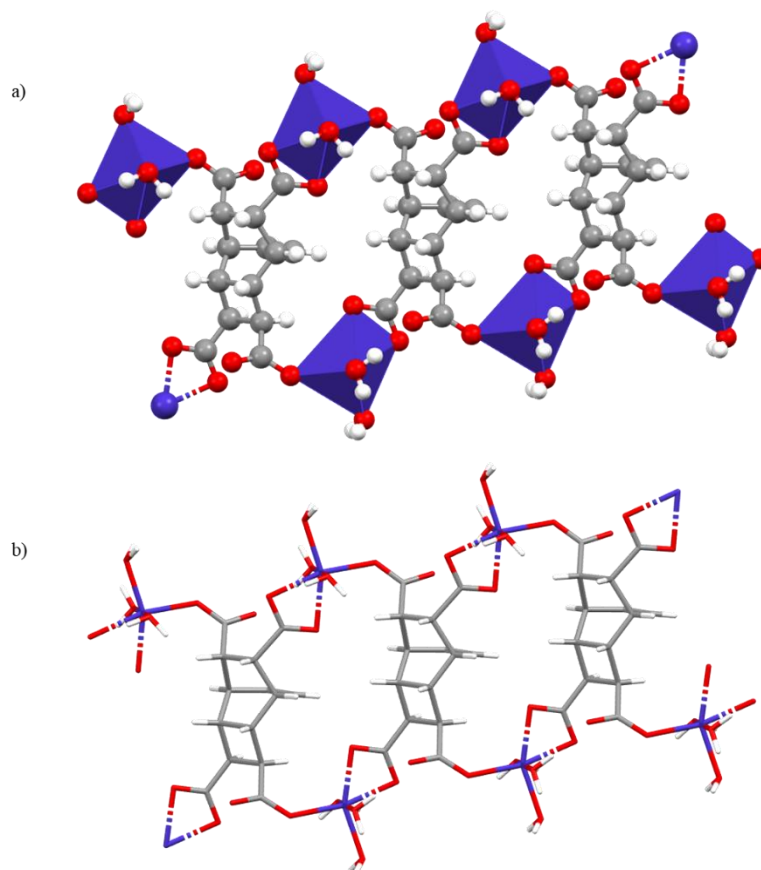


**Figure 24:** Side view of the Co-CBTA-2 complex shown in polyhedral style; b) Side view of the 2D Co-CBTA-2 complex shown in capped sticks style.

### 3.1.8. Thermochromic Properties

The cobalt complex synthesized from CBTA-2 showed interesting thermochromic properties. When heated to 200 °C for 1 hour in an oven, the pink colored complex crystals turned into purple, probably due to the loss of water from the complex.<sup>104</sup> A comparison of the complex appearance at room temperature and after the thermal exposure is shown in Figure 25. The purple color of the complex did not change when the sample was exposed to room temperature and to air for a month. It is known that color changes of metal complexes because of temperature variation are mainly caused



by solid-solid phase transitions due to changes in metal coordination geometry, coordination number, and/or the coordinated ligands.<sup>46, 104</sup>

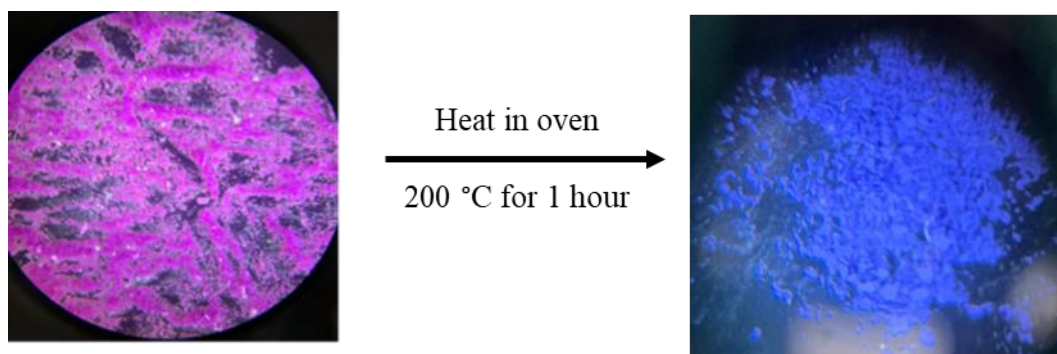


**Figure 25:** Thermochromic behavior of Co-CBTA-2 complex

### 3.1.9. Initial Thermal Properties of Co-CBTA-2 Complex

The thermogravimetric analysis of Co-CBTA-2 complex with or without a heating pretreatment under a nitrogen atmosphere at a heating rate of 20 °C/min and the corresponding DTG curves are shown in Figure 26. For comparison, the thermal decomposition profile of CBTA-2 is reported in Figure 18. The thermal decomposition of CBTA-2 shows no degradation below 220 °C. According to the TGA profile in Figure 26a (pink curve), the complex undergoes decomposition in three stages. The complex starts showing a weight loss of about 2.9 % due to removal of one molecule of coordinated H<sub>2</sub>O (calcd.: 2.9 %) in the crystalline sample around 103 °C. The complex then successively loses two more molecules of H<sub>2</sub>O at about 212 °C (calcd.: 7.2 %). At around 406 °C, the complex starts to lose weight in parallel with the heated complex.

The complex had its  $T_{10}$  and  $T_d$  at 262 °C and 543 °C, respectively. To experimentally demonstrate the loss of water during heating, the purple crystals which were obtained from heating the Co-CBTA-2 complex as previously described were subjected to TGA analysis. The data is shown in Figure 26 (blue curve), where it shows that the complex does not lose weight until 409 °C. At this temperature the unheated Co-CBTA-2 complex had lost the final water molecule and had a degradation pattern similar to the heated sample. The DTG plot (Figure 26b) also shows a peak at this temperature where the peaks of heated and unheated samples almost align. The thermal analysis results indicated that Co-CBTA-2 has good thermal stability which is required for MOF synthesis.<sup>43, 100</sup>

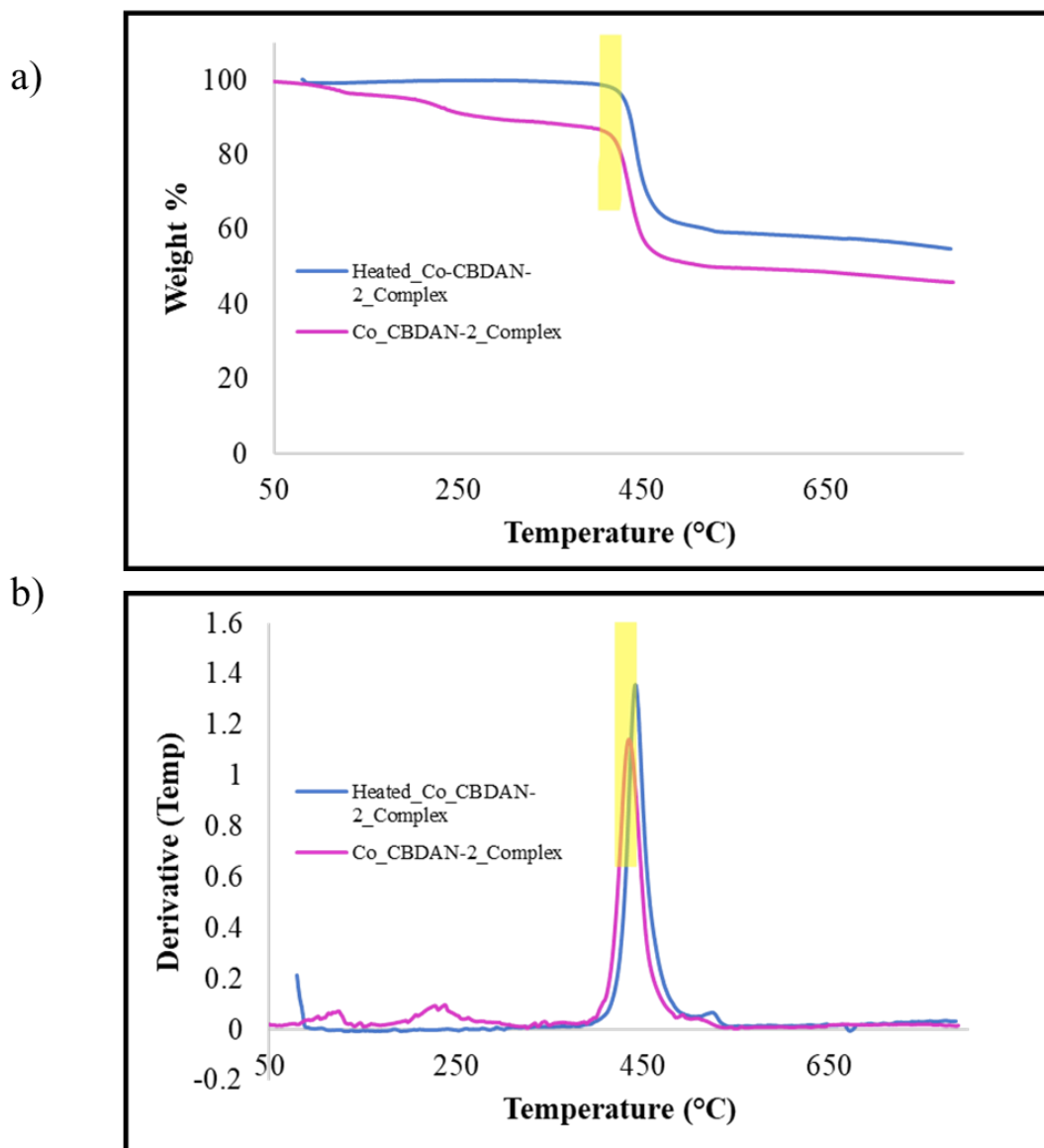


**Figure 26:** TGA and DTG curves of Co-CBTA-2 complex (heated and unheated); (a) TGA curves recorded from 50 °C to 600 °C with a heating rate of 20 °C·min<sup>-1</sup> under N<sub>2</sub> atmosphere. (b) DTG curves recorded from 50 °C to 600 °C with a heating rate of 20 °C·min<sup>-1</sup> under N<sub>2</sub> atmosphere.

### 3.1.10. Synthesis of Cyclobutane-containing Diacids from CBDAN-2

CBDAN-2 has already been shown to be a versatile building block in material synthesis. To further show its potential in material synthesis, two cyclobutane-

containing diacids (CBDAs) were synthesized from CBDAN-2. The CBDAs were synthesized from the reaction of CBDAN-2 and benzylamine or aniline. The synthesis of CBDAs from CBDAN-2 followed a general pattern. Briefly, nucleophiles readily reacted with the dianhydride yielding the diacids. The order of reactivity of amines was  $1^\circ > 2^\circ$ . The  $1^\circ$  amines reacted upon addition to the mixture and the reaction completed within minutes. Based on our previous knowledge, a solvent in which CBDAN-2 had low solubility was selected for the reactions. The goal was to reduce solubility and slow the reaction in such a way that as soon as CBDAN-1 dissolves in the solvent, the nucleophile reacts instantaneously and the trans product is favored.

### 3.2. Conclusion

An aliphatic carboxylic dianhydride monomer with cyclobutane ring was synthesized from biomass derived chemicals. This monomer was characterized and used to synthesize cyclobutane containing polyimides with 2,2-bis[4-(4-aminophenoxy)phenyl]hexafluoropropane, 2,2-bis(3-amino-4-hydroxyphenyl)hexafluoropropane and hexane-1,6-diamine. Heavy molecular weight polyimides were difficult to fully characterize due to their poor solubility in conventional solvents, as such a model imide between CBDAN-2 and *n*-butylamine was synthesized. The model imide was used to confirm the successful synthesis of the polyimides and to confirm the presence of the cyclic imide bond. The imide was synthesized using a typical two-step process of synthesizing polyimides, i.e., through a polyamic acid and then cyclocondensation (imidization). The synthesized polyimides showed interesting characteristics such as high thermal and chemical resistance.

CBDAN-2 was shown to be a versatile intermediate in material synthesis. This was done by making derivatives of CBDAN-2 with potential in material synthesis. CBDAN-2 was successfully converted to CBTA-2. CBTA-2 was then used to successfully synthesize a metal-organic material with  $\text{Co}(\text{NO}_3)_2 \cdot 6\text{H}_2\text{O}$ . The metal-organic material showed desired properties such as good thermal resistance and interesting thermochromic attributes. To further emphasize the versatile nature of CBDAN-2, a couple of cyclobutane-containing dicarboxylic acids (CBDAs) were synthesized using aniline and benzylamine. These dicarboxylic acids could be used in the synthesis of polyesters.

### **3.3. Experimental Section**

#### **3.3.1 Chemicals and measurements**

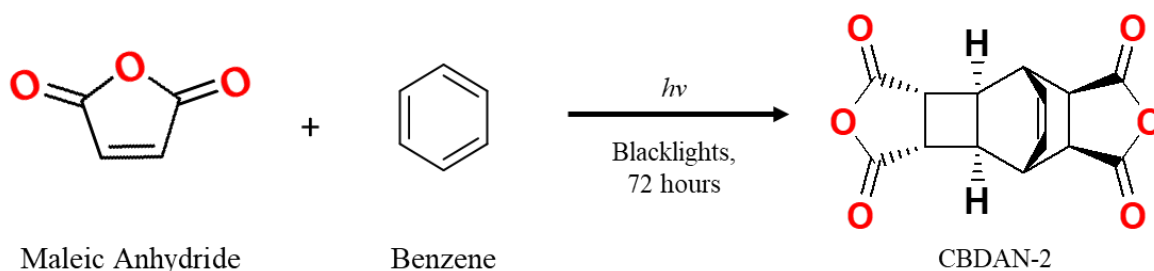
All chemicals were purchased from Alfa Aesar, Sigma-Aldrich, or Acros, and used without further purification. Blacklight used in the photoreaction was Fiet Electric 7-watt LED bulb or 15W Eiko EK15526 F15T8/BL. The solution phase nuclear magnetic resonance spectra (NMR) were recorded with Bruker AVANCE ( $^1\text{H}$ : 500 MHz,  $^{13}\text{C}$ : 125 MHz). Proton and carbon chemical shifts were reported in ppm downfield from tetramethyl silane (TMS) and were expressed in part per million. Spin-spin coupling constants,  $J$ , are given in Hz. Spectra were recorded in  $\text{DMSO-d}_6$  unless otherwise stated. Single crystals of CBDAN-2 precipitated out of solution and were used as such for x-ray analysis. Single crystals of CBTIM-2 were grown by dissolving it in methanol and slowly evaporating the solvent. Single crystal X-ray data were collected on a Bruker Kappa Apex II Duo X-Ray Diffractometer with  $\text{Cu } K\alpha$  ( $\lambda = 1.54178 \text{ \AA}$ ). Infrared

spectroscopy (IR) was conducted on a Thermo Scientific Nicolet iS5 FT-IR spectrometer. Differential scanning calorimetry (DSC) was conducted on a Perkin Elmer Jade DSC with a ramping rate of 20 °C min<sup>-1</sup> under nitrogen protection. Heat flow was recorded from both the first heating and cooling curve. Thermogravimetric analysis (TGA) was carried out with a Hi-Res TGA Q500 from TA Instruments using alumina pans at a heating rate of 20 °C min<sup>-1</sup> under nitrogen with a sample weight of about 10 mg. Gel Permeation Chromatography (GPC) samples were analyzed using a GPC system (EcoSEC HLC-8320GPC, Tosoh Bioscience, Japan) with a differential refractometer (DRI) detector. Separations were performed using two TSKgel SuperH3000 6.00 mm ID× 15 cm columns with an eluent flow rate of 0.35 mL min<sup>-1</sup>. The columns and detectors were thermostated at 40 °C. The eluent used was tetrahydrofuran (THF). Samples were prepared at about 10 mg mL<sup>-1</sup> in the eluent and allowed to dissolve at ambient temperature for several hours. Samples were filtered through 0.2 µm filters and the injection volume was 40 µL for each sample. Calibration was conducted using PS standards (Agilent EasiVial PS-H 4mL).

### **3.3.2. Synthesis of tricyclo[4.2.2.0<sup>2,5</sup>]dec-7-ene-3,4,9,10-tetracarboxylic dianhydride (CBDAN-2) from benzene and maleic anhydride**

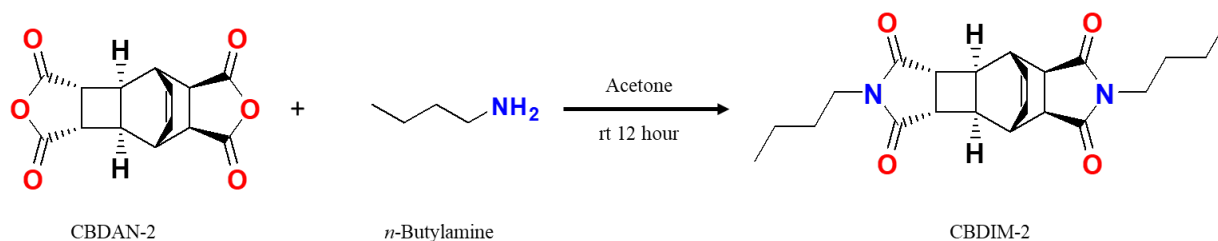
CBDAN-2 was prepared by dissolving 0.5 g (5 mmol) of MAn in 20 mL of benzene in a 20 mL cornil vial and irradiated between four black lights for 72 hours. The bulbs were placed two on each side of the cornil flask. Crystals of CBDAN-2 grew in the vial as the reaction proceeded. After 72 hours, the crystals were scrubbed out, washed with ethyl acetate, and dried at room temperature for residual solvent to evaporate. About

0.56 g of CBDAN-2 (41 %) were obtained. The product was characterized using  $^1\text{H}$  and  $^{13}\text{C}$  NMR, FT-IR spectroscopy, and X-ray crystallography. The melting point was shown to be  $356\text{ }^\circ\text{C}$ .  $^1\text{H}$  NMR  $\delta$  (ppm): 6.45 (d,  $J = 5$ , 2H,  $\text{CH}=\text{CH}$ ), 3.20 - 3.29 (m, 4H,  $\text{CH}$ -cyclobutane), 2.84 - 2.89, (m, 4H,  $\text{CH}$ -cyclobutane).  $^{13}\text{C}$  NMR  $\delta$  (ppm): 174, 173 (C=O), 133 (C=C), 42, 42 (cyclobutane), 38, 34 (cyclohexane). FT-IR (solid)  $\bar{\nu}_{\text{max}}$  ( $\text{cm}^{-1}$ ): 2957 (aliphatic  $\text{sp}^2$  C-H), 1849 (C=C), 1771 (acid anhydride C=O).



**Scheme 20:** Synthesis of CBDAN-2

### 3.3.3. Synthesis of 5,12-Dibutyl-5,12-diazapentacyclo[7.5.2.0<sub>2</sub>,8.0<sub>3</sub>,7.0<sub>10</sub>,14]hexadec-15-ene-4,6,11,13-tetrone (CBTIM-2) from CBDAN-2.



**Scheme 21:** Synthesis of CBDIM-2

CBTIM-2 was synthesized from CBDAN-2 and *n*-butylamine through a condensation reaction. A paste of CBDAN-2 with a solid content 15 % wt was prepared by placing

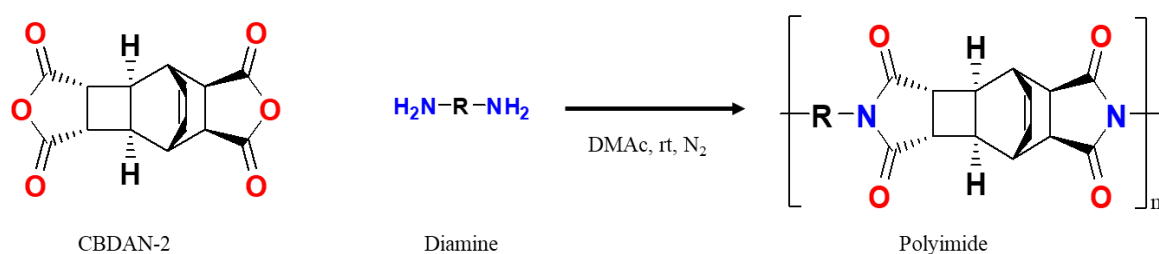
one gram of CBDAN-2 in 10 mL of acetone in a 100 mL three-neck flask equipped with a nitrogen inlet/outlet, and a mechanical stirrer. A sample of 360  $\mu$ L n-butylamine was dropwise added to the flask. The reaction mixture was stirred at room temperature for 12 h under N<sub>2</sub> protection. The AA formed precipitated out of the solution. The solvent was removed from the precipitate formed by heating at 80 °C for an hour. The product obtained was essentially pure and needed no further purification. The precipitate was heated at 100 °C for an hour then 120 °C for an hour and finally at 180 °C for 12 hour yielding pure CBTIM-2. <sup>1</sup>H NMR  $\delta$  (ppm): 6.22 (t, *J* = 5, 10, 2H, CH=CH) 3.29 (q, *J* = 5, 15, 4H, CH-cyclobutane) 3.20 (q, *J* = 5, 15, 2H, CH-cyclohexane) 2.44 - 2.77 (m, 2H) 1.37 - 1.43 (m, 2H) 1.28 - 1.31 (m, 2H) 1.26 - 1.27 (m, 2H) 1.20 - 1.22 (m, 2H) 1.09 - 1.16 (m, 6H, 2xCH<sub>3</sub>) ppm. <sup>13</sup>C NMR  $\delta$  (ppm): 178.42 177.87 131 (C=C), 41, 40 (CH-cyclobutane) 37, 37, 34, (CH-cyclohexane), 29, 29 (CH<sub>2</sub>), 19, 19 (CH<sub>2</sub>), 13, 13 (CH<sub>3</sub>). FT-IR (solid)  $\bar{\nu}_{\max}$  (cm<sup>-1</sup>): 2929 (aliphatic sp<sup>2</sup> C-H), 1760 (C=C), 1685 (carbonyl C=O).

#### **3.3.4. General synthesis of polyimides from CBDAN-2.**

Polyimides were synthesized from CBDAN-2 and diamines through a polycondensation reaction. A paste of CBDAN-2 with a solid content 15 % wt was prepared by placing 3.6 mmol of CBDAN-2 and 3.6 mmol of the appropriate diamine in 8 mL of DMAc in a 100 mL three-neck flask equipped with a nitrogen inlet/outlet, and a mechanical stirrer. The reaction mixture was stirred at room temperature for 24 h under N<sub>2</sub> protection for 2 hours and then vacuum until a viscous polyamic (PAA) solution was formed. The viscous solution was cooled and added to methanol to

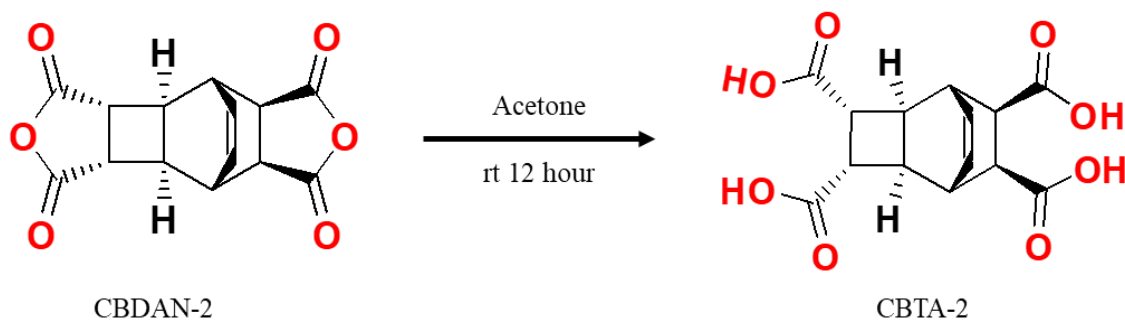


precipitate the PAA formed. The precipitate was further washed three times in a 1:1 solution of methanol/water. The solvent was removed from the product by heating at 80 °C for an hour. The product was then heated at 120 °C for an hour then at 200 °C for an hour and finally at 280 °C for 24 hours yielding the polyimide. The yield of this polyimide was 82.2 %.



**Scheme 22:** General method for synthesis of polyimides

### 3.3.5. Synthesis of tricyclo[4.2.2.0<sub>2,5</sub>]dec-7-ene-3,4,9,10-tetracarboxylic acid (CBTA-2) from CBDAN-2



**Scheme 23:** Synthesis of CBTA-2

#### Method I:

CBDAN-2 (1.02g, 2.80 mmol) was added to a 50 mL mixture of water and ethyl acetate (3:1) in a round bottom flask. The mixture was stirred under reflux for 6 hours.

CBDAN-2 dissolves in water and was converted to CBTA-2. After 6 hours, the solution was filtered, and the water/ ethyl acetate evaporated using a rotavapor leaving the white product which is essentially pure. About 1.00 g of CBTA-2 (> 96 %) was obtained. The product was characterized using  $^1\text{H}$  and  $^{13}\text{C}$  NMR, FT-IR spectroscopy, and X-ray crystallography.

### **Method II:**

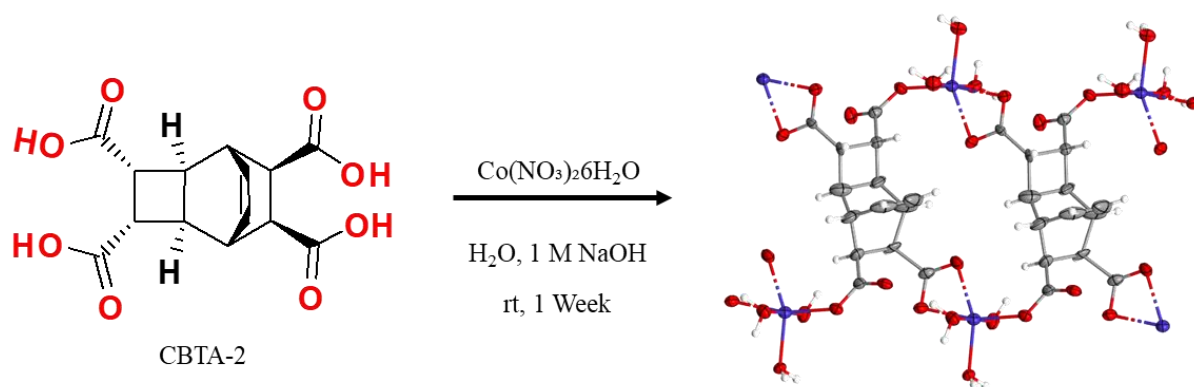
CBDAN-2 (1.00g, 2.80 mmol) was added to a 50 mL solution of 1.0 M NaOH in a round bottom flask. The mixture was stirred under reflux for 2 hours. CBDAN-2 dissolves in the solution and is converted to CBTA-2. After 2 hours, the solution was filtered, and HCl was added dropwise to precipitate the product out of solution. The slightly brown product, which was essentially pure, was isolated with no further purification needed. About 0.90 g of CBTA-2 (> 90 %) is obtained. The product was characterized using  $^1\text{H}$  and  $^{13}\text{C}$  NMR, FT-IR spectroscopy, and X-ray crystallography. The melting point was measured to be 242 °C.

$^1\text{H}$  NMR  $\delta$  (ppm): 12.01 (s, 4H, COOH) 6.31 (d,  $J = 5$ , 2H,  $\text{CH}=\text{CH}$ ), 2.80 – 2.89 (m, 4H,  $\text{CH}$ -cyclobutane), 2.60 - 2.63 (m, 4H,  $\text{CH}$ -cyclohexane).  $^{13}\text{C}$  NMR  $\delta$  (ppm): 173, 173 (COOH), 132 (C=C), 45, 41 ( $\text{CH}$ -cyclobutane), 38, 36 ( $\text{CH}$ -cyclohexane). FT-IR (solid)  $\bar{\nu}_{\text{max}}$  ( $\text{cm}^{-1}$ ): 3300/2700 (carboxylic acid OH), 2966 (C-H), 2364 (C=C stretch), 1733/1704 (carboxylic acid C=O).

### **3.3.6. Synthesis of Co-CBTA-2 Complex**

Pink colored crystals of Co-CBTA-2 complex were obtained from a methanol – water solution (1:1 ratio). Briefly, 236 mg (1.30 mmol) of  $\text{Co}(\text{NO}_3)_2 \cdot 6\text{H}_2\text{O}$  and 100 mg (0.32

mmol) of CBTA-2 were each separately dissolved in 10 mL of water and methanol, respectively. The  $\text{Co}(\text{NO}_3)_2 \cdot 6\text{H}_2\text{O}$  solution was added dropwise to the CBTA-2 solution and stirred for 10 minutes to ensure complete homogenization. After homogenization, a 1.0 M solution of NaOH was added dropwise to the reaction mixture. Upon addition of the NaOH solution, little precipitates were formed which completely disappeared upon stirring. The NaOH solution was added until a slight amount of precipitate persisted after stirring for about 15 minutes. The precipitate was filtered out, and the filtrate was kept at room temperature for several days to crystalize. The crystals were washed with water and methanol, respectively, and allowed to be dried in vacuum overnight. The yield of Co-CBTA-2 complex crystals was 52% based on the metal salt.

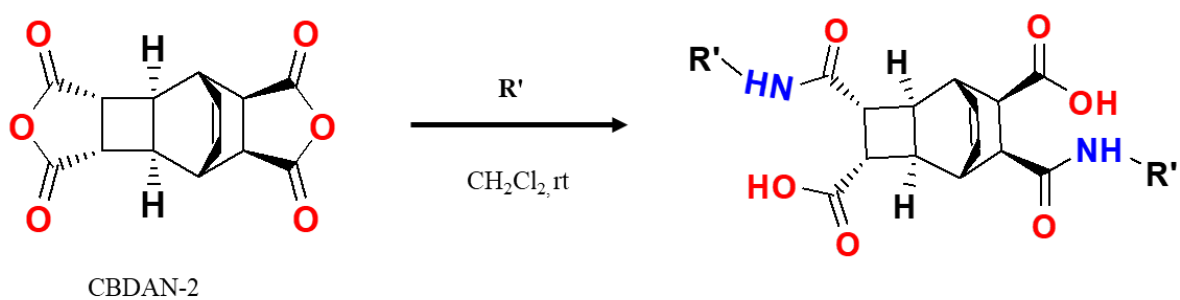


**Scheme 24:** Synthesis of Co-CBTA-2 complex

### 3.3.7. Synthesis of Cyclobutane-containing Diacids from CBDAN-2

In an oven-dried round-bottom flask, CBDAN-2 (2.0 g, 7.3 mmol), was placed in 100.0 mL dichloromethane. A solution of aniline or benzylamine (2:1 ratio with CBDAN-2), was slowly added to the flask. The reaction mixture was stirred at room temperature for 4 or 12 hours respectively. The product precipitated out of solution as the reaction

proceeded and completion of reaction was checked by recording the  $^1\text{H}$  NMR spectra of the solution. The pure product was filtered out of the solvent and dried before characterization.



**Scheme 25:** General method for synthesis of CBDAXs

## CHAPTER FOUR

### Preliminary Exploration of the Photoreactivity and Applications of Some 2(5H)-Furanones

#### 4.0. Introduction

Today, research in sustainable, and renewable sources of raw materials is gaining much attention. This is because nonrenewable sources are feared to deplete soon and the cost of their exploitation on our environment is devastating.<sup>105, 106, 106</sup> Manufacturing new materials from biobased precursors is limited because there are only a few precursors available.<sup>54, 107</sup> Derivatizing the currently available biomass-based building blocks to make a library of precursor chemicals will set the pathway to gradually reduce our current reliance on petrochemicals, leading to the progressive transition to a full bio-based future.<sup>54, 107, 108</sup> Polymers derived from biomass-derived diacids and diols containing cyclobutane rings have been shown to provide desired attributes such as semi-rigidity and good glass-transition temperatures.<sup>10, 38, 39</sup> Inspired by the plethora of possibilities from results of the previous study on the reactions of maleic anhydride and its derivatives, it was thought that studies could be carried out using 2(5H)-furanone and its derivatives. These olefinic furanones share several features in common with furanediones and as such they might share some reactions in common.

Furanones are produced naturally by plants and used to inhibit bacterial colonization.<sup>109-111</sup> They have significant applications in the pharmaceutical industries to produce biofilms used to inhibit gram-negative bacteria.<sup>112</sup> Furanones have also become known as promising anti-inflammatory, anti-cancer, analgesic, anticonvulsant, antifungal, antioxidant, and antiulcer agents.<sup>111, 113, 114</sup> Their five-membered

heteroatomic ring in biologically active compounds provides the motif involved in their mechanism of action.<sup>113</sup> They are synthesized from the biomass via furfural in some cases utilizing photocatalysis and electrocatalysis.<sup>23 115 116</sup>

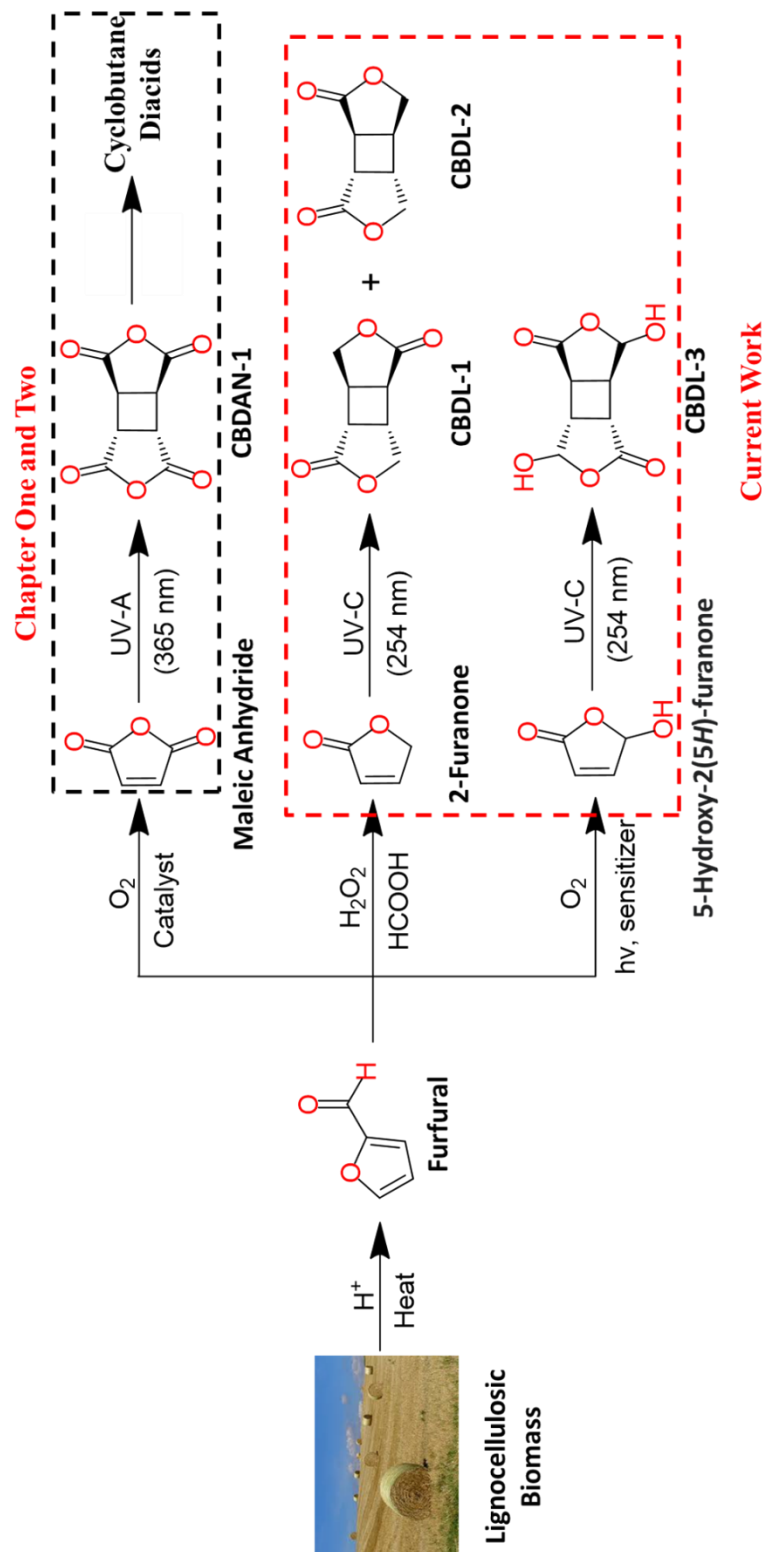
Their applications in the synthesis of polymers have however been overlooked.<sup>117, 118</sup> There has been some setback in this area with mostly five membered ring monolactones in ring opening polymerization reactions.<sup>117, 119</sup> Nonetheless, biodegradable Gemini surfactants or twin-tail amphoteric surfactants have been synthesized from 2(5H)-furanone and fatty acid amines.<sup>120-122</sup> Hydroxyl-furanones have also been used in the synthesis of sulfonated surfactants.<sup>118, 121, 123</sup> Dilactones obtained via dimerization of olefinic cyclic lactones have however not been explored. Moreover, hydrolysis of these dilactones would yield diacids and diols, which are the precursors to polyester synthesis. These diacids and diols, if they possess desired thermal properties for polymeric precursors, will make them precursors for polymer synthesis. Also, some might yield reactive dicarbonyl, which would make them intermediates in organic synthesis.

The goal of this study was to explore the dimerization of biomass-derived 2(5H)-furanone, 5-hydroxy-2(5H)-furanone, 4-methyl-2(5H)-furanone, and 3-methyl-2(5H)-furanone. Also, the thermal stability of the dilactones formed was investigated using thermal decomposition analysis.

#### **4.0.1. Background, Hypothesis and Concept**

2(5H)-Furanone was synthesized by the catalytic oxidation of furfural using H<sub>2</sub>O<sub>2</sub>.<sup>120, 124, 125</sup> Even though both heterogeneous and homogeneous catalysis can be deployed,

the latter had higher yields.<sup>124, 125</sup> Ongoing research in this area involves improving the yields, for which biphasic systems have worked well. Difficulties in the recovery of the homogeneous catalysts and separation of products has also attracted the deployment of environmentally friendly and inexpensive oxidants using non-metallic catalytic systems.<sup>110, 124</sup> 5-Hydroxy-2(5H)-furanone, on the other hand, can be obtained from photooxidation of furfural using singlet oxygen with a photosensitizer.<sup>116, 126</sup> It can also be synthesized from furfural electrochemically using hydrogen peroxide as a catalyst.<sup>127</sup> Other furanone derivatives can be synthesized from furfural using similar methods. The biomass is an attractive source to obtain sustainable precursors to materials. In the first and second chapter of this dissertation CBDAN-1 was shown to represent a versatile platform for the synthesis of several diacids. The furanedione used to synthesize CBDAN-1 shares several features in common with olefinic furanones. We therefore hypothesized that some olefinic furanones will photo-dimerize to form cyclobutane-containing difuranones. Scheme 4-1 shows the similarities of the previous work to this current one.



**Scheme 26:** Project concept



#### 4.0.2. Study Design

The furanones chosen for this study are: 2(5H)-furanone, 5-hydroxy-2(5H)-furanone, 4-methyl-2(5H)-furanone, and 3-methyl-2(5H)-furanone. Photochemical reactions in solid-state are governed by the molecule's topochemical crystal lattice packing and the light (energy) source providing photons to activate the reacting species. In this regard, reaction in the solid state will only occur if the configuration of the molecules and distance from the closest molecule in the crystal lattice agree with the Schmidt principle.<sup>2</sup> Moreover, the light source must be producing photons with the sufficient energy to activate reacting molecules. Finding olefins that have the appropriate crystal packing and sorting the light source, which will activate the reacting molecules, is the most important step for a successful photodimerization reaction design. However, photosensitizers are sometimes used to circumvent such problems and activate reacting species. This only adds to the complexity of the setup and is unsuccessful in many cases. In this study, the starting materials are liquid therefore their direct crystal structures cannot be obtained. To evaluate their photoreactivities, only screening experiments can be validated.

To achieve this screening an appropriate UV source must be used for irradiation. Therefore, the UV-Vis spectra of 2(5H)-furanone, 5-hydroxy-2(5H)-furanone, 4-methyl-2(5H)-furanone, and 3-methyl-2(5H)-furanone were obtained (Figure 4-1). The UV-vis showed that the compounds showed absorbance between 251 nm and 400 nm. This region is contained within the region defined by ECO-UV in chapter one. Therefore, lamps producing UV- A, B or C could be tested. Their absorption spectra

also indicated that the maximum absorption occurred at 268 nm, 259 nm, 256 (291) nm, and 280 nm for 4-methyl-2(5H)-furanone, 3-methyl-2(5H)-furanone, 2(5H)-furanone, and 5-hydroxy-2(5H)-furanone, respectively. Lamps producing UV-A, B and C were used to screen the various furanones. No obvious reaction was observed when lamps producing UV-A, or B were used for photoreaction for either compound. However, 2(5H)-furanone, 3-methyl-2(5H)-furanone, and 5-hydroxy-2(5H)-furanone molecules were excited and dimerized when lamps producing UV-C (254 nm) were used.

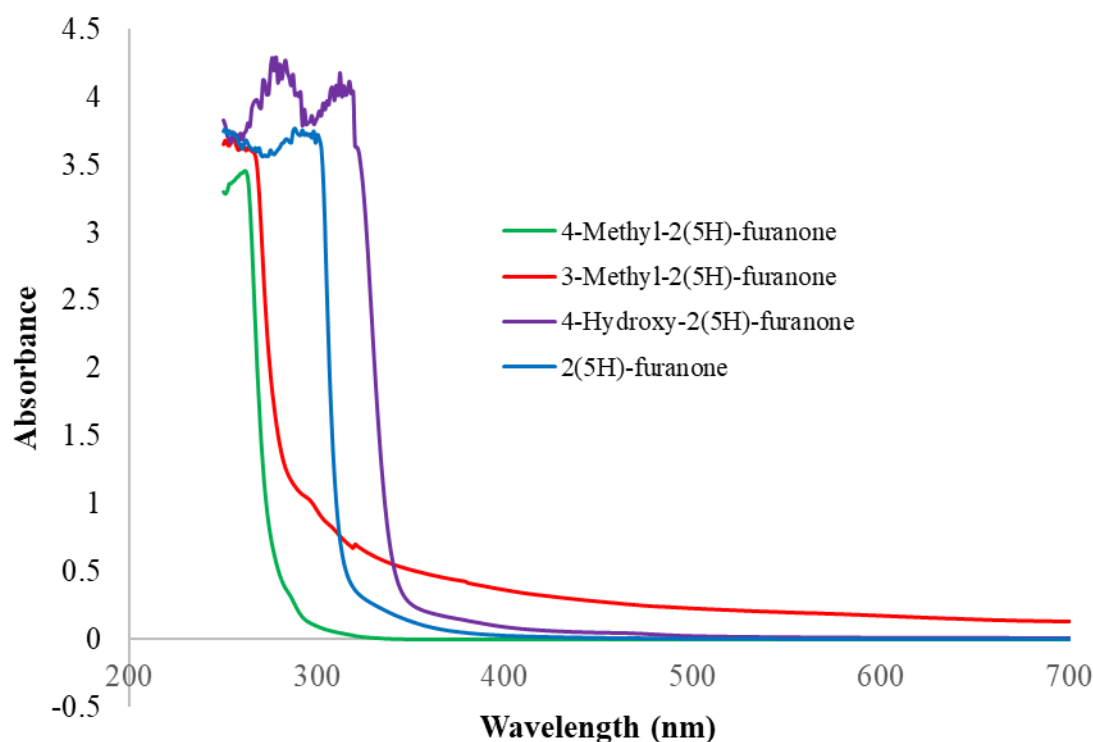


**Figure 27:** UV-Vis absorbance of 5-hydroxy-2(5H)-furanone, 2(5H)-furanone, 3-methyl-2(5H)-furanone, and 4-methyl-2(5H)-furanone in ethanol.

## **4.1. Results and Discussion**

### **4.1.1. Synthesis of Cyclobutane Dilactone-1&2 (CBDL-1&2) from 2(5H)-Furanone**

CBDL-1 and CBDL-2 were synthesized through a [2+2] photodimerization in the solid state under UV-C of 2(5H)-furanone. Germicidal lamps (UV-C; 254 nm) excited molecules of 2(5H)-furanone to react forming the dimer. Crystallography revealed the structure of CBDL-1 and CBDL-2 to be consistent with the cis-trans-cis conformation (Figure 28). In the synthesis of CBDL-1 and CBDL-2, the liquid 2(5H)-furanone was placed on a quartz glass and irradiated with germicidal lamps. The reaction was observed to occur because the liquid solidified during the experiment. The reaction was completed within 24 hours reaching a 90 % conversion. The pure powder was obtained after recrystallization in methanol.

The reaction product was characterized using  $^1\text{H}$  NMR,  $^{13}\text{C}$  NMR, FT-IR spectroscopic and crystallography. This reaction is also possible in the solution phase. In the solution phase reaction, 2(5H)-furanone was dissolved in acetone in a round bottom quartz glass and irradiated between two germicidal lamps. A precipitate, which is the product, was formed as the reaction proceeded. This precipitate was filtered and used for analysis which showed the mixture of head-to-head and head to tail products. It is interesting to note that in the solution phase reaction, the head-to-tail product dominate to give a ratio of about 20:80 CBDL-1 and CBDL-2 respectively.

#### 4.1.2. Description of CBDL-1 and CBDL-2 Structure

The single crystals of CBDL-1 and CBDL-2 were grown directly by slow evaporation in methanol. The crystals were monoclinic with a P 21/n space group. The crystal structure revealed that two different products were formed, i.e., the head-to-head and head-to-tail [2+2] photodimerized products in equal proportions. The cyclobutane ring in each product adopts a different conformation. The head-to-tail product adopts a planar configuration, while the head-to-head product adopts a puckered configuration. This indicates that there is less flexibility between the four-membered ring structure. The single crystal reveals a carbon-carbon bond distance of around 1.562 and 1.547 Å for the puckered and planar conformations, respectively (Figure 28). The lactone groups on opposite sides of the cyclobutane ring have an angle between them of about 180°. The distance between the two lactone groups is 5.295 and 5.247 Å apart for the puckered and planar conformations respectively. This distance is like the distance between the two anhydride groups in the building block CBDAN-1, which is 5.297 Å. This makes this CBDL-1&2 an interesting molecule to explore in polymer and organic synthesis. The limited conformational flexibility of the cyclobutane ring is expected to give CBDL-1 and CBDL-2 a unique semi-rigid character like other cyclobutane-containing monomers.<sup>67, 68</sup>

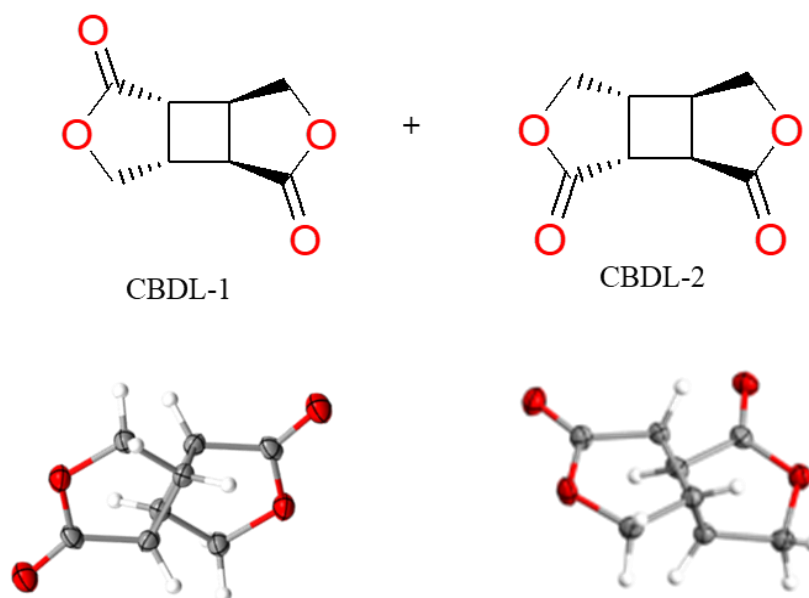


**Figure 28:** Chemical and x-ray single-crystal structure of CBDL-1 and CBDL-2: One molecule shown as Oak Ridge Thermal Ellipsoid Plot (ORTEP) representing 50% electron density.

#### 4.1.3. Synthesis of Cyclobutane Dilactone-3 (CBDL-3) from 5-Hydroxy-2(5H)-Furanone

CBDL-3 was synthesized through a [2+2] photodimerization in the solid-state under UV-C of 5-hydroxy-2(5H)-furanone. Germicidal lamps (UV-C; 254 nm) excited molecules of 5-hydroxy-2(5H)-furanone to react forming the dimer. In the synthesis of CBDL-3, powder 5-hydroxy-2(5H)-furanone was placed on a quartz glass plate and sandwiched between four germicidal lamps. The progress of the reaction was monitored through  $^1\text{H}$  NMR, the appearance of the cyclobutane peak and the disappearance of the olefin peaks indicated the reaction progress. The reaction was completed after about 24 hours reaching about a 98 % conversion. The pure powder obtained was recrystallized

in methanol to obtain the pure product. This solvent free reaction is possible because the crystal packing of the molecules follow the Schmid's principle of photodimerization. The reaction product was characterized using  $^1\text{H}$  NMR,  $^{13}\text{C}$  NMR, FT-IR spectroscopic, and X-ray crystallography.

#### **4.1.4. Synthesis of Cyclobutane Dilactone-4&5 (CBDL-4&5) from 3-methyl-2(5H)-Furanone**

CBDL-4 and CBDL-5 were synthesized through a [2+2] photodimerization in solution under UV-C of 3-methyl-2(5H)-furanone. Germicidal lamps (UV-C; 254 nm) excited molecules of 3-methyl-2(5H)-furanone to react forming the dimer. NMR analysis revealed that both the head-head and head-tail product are formed in the ration of about 20:80 to give CBDL-4 and CBDL-5 respectively. In the synthesis of CBDL-1 and CBDL-2, the liquid 3-methyl-2(5H)-furanone was dissolved in acetone in a quartz round bottom flask and irradiated with germicidal lamps. The reaction was completed after about 24 hours reaching about a 90 % conversion. The solvent was evaporated giving a powder which is essentially pure after recrystallization in methanol. The reaction product was analyzed using  $^1\text{H}$  NMR,  $^{13}\text{C}$  NMR, and FT-IR spectroscopy. It is worth noting that in solid phase this reaction was not possible even though 3-methyl-2(5H)-furanone is a liquid.

#### **4.1.5. Initial Thermal Studies on CBLAC-1, CBDL-2, and CBLAC-3**

Studies on the thermal properties of precursors to polymers often give insights in the molecule's stability during polymer synthesis because sometimes polymer synthetic methods require high temperatures to maximize condensation. Thermogravimetric

analysis showed that both CBDL-1, CBDL-2, and CBDL-3 have good stability (Table 10). This shows that the cyclobutane ring in CBDL-1, CBDL-2, and CBDL-3 is stable to be incorporated in polymers. This comes as no surprise since the cyclobutane ring has previously been shown to possess good thermal, physical and chemical properties.<sup>38-42</sup> CBDL-1 and CBDL-2 starts rapidly losing weight at temperatures around 220 °C and at 257 °C, 50 % of its weight has been lost (Figure 29). This is slightly lower than CBDAN-1 which had its T<sub>5</sub>, T<sub>10</sub> and T<sub>d</sub> at 315 °C, 342 °C and 368 °C, respectively. This implies CBDL-1 and CBDL-2 are less stable than CBDAN-1. On the other hand, CBDL-3 decomposes in two stages. It first starts losing weight at about 176 °C where its first decomposition cycle begins. The second decomposition cycle begins at 260 °C where it remains stable and only loses weight slightly. At 600 °C about 30 % of the compound had not decomposed. At this temperature most organic monomers would have completely lost their weight; only polymeric materials would be expected to be undecomposed at this temperature. A possible explanation to this observation is that there is a ring opening and possible polymerization of the carbonyl functional group. The ring opening is possibly associated with decarboxylation. This is because elimination of a CO<sub>2</sub> molecule will lead to a 22 % weight loss, but the TGA has 20 % loss corresponding to the first decomposition.

**Table 10:** Thermogravimetric analysis of CBLAC-1 and CBDL-2 and CBLAC-3

SN	T <sub>5</sub> (°C)	T <sub>10</sub> (°C)	T <sub>d</sub> (°C)
<b>CBLAC-1 and CBDL-2</b>	235	257	311
<b>CBLAC-3</b>	180	200	389

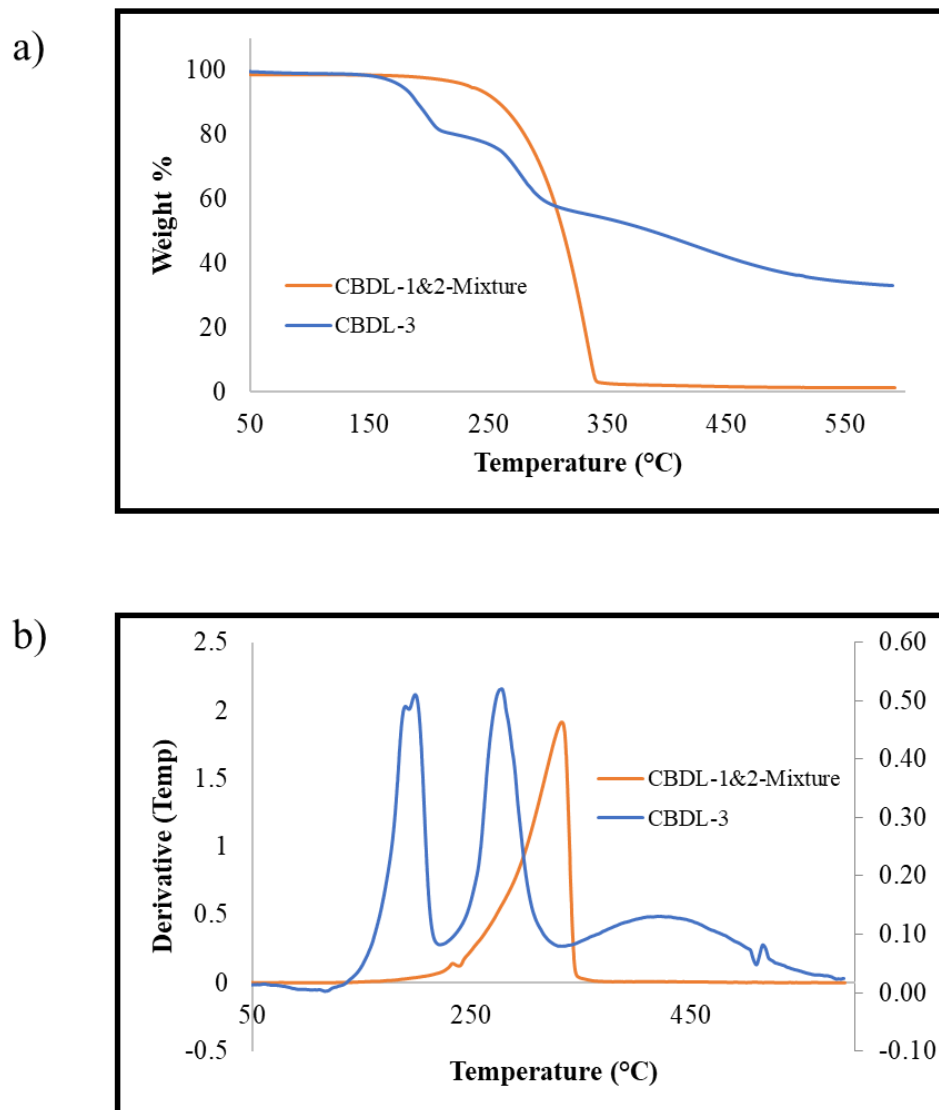


**Figure 29:** TGA and DTG curves of CBDL-1 and CBDL-2 recorded from 0 °C to 600 °C with a heating rate of 20 °C·min<sup>-1</sup> under N<sub>2</sub> atmosphere, **b)** DTG curves of CBDL-1 and CBDL-2 recorded from 0 °C to 600 °C with a heating rate of 20 °C·min<sup>-1</sup> under N<sub>2</sub> atmosphere

#### 4.2. Conclusion

Dimerization of 2(5H)-furanone, 5-hydroxy-2(5H)-furanone, and 3-methyl-2(5H)-furanone was achieved. The initial thermal stability study of the dilactones formed



showed that these precursors have high decomposition temperatures comparable to other monomers used in polymer synthesis.

### **4.3. Experimental Section**

#### **4.3.1. Materials and Procedures**

All chemicals were purchased from Alfa Aesar, Sigma-Aldrich, or Acros, and used without further purification. Germicidal lamps used in the photoreaction was Germicidal lamp T5 G5 39/ 41W ozone free Sankyo Denki Co., ltd. The solution phase nuclear magnetic resonance spectra (NMR) were recorded with Bruker AVANCE (<sup>1</sup>H: 500 MHz, <sup>13</sup>C: 125 MHz). Proton and carbon chemical shifts were reported in ppm downfield from tetramethylsilane (TMS). Single crystal X-ray data were collected on a Bruker Kappa Apex II Duo X-Ray Diffractometer with Cu K $\alpha$  ( $\lambda = 1.54178 \text{ \AA}$ ). Infrared spectroscopy (IR) was recorded on Thermo Scientific Nicolet iS5 FT-IR spectrometer. Thermogravimetric analysis (TGA) was carried out with a Hi-Res TGA Q500 from TA Instruments using alumina pans at a heating rate of  $20 \text{ }^\circ\text{C}\cdot\text{min}^{-1}$  under nitrogen with a sample weight of about 10 mg.

#### **4.3.2. Synthesis of Cyclobutane Dilactone-1&2 from 2(5H)-Furanone**

##### **Method I:**

One milliliter (14 mmol) of 2(5H)-furanone was placed on a quartz glass slide and evenly distributed to form a thin layer. The quartz slide was sandwiched between two germicidal lamps (UV-C) with the lower back part touching one lamps and the upper at about 2 mm from the second lamps. The reaction proceeded in liquid state and the liquid turned into solid as the reaction proceeded. The reaction completed after 48 hours

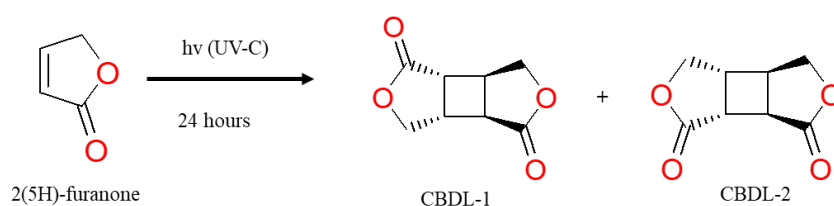
with a greater than 90 % conversion rate. The product was characterized using  $^1\text{H}$  NMR,  $^{13}\text{C}$  NMR and FT-IR spectroscopy.

### Method II:

1.0 mL of 2(5H)-furanone (14.0 mmol) and 50.0 mL of acetone were placed in a 100.0 mL round bottom quartz flask. The flask was sandwiched between four germicidal lamps (UV-C; 254 nm) and irradiated while stirring. The lamps were about 2 mm from the flask and the irradiation lasted 24 hours. The product precipitated out of solution. After 24 hours, the precipitate was filtered, and the resulting powder was the product, which was recrystallized in ethanol. The reaction had a greater than 92 % yield. The product was analyzed using  $^1\text{H}$  NMR,  $^{13}\text{C}$  NMR, FT-IR spectroscopy, and X-ray crystallography.

**CBDL-1:**  $^1\text{H}$  NMR  $\delta$  (ppm): 4.51 (m, 4H,  $\text{OCH}_2$ ) 3.15 - 3.26 (m, 4H,  $\text{CH}$ -cyclobutane).  
 $^{13}\text{C}$  NMR  $\delta$  (ppm): 171 (C=O), 41 ( $\text{CH}$ -cyclobutane). FT-IR (solid)  $\bar{\nu}_{\text{max}}$  ( $\text{cm}^{-1}$ ): 2980 (aliphatic  $\text{sp}^3$  C-H), 1757 (carbonyl C=O).

**CBDL-2:**  $^1\text{H}$  NMR  $\delta$  (ppm): 4.46 (m, 4H,  $\text{OCH}_2$ ) 3.25 3.17 (m, 4H,  $\text{CH}$ -cyclobutane).  
 $^{13}\text{C}$  NMR  $\delta$  (ppm): 172 (C=O), 41 ( $\text{CH}$ -cyclobutane). FT-IR (solid)  $\bar{\nu}_{\text{max}}$  ( $\text{cm}^{-1}$ ): 2919 (aliphatic  $\text{sp}^3$  C-H), 1757 (carbonyl C=O).

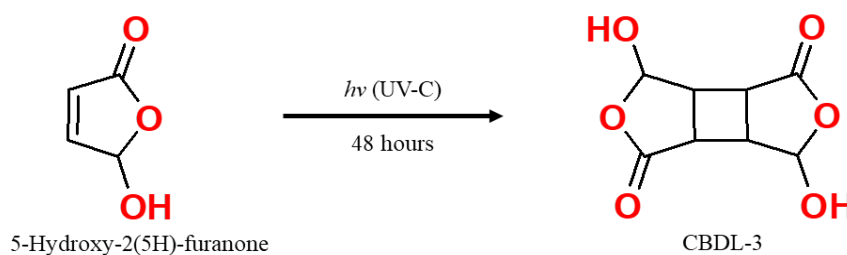


**Scheme 27:** Synthesis of CBDL-1&2

### 4.3.3. Synthesis of Cyclobutane Dilactone-3 from 5-Hydroxy-2(5H)-Furanone

5-Hydroxy-2(5H)-furanone powder (1.00 g, 1.00 mmol) was placed on a quartz glass slide and evenly distributed to form a thin layer. The quartz slide was placed between two germicidal lamps (UV-C) with the lower back part touching one lamp the upper at about 2 mm from the second lamp. The reaction proceeded in the solid state and the powder was mixed every six hours to ensure that all powder was exposed to the light source. The reaction was completed after 48 hours with a greater than 99 % conversion rate. The product was characterized using  $^1\text{H}$  NMR,  $^{13}\text{C}$  NMR and FT-IR spectroscopy.

$^1\text{H}$  NMR  $\delta$  (ppm): 6.56 (s, 2H, OH) 4.58 (d,  $J = 5$ , 2H, cyclobutane), 4.17 (d,  $J = 15$ , 2H, cyclobutane), 3.32 (s, 2H, CH-OH).  $^{13}\text{C}$  NMR  $\delta$  (ppm): 172 (C=O), 78 COOC-OH, 70, 54 (CH-cyclobutane). FT-IR (solid)  $\bar{\nu}_{\text{max}}$  ( $\text{cm}^{-1}$ ): 3362 (alcohol-OH), 1734 (carbonyl C=O).



**Scheme 28:** Synthesis of CBDL-3

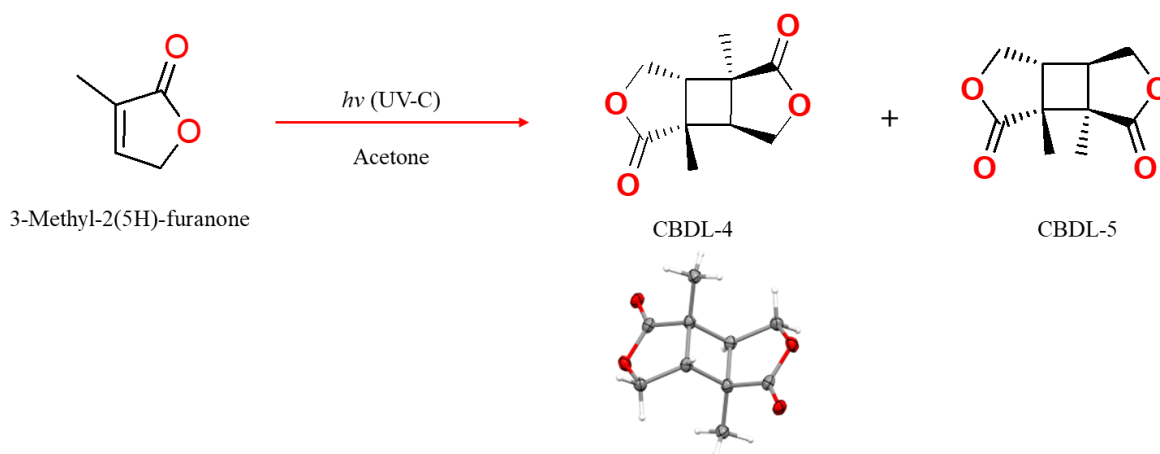
### 4.3.4. Synthesis of Cyclobutane Dilactone- 4 and 5 from 3-Methyl-2(5H)-furanone

3-methyl-2(5H)-furanone (1.0 mL, 11.2 mmol) and 50 mL of acetone were placed in a 100 mL round bottom quartz flask. The flask was sandwiched between four germicidal lamps (UV-C; 254 nm) and irradiated while stirring. The lamps were about 2 mm from

the flask and the irradiation lasted 24 hours. After 24 hours, the solvent was evaporated on a rotavapor. The resulting powder was the product, which was recrystallized in methanol. The reaction had a greater than 92 % yield. The product was analyzed using  $^1\text{H}$  NMR,  $^{13}\text{C}$  NMR, FT-IR spectroscopy, and X-ray crystallography.

**CBDL-4:**  $^1\text{H}$  NMR  $\delta$  (ppm): 4.51 (m, 4H,  $\text{OCH}_2$ ) 3.15 - 3.26 (m, 4H,  $\text{CH}$ -cyclobutane).  
 $^{13}\text{C}$  NMR  $\delta$  (ppm): 171 (C=O), 41 ( $\text{CH}$ -cyclobutane). FT-IR (solid)  $\bar{\nu}_{\text{max}}$  ( $\text{cm}^{-1}$ ): 2980 (aliphatic  $\text{sp}^3$  C-H), 1757 (carbonyl C=O).

**CBDL-5:**  $^1\text{H}$  NMR  $\delta$  (ppm): 4.46 (m, 4H,  $\text{OCH}_2$ ) 3.25 3.17 (m, 4H,  $\text{CH}$ -cyclobutane).  
 $^{13}\text{C}$  NMR  $\delta$  (ppm): 172 (C=O), 41 ( $\text{CH}$ -cyclobutane). FT-IR (solid)  $\bar{\nu}_{\text{max}}$  ( $\text{cm}^{-1}$ ): 2919 (aliphatic  $\text{sp}^3$  C-H), 1757 (carbonyl C=O).



**Scheme 29:** Synthesis of CBDL-4&5

## CHAPTER FIVE

### Conclusions and Perspectives

Transitioning from fossil fuel-based chemicals to more environmentally favorable and sustainable products require a thorough exploration of the available biomass precursors. Considering that fossil fuels only provide us with hydrocarbons, oxygen must be introduced into these molecules via very vigorous oxidative methods. The biomass contains molecules with the essential functional groups we need to synthesis di- and tetracarboxylic acids much easily. Tetracarboxylic acids and dicarboxylic acids are very important molecules that can be used to make polyester, polyimides, polyamides etc. The di- and tetraacids provided by fossil fuels already overwhelm current material industry. There is therefore the need to look for new molecules or alternative methods to obtain these molecules that are sustainable and safe.

This dissertation has shown examples of either totally biomass derived or semi biomass derived molecules that can be optimized to provide us with interesting alternate materials precursors. Figure 31 summarizes the several platform molecules that have been synthesized from this work. These molecules could be exploited further as it was in chapter two to synthesize many very interesting monomers. Also, CBDANs and CBDLs with great potential have been introduced and a new field has been opened where the potentials of these molecules can be studied. In future work the library of dicarboxylic acids will continue to be developed to obtain a huge repertoire. Also, materials will be synthesized from these molecules and their properties studied.

Ultimately the effects of backbone changes will give insights into which back bone will provide desired properties.

Chapter three showed how these dianhydrides can be used to synthesize important polyimides. For example, Figure 30 compares thin films of two polyimides synthesized in chapter three to Kapton, Dupont's commercial polyimide tape. Also, the carboxylic acid derivative of CBDAN-2 was used to synthesize a MOM which could open the gate way of their potential application in MOFs synthesis.

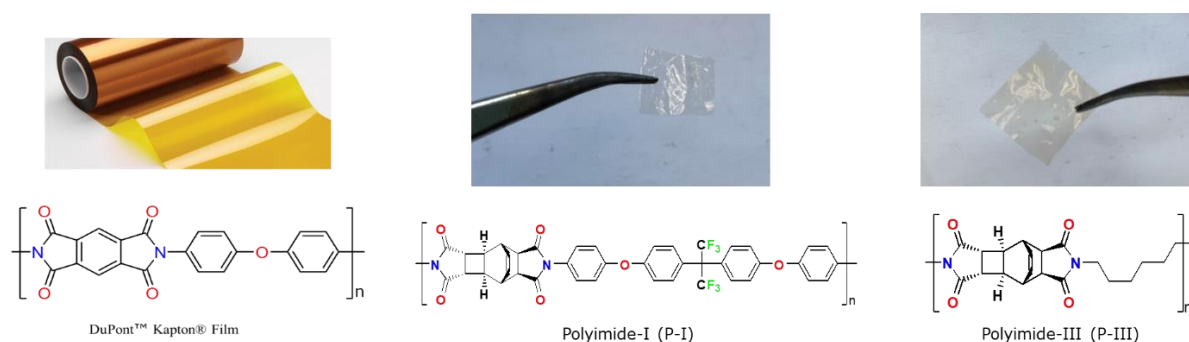


**Figure 30:** Comparison of Kapton and polyimides synthesized from CBDAN-2

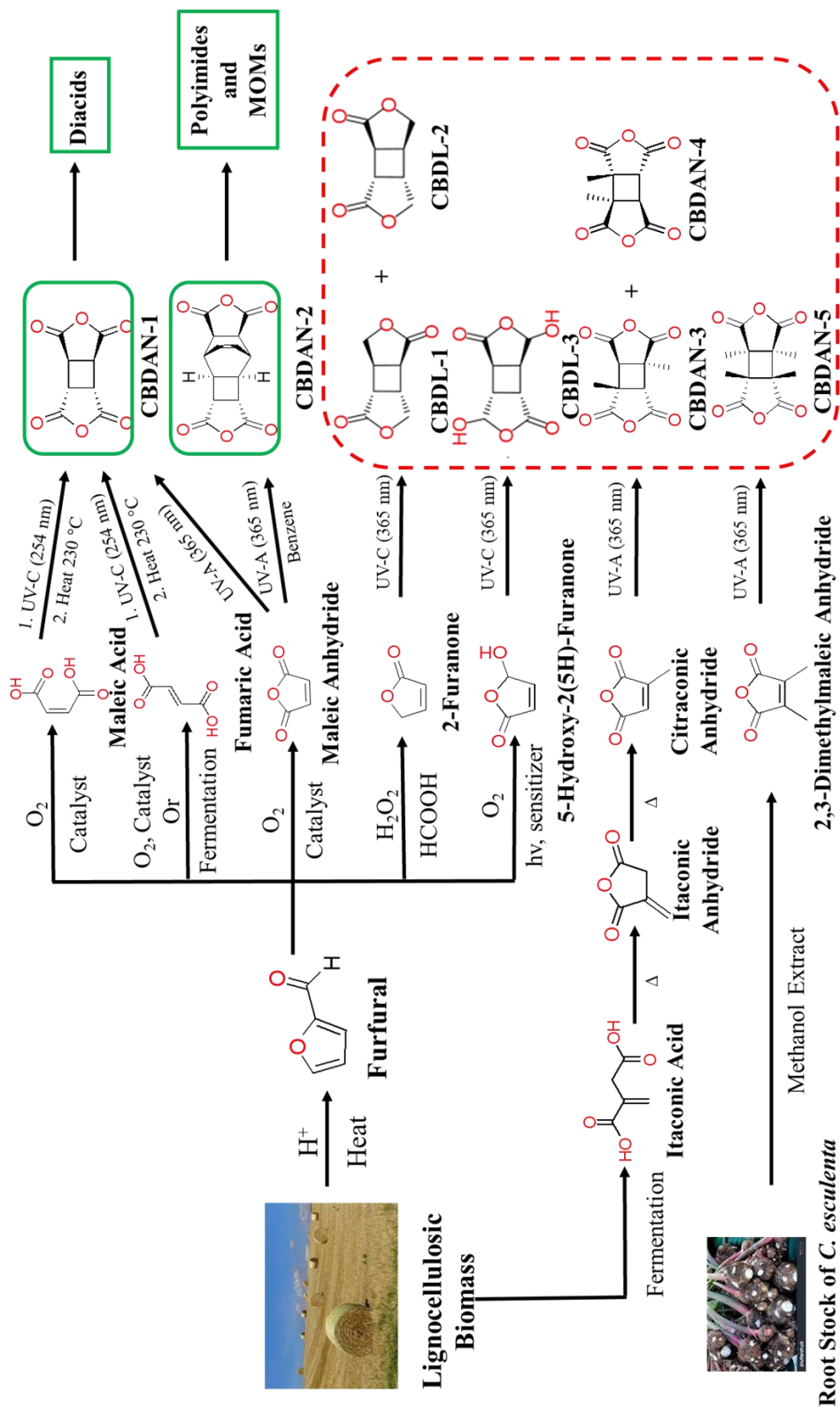


**Figure 31:** Project summary, emphasizing the biomass origin of starting material

## APPENDICES

### Appendix A: Crystal Data

**Table 11:** Table A-1: Crystal data of CBDAN-1, CBTA-1, sublime FA

Crystal	CBDAN-1	CBTA-1	Sublime FA	CBTA-4
Formula	C <sub>8</sub> H <sub>4</sub> O <sub>6</sub>	C <sub>8</sub> H <sub>8</sub> O <sub>8</sub>	C <sub>4</sub> H <sub>4</sub> O <sub>4</sub>	C <sub>10</sub> H <sub>12</sub> O <sub>8</sub>
FW	196.11	232.14	116.07	260.20
Crystal system	orthorhombic	monoclinic	triclinic	monoclinic
Space group	P b c a	P 21/c	P -1	P21/c
a (Å)	6.3989 (2)	5.3746 (2)	4.4012 (4)	10.8937(4)
b (Å)	10.1449 (3)	12.2527 (4)	5.1740 (6)	7.7271(3)
c (Å)	11.2883 (3)	6.4760 (2)	5.3469 (6)	13.7332(5)
α (°)	90	90	87.381 (7)	90
β (°)	90	93.797 (2)	70.636 (5)	104.657(2)
γ (°)	90	90	85.305 (5)	90
V (Å <sup>3</sup> )	732.79 (4)	425.53 (2)	114.46 (2)	1118.40(7)
Temp. (K)	110	111	273	104.99
ρ <sub>calc</sub> (g.cm <sup>-3</sup> )	1.778	1.812	1.684	1.545
μ (mm <sup>-1</sup> )	1.390	1.484	1.379	1.194
Radiation type	CuKα	CuKα	CuKα	CuKα
F (000)	400	240.0	60.0	544.0
No of measured refl.	648	758	394	9318
R (reflections)	0.0351	0.0307 (724)	0.0771 (389)	0.0368
wR2 (reflections)	0.0894	0.0803 (758)	0.2173 (394)	0.0917
Data completeness	1.000	1.000	0.983	1.067
Bond precision C-C (Å)	0.0091	0.0019	0.0035	0.0030



**Table 12:** Crystal data of CBDAx-1 through CBDAx-4

Crystal	CBDAx-1	CBDAx-2 (cis)	CBDAx-3	CBDAx-4
Formula	C <sub>30</sub> H <sub>44</sub> N <sub>4</sub> O <sub>6</sub>	C <sub>21</sub> H <sub>22</sub> N <sub>2</sub> O <sub>7</sub>	C <sub>20</sub> H <sub>30</sub> N <sub>2</sub> O <sub>6</sub>	C <sub>18</sub> H <sub>34</sub> N <sub>2</sub> O <sub>8</sub>
FW	556.69	414.40	394.46	406.47
Crystal size [mm]	0.25 × 0.25 × 0.04	0.22 × 0.12 × 0.1	0.2 × 0.12 × 0.06	0.286 × 0.137 × 0.112
Crystal system	Monoclinic	Triclinic	Monoclinic	Triclinic
Space group	P2 <sub>1</sub> /c	P-1	P2 <sub>1</sub> /c	P-1
a (Å)	13.8220(11)	9.1926(3)	15.1412(9)	6.4881(3)
b (Å)	8.3125(5)	10.4784(4)	6.7366(4)	6.9934(3)
c (Å)	12.5437(9)	10.8258(4)	9.7556(6)	12.0221(5)
α (Å)	90	98.294(2)	90	81.038(2)
β (Å)	95.130(6)	101.496(2)	104.188(4)	85.749(2)
γ (Å)	90	97.862(2)	90	81.9490(10)
V (Å <sup>3</sup> )	1435.44(18)	996.33(6)	964.72(10)	532.76(4)
Z	2	2	2	1
Temp. (K)	107.0	104.99	273.15	296.15
ρ <sub>calc</sub> (g.cm <sup>-3</sup> )	1.288	1.381	1.358	1.267
μ (mm <sup>-1</sup> )	0.730	0.878	0.827	0.829
Radiation type	CuKα (λ = 1.54178)	CuKα (λ = 1.54178)	CuKα (λ = 1.54178)	CuKα (λ = 1.54178)
F (000)	600.0	436.0	424.0	220.0
No of measured refl.	2542	3514	11383	11411
R (reflections)	0.0589 (1778)	0.0454 (3187)	0.0447 (1342)	0.0346 (1842)
wR2 (reflections)	0.1624 (2526)	0.1309 (3514)	0.1044 (1695)	0.0923 (1892)
Data completeness	0.994	0.995	0.998	0.996
Theta (max)	66.678	66.752	66.651	66.676
Npar	183	276	128	133
S	1.022	1.034	1.052	1.073
Bond precision C-C (Å)	0.0041 A	0.0031	0.0030	0.0016

**Table 13:** Crystal data of CBDAN-2, CBTA-2\_Co Complex and model compound

Crystal	CBDAN-2	CBTA-2_Co Complex	Polyimide CBDAN-2 & <i>n</i> -butylamine
Formula	C <sub>14</sub> H <sub>10</sub> O <sub>6</sub>	C <sub>14</sub> H <sub>22</sub> Co <sub>2</sub> O <sub>14</sub>	C <sub>44</sub> H <sub>56</sub> N <sub>4</sub> O <sub>8</sub>
FW	352.33	532.17	768.92
Crystal size [mm]	n/a	0.192 × 0.088 × 0.06	0.208 × 0.166 × 0.075
Crystal system	Monoclinic	Monoclinic	Monoclinic
Space group	P 21/c	Pn	P21/c
a (Å)	9.7689 (4)	6.4107(2)	16.4125(4)
b (Å)	6.5782 (3)	6.9435(2)	6.38000(10)
c (Å)	25.6077 (11)	22.5110(7)	18.8408(5)
α (°)	90	90	90
β (°)	95.804 (3)	92.383(2)	101.657(2)
γ (°)	90	90	90
Theta (max)	66.841	66.646	66.728
V (Å <sup>3</sup> )	1637.16 (12)	1001.16(5)	1932.16(8)
Temp. (K)	110	104.99	273.15
ρ <sub>calc</sub> (g.cm <sup>-3</sup> )	1.429	1.765	1.322
μ (mm <sup>-1</sup> )	0.888	13.650	0.737
Radiation type	CuKα (λ = 1.54178)	CuKα (λ = 1.54178)	CuKα (λ = 1.54178)
F (000)	736.0	544.0	824.0
No of measured refl.	2913	11039	20692
R (reflections)	0.0383 (2367)	0.0543(2865)	0.0412(2754)
wR2 (reflections)	0.1006 (2879)	0.1489(3307)	0.1052(3420)
Data completeness	0.988	1.032	0.999
Bond precision C-C (Å)	0.0024	0.0196	0.0025 A

**Table 14:** Crystal data of CBDLs

Crystal	CBDL-1&2 (Mixture)	CBDL-1	CBDL-4
Formula	C <sub>8</sub> H <sub>8</sub> O <sub>4</sub>	C <sub>8</sub> H <sub>8</sub> O <sub>4</sub>	C <sub>10</sub> H <sub>12</sub> O <sub>4</sub>
FW	168.14	168.14	196.20
Space group	P 1 2 <sub>1</sub> /n 1	P 2 <sub>1</sub> /c	P 2 <sub>1</sub> /n
a (Å)	6.4138(4)	5.9890 (2)	6.4629 (2)
b (Å)	16.0057(7)	11.1678 (4)	6.4707(2)
c (Å)	10.1088(4)	5.2504 (2)	10.6364(4)
α (Å)	90	90	90
β (Å)	97.820(2)	108.433(3)	100.776(2)
γ (Å)	90	90	90
V (Å <sup>3</sup> )	1028.09(9)	333.15 (2)	436.96(3)
Temp. (K)	105	108.38	107.02
ρ <sub>calc</sub> (g.cm <sup>-3</sup> )	1.630	1.676	1.491
μ (mm <sup>-1</sup> )	1.132	1.165	0.972
Radiation type	CuKα (λ = 1.54178)	CuKα (λ = 1.54178)	CuKα (λ = 1.54178)
F (000)	528.0	176.0	208.0
No of measured refl.	1817	2570	3768
R (reflections)	0.1074(1441)	0.0385 (551)	0.0512( 748)
wR2 (reflections)	0.3263(1809)	0.1081 (587)	0.1337( 771)
Data completeness	0.996	1.000	0.999
Bond precision C-C (Å)	0.0072	0.0023	0.0030

## **Appendix B**

### **Selected NMR and FT-IR Spectra of Synthesized Compounds**

PROTON

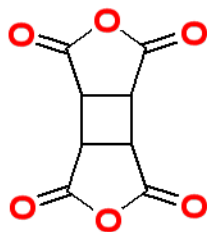


Current Data Parameters  
NAME Dec02-2019-dnke  
EXPNO 3  
PROCNO 1

F2 - Acquisition Parameters  
Date\_ 20191202  
Time 21.43  
INSTRUM spect  
PROBHD 5mm BBO BB-1H-  
PULPROG zg30  
TD 65336  
SOLVENT DMSO  
NS 16  
DS 2  
SWH 10330.578 Hz  
FIDRES 0.157632 Hz  
AQ 3.1720407 sec  
RG 812.7  
DW 48.400 usec  
DE 6.00 usec  
TE 291.2 K  
D1 1.00000000 sec  
TD0 1

===== CHANNEL f1 =====  
NUC1 1H  
P1 9.25 usec  
PL1 -6.00 dB  
SFO1 500.1330885 MHz

F2 - Processing parameters  
SI 32768  
SF 500.1300027 MHz  
WDW EM  
SSB 0  
LB 0.30 Hz  
GB 0  
PC 1.00



3.86

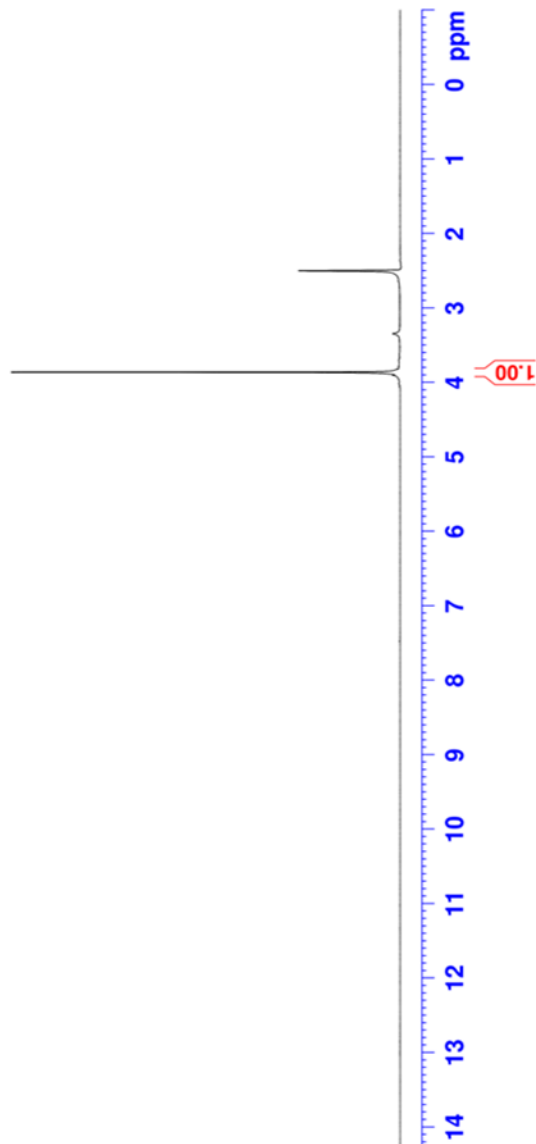


Figure 32: <sup>1</sup>H NMR spectrum of CBDAN-1 in DMSO-d<sub>6</sub> at room temperature



Current Data Parameters  
NAME Sep03-2018-dike  
EXPNO 14  
PROCNO 1

F2 - Acquisition Parameters

Date\_ 20180903  
Time 15.40  
INSTRUM spect  
PROBHD 5mm BBO BB-1H-  
PULPROG zgpg30  
TD 65536  
SOLVENT Acetone  
NS 1024  
DS 4  
SWH 30030.029 Hz  
FIDRES 0.458222 Hz  
AQ 1.0912410 sec  
RG 14456.5  
DM 16.650 usec  
DE 6.00 usec  
TE 340.2 K  
D1 2.00000000 sec  
d11 0.03000000 sec  
DELTA 1.89999998 sec  
TD0 1

===== CHANNEL f1 =====  
NUC1 13C  
P1 8.00 usec  
PL1 0.00 dB  
SFO1 125.7703643 MHz

===== CHANNEL f2 =====  
CPDPRG2 waltz16  
NUC2 1H  
PCPD2 80.00 usec  
PL2 -6.00 dB  
PL12 12.74 dB  
PL13 15.74 dB  
SFO2 500.1320005 MHz

F2 - Processing parameters  
SI 32768  
SF 125.7577390 MHz  
EM  
WDW 0  
SSB 0  
LB 1.00 Hz  
GB 0  
PC 1.40

MAD Xtals  
C13CPD

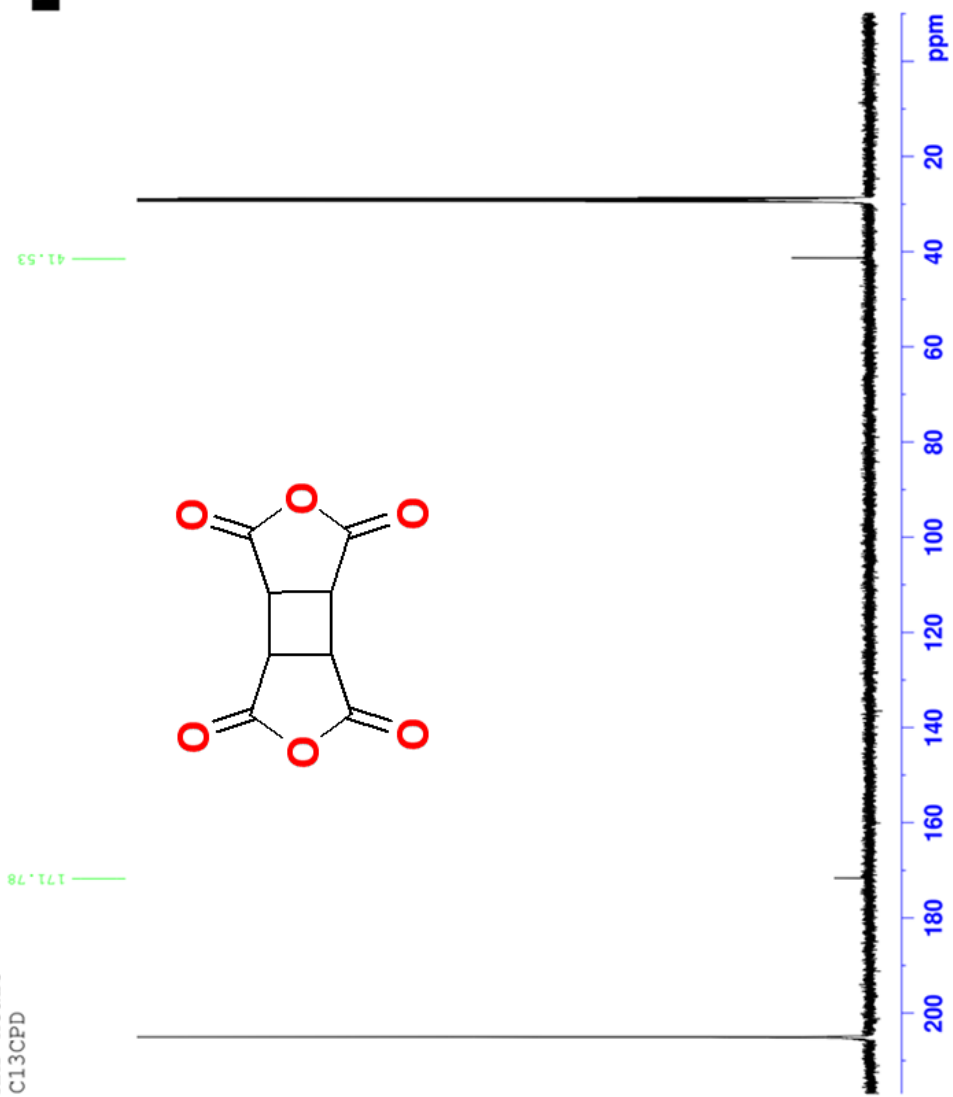


Figure 33:  $^{13}\text{C}$  NMR spectrum of CBDAN-1 in Acetone- $\text{d}_6$  at room temperature

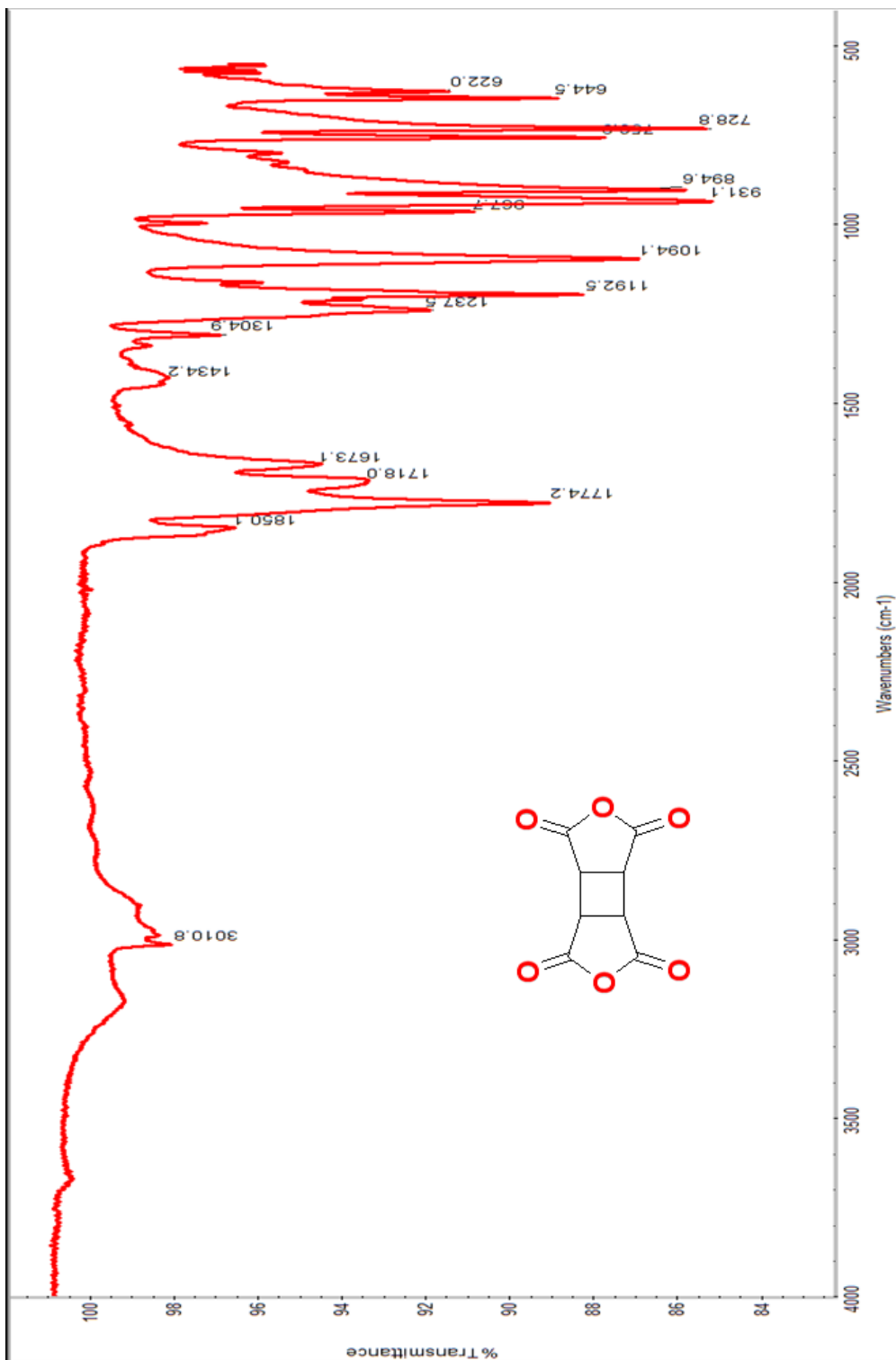


Figure 34: FT-IR spectrum of CBDAN-1

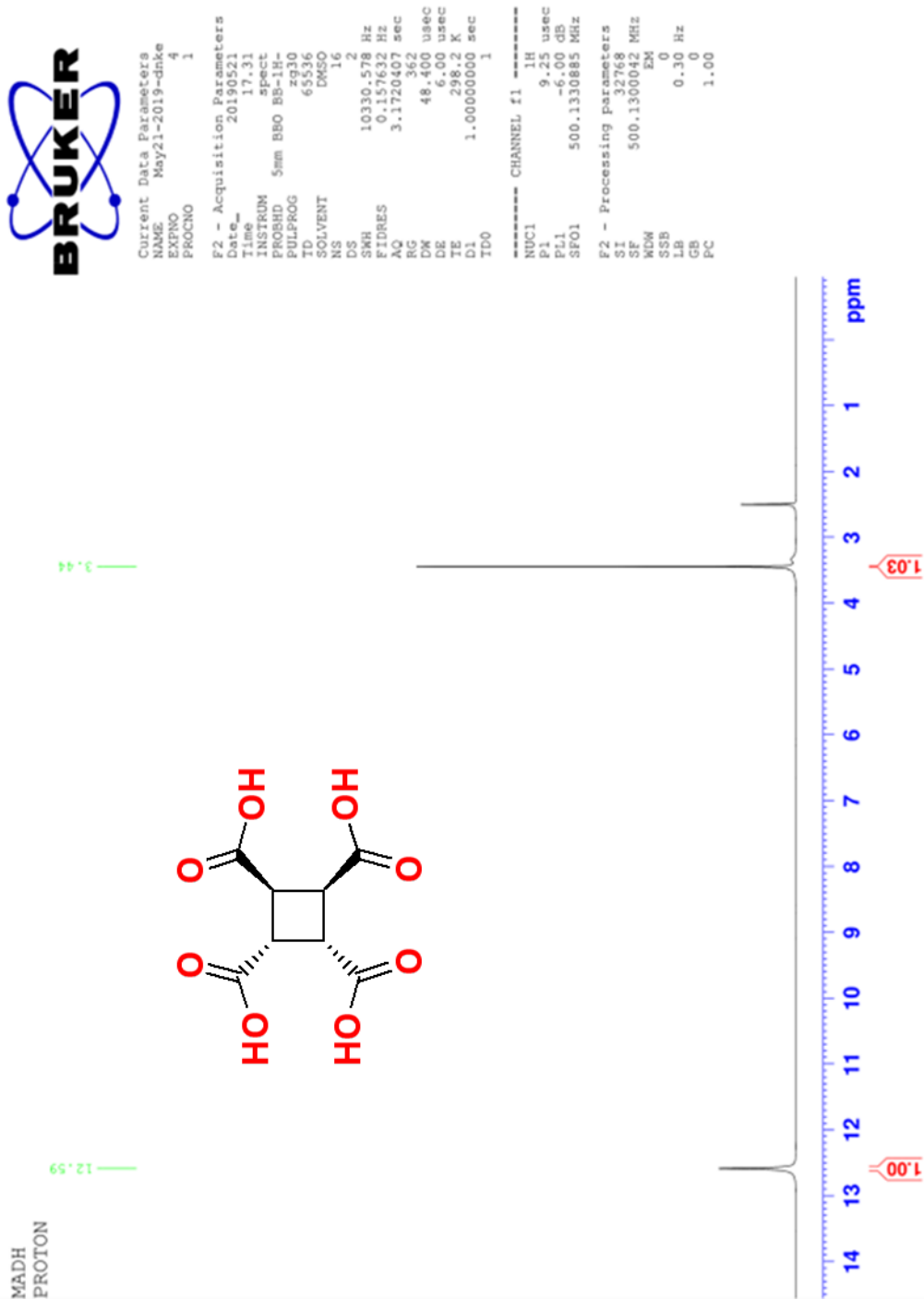


Figure 35:  $^1\text{H}$  NMR spectrum of CBTA-1 in  $\text{DMSO-d}_6$  at room temperature



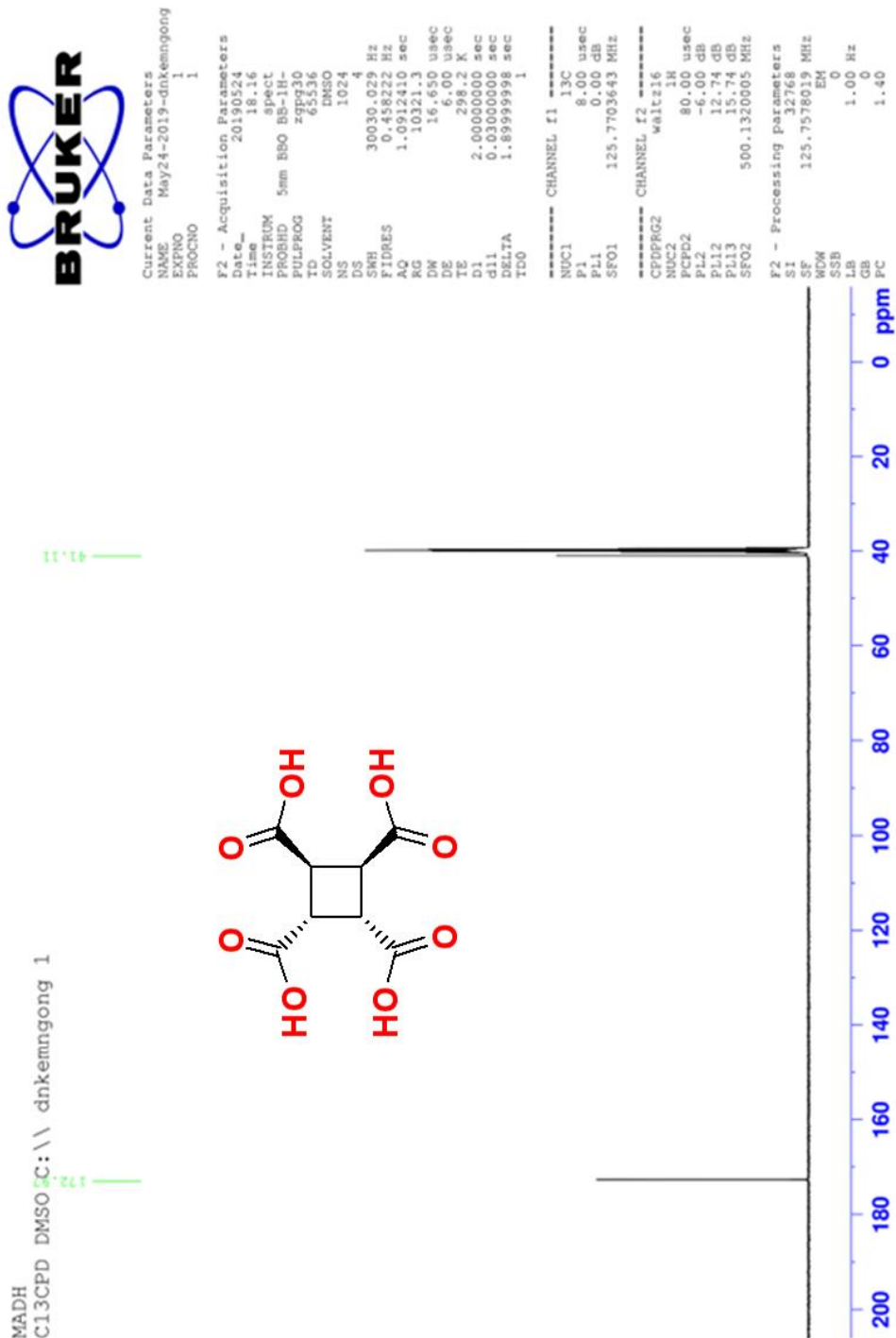
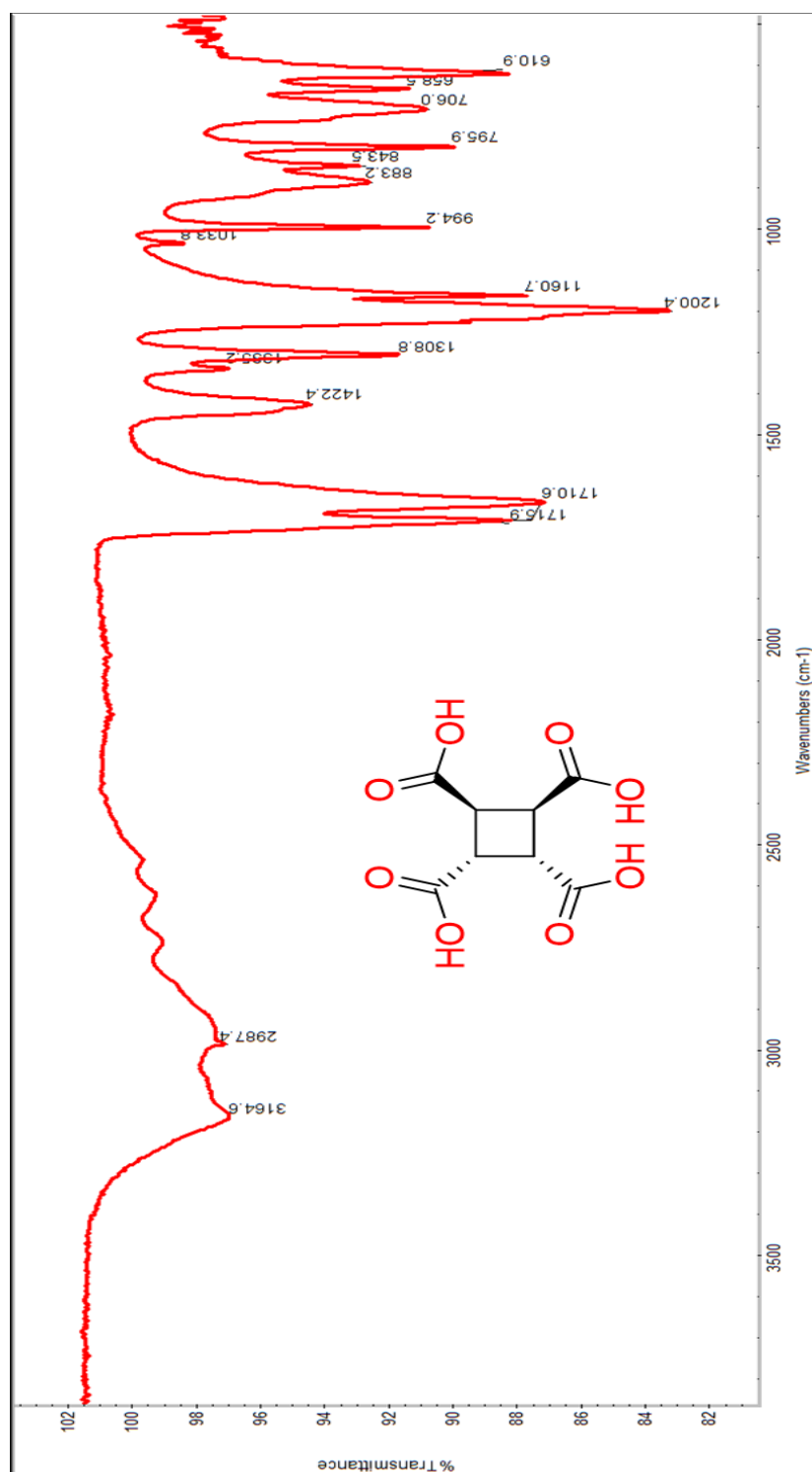


Figure 36:  $^{13}\text{C}$  NMR spectrum of CBTA-1 in DMSO- $d_6$  at room temperature



**Figure 37:** FT-IR spectrum of CBTA-1

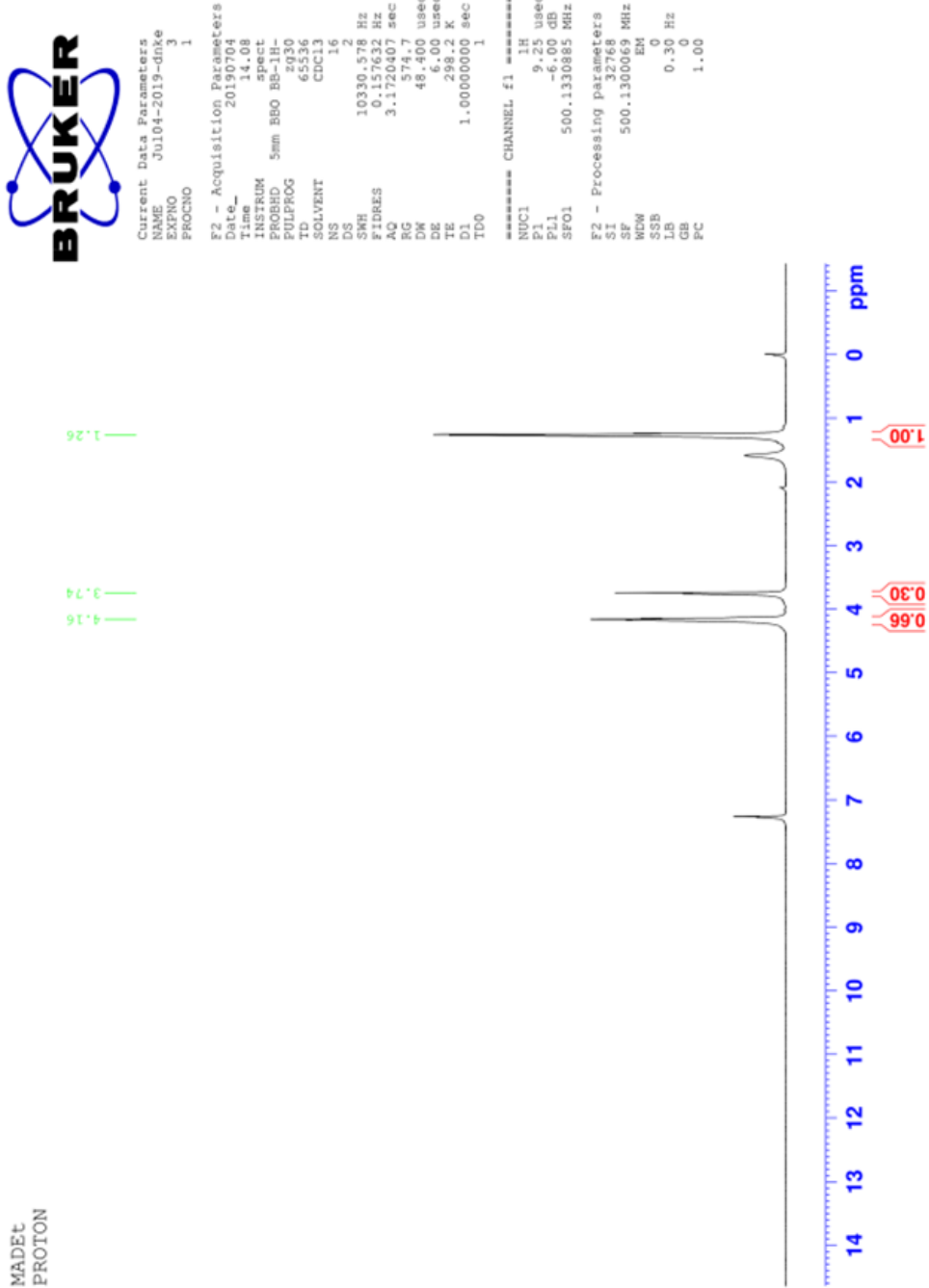


Figure 38:  $^1\text{H}$  NMR spectrum of CBTE-1 in  $\text{DMSO-d}_6$  at room temperature

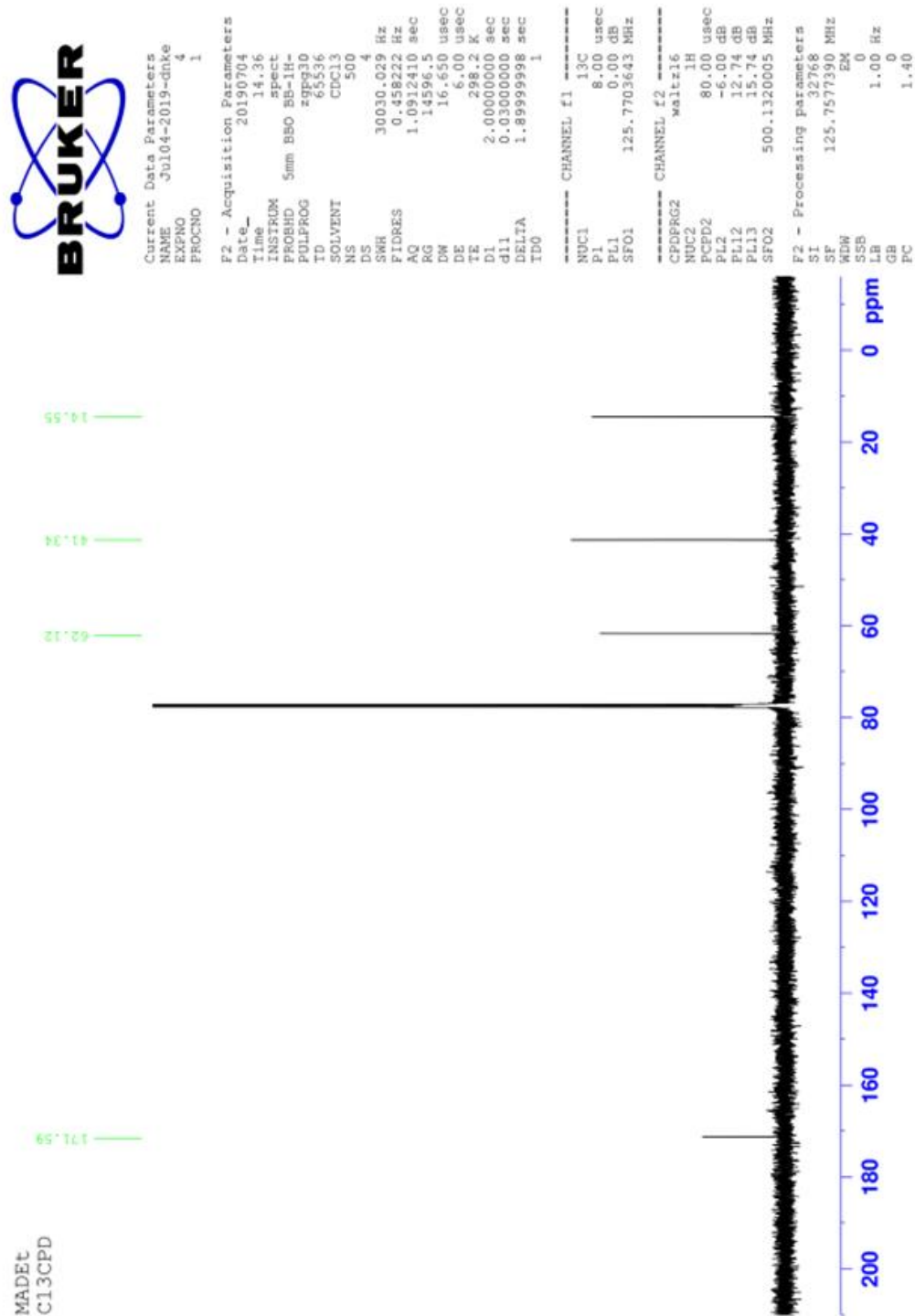
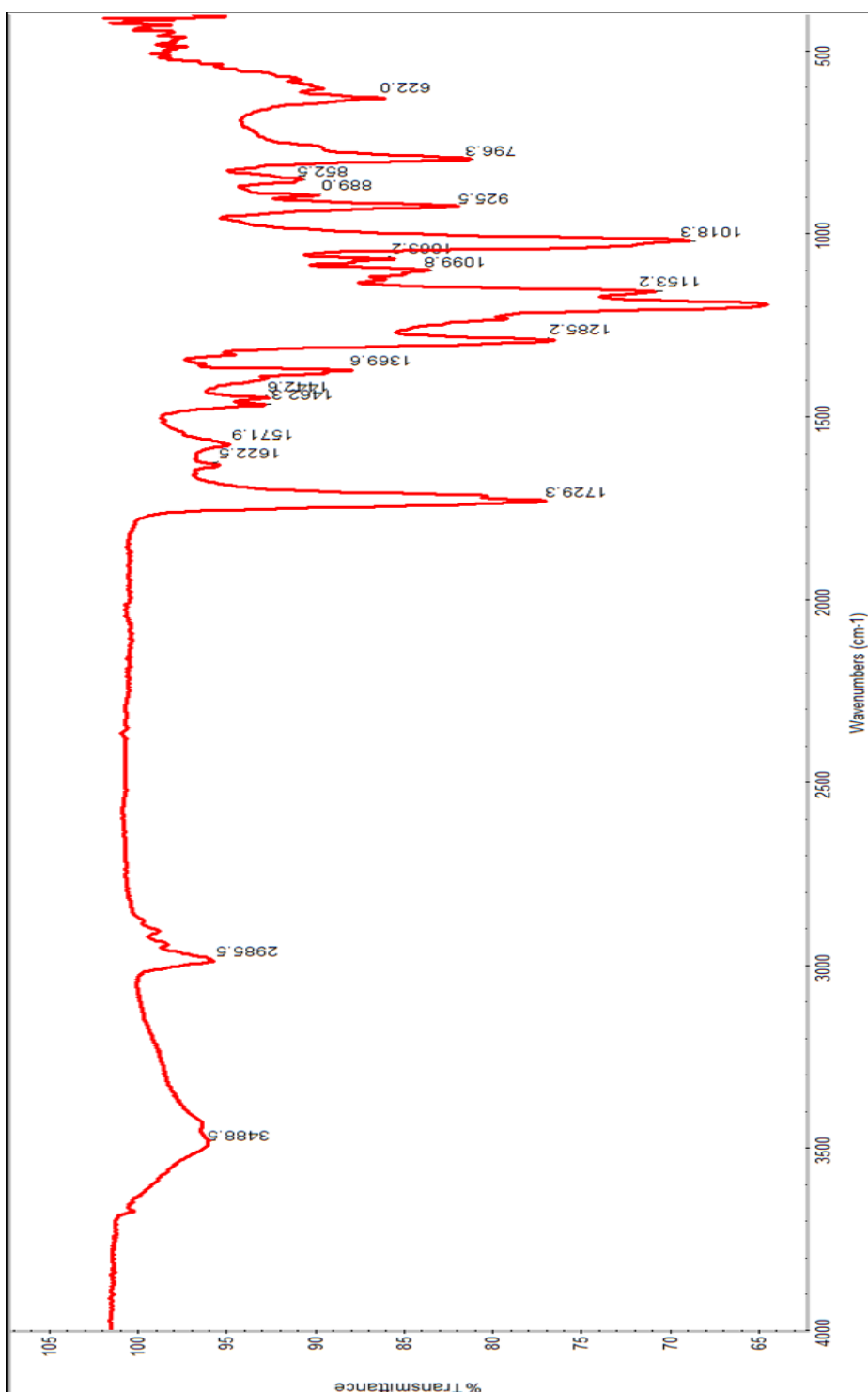
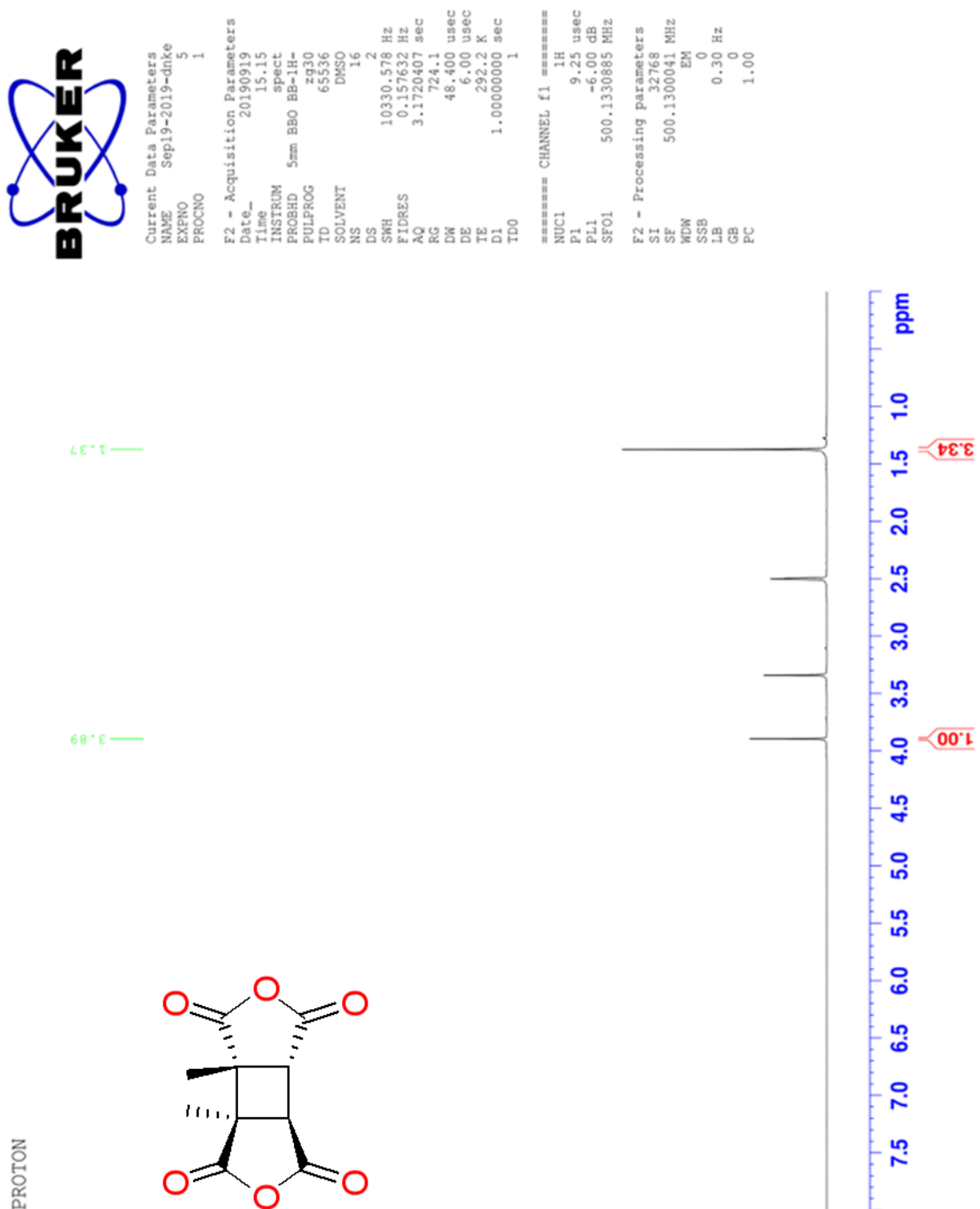


Figure 39:  $^{13}\text{C}$  NMR spectrum of CBTE-1 in  $\text{DMSO-d}_6$  at room temperature



**Figure 40:** FT-IR spectrum of CBTE-1



**Figure 41:**  $^1\text{H}$  NMR spectrum of CBDAN-4 in  $\text{DMSO-d}_6$  at room temperature

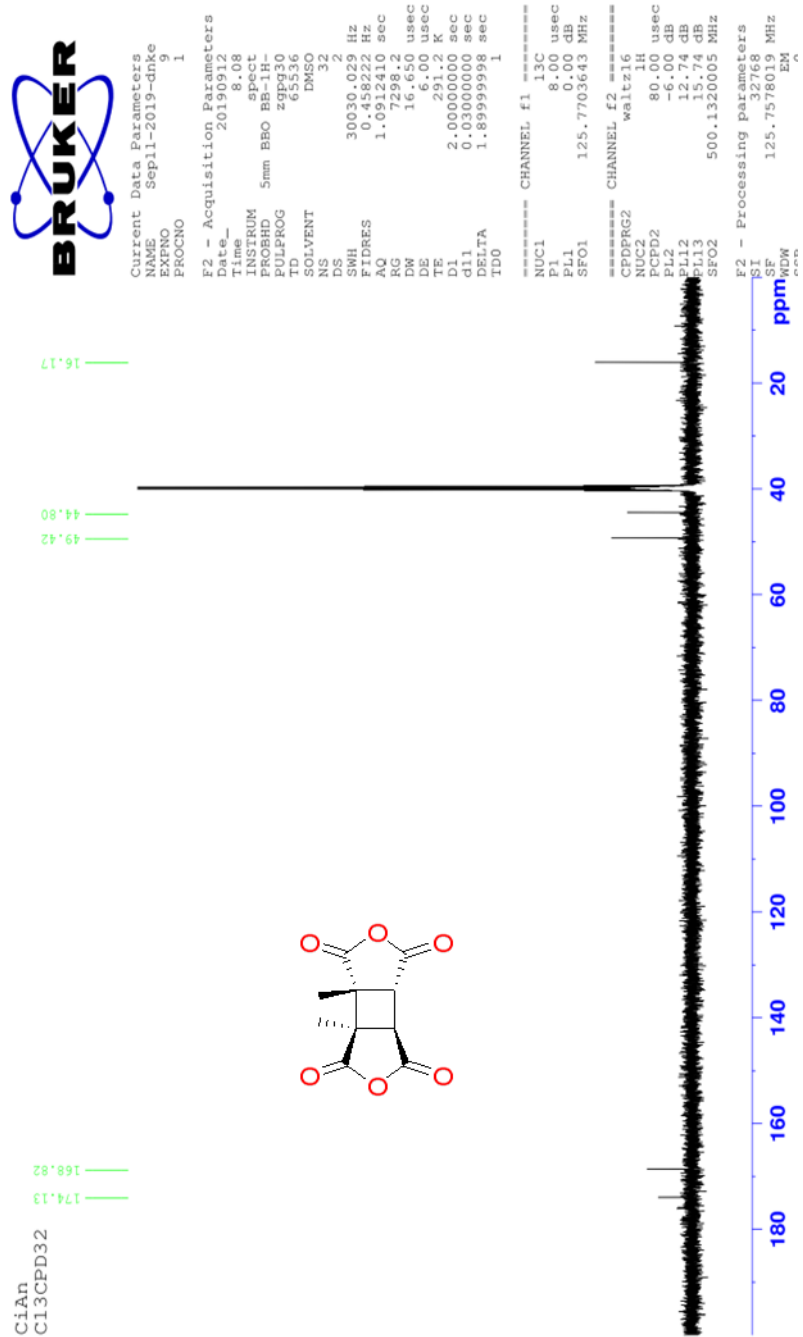


**Figure 42:**  $^{13}\text{C}$  NMR spectrum of CBDAN-4 in  $\text{DMSO-d}_6$  at room temperature

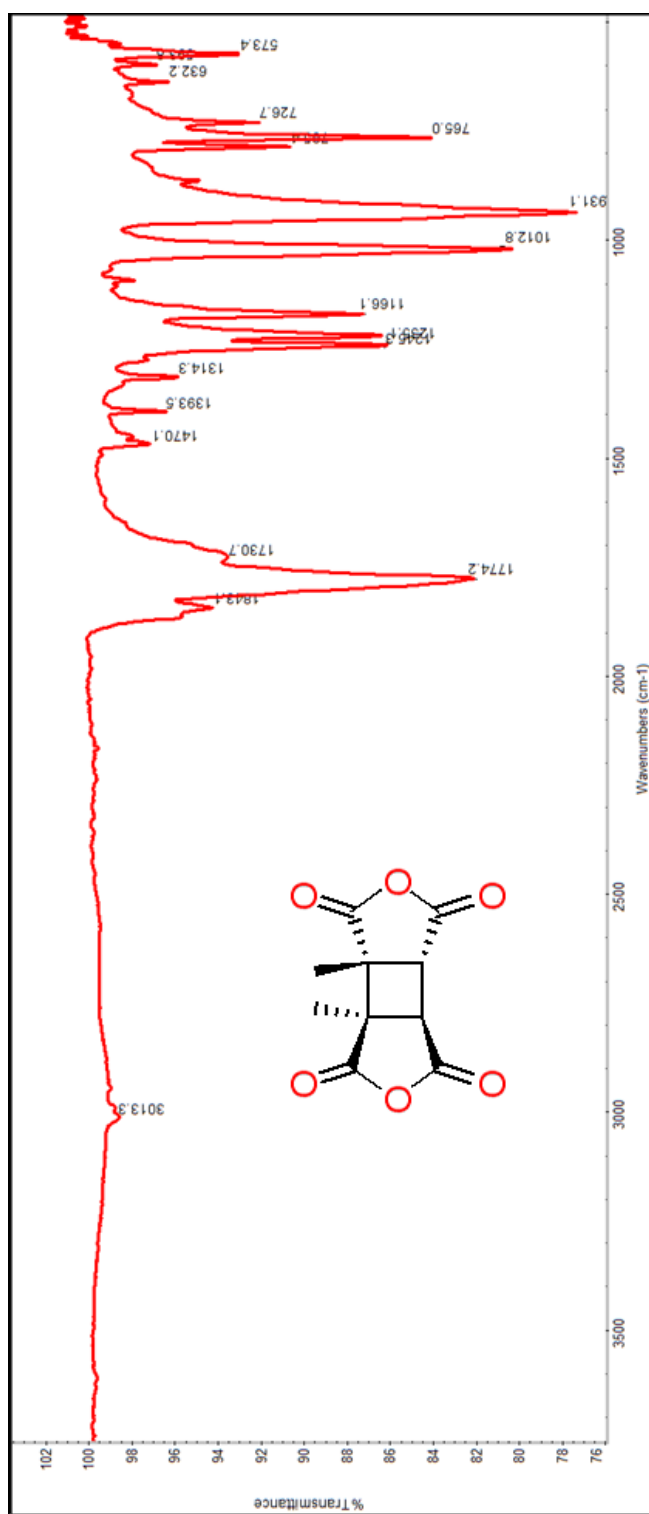


**Figure 43:** FT-IR spectrum of CBDAN-4



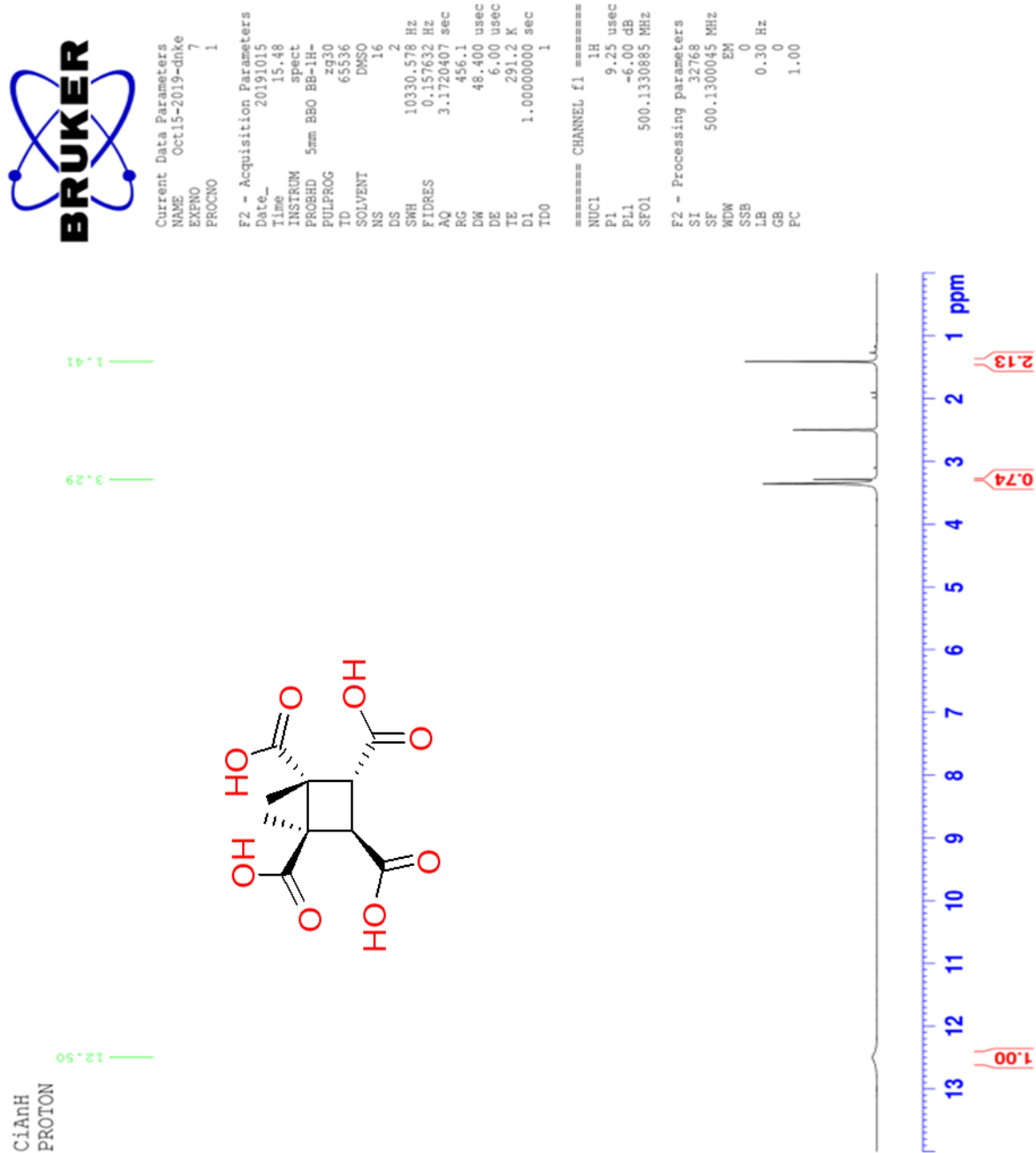


**Figure 44:**  $^1\text{H}$  NMR spectrum of CBTA-4 in  $\text{DMSO-d}_6$  at room temperature

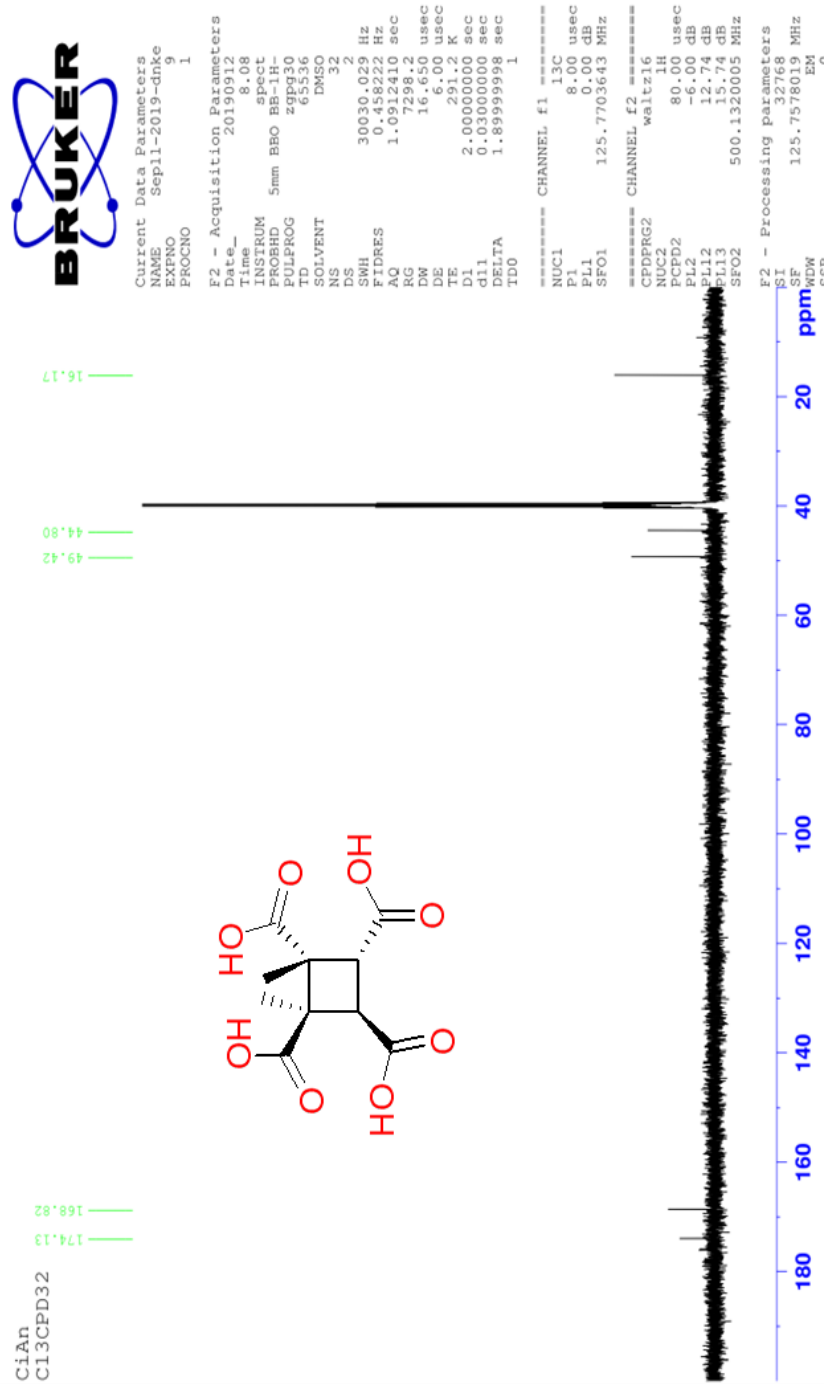


**Figure 45:**  $^{13}\text{C}$  NMR spectrum of CBTA-4 in  $\text{DMSO-d}_6$  at room temperature

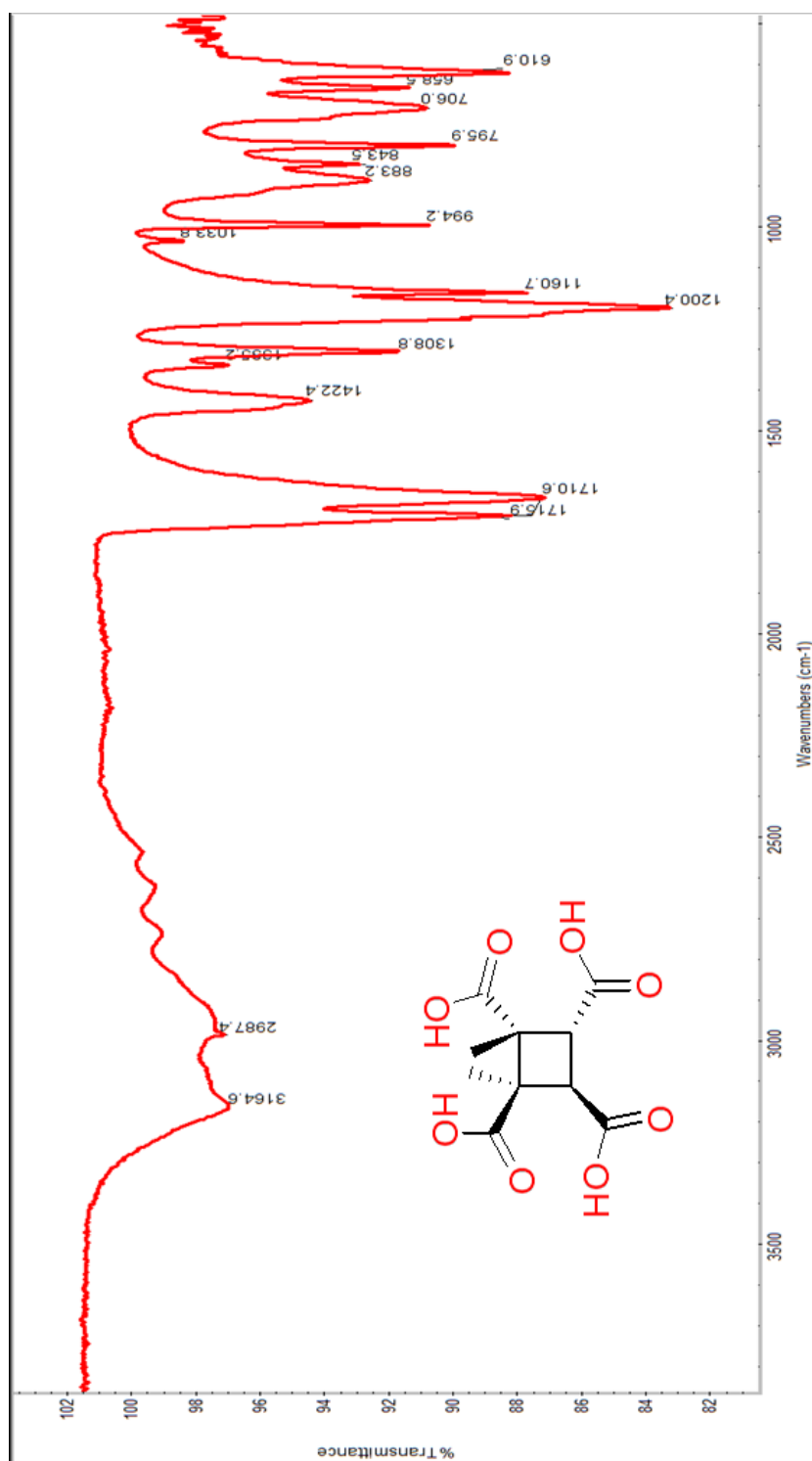


**Figure 46:** FT-IR spectrum of CBTA-4

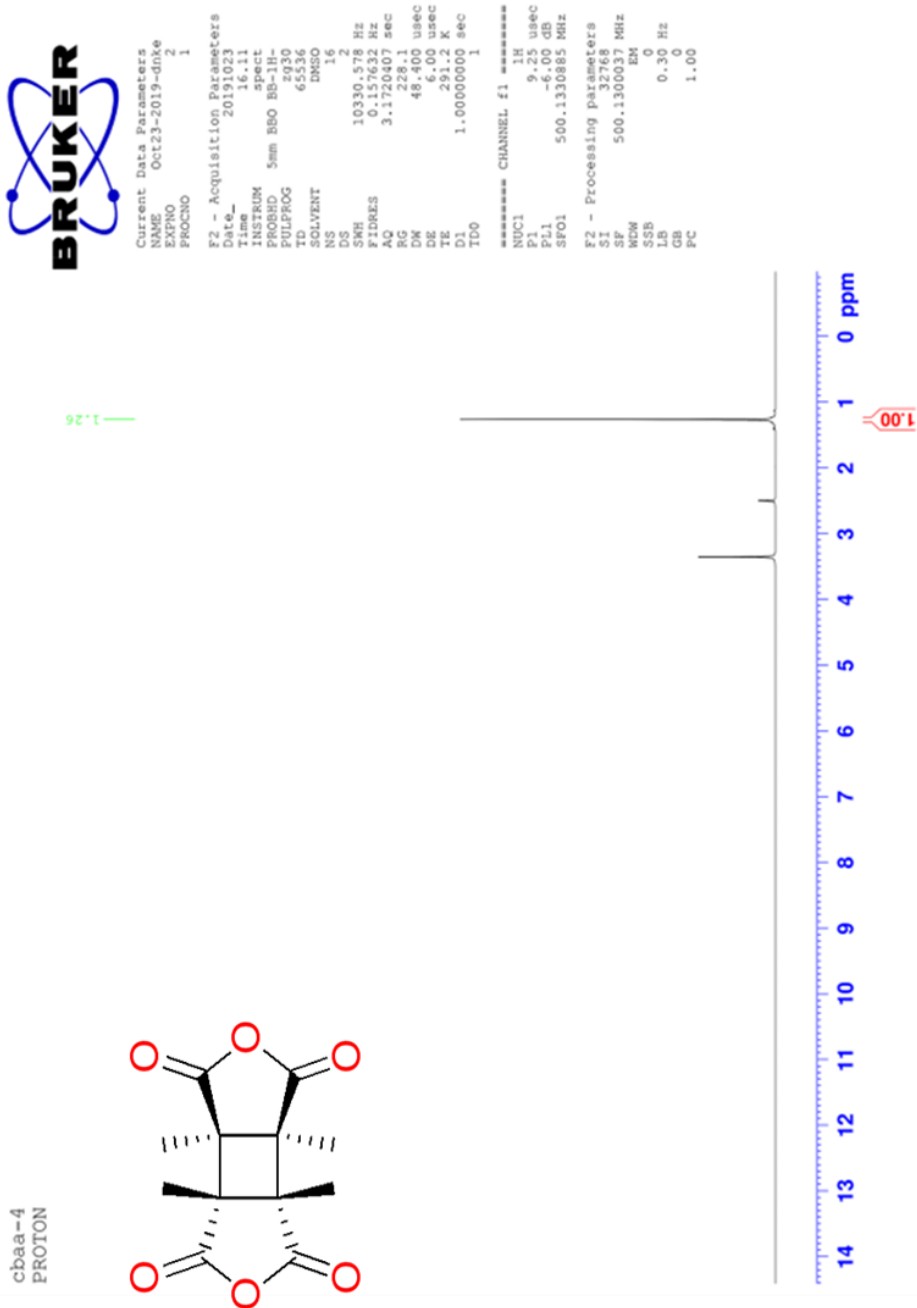
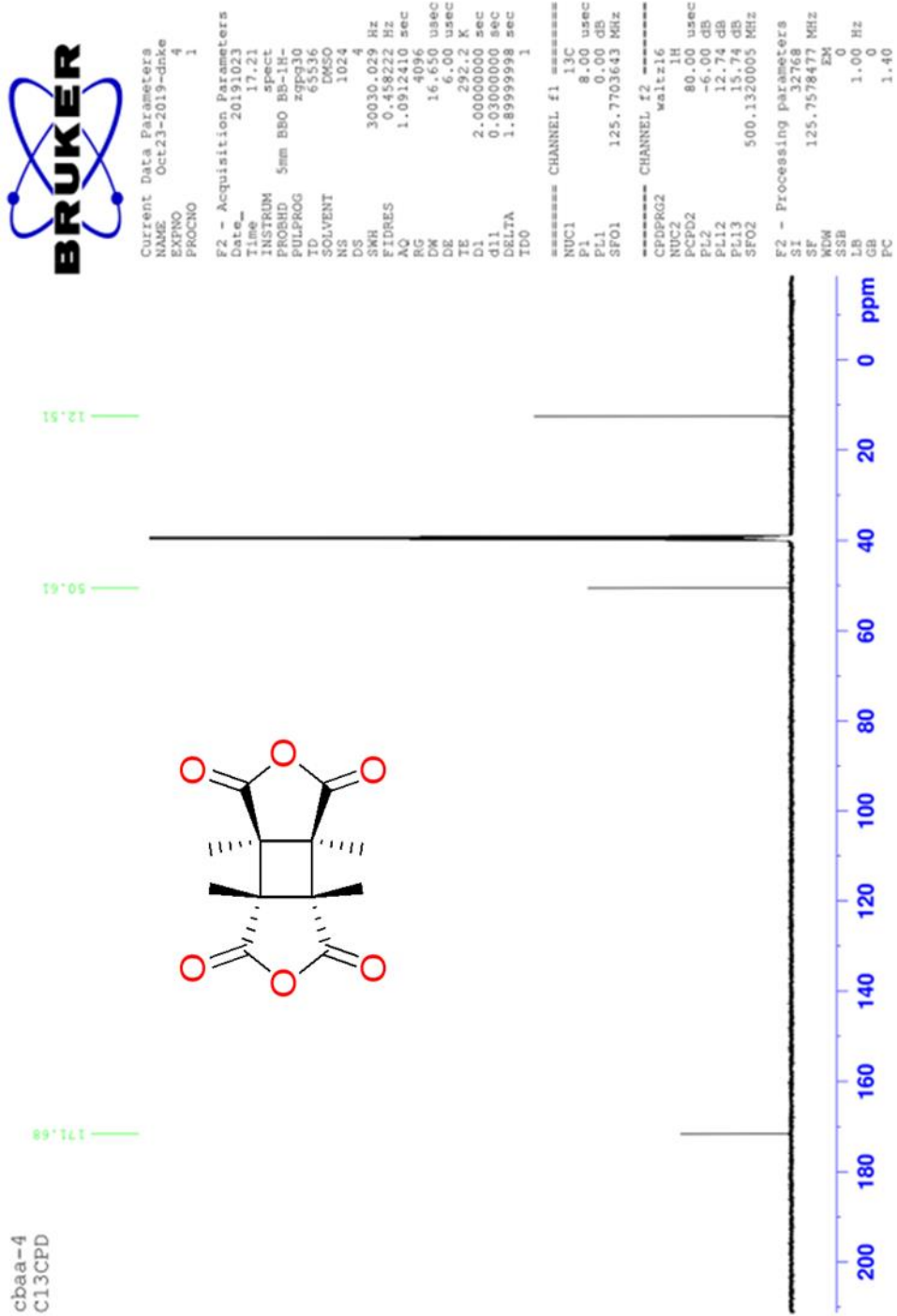
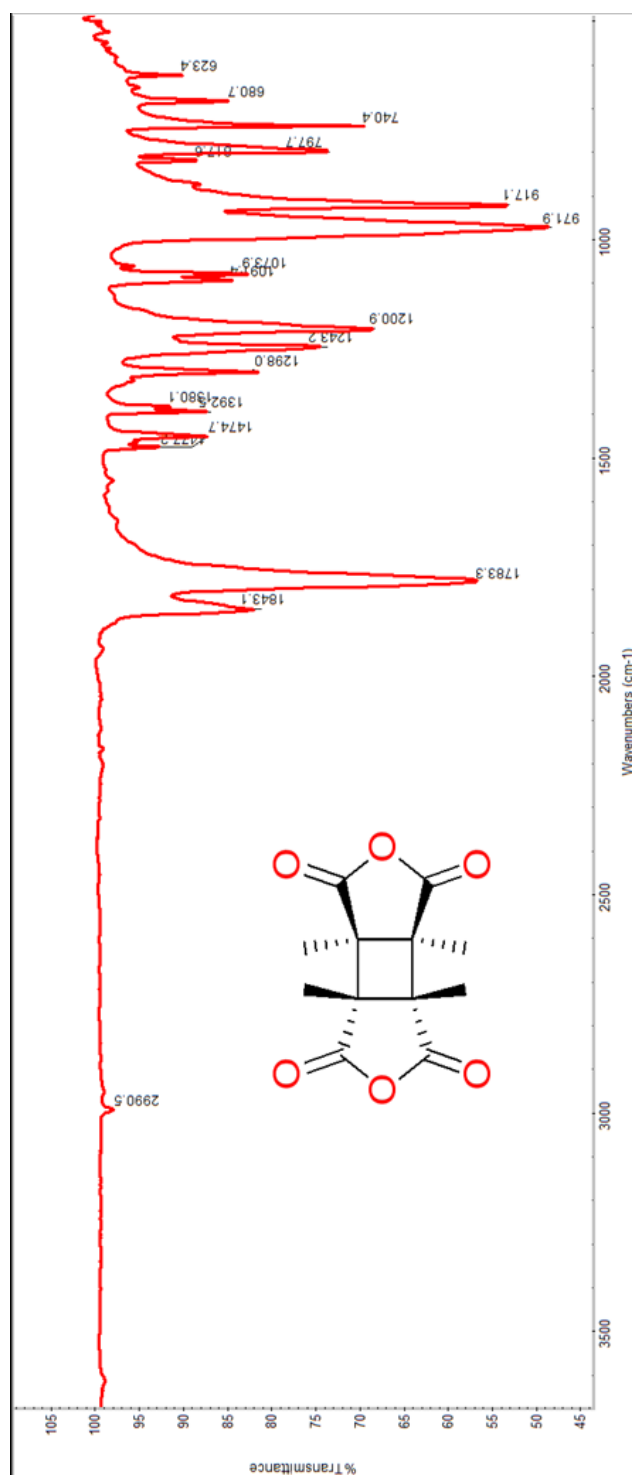


Figure 47:  $^1\text{H}$  NMR spectrum of CBDAN-5 in  $\text{DMSO-d}_6$  at room temperature



**Figure 48:**  $^{13}\text{C}$  NMR spectrum of CBDAN-5 in  $\text{DMSO-d}_6$  at room temperature



**Figure 49:** FT-IR spectrum of CBDAN-5

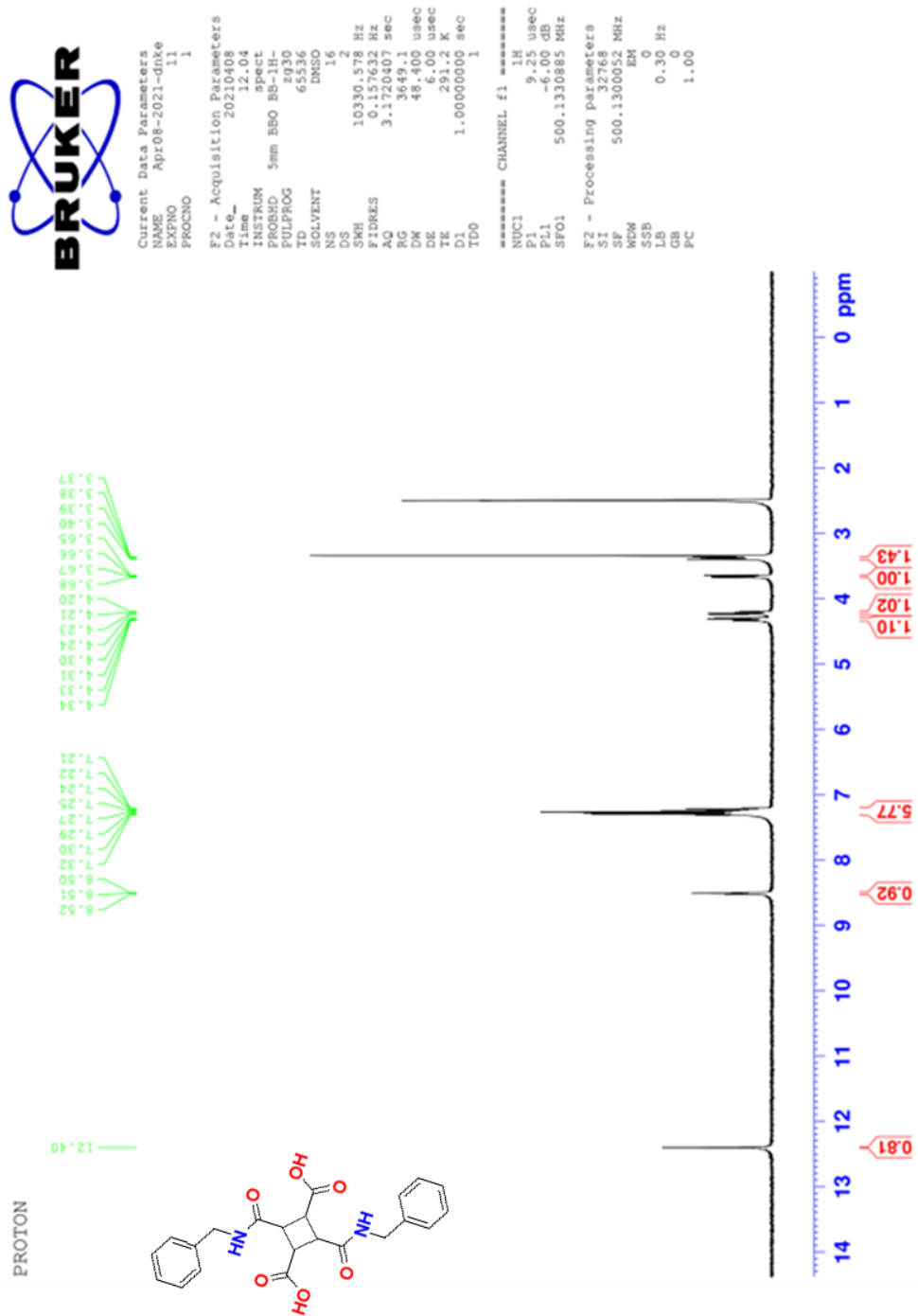


Figure 50:  $^1\text{H}$  NMR spectrum of CBDax-1 in  $\text{DMSO-d}_6$  at room temperature

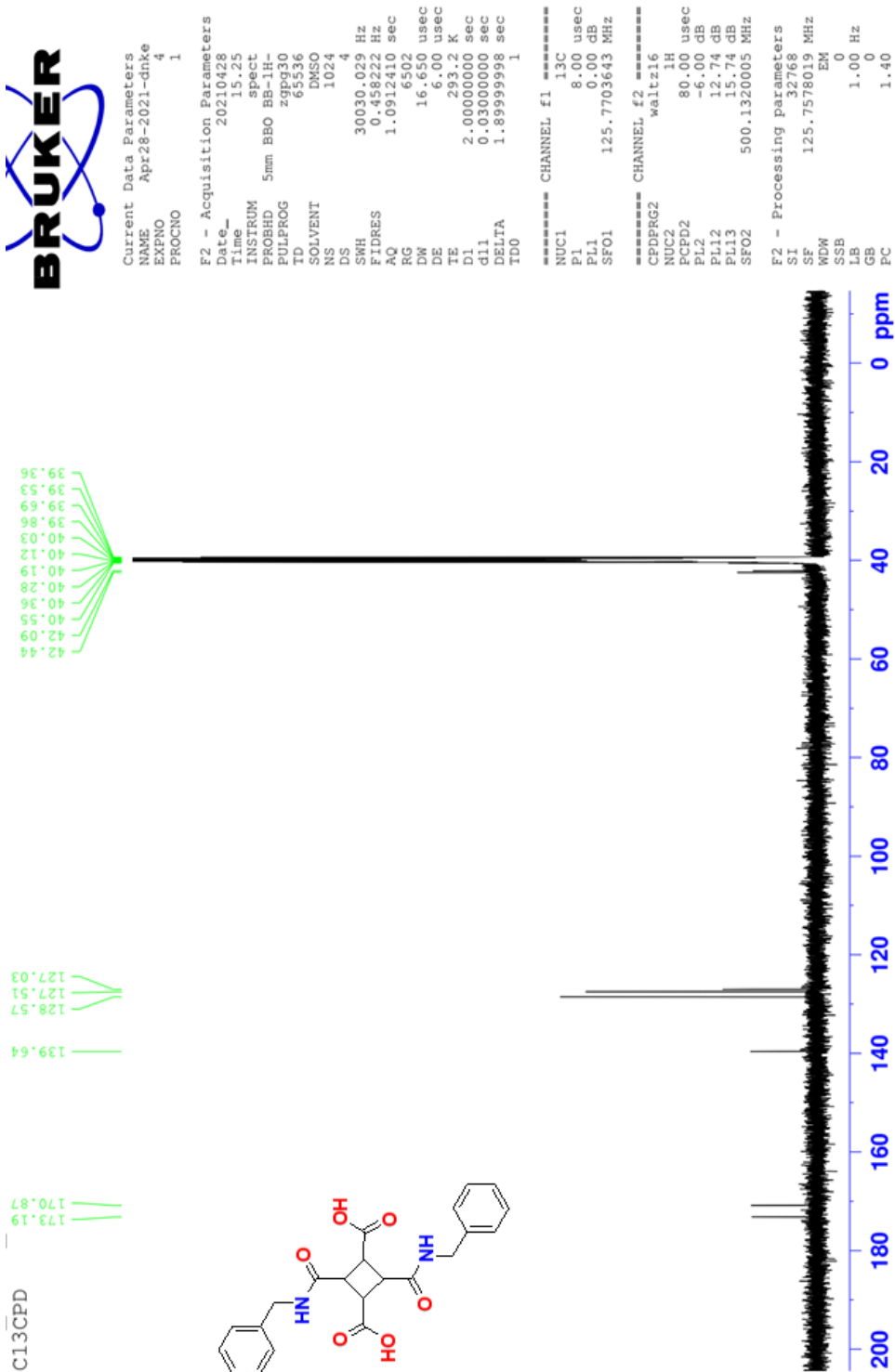
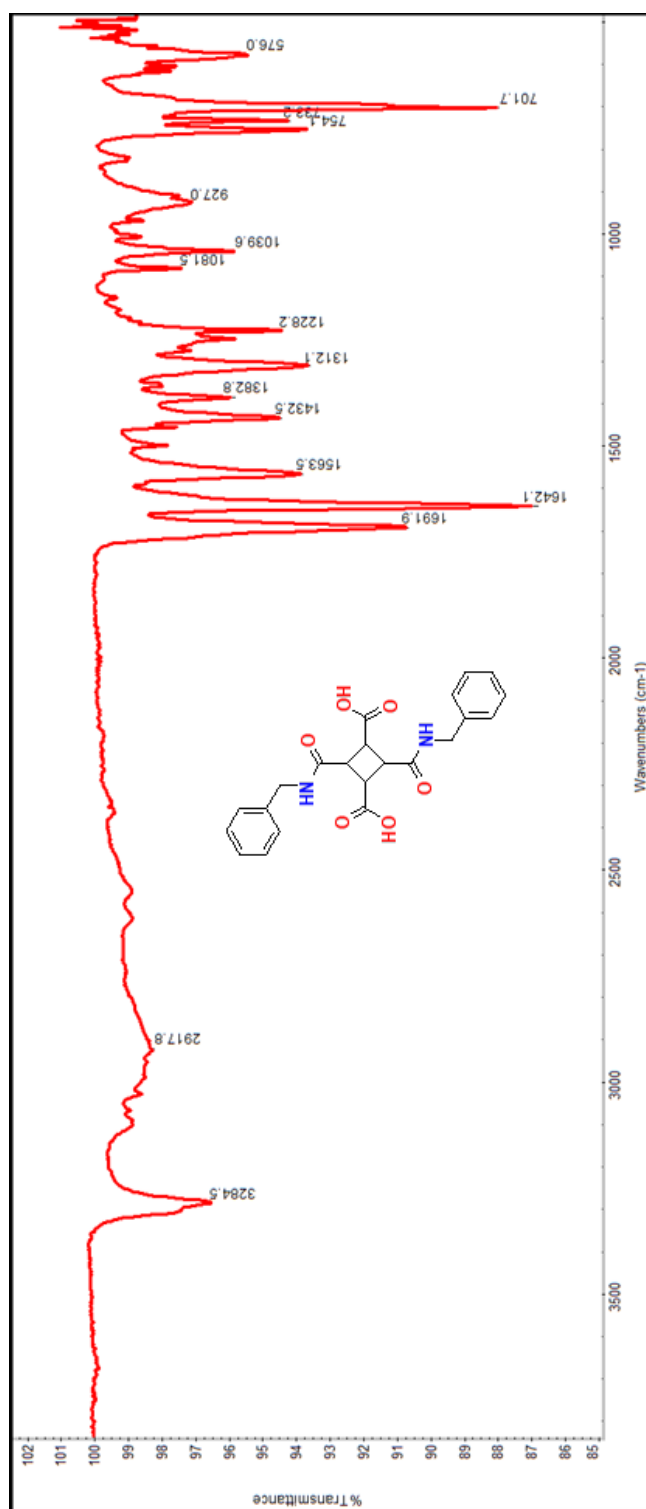
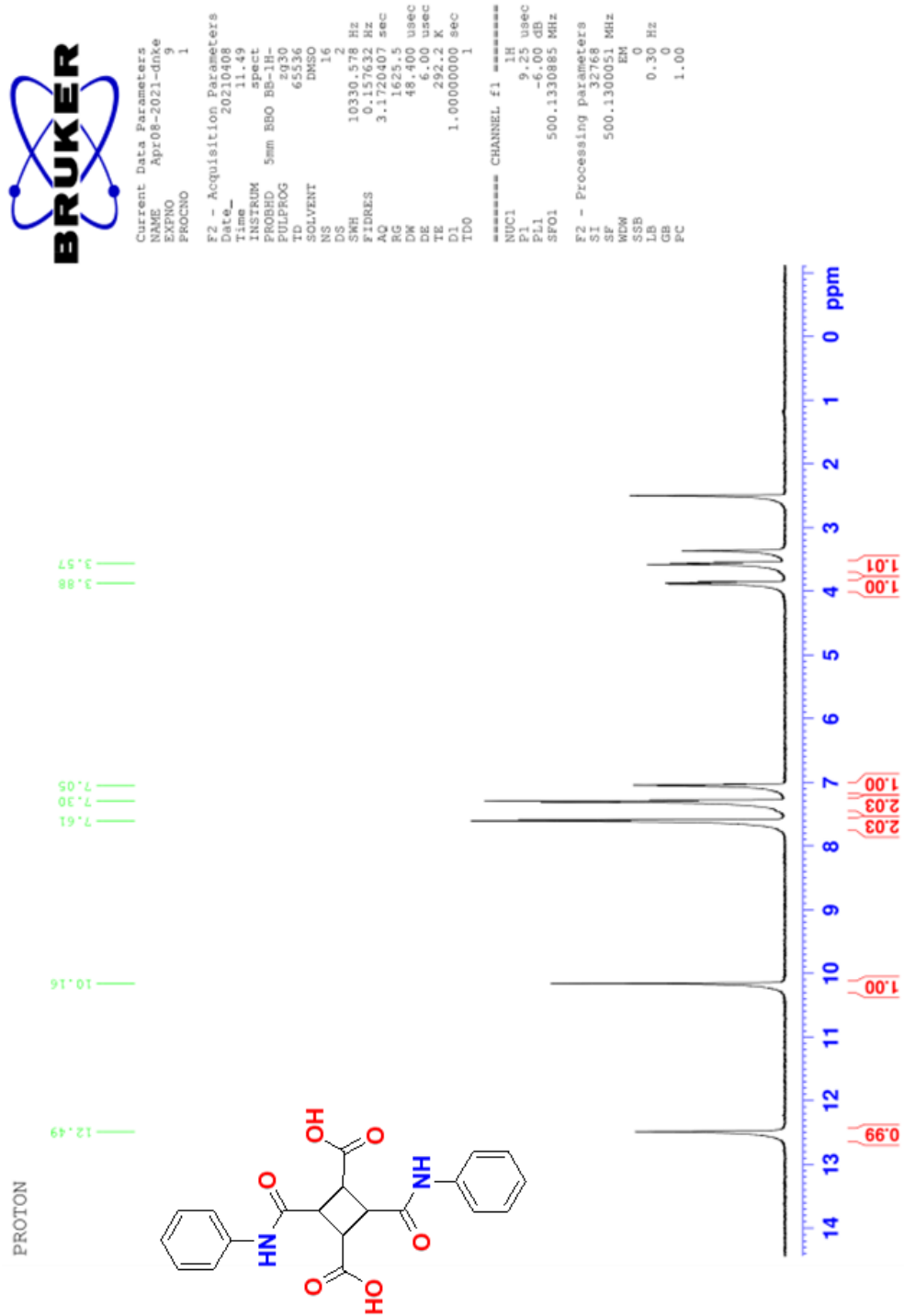


Figure 51:  $^{13}\text{C}$  NMR spectrum of CBDAx-1 in DMSO- $d_6$  at room temperature





**Figure 52:** FT-IR spectrum of CBDAx-1



**Figure 53:**  $^1\text{H}$  NMR spectrum of CBDax-2 in  $\text{DMSO-d}_6$  at room temperature



Current Data Parameters  
NAME Apr21-2021-dnke  
EXPNO 4  
PROCNO 1

F2 - Acquisition Parameters  
Date\_ 20210421  
Time 21.37  
INSTRUM spect  
PROBHD 5mm BBO BB-1H-  
PULPROG zgpg30  
TD 65536  
SOLVENT DMSO  
NS 1024  
DS 4  
SWH 30030.029 Hz  
FIDRES 0.458222 Hz  
AQ 1.0912410 sec  
RG 7298.2  
DW 16.650 usec  
DE 6.00 usec  
TE 292.2 K  
D1 2.00000000 sec  
d11 0.03000000 sec  
DELTA 1.89999998 sec  
TD0 1

===== CHANNEL f1 =====  
NUC1 13C  
P1 8.00 usec  
PL1 0.00 dB  
SFO1 125.7703643 MHz

===== CHANNEL f2 =====  
CPDPRG2 waltz16  
NUC2 1H  
PCPD2 80.00 usec  
PL2 -6.00 dB  
PL12 12.74 dB  
PL13 15.74 dB  
SFO2 500.1320005 MHz

F2 - Processing parameters  
SI 32768  
SF 125.7578019 MHz  
WDW EM  
SSB 0  
LB 1.00 Hz  
GB 0  
PC 1.40

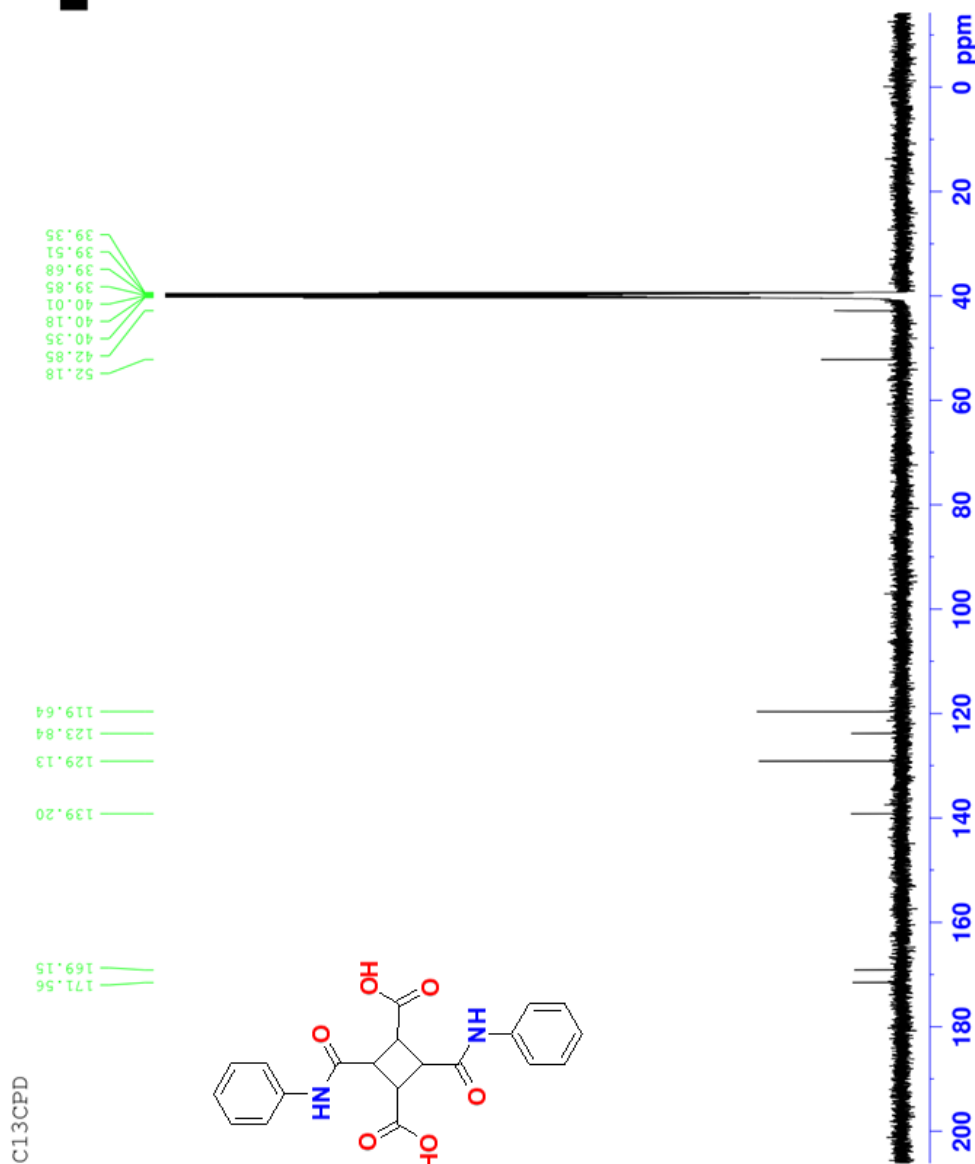
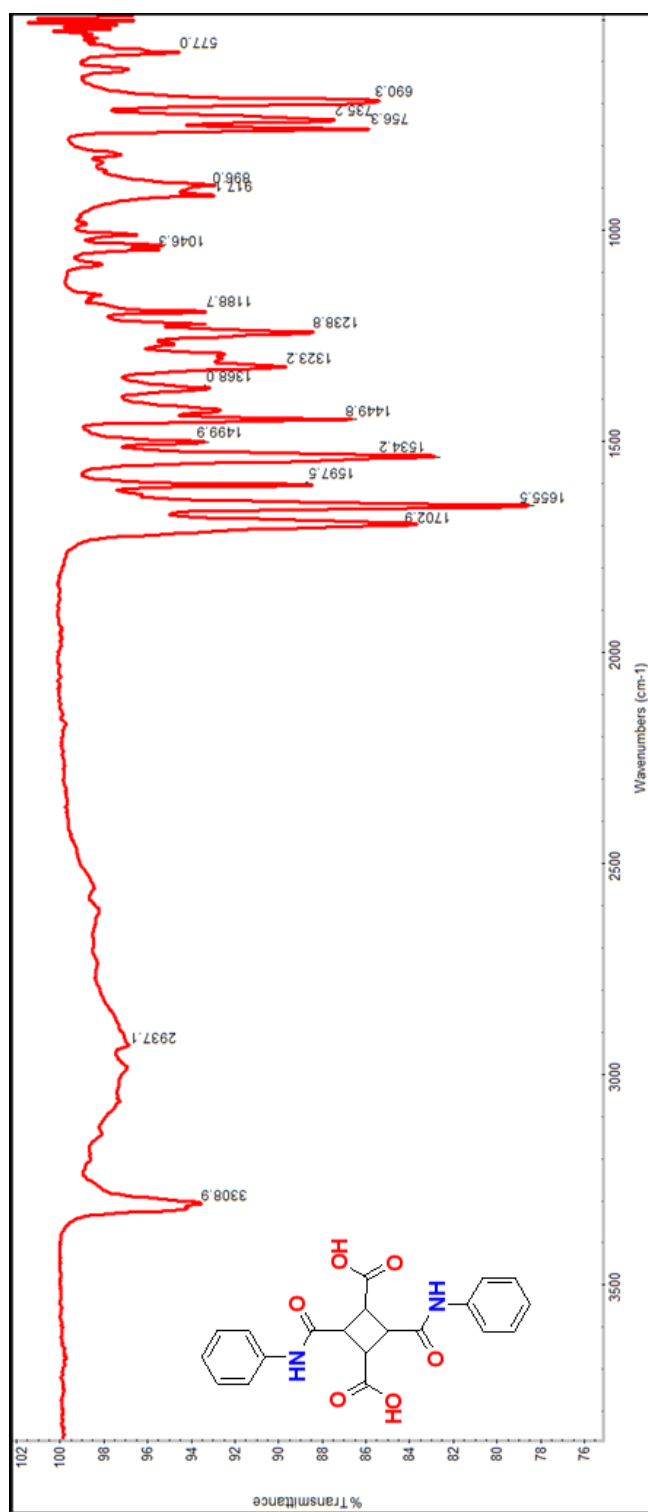
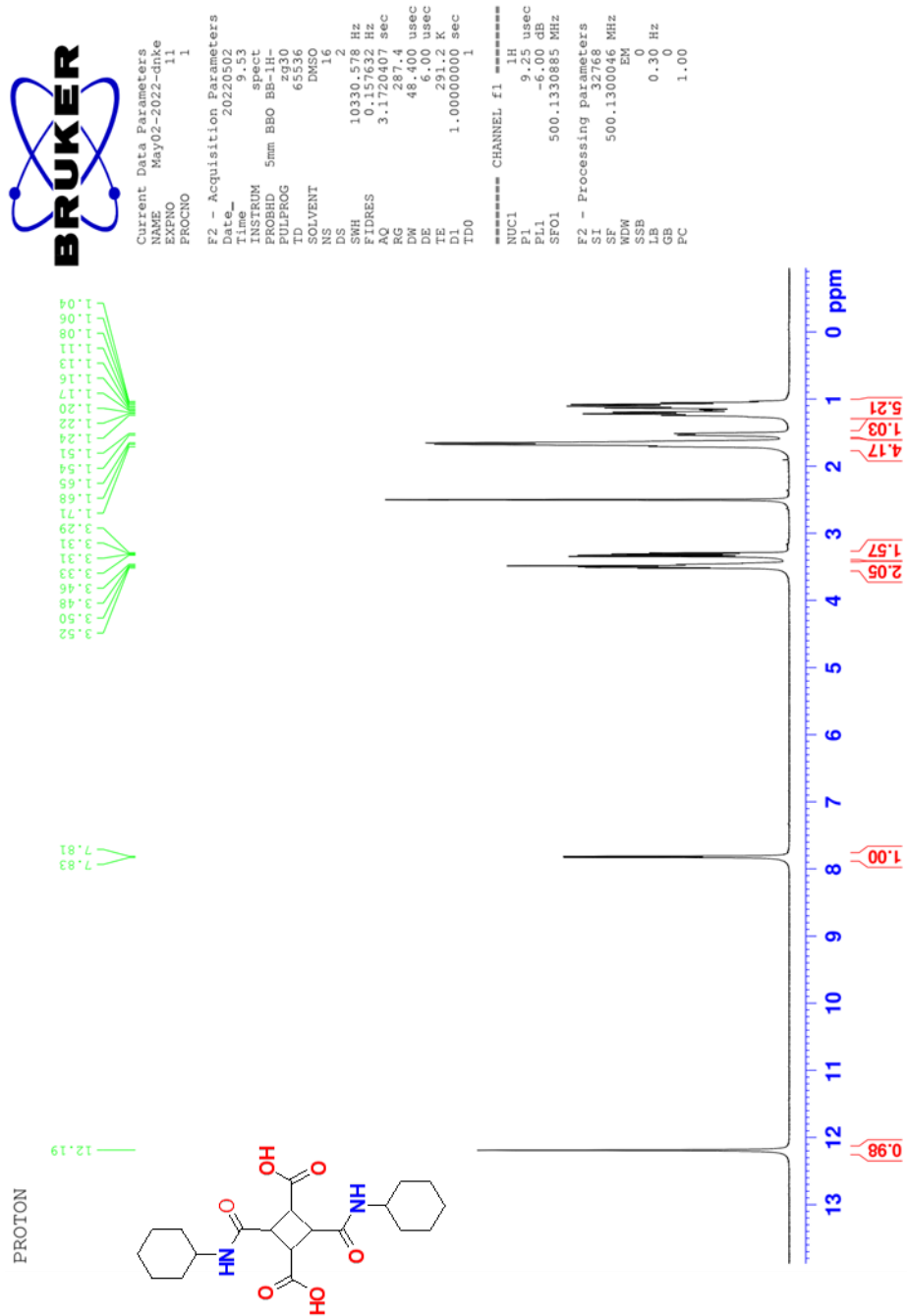


Figure 54: <sup>13</sup>C NMR spectrum of CBDAX-2 in DMSO-d<sub>6</sub> at room temperature



**Figure 55:** FT-IR spectrum of CBDAx-2



**Figure 56:**  $^1\text{H}$  NMR spectrum of CBDax-3 in  $\text{DMSO-d}_6$  at room temperature



Current Data Parameters  
NAME May02-2022-dnke  
EXPNO 15  
PROCNO 1

F2 - Acquisition Parameters  
Date\_ 20220502  
Time 12.00  
INSTRUM spect  
PROBHD 5mm BBO BB-1H  
PULPROG zgpg30  
TD 65536  
SOLVENT DMSO  
NS 1024  
DS 4  
SWH 30030.029 Hz  
FIDRES 0.458222 Hz  
AQ 1.0912410 sec  
RG 13004  
DW 16.650 usec  
DE 6.00 usec  
TE 292.2 K  
D1 2.00000000 sec  
d11 0.03000000 sec  
DELTA 1.89999998 sec  
TD0 1

===== CHANNEL f1 =====  
NUC1 13C  
P1 8.00 usec  
PL1 0.00 dB  
SFO1 125.7703643 MHz

===== CHANNEL f2 =====  
CFPRG2 waltz16  
NUC2 1H  
PCPD2 80.00 usec  
PL2 -6.00 dB  
PL12 12.74 dB  
PL13 15.74 dB  
SFO2 500.1320005 MHz

F2 - Processing parameters  
SI 32768  
SF 125.7578519 MHz  
MVM EM  
SSB 0  
LB 1.00 Hz  
GB 0  
PC 1.40

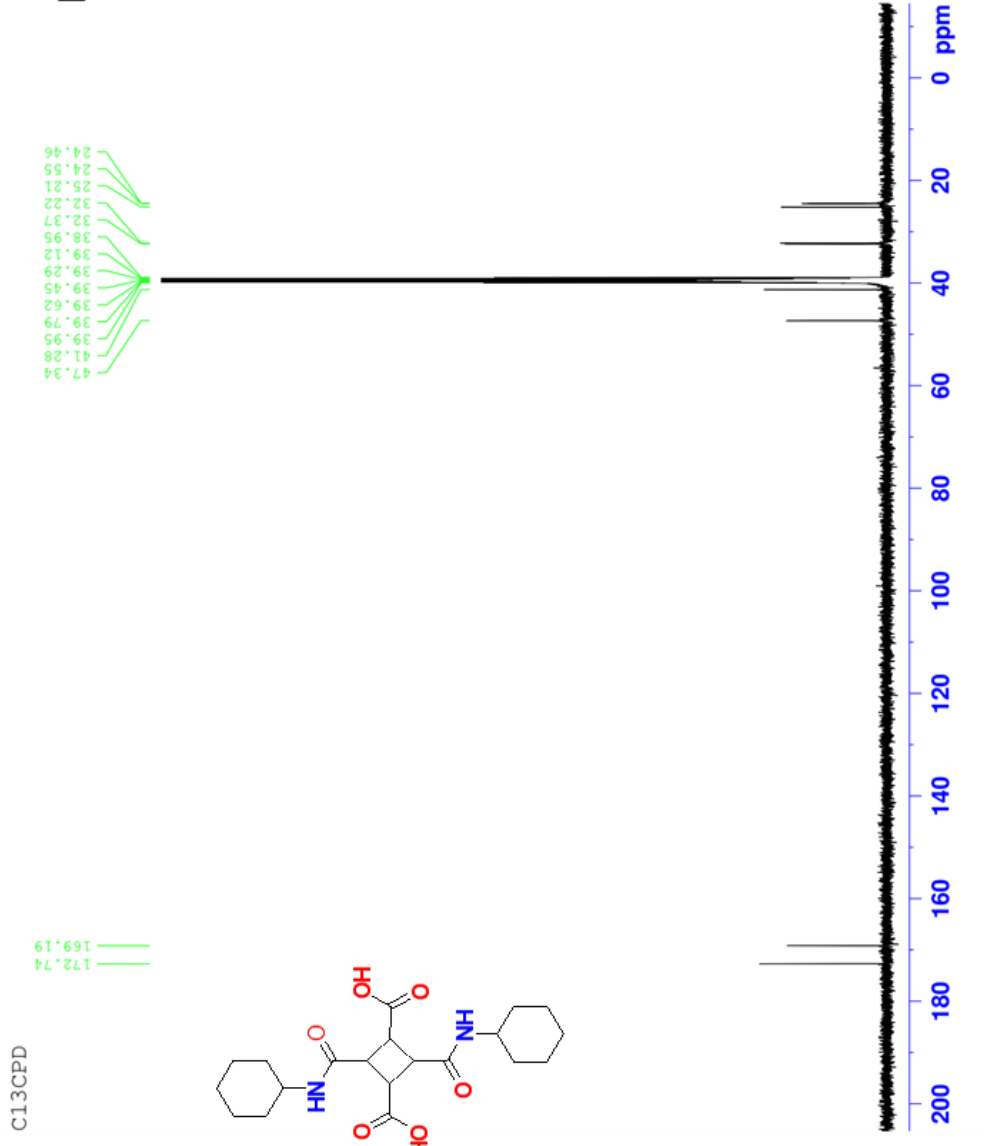


Figure 57: <sup>13</sup>C NMR spectrum of CBDax-3 in DMSO-d<sub>6</sub> at room temperature

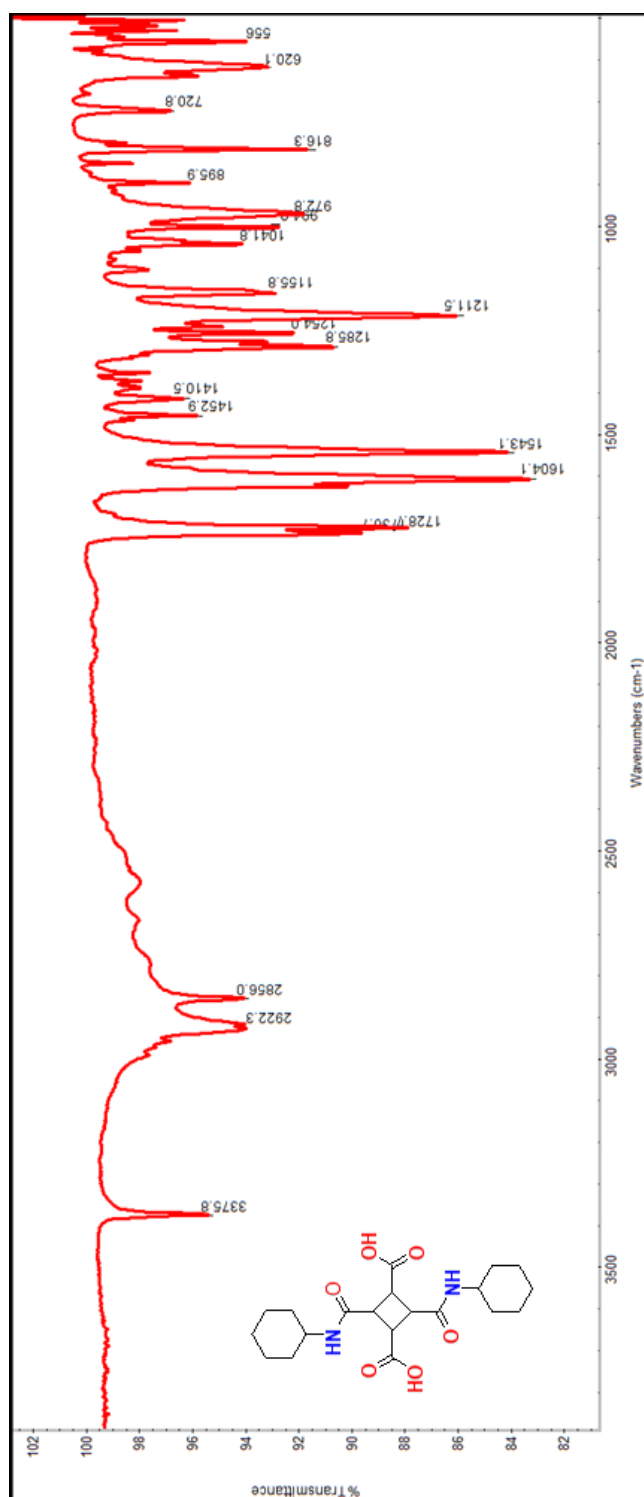


Figure 58: FT-IR spectrum of CBDAx-3

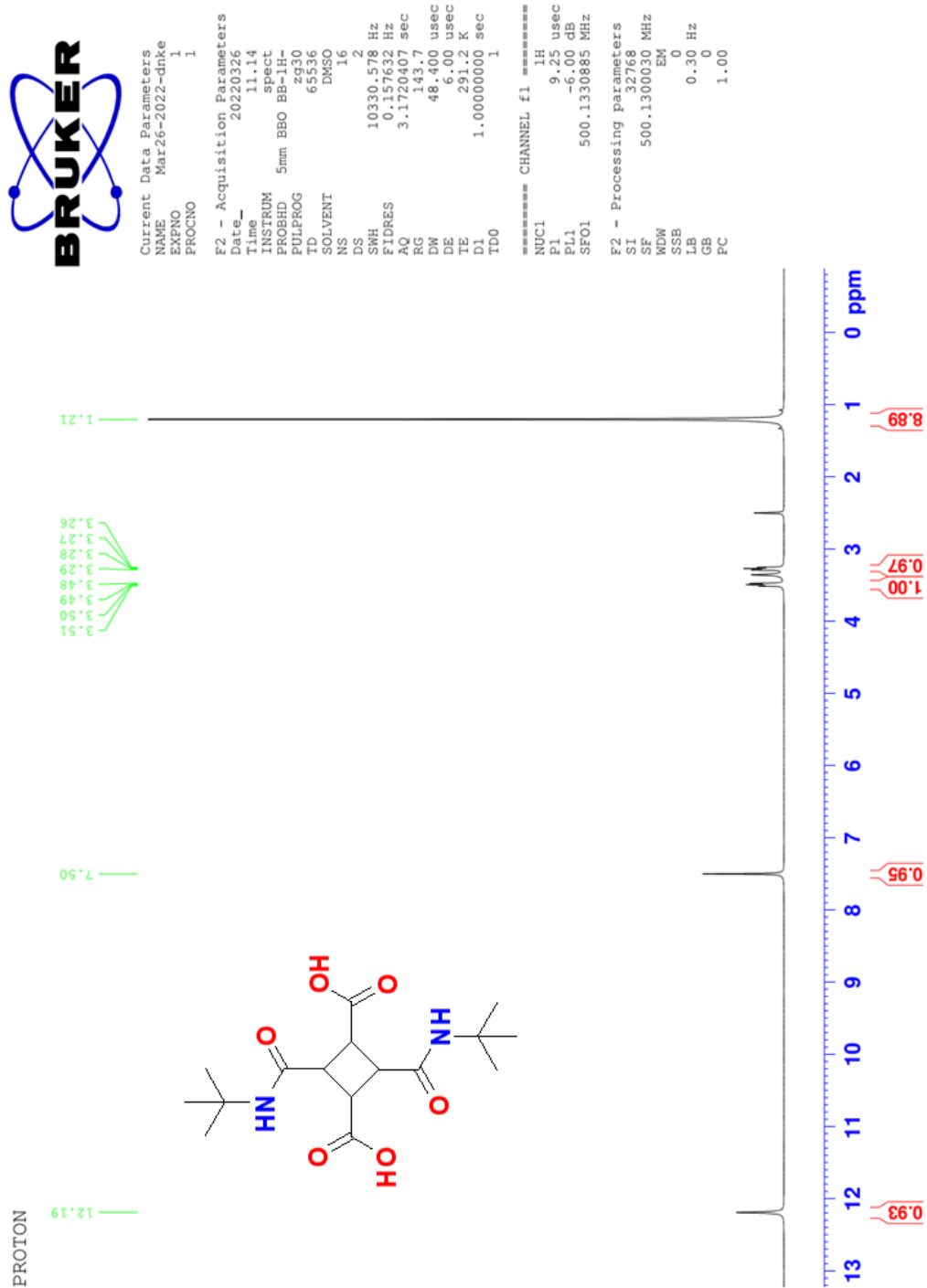


Figure 59:  $^1\text{H}$  NMR spectrum of CBDax-4 in  $\text{DMSO-d}_6$  at room temperature



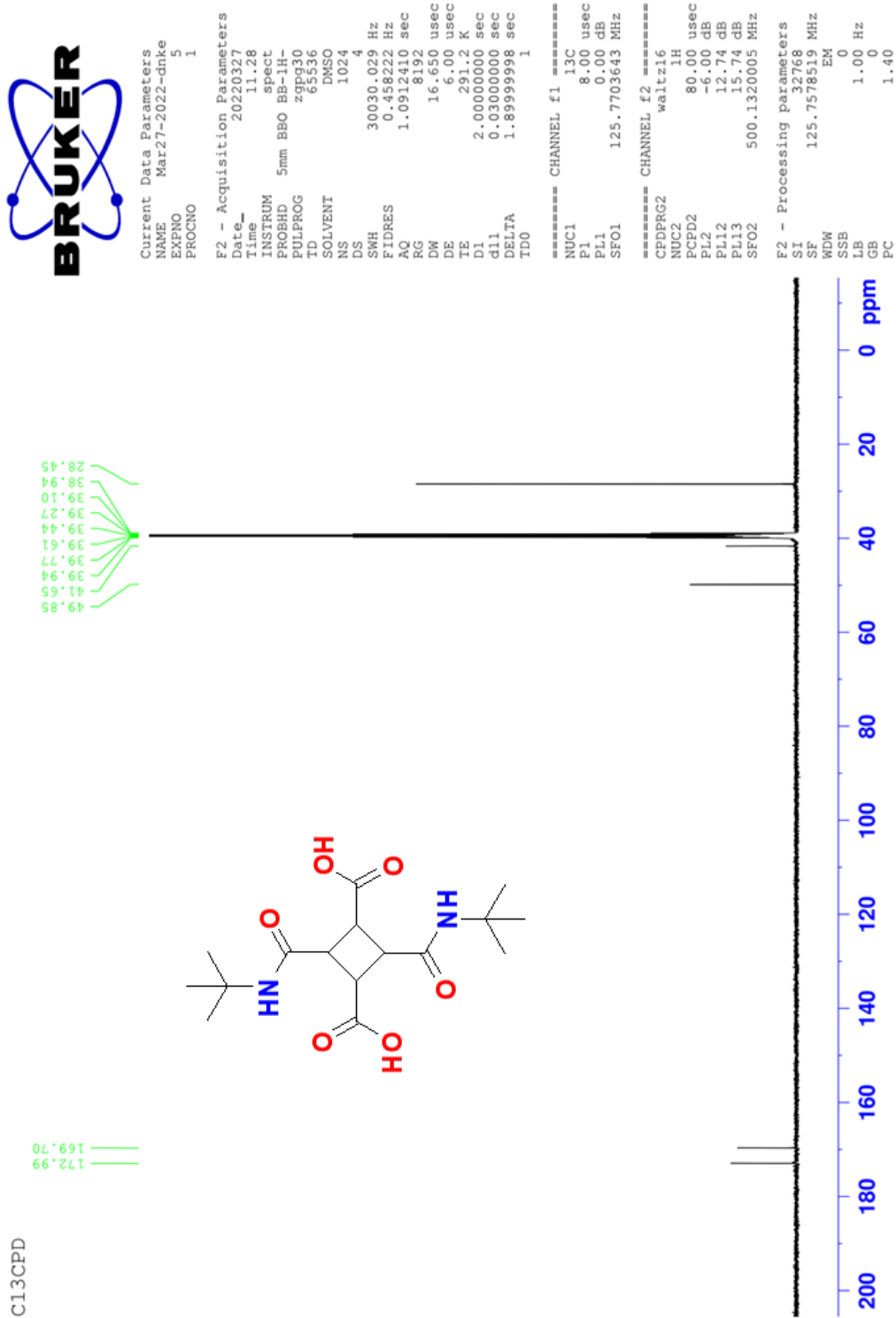
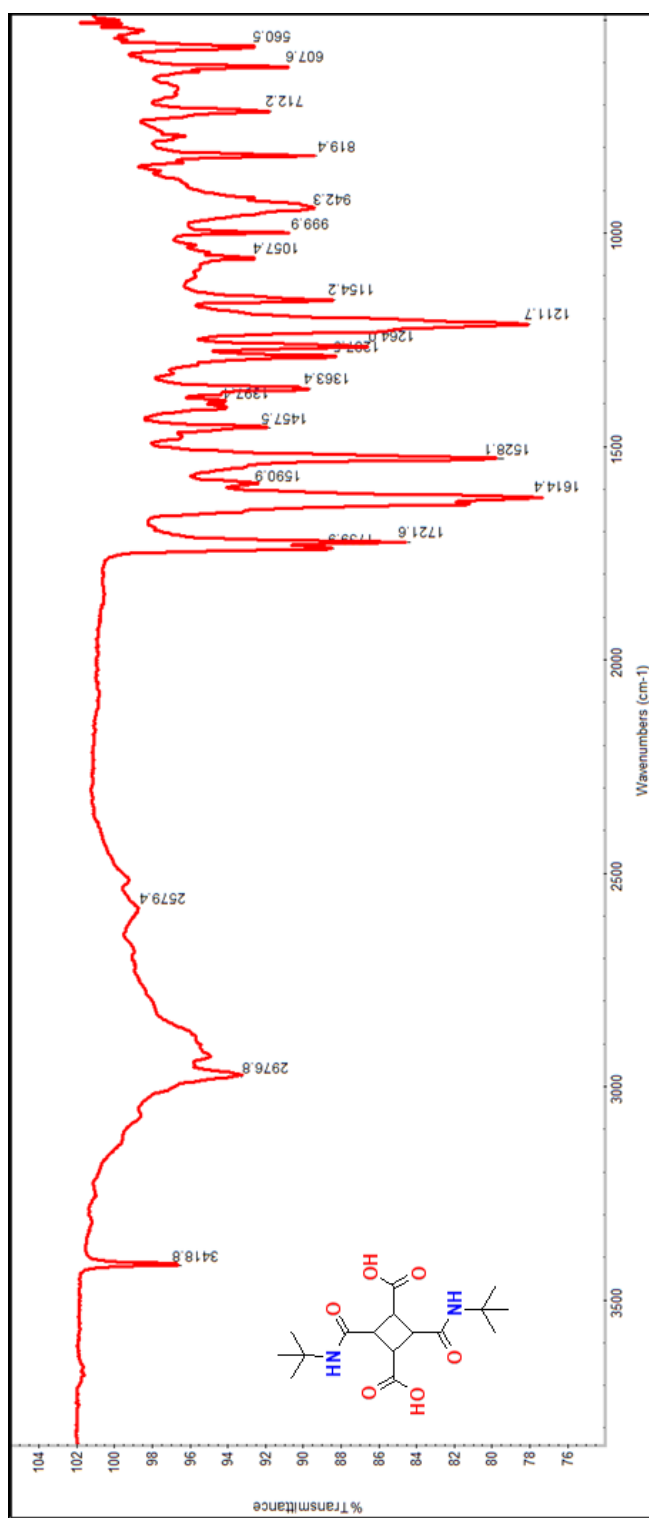


Figure 60: <sup>13</sup>C NMR spectrum of CBDax-4 in DMSO-d<sub>6</sub> at room temperature



**Figure 61:** FT-IR spectrum of CBDAx-4

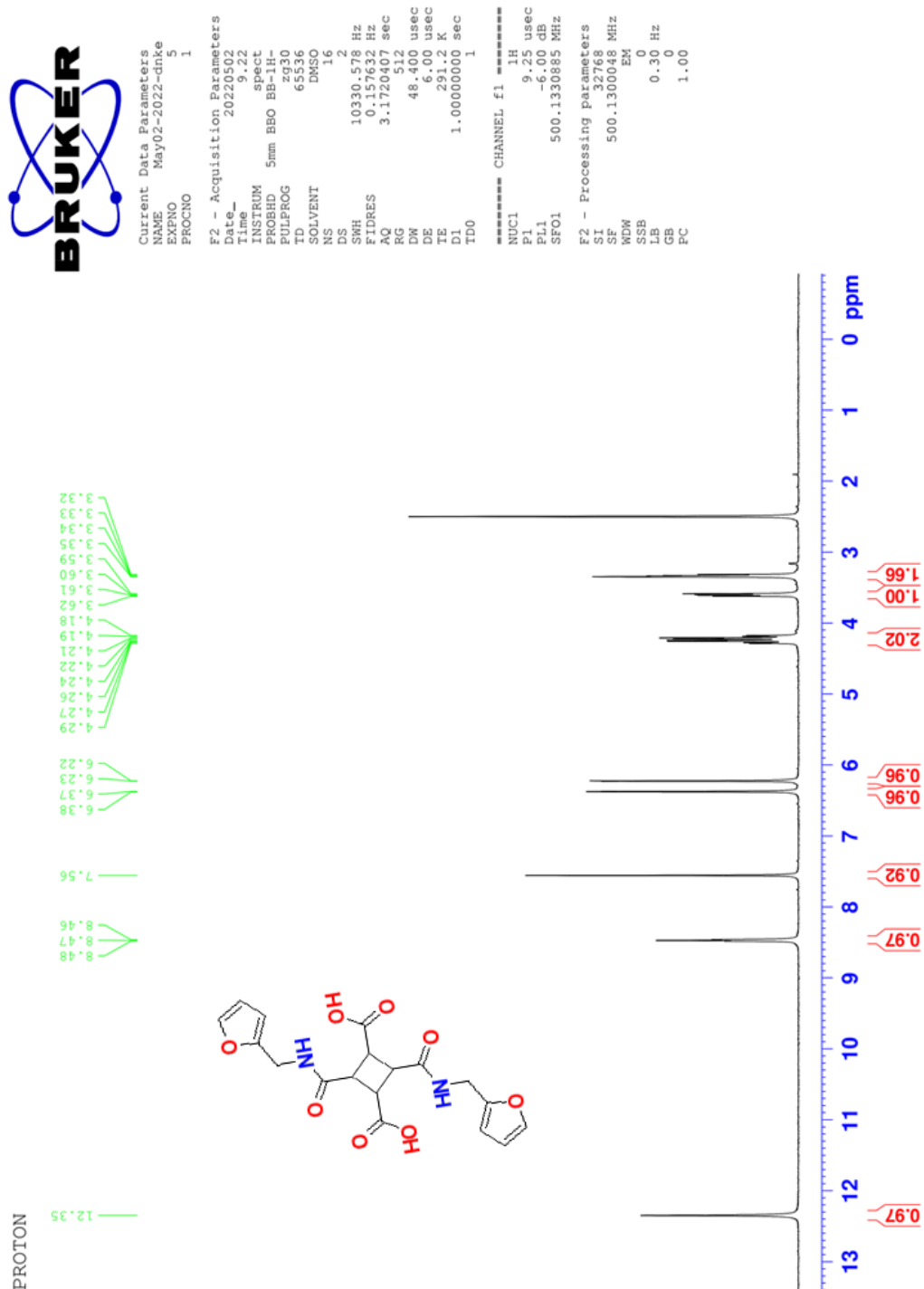


Figure 62: <sup>1</sup>H NMR spectrum of CBDAx-5 in DMSO-d<sub>6</sub> at room temperature

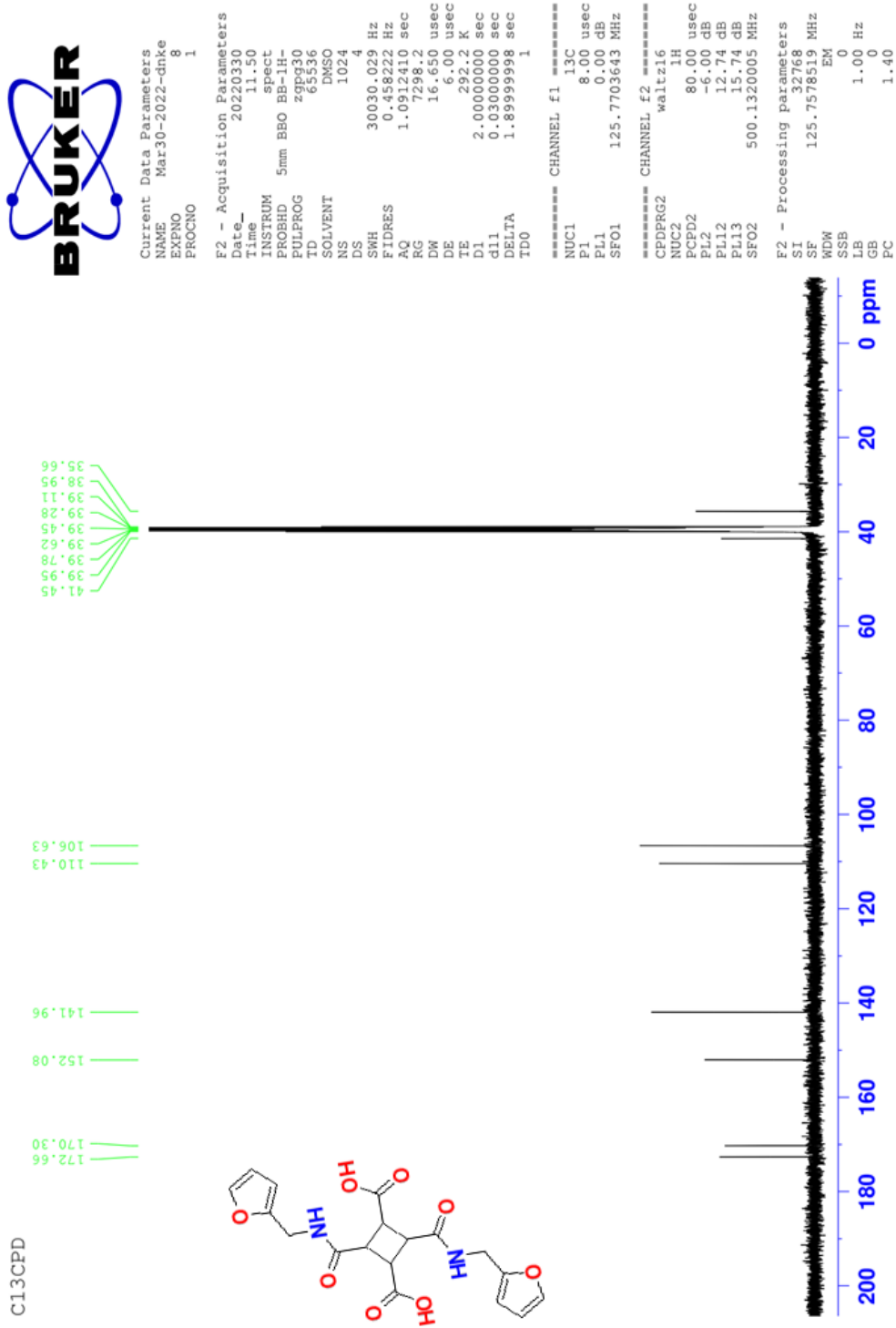
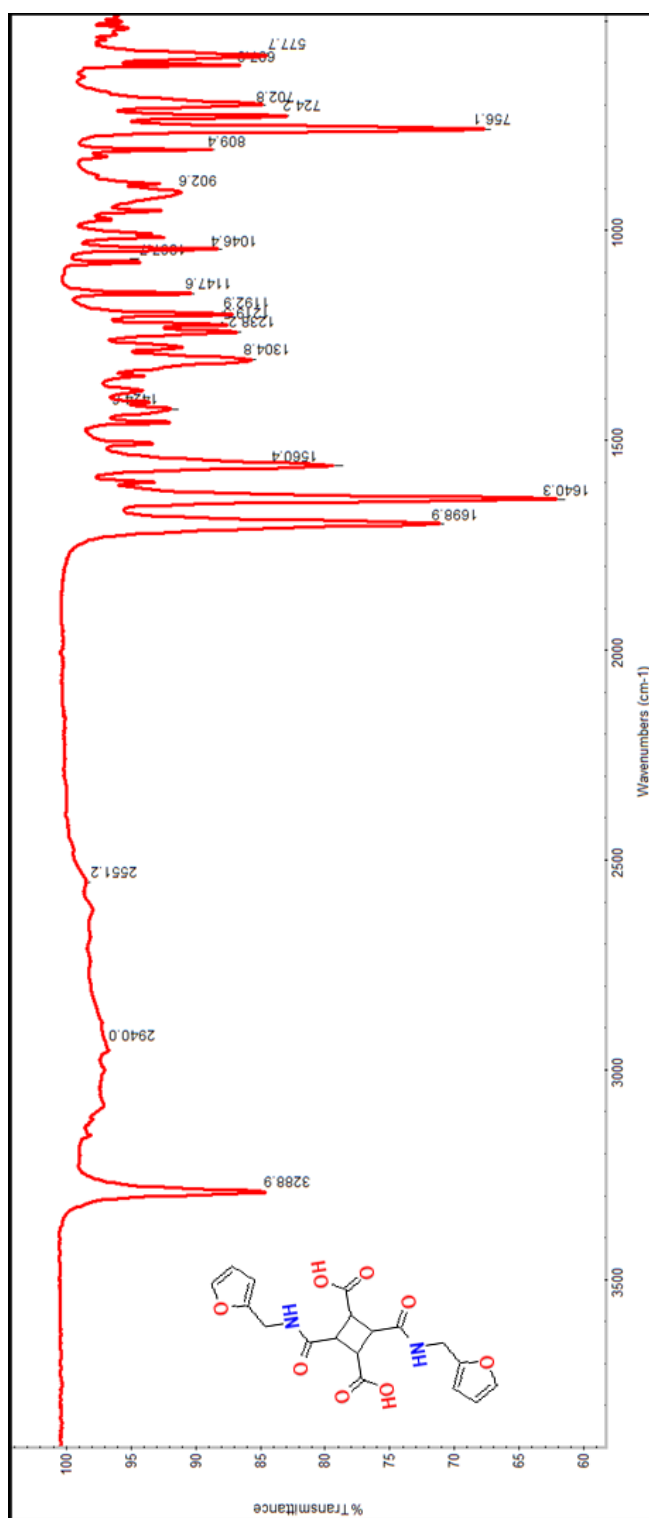
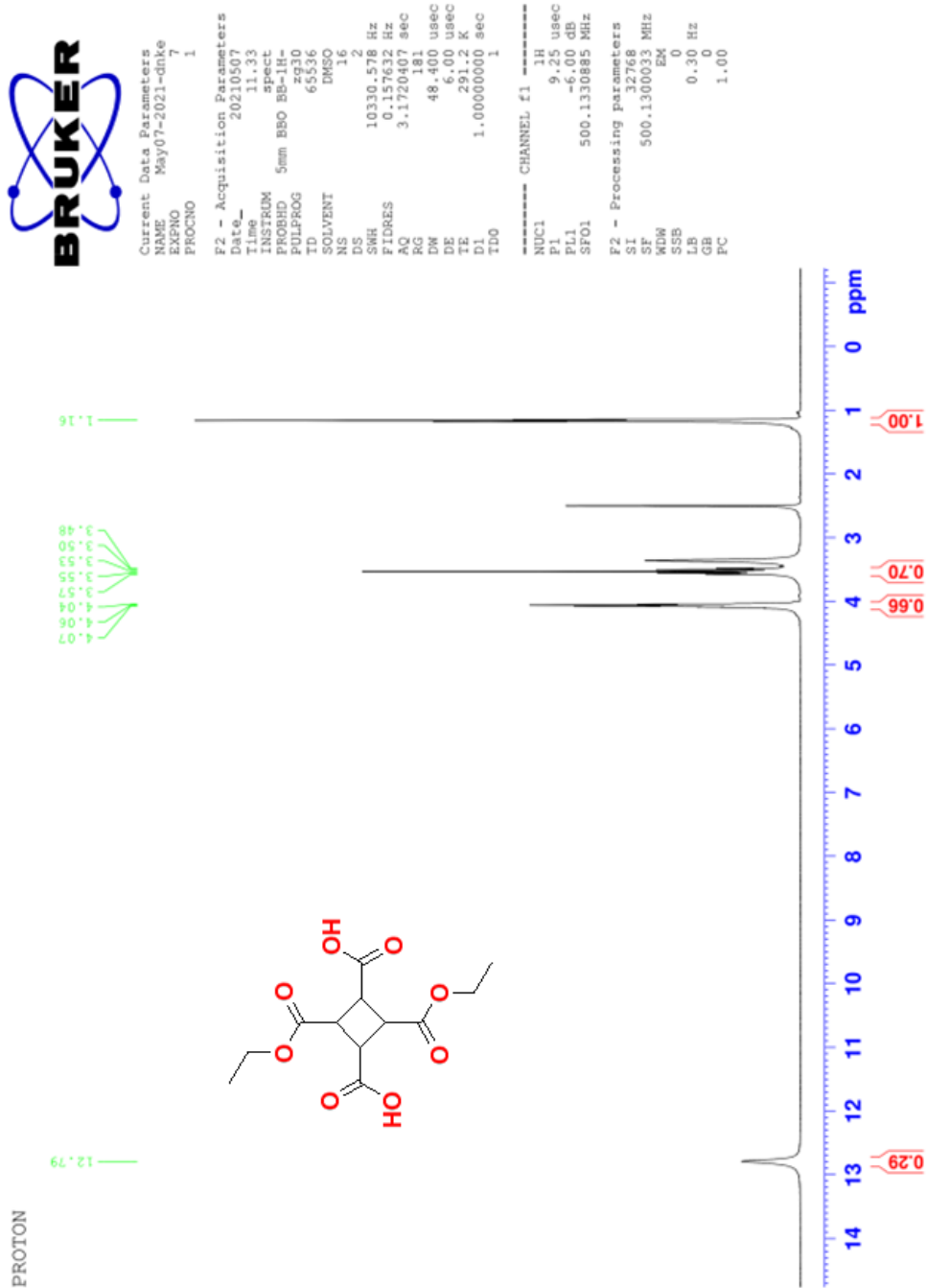


Figure 63:  $^{13}\text{C}$  NMR spectrum of CBDax-5 in  $\text{DMSO-d}_6$  at room temperature



**Figure 64:** FT-IR spectrum of CBDAX-5



**Figure 65:**  $^1\text{H}$  NMR spectrum of CBDax-6 in  $\text{DMSO-d}_6$  at room temperature

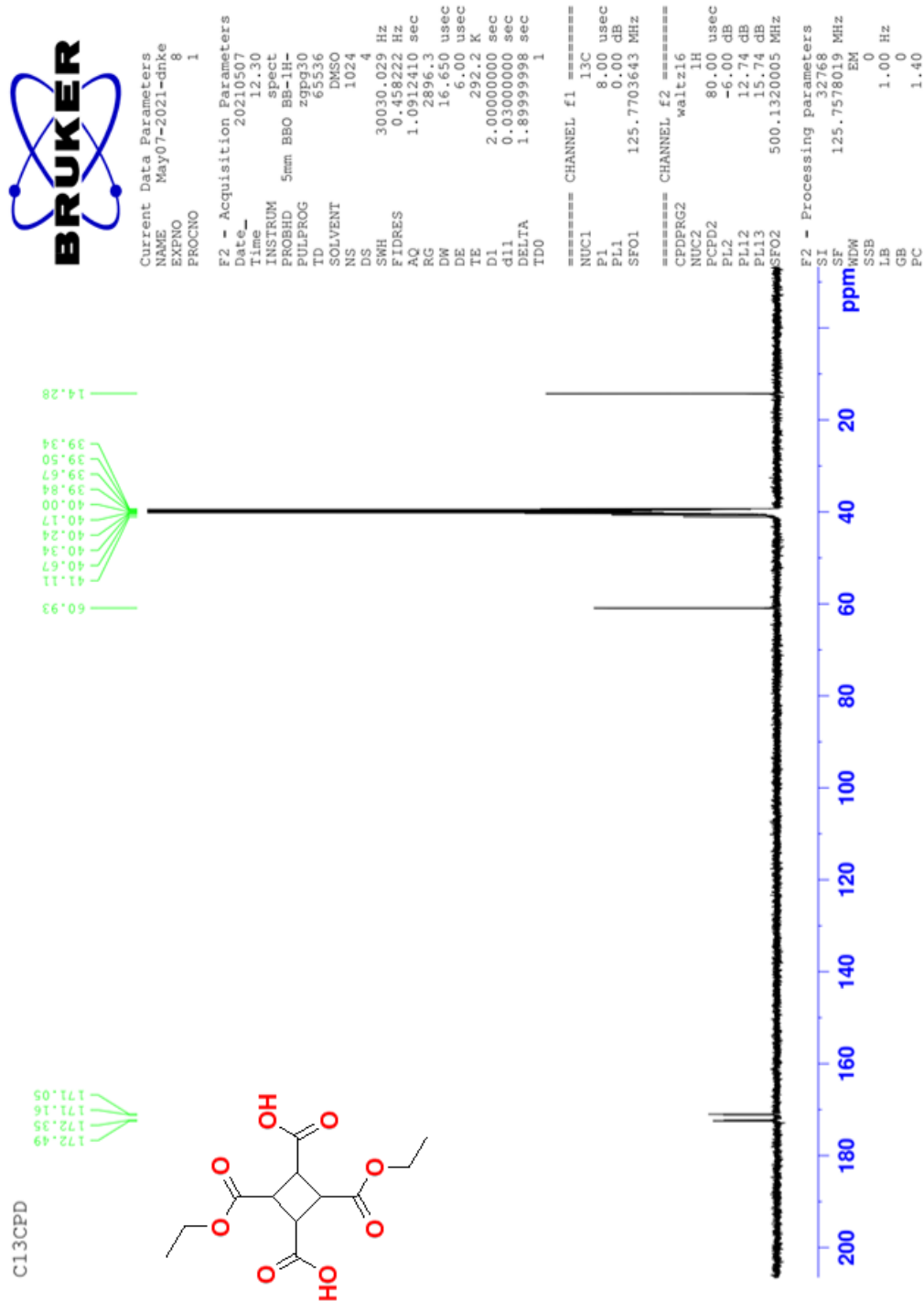


**Figure 66:**  $^{13}\text{C}$  NMR spectrum of CBDAX-6 in DMSO- $d_6$  at room temperature

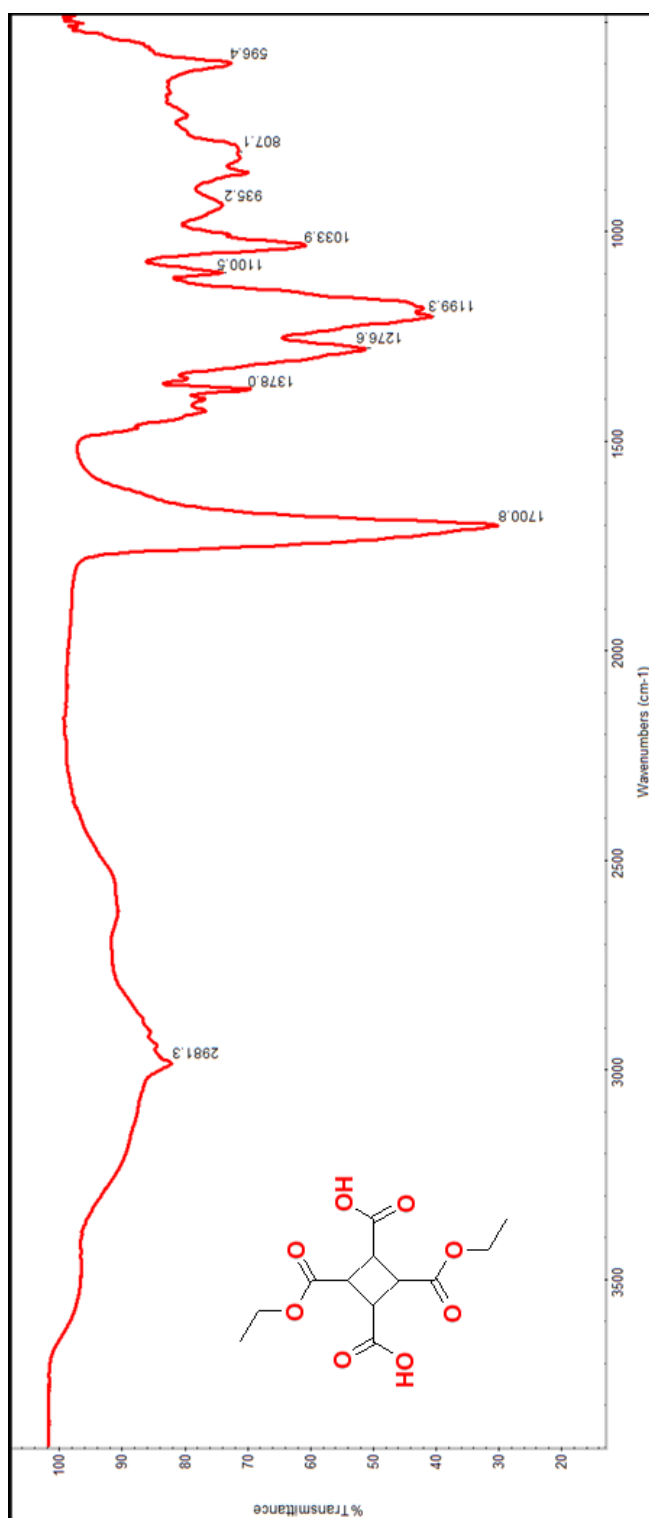


**Figure 67:** FT-IR NMR spectrum of CBDax-6



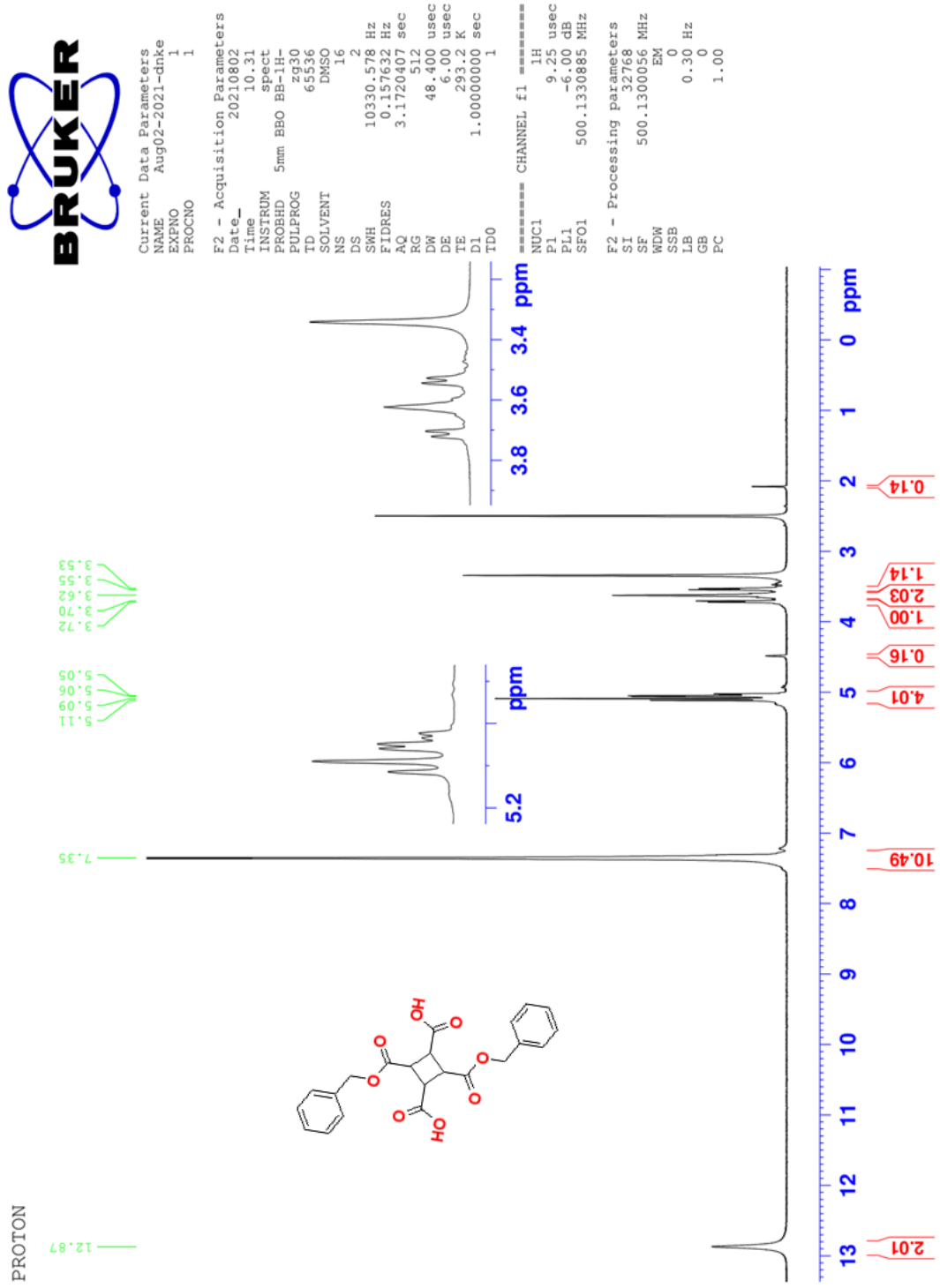


Figure 68: <sup>1</sup>H NMR spectrum of CBDAx-7 in DMSO-d<sub>6</sub> at room temperature

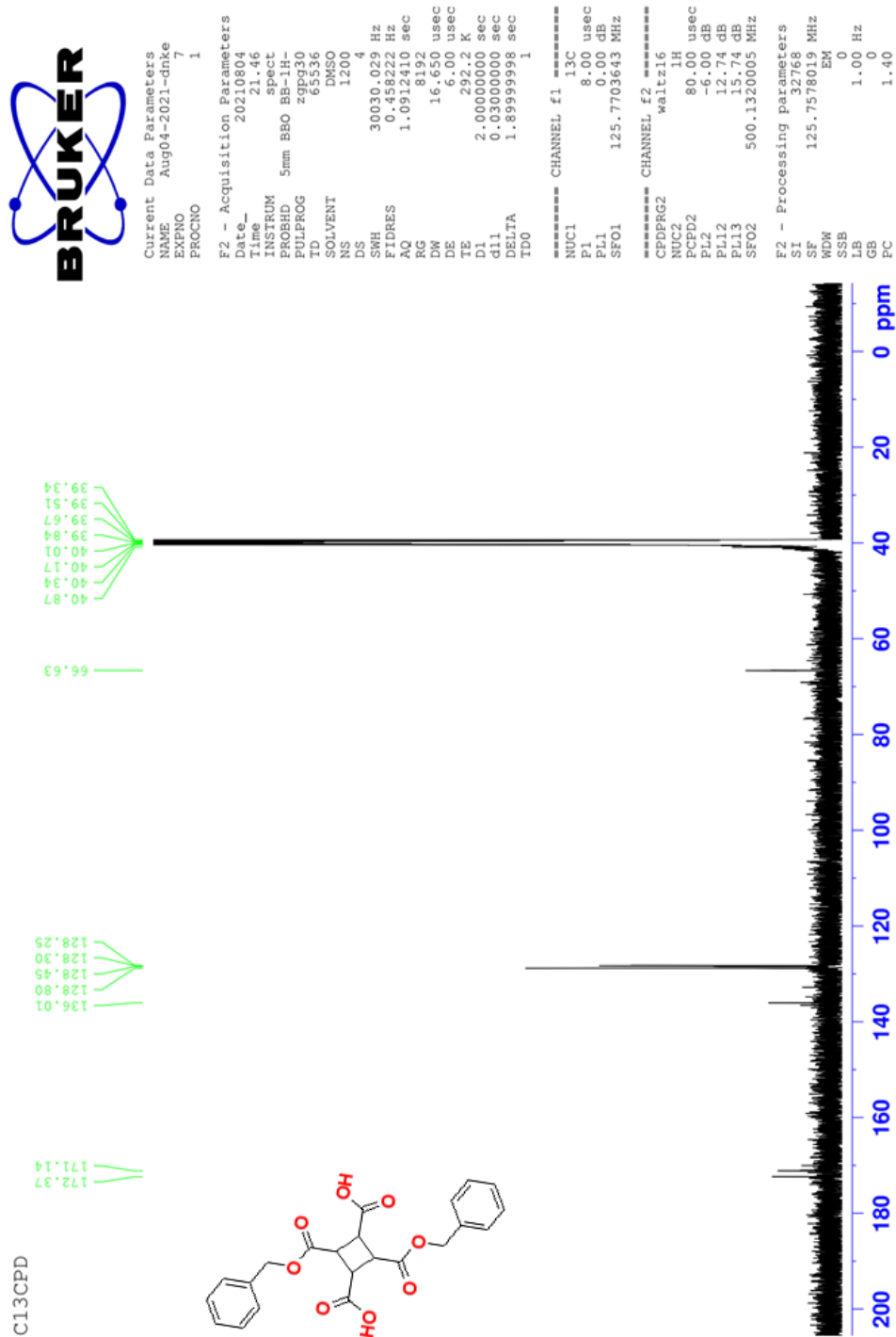
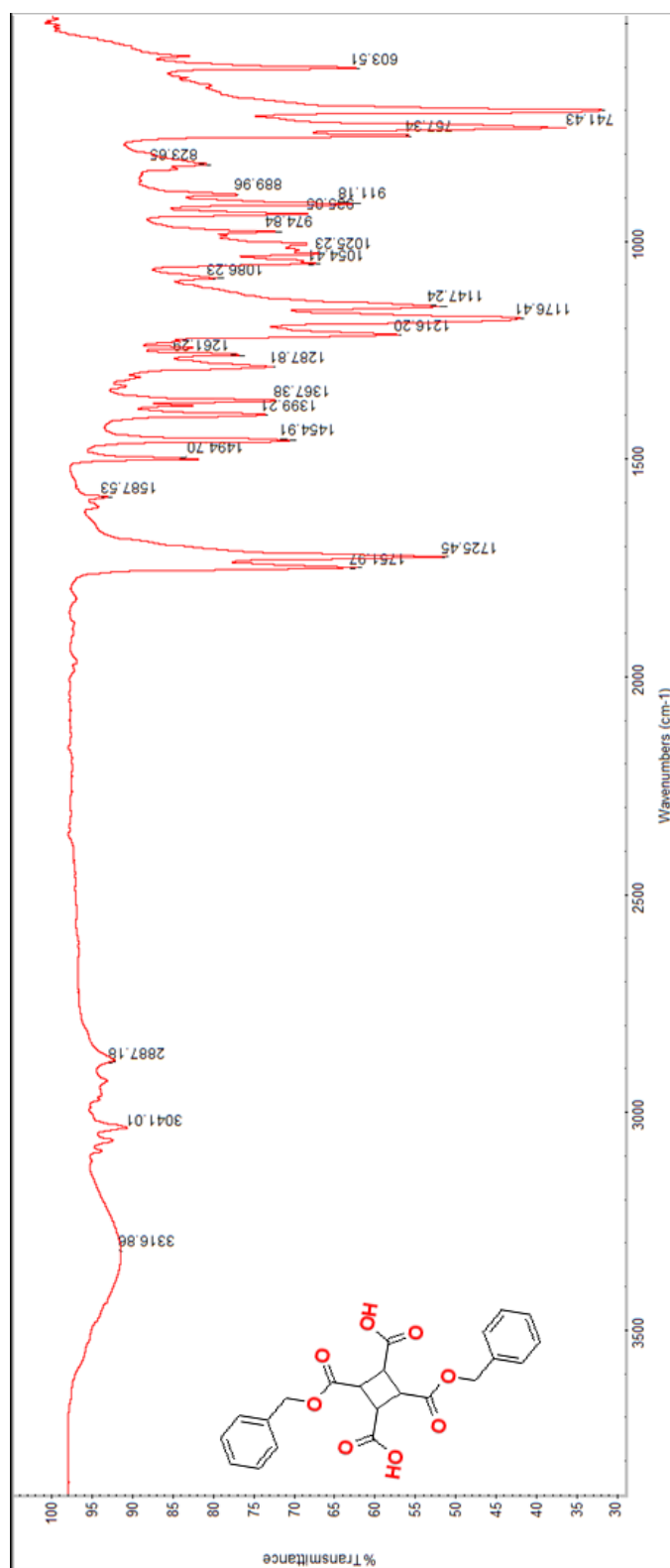
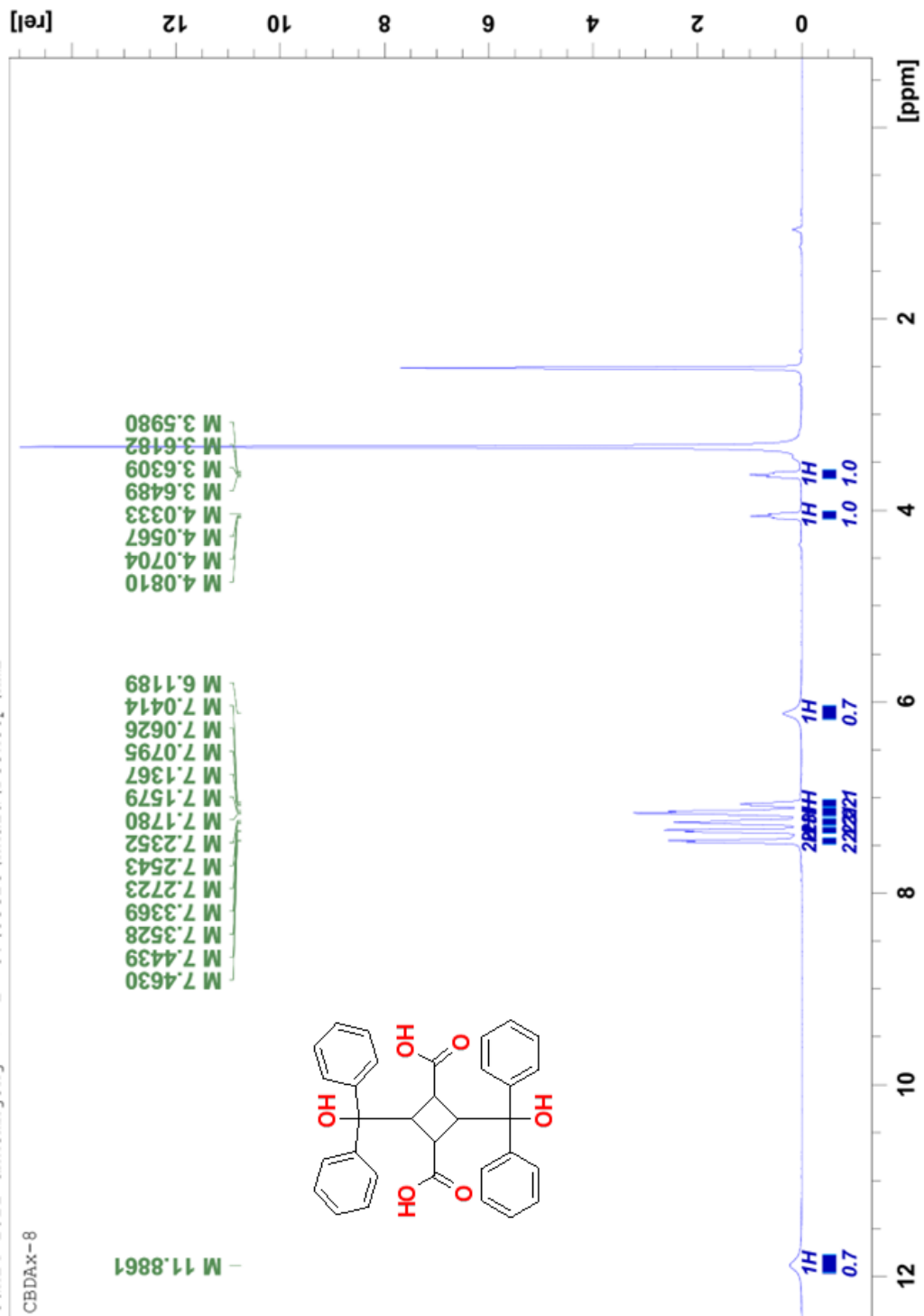


Figure 69:  $^{13}\text{C}$  NMR spectrum of CBDAx-7 in  $\text{DMSO-d}_6$  at room temperature



**Figure 70:** FT-IR NMR spectrum of CBDax-7



**Figure 71:** <sup>1</sup>H NMR spectrum of CBDax-8 in DMSO-d<sub>6</sub> at room temperature



C13CPD

Current Data Parameters  
NAME Feb11-2022-dnke  
EXPNO 1  
PROCNO 1

F2 - Acquisition Parameters  
Date\_ 20220211  
Time 9.10  
INSTRUM spect  
PROBHD 5mm BBO BB-1H-  
PULPROG zgpg30  
ID 65536  
SOLVENT DMSO  
NS 1024  
DS 4  
SWH 30030.029 Hz  
FIDRES 0.458222 Hz  
AQ 1.0912410 sec  
RG 5160.6  
DE 16.650 usec  
TE 291.2 K  
D1 2.00000000 sec  
d11 0.03000000 sec  
DELTA 1.89999998 sec  
TD0 1

==== CHANNEL f1 =====  
NUC1 13C  
P1 8.00 usec  
PL1 0.00 dB  
SFO1 125.7703643 MHz

==== CHANNEL f2 =====  
CPDPRG2 waltz16  
NUC2 1H  
PCPD2 80.00 usec  
PL2 -6.00 dB  
PL12 12.74 dB  
PL13 15.74 dB  
SFO2 500.1320005 MHz

F2 - Processing parameters  
SI 32768  
SF 125.7578519 MHz  
WDW EM

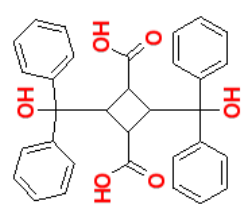
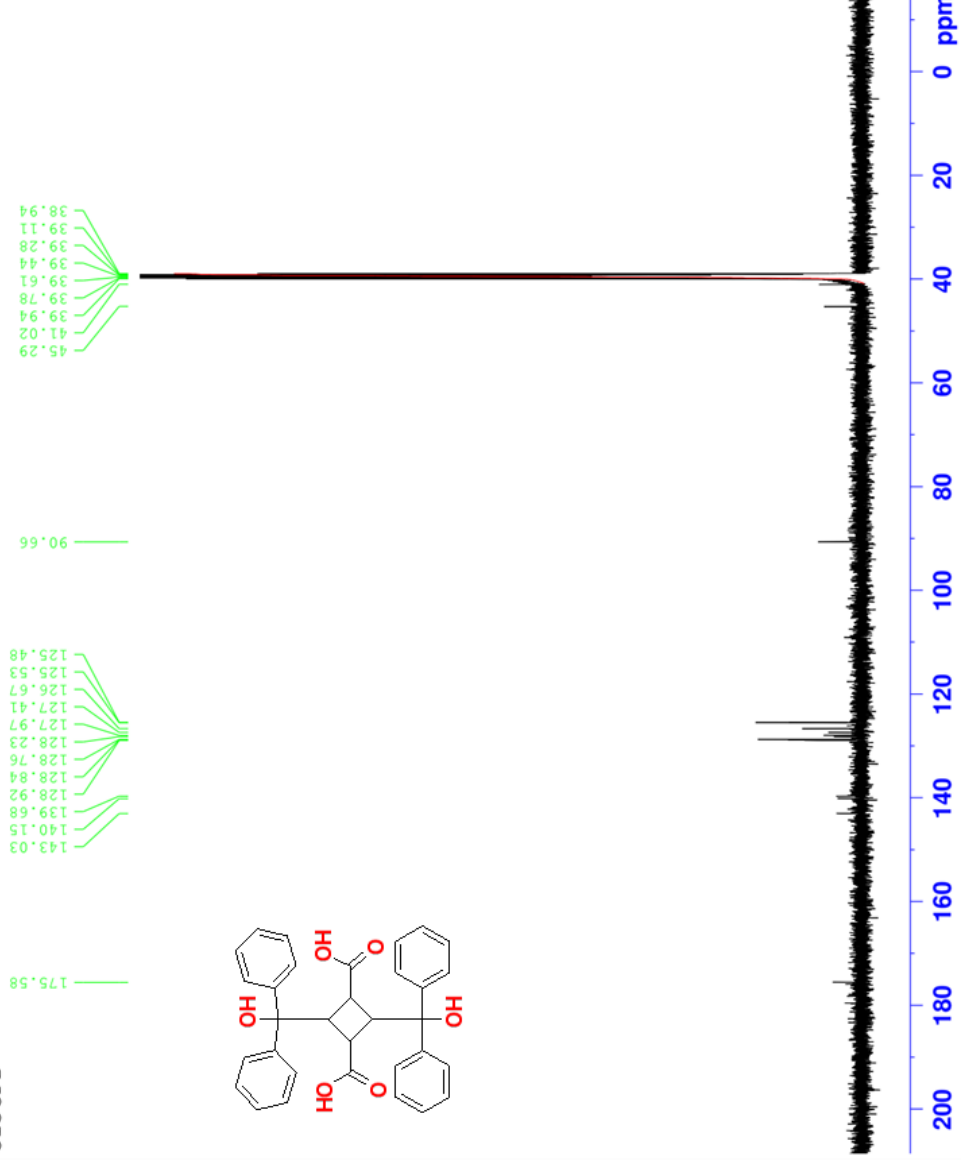


**Figure 72:**  $^{13}\text{C}$  NMR spectrum of CBDAx-8 in  $\text{DSMO-d}_6$  at room temperature

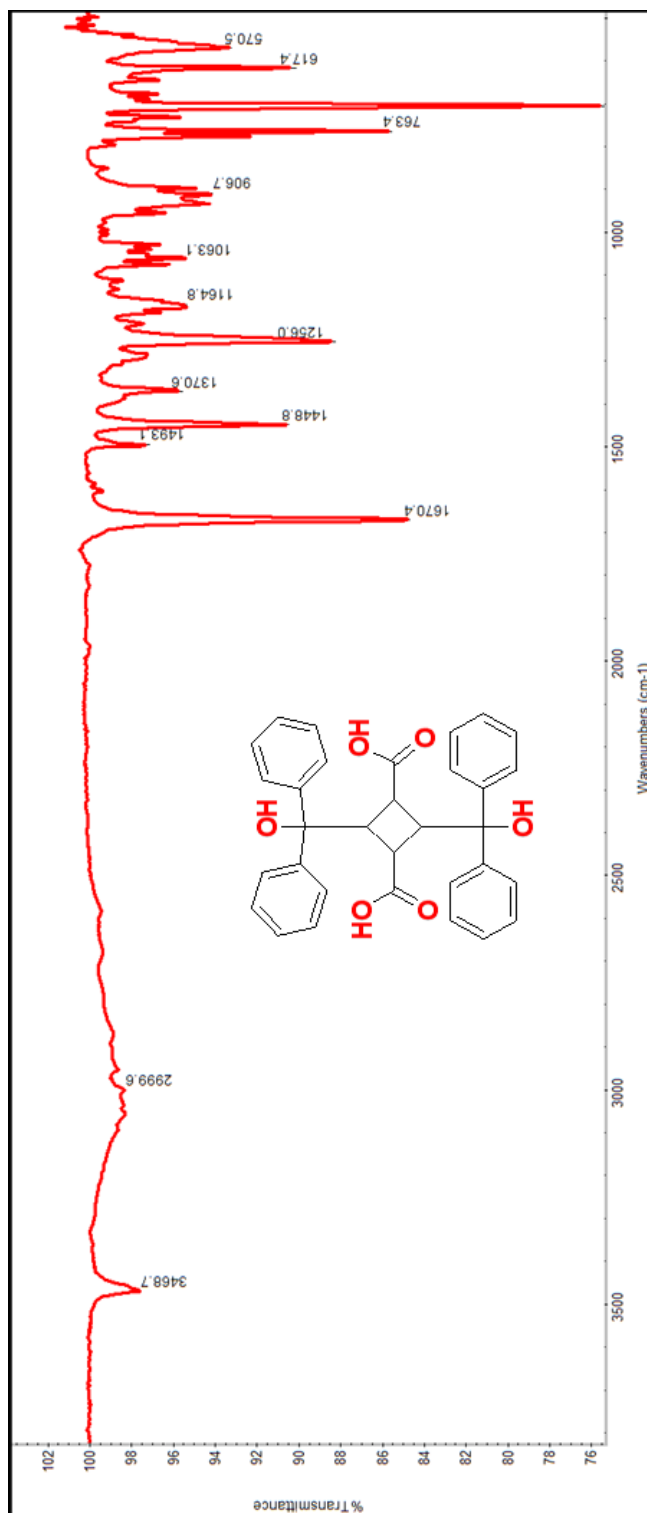


**Figure 73:** FT-IR NMR spectrum of CBDAx-8



Current Data Parameters  
NAME Apr22-2021-dnke  
EXPNO 1  
PROCNO 1

F2 - Acquisition Parameters  
Date\_ 20210422  
Time 10.26  
INSTRUM spect  
PROBHD 5mm BBO BB-IH-  
PULPROG zg30  
TD 65536  
SOLVENT DMSO  
NS 16  
DS 2  
SWH 10330.578 Hz  
FIDRES 0.157632 Hz  
AQ 3.1720407 sec  
RG 362  
DW 48.400 usec  
DE 6.00 usec  
TE 291.2 K  
D1 1.00000000 sec  
TD0 1

===== CHANNEL f1 =====  
NUC1 1H  
P1 9.25 usec  
PL1 -6.00 dB  
SFO1 500.1330885 MHz

F2 - Processing parameters  
SI 32768  
SF 500.1300040 MHz  
WDW EM  
SSB 0  
LB 0.30 Hz  
GB 0  
PC 1.00

PROTON

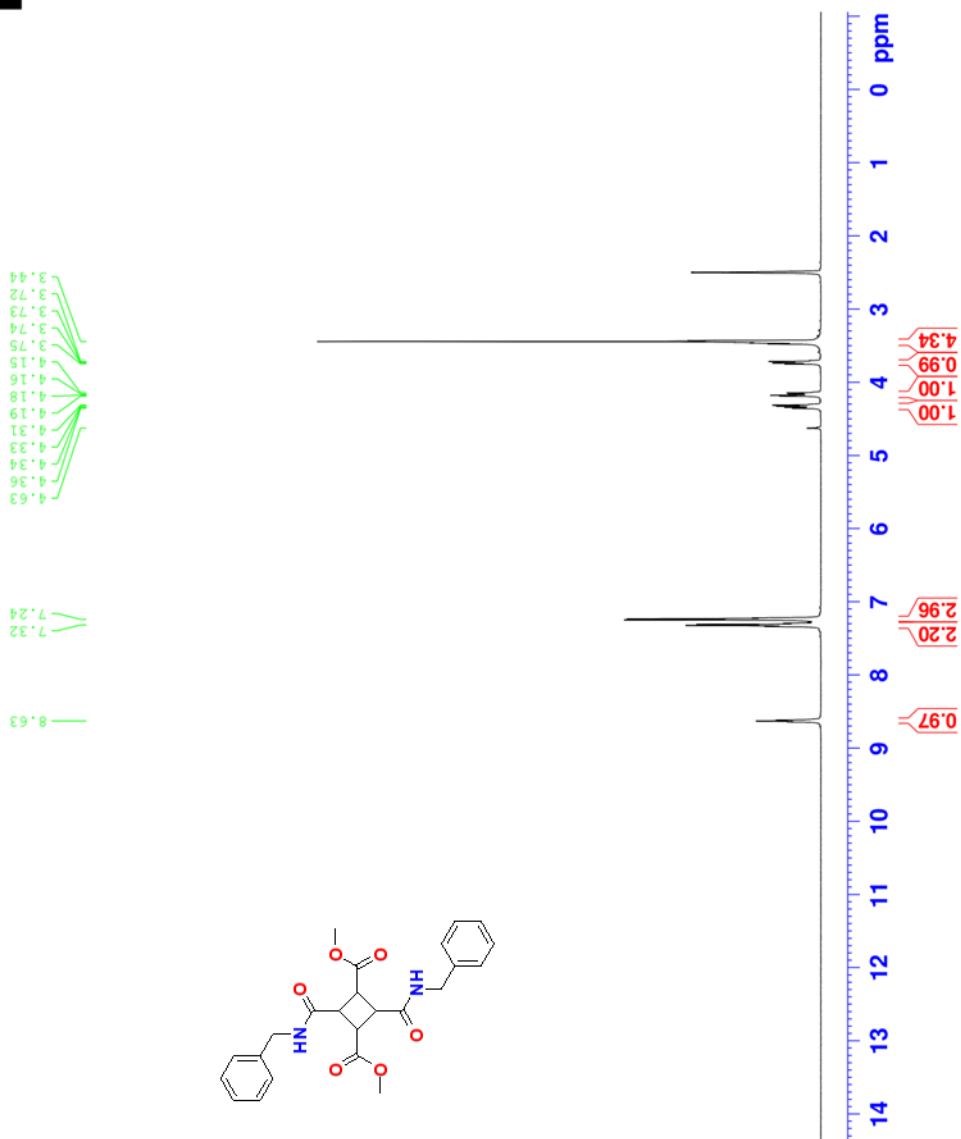
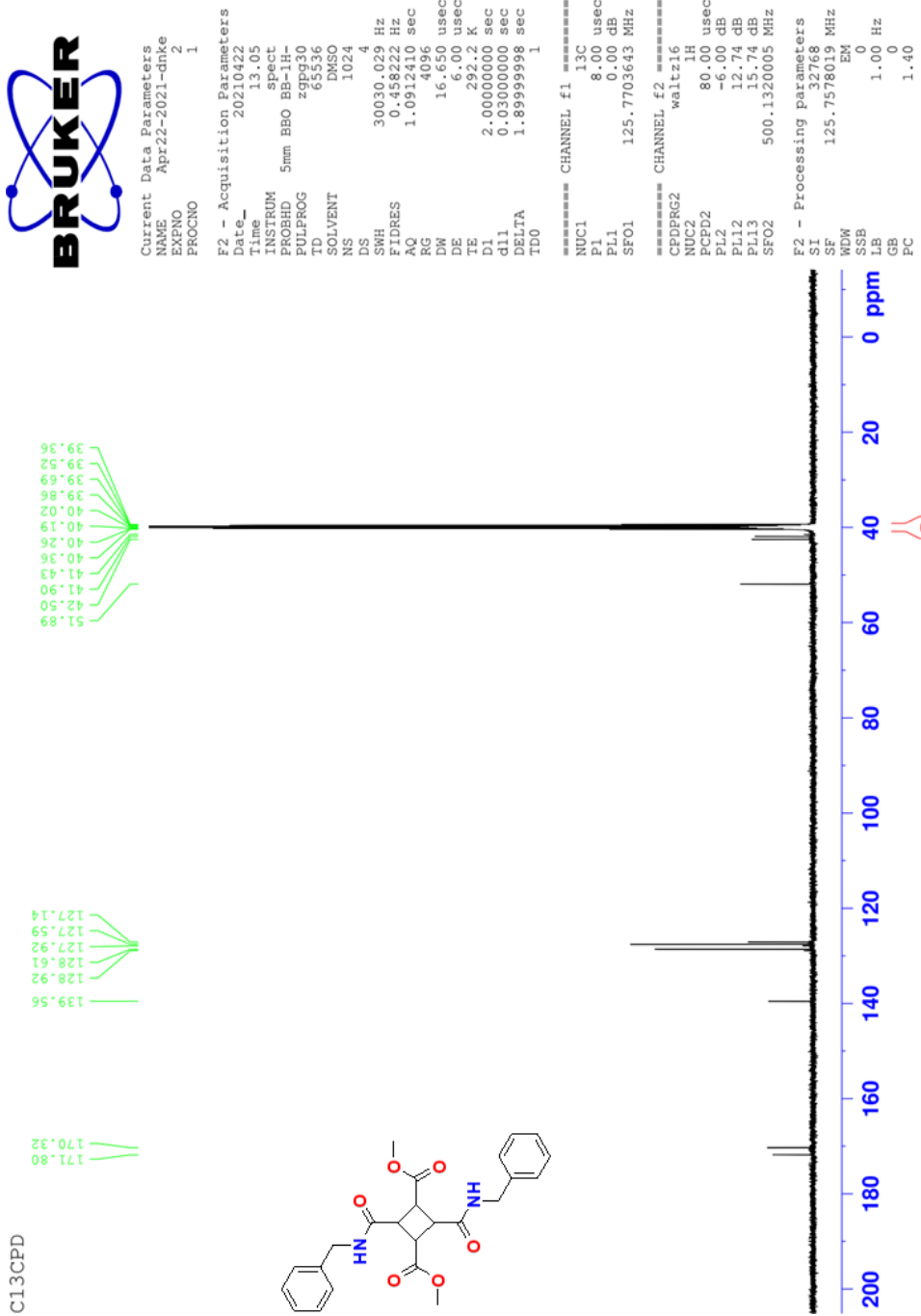


Figure 74:  $^1\text{H}$  NMR spectrum of CBDEx-1 in DMSO- $d_6$  at room temperature



**Figure 75:**  $^{13}\text{C}$  NMR spectrum of CBDEx-1 in  $\text{DMSO-d}_6$  at room temperature



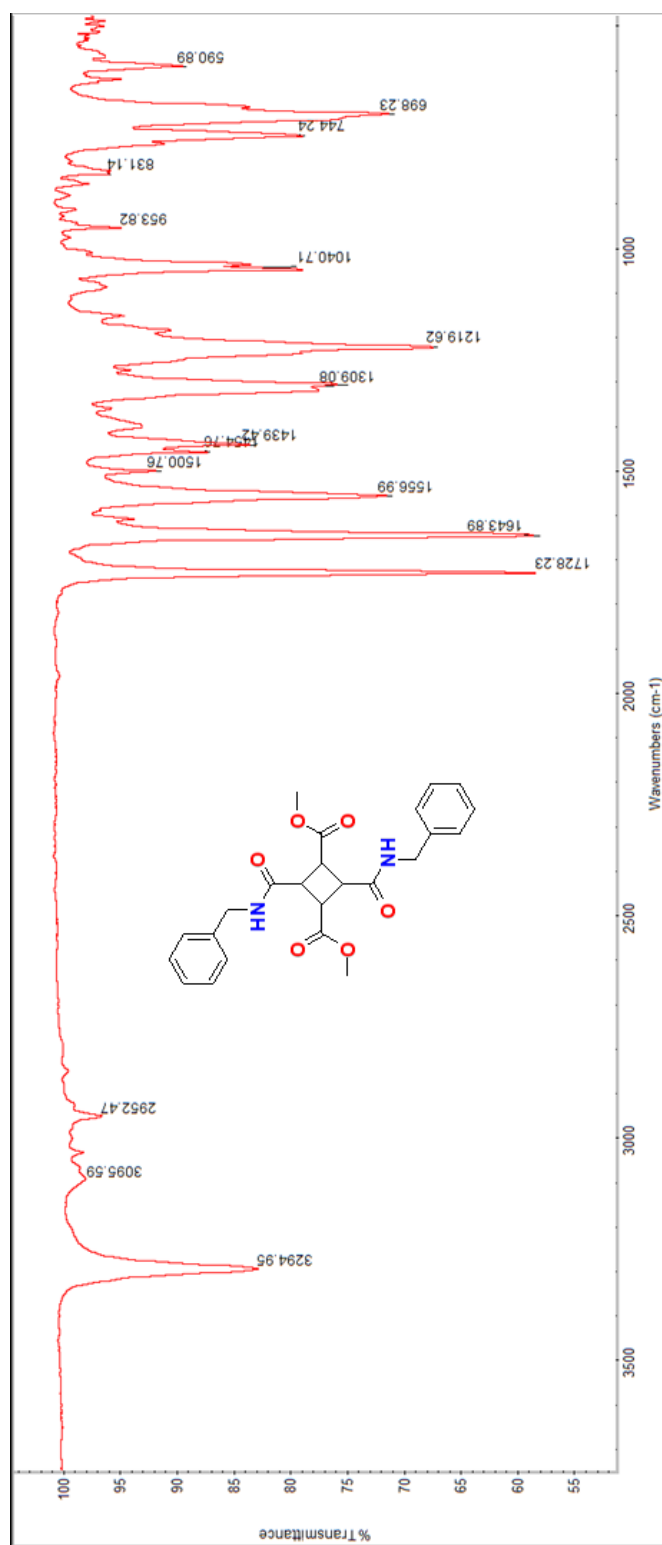
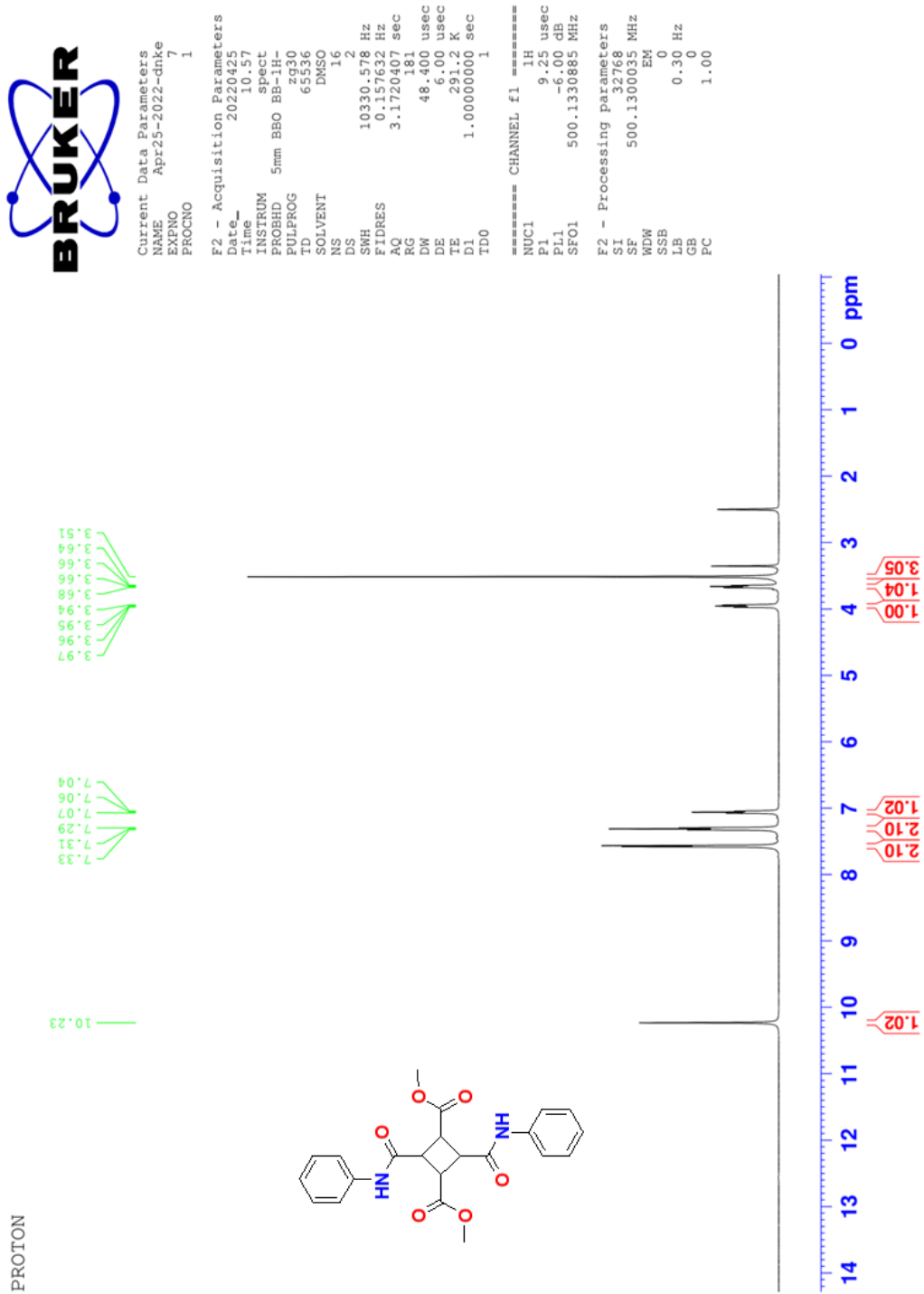


Figure 76: FT-IR NMR spectrum of CBDEx-1



**Figure 77:**  $^1\text{H}$  NMR spectrum of CBDEx-2 in DMSO- $d_6$  at room temperature

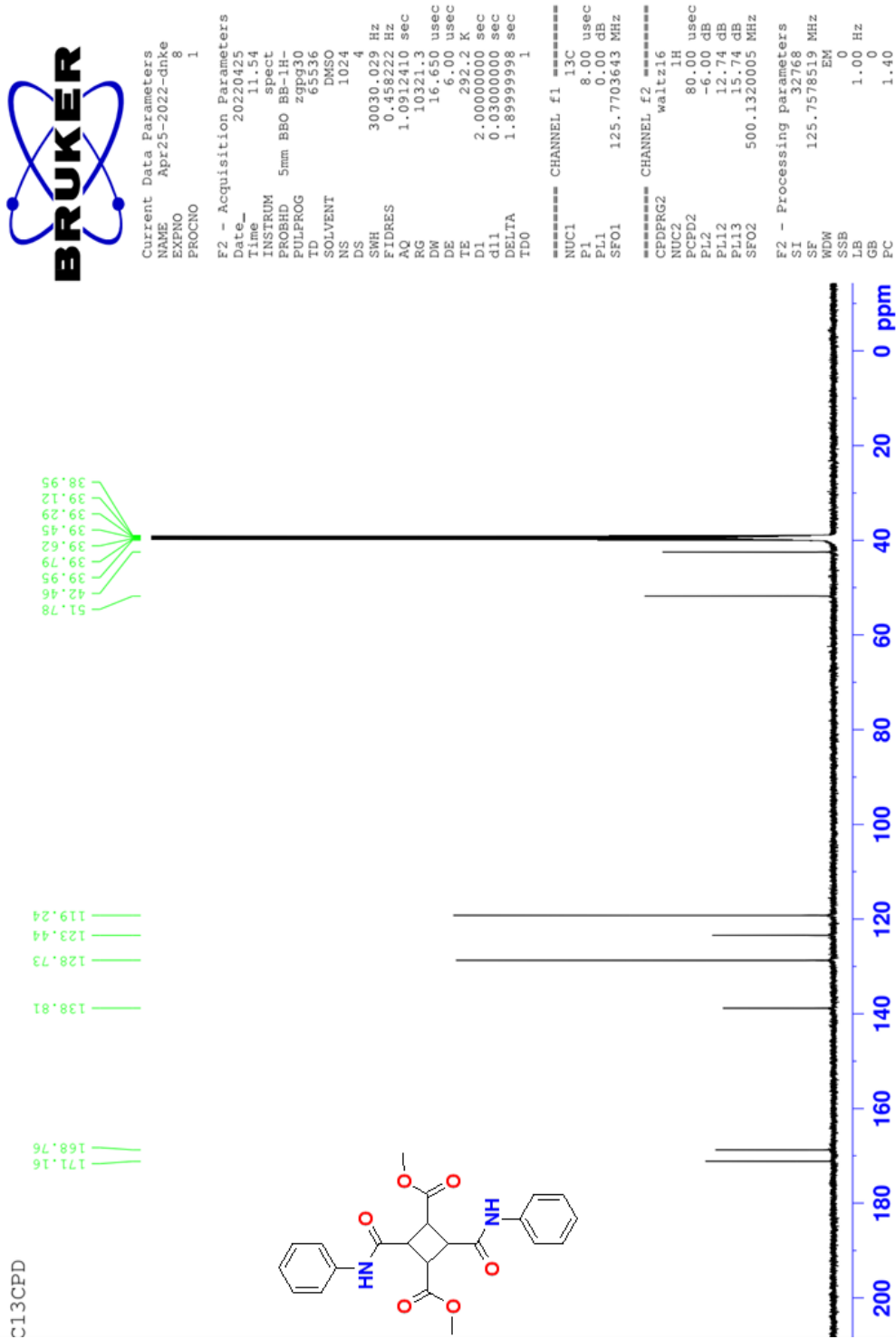
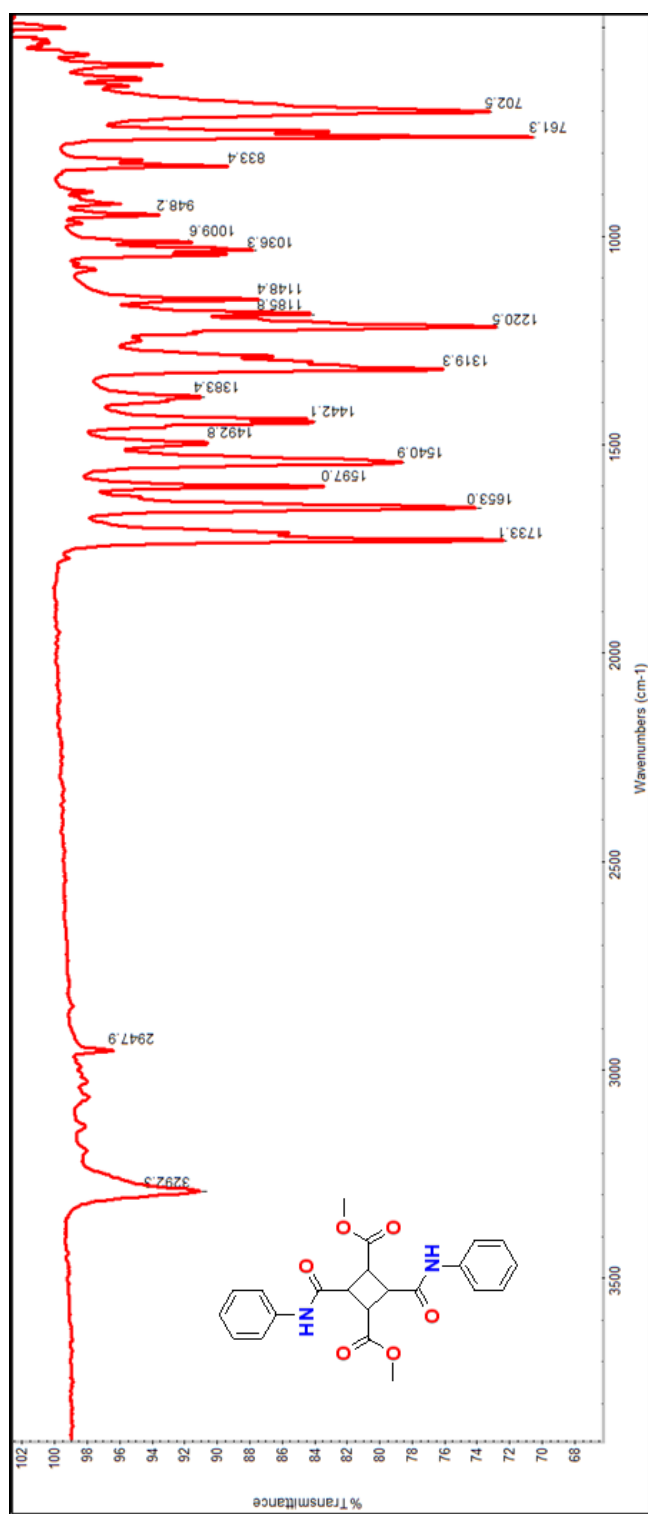
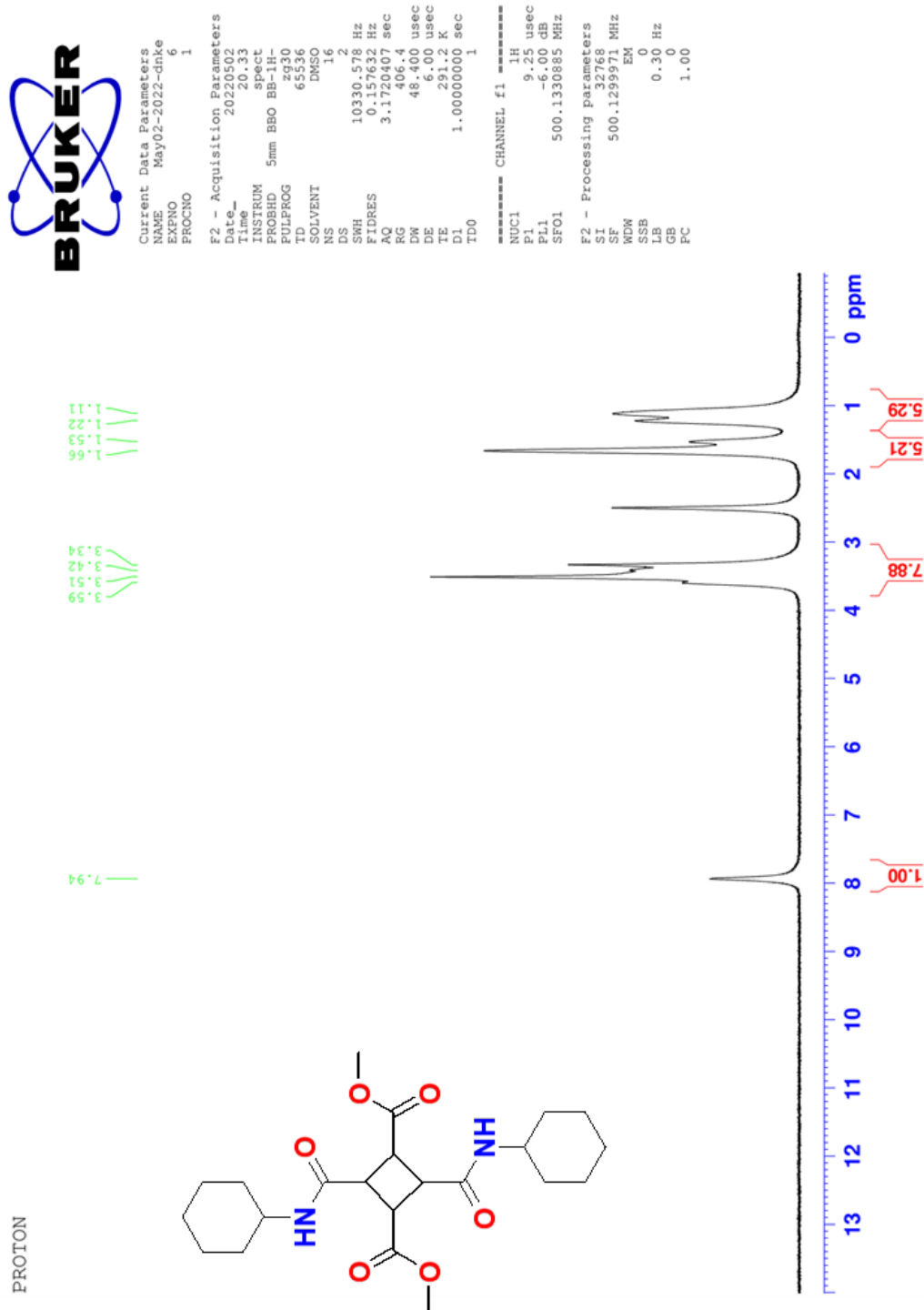


Figure 78:  $^{13}\text{C}$  NMR spectrum of CBDEx-2 in  $\text{DMSO-d}_6$  at room temperature



**Figure 79:** FT-IR NMR spectrum of CBDEx-2



**Figure 80:**  $^1\text{H}$  NMR spectrum of CBDEx-3 in  $\text{DMSO-d}_6$  at room temperature

**Figure 81:**  $^{13}\text{C}$  NMR spectrum of CBDEx-3 in  $\text{DSMO-d}_6$  at room temperature

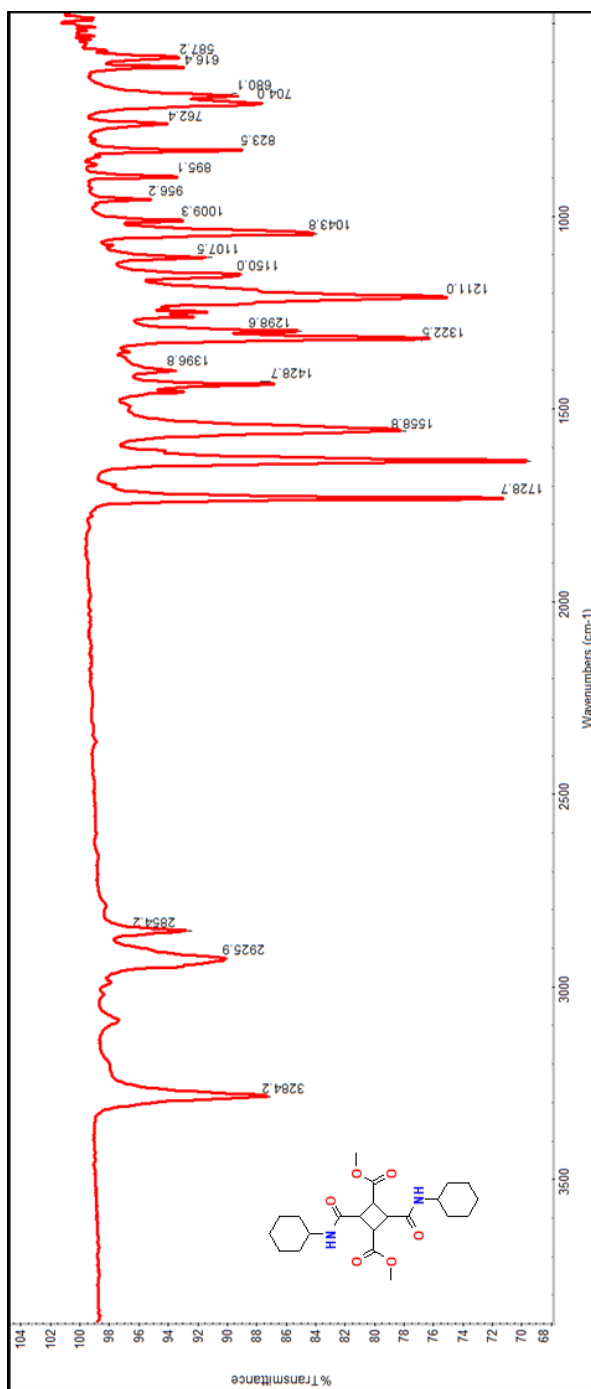


**Figure 82:** FT-IR NMR spectrum of CBDEx-3



Current Data Parameters  
NAME May02-2022-dnke  
EXPNO 1  
PROCNO 1

F2 - Acquisition Parameters  
Date\_ 20220502  
Time 9.07  
INSTRUM spect  
PROBHD 5mm BBO BB-1H-  
PULPROG zg30  
TD 65536  
SOLVENT DMSO  
NS 16  
DS 2  
SWH 10330.578 Hz  
FIDRES 0.157632 Hz  
AQ 3.1720407 sec  
RG 406.4  
DE 48.400 usec  
TE 291.2 K  
D1 1.00000000 sec  
TD0 1

===== CHANNEL f1 =====  
NUC1 1H  
P1 9.25 usec  
PL1 -6.00 dB  
SFO1 500.1330885 MHz

F2 - Processing parameters  
SI 32768  
SF 500.1300038 MHz  
MEM  
SSB 0  
LB 0.30 Hz  
GB 0  
PC 1.00

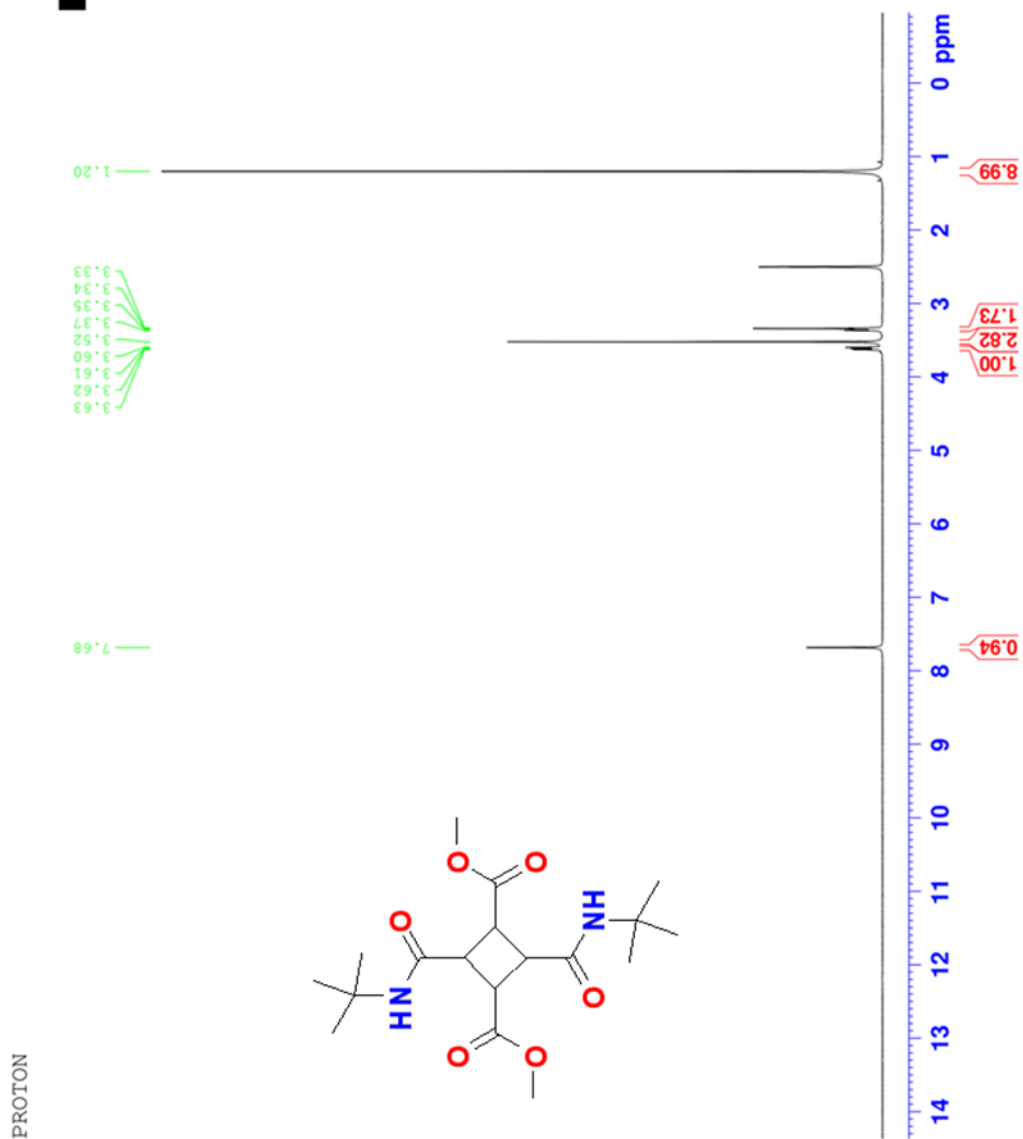


Figure 83:  $^1\text{H}$  NMR spectrum of CBDEx-4 in DMSO- $d_6$  at room temperature



Current Data Parameters  
 NAME May02-2022-drke  
 EXPNO 13  
 PROCNO 1

F2 - Acquisition Parameters  
 Date\_ 20220502  
 Time 10:55  
 INSTRUM spect  
 PROBHD 5mm BBO BB-1H  
 PULPROG zgpg30  
 TD 65536  
 SOLVENT DMSO  
 NS 1024  
 DS 4  
 SWH 30030.029 Hz  
 FIDRES 0.458222 Hz  
 AQ 1.0912410 sec  
 RG 14596.5  
 DW 16.650 usec  
 DE 6.00 usec  
 TE 292.2 K  
 D1 2.00000000 sec  
 d11 0.03000000 sec  
 DELTA 1.89999998 sec  
 TDO 1

===== CHANNEL f1 =====  
 NUC1 13C  
 P1 8.00 usec  
 PL1 0.00 dB  
 SFO1 125.7703643 MHz

===== CHANNEL f2 =====  
 CPDPRG2 waltz16  
 NUC2 1H  
 PCPD2 80.00 usec  
 PL2 -6.00 dB  
 PL12 12.74 dB  
 PL13 15.74 dB  
 SFO2 500.1320005 MHz

F2 - Processing parameters  
 SI 32768  
 SF 125.7578519 MHz  
 MDW EM 0  
 SSB 0  
 LB 1.00 Hz  
 GB 0  
 BR 1 an

C13CPD

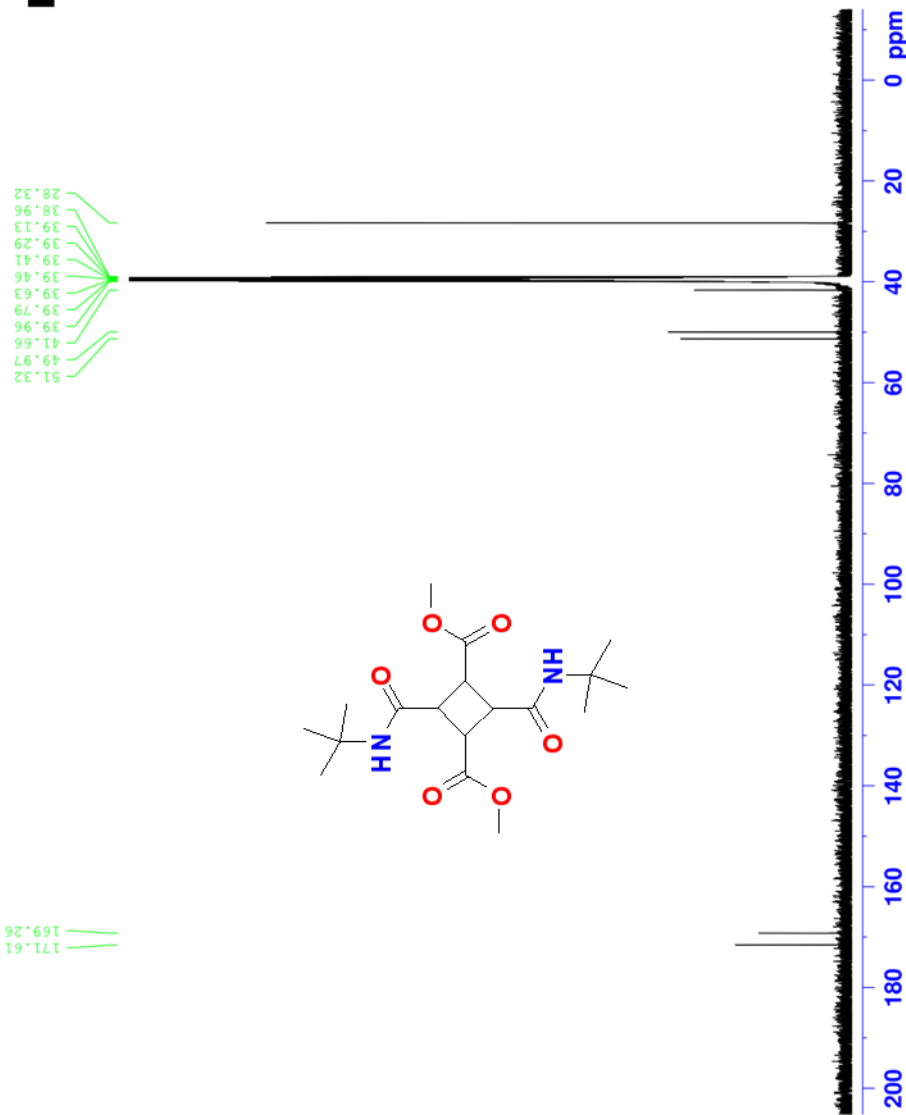


Figure 84: <sup>13</sup>C NMR spectrum of CBDEx-4 in DMSO-d<sub>6</sub> at room temperature



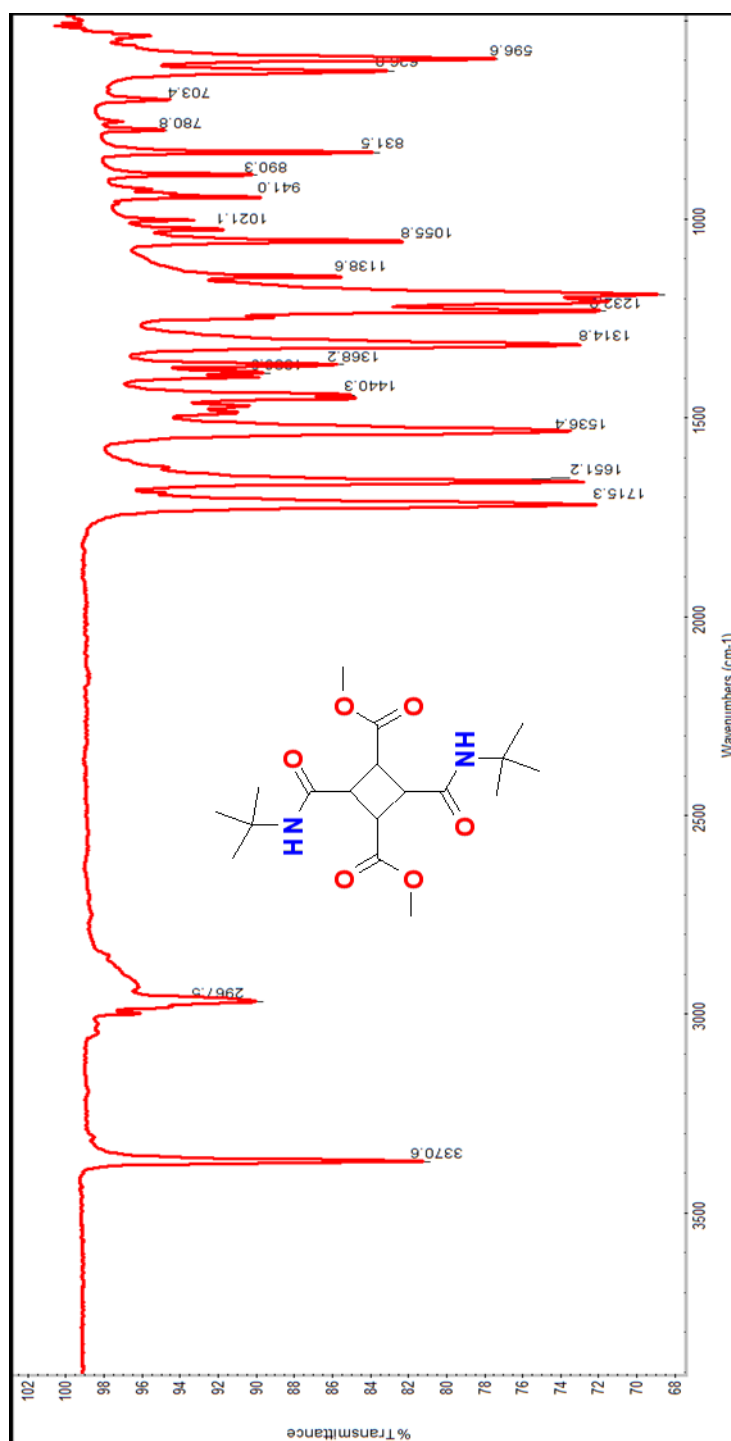


Figure 85: FT-IR NMR spectrum of CBDEx-4

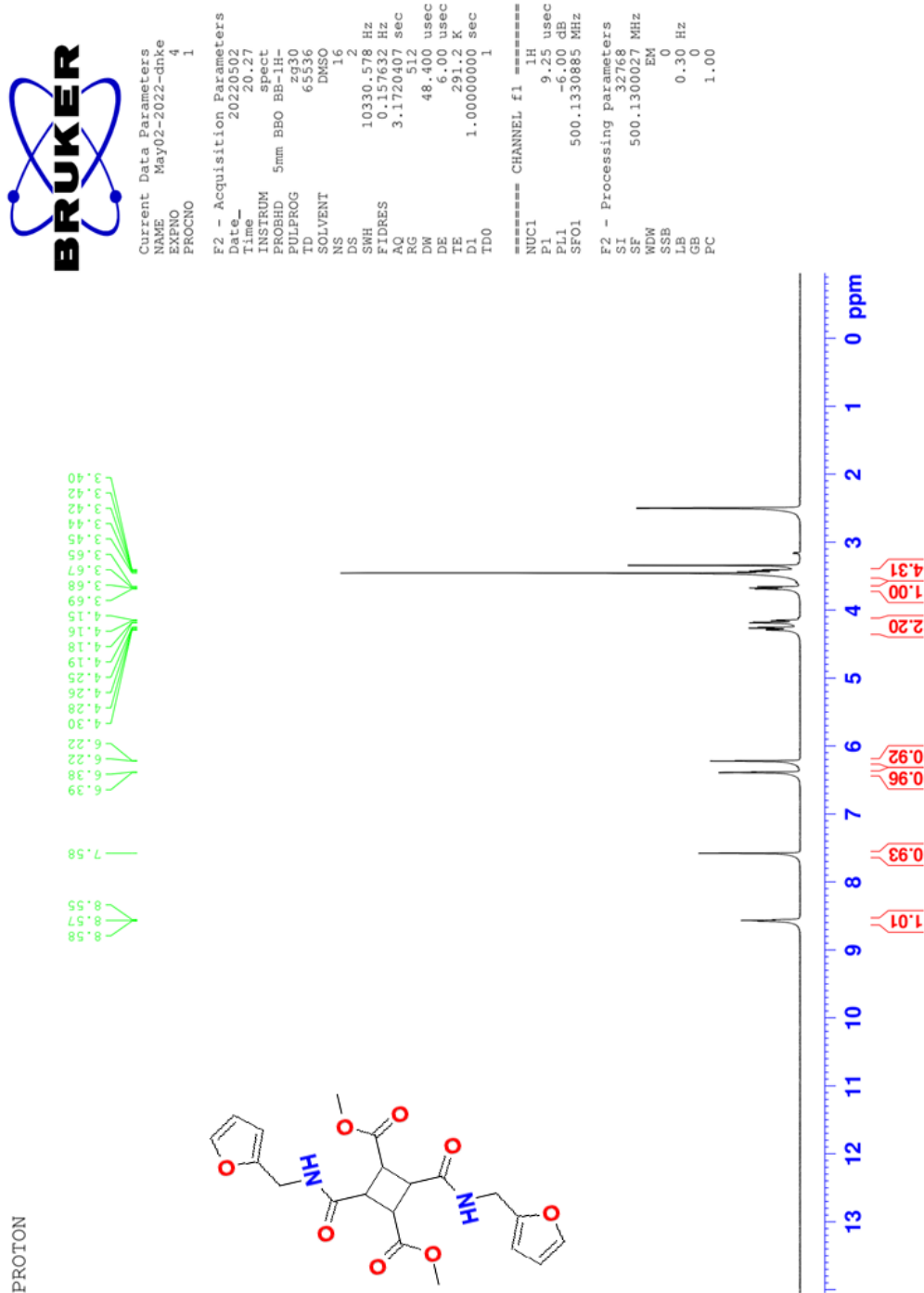
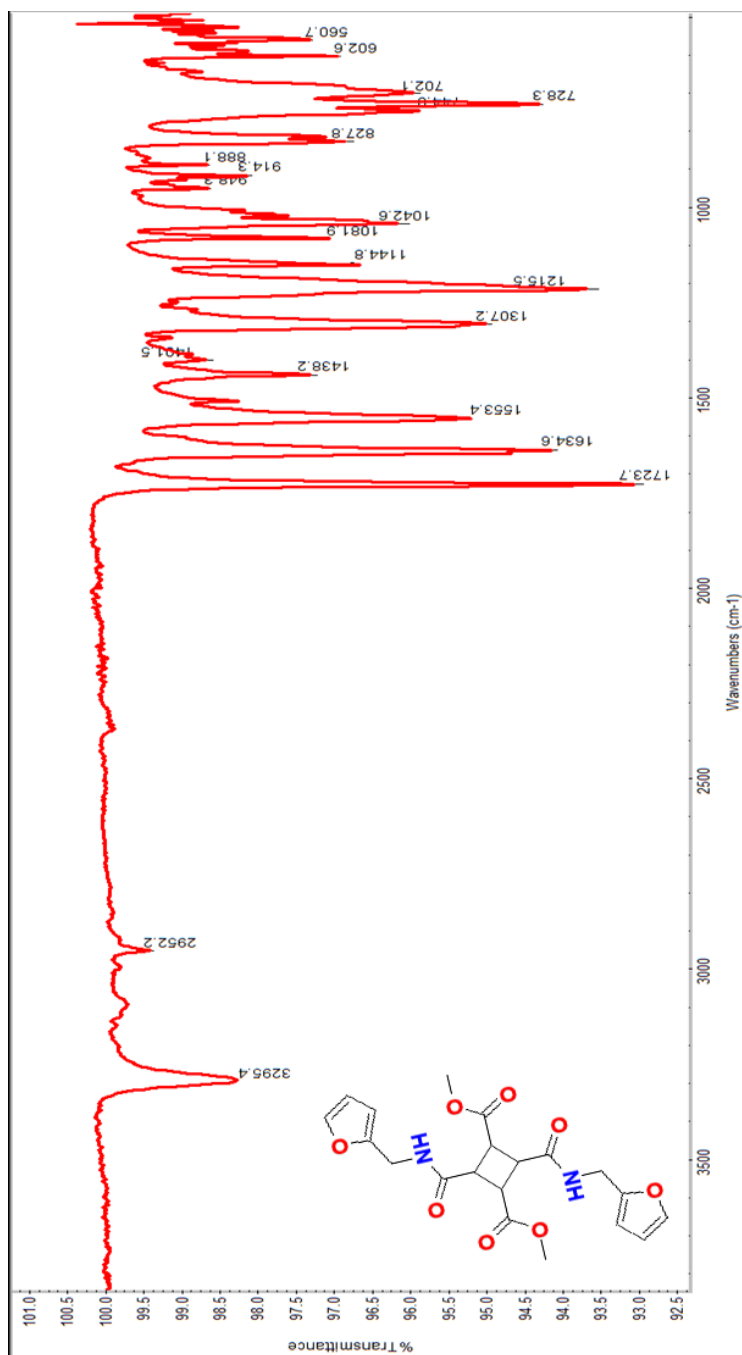


Figure 86: <sup>1</sup>H NMR spectrum of CBDEx-5 in DMSO-d<sub>6</sub> at room temperature

**Figure 87:**  $^{13}\text{C}$  NMR spectrum of CBDEx-5 in  $\text{DSMO-d}_6$  at room temperature



**Figure 88:** FT-IR NMR spectrum of CBDEx-5



Current Data Parameters  
NAME Feb06-2020-dnke  
EXPNO 1  
PROCNO 1

F2 - Acquisition Parameters  
Date\_ 20200206  
Time 12.50  
INSTRUM spect  
PROBHD 5mm BBO BE-IH-  
PULPROG zg30  
TD 65536  
SOLVENT DMSO  
NS 16  
DS 2  
SWH 10330.578 Hz  
FIDRES 0.157632 Hz  
AQ 3.1720407 sec  
RG 512  
DM 48.400 usec  
DE 6.00 usec  
TE 290.2 K  
D1 1.00000000 sec  
TDO 1

----- CHANNEL f1 -----  
NUC1 1H  
P1 9.25 usec  
PL1 -6.00 dB  
SFO1 500.1330885 MHz

F2 - Processing parameters  
SI 32768  
SF 500.129995 MHz  
WDW EM  
SSB 0  
LB 0.30 Hz  
GB 0  
PC 1.00

Bn\_MAD\_tga\_hold\_335 0C\_20 mins  
PROTON

6.44  
3.27  
3.25  
3.23  
3.21  
3.19

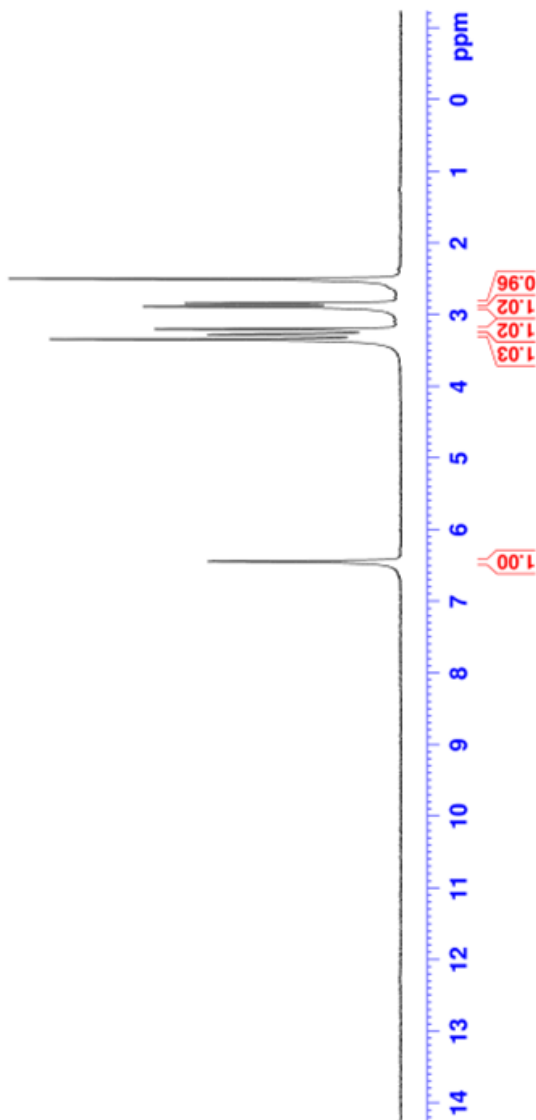
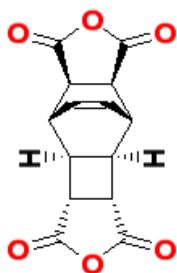
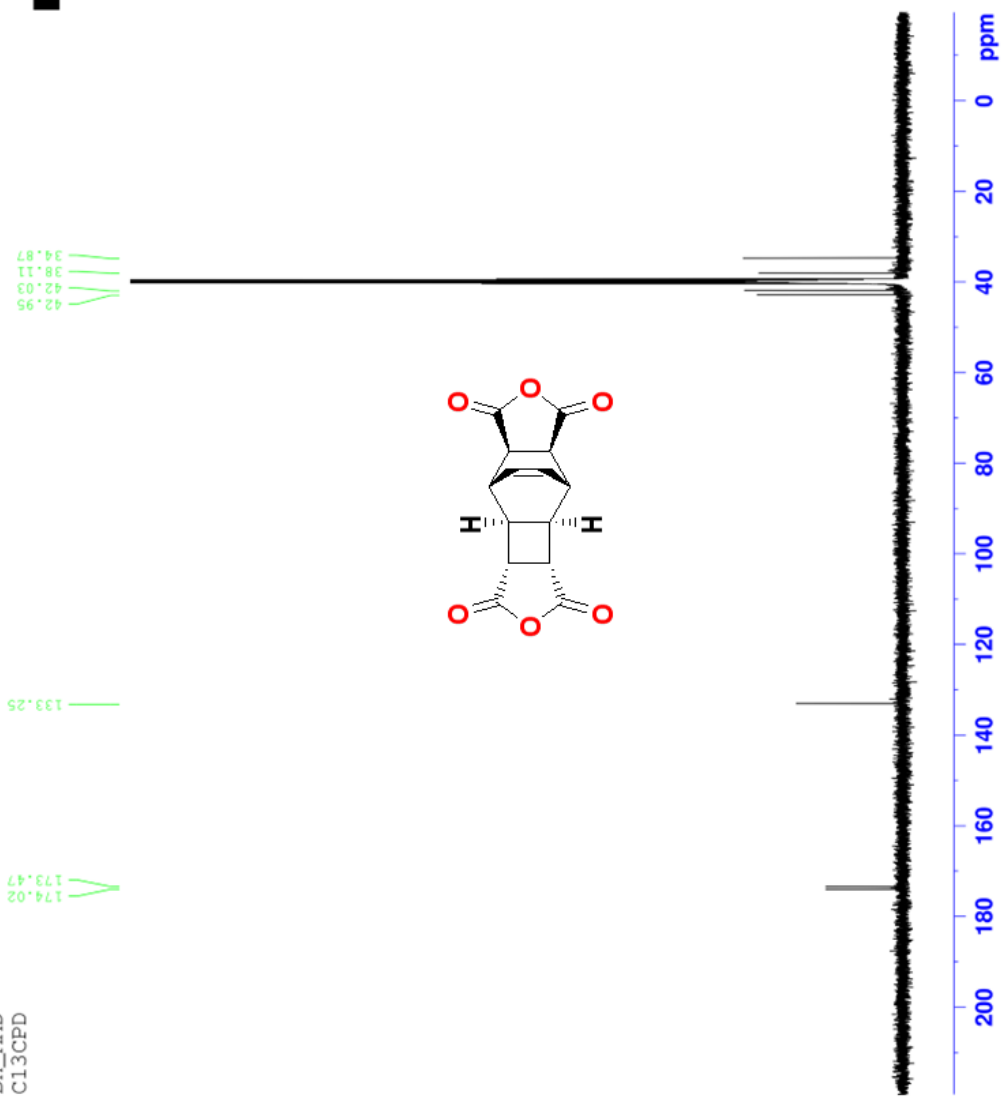


Figure 89:  $^1\text{H}$  NMR spectrum of CBDAN-2 in  $\text{DMSO-d}_6$  at room temperature



B0\_MAD  
C13CPD



Current Data Parameters  
NAME Oct25-2019-drke  
EXPNO 12  
PROCNO 1

F2 - Acquisition Parameters  
Date\_ 20191025  
Time 18:50  
INSTRUM spect  
PROBHD 5mm BBO BB-1H-  
PULPROG zgpg30  
TD 65536  
SOLVENT DMSO  
NS 1024  
DS 4  
SWH 30030.029 Hz  
FIDRES 0.458222 Hz  
AQ 1.0912410 sec  
RG 2896.3  
DW 16.650 usec  
DE 6.00 usec  
TE 292.2 K  
D1 2.00000000 sec  
d11 0.03000000 sec  
DELTA 1.89999998 sec  
TDO 1

===== CHANNEL f1 =====  
NUC1 13C  
P1 8.00 usec  
PL1 0.00 dB  
SFO1 125.7703643 MHz

===== CHANNEL f2 =====  
CPDPRG2 waltz16  
NUC2 1H  
PCPD2 80.00 usec  
PL2 -6.00 dB  
PL12 12.74 dB  
PL13 15.74 dB  
SFO2 500.1320005 MHz

F2 - Processing parameters  
SI 32768  
SF 125.7578019 MHz  
MDW EM  
SSB 0  
LB 1.00 Hz  
GB 0  
PC 1.40

Figure 90: <sup>13</sup>C NMR spectrum of CBDAN-2 in DMSO-d<sub>6</sub> at room temperature

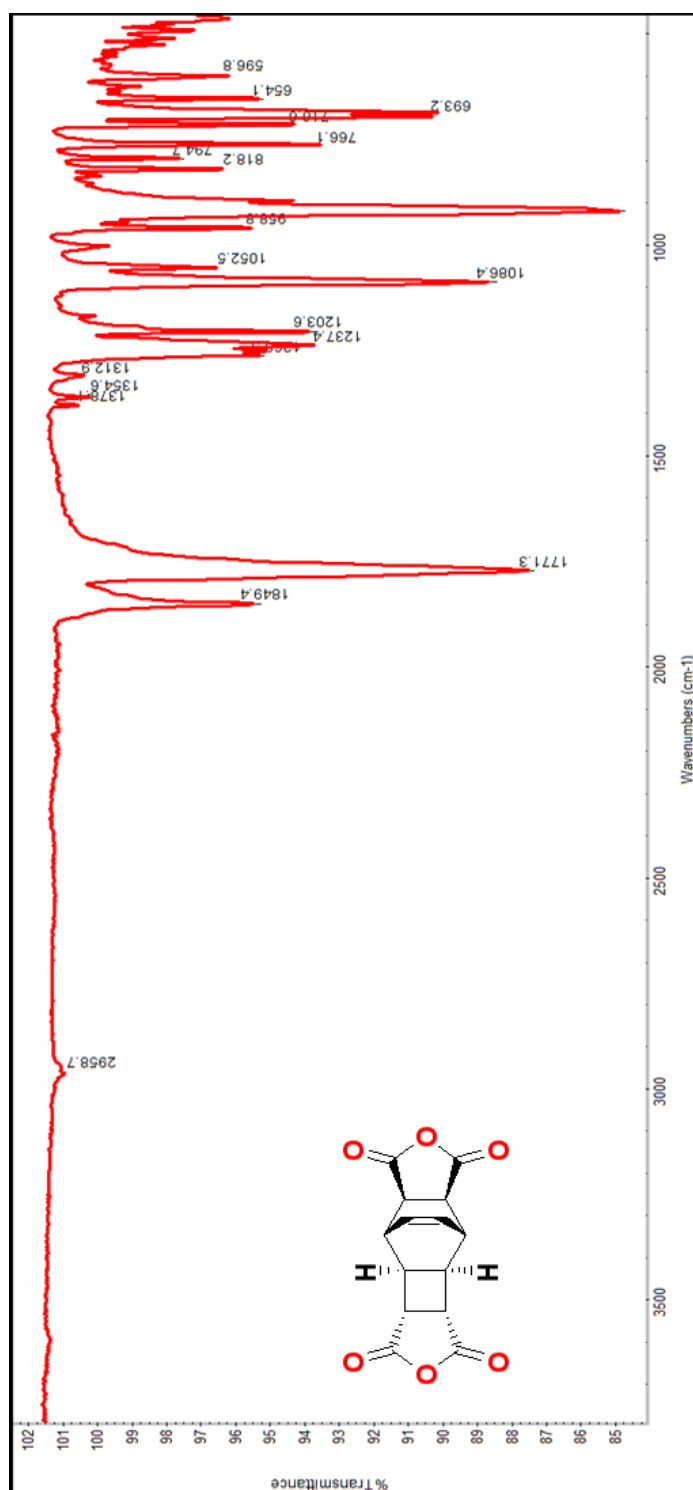


**Figure 91:** FT-IR NMR spectrum of CBDAN-2



Current Data Parameters  
NAME Jan11-2021-dm6  
EXPNO 3  
PROCNO 1

F2 - Acquisition Parameters  
Date\_ 20210111  
Time\_ 14.10  
INSTRUM spect  
PROBHD 5mm BBO BB-1H-  
PULPROG zg30  
TD 65536  
SOLVENT DMSO  
NS 16  
DS 2  
SWH 10330.578 Hz  
FIDRES 0.157632 Hz  
AQ 3.1720407 sec  
RG 1625.5  
DW 48.400 usec  
DE 6.00 usec  
TE 292.2 K  
D1 1.0000000 sec  
TD0 1

===== CHANNEL f1 =====  
NUC1 1H  
P1 9.25 usec  
PL1 -6.00 dB  
SFO1 500.1330885 MHz

F2 - Processing parameters  
SI 32768  
SF 500.1300069 MHz  
WDW EM  
SSB 0  
LB 0.30 Hz  
GB 0  
PC 1.00

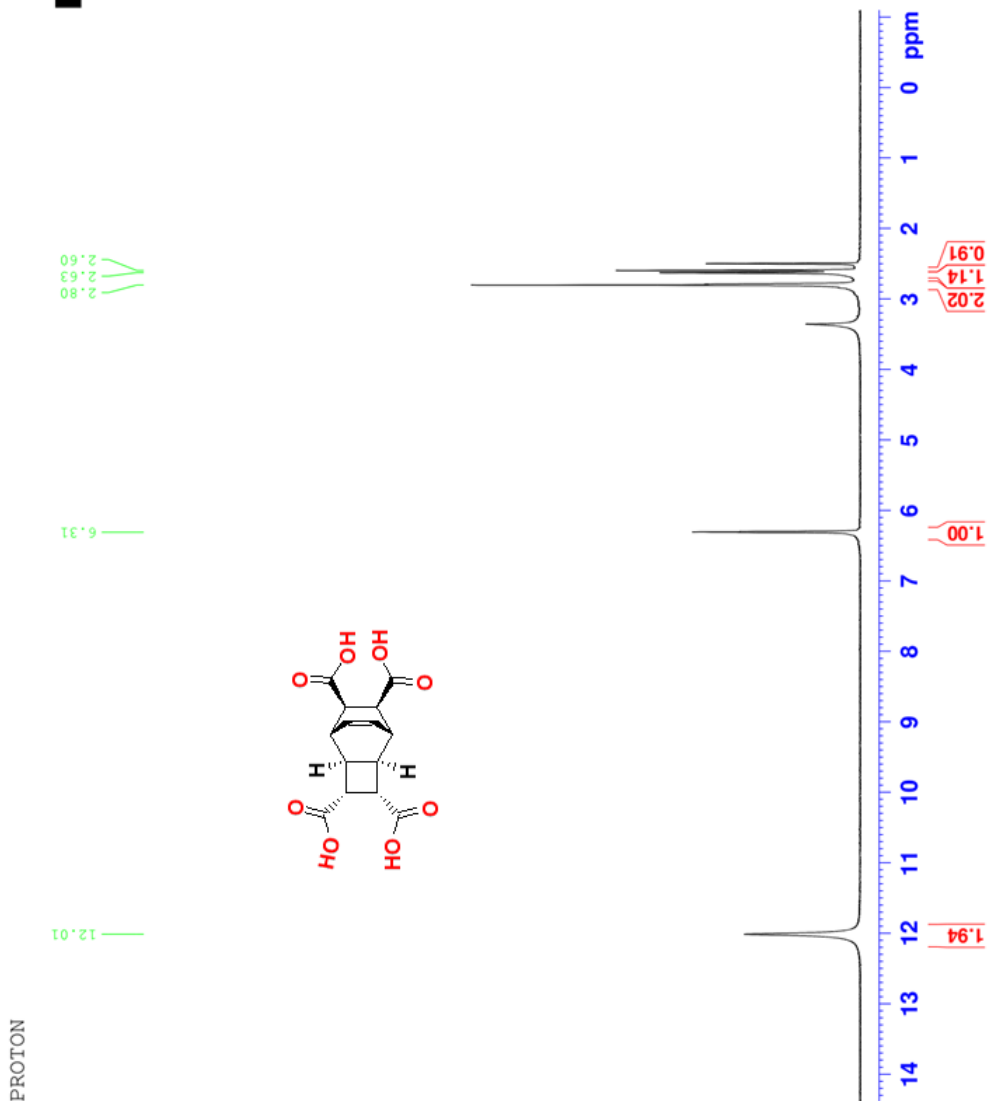


Figure 92:  $^1\text{H}$  NMR spectrum of CBTA-2 in  $\text{DMSO-d}_6$  at room temperature

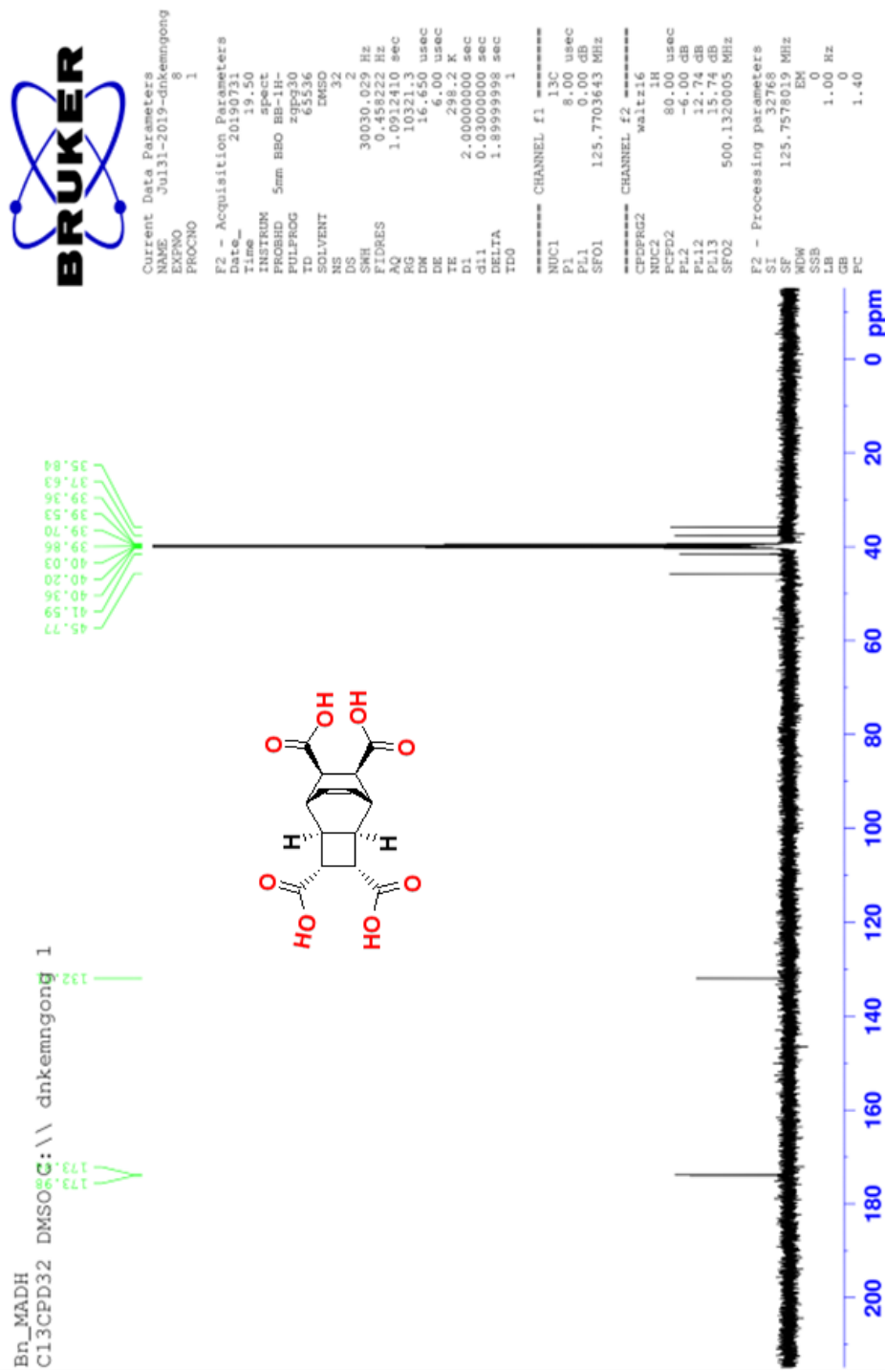
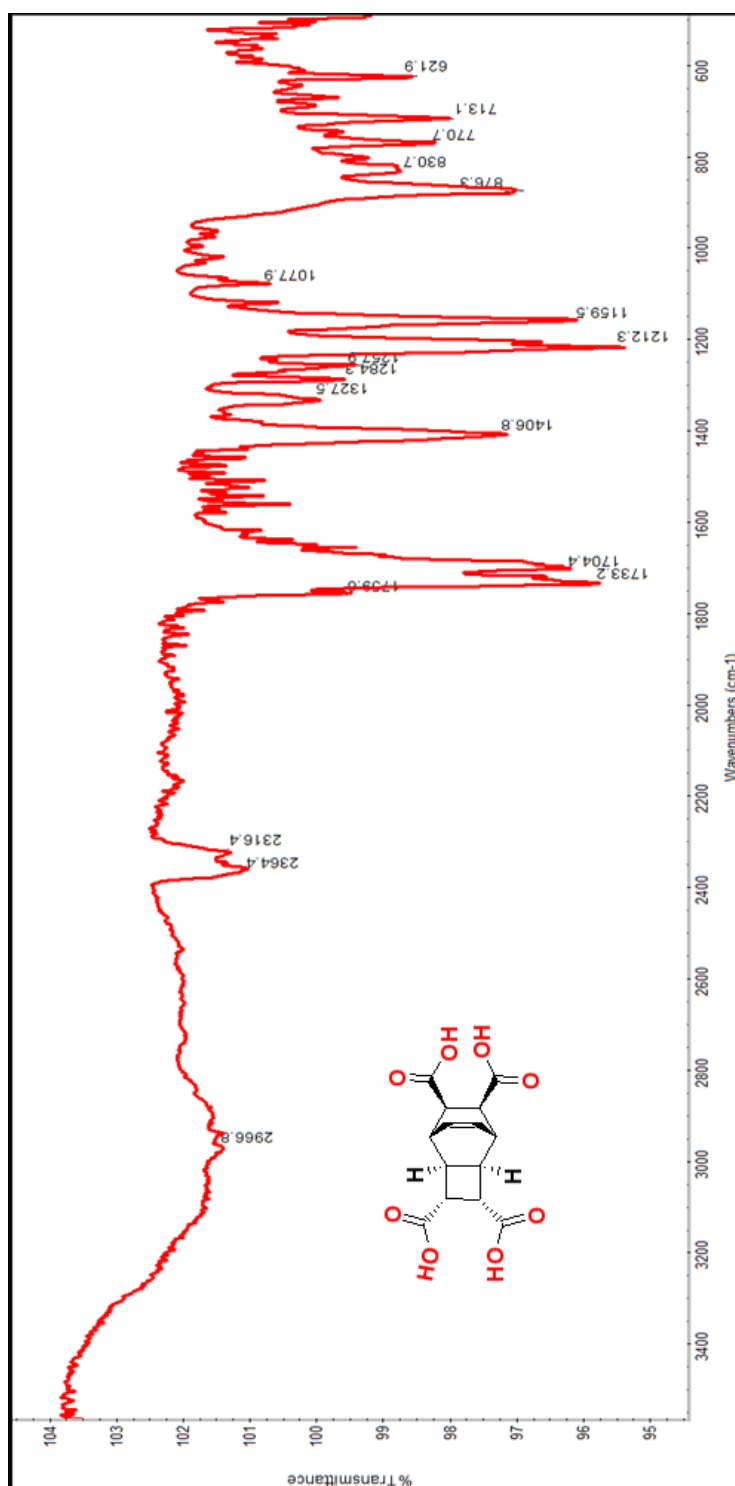


Figure 93:  $^{13}\text{C}$  NMR spectrum of CBTA-2 in DMSO- $d_6$  at room temperature





**Figure 94:** FT-IR NMR spectrum of CBTA-2

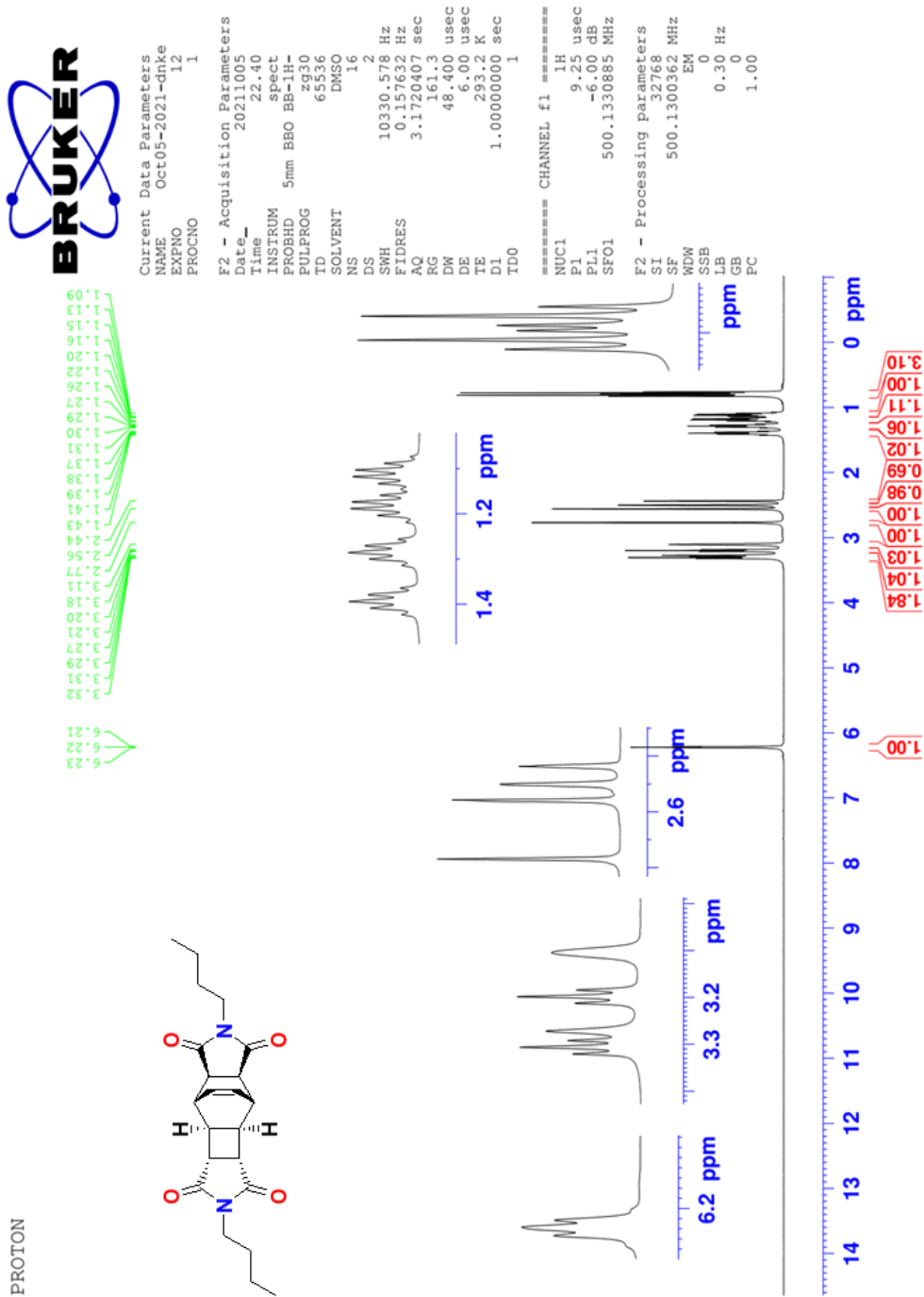


Figure 95:  $^1\text{H}$  NMR spectrum of CBDIM-2 in  $\text{DMSO-d}_6$  at room temperature



Current Data Parameters  
NAME Apr26-2022-dnke  
EXPNO 9  
PROCNO 1

F2 - Acquisition Parameters  
Date\_ 20220426  
Time 12.50  
INSTRUM spect  
PROBHD 5mm BBO BB-1H-  
PULPROG zgpg30  
TD 65536  
SOLVENT DMSO  
NS 1024  
DS 4  
SMH 30030.029 Hz  
FIDRES 0.458222 Hz  
AQ 1.0912410 sec  
RG 8192  
DW 16.650 usec  
DE 6.00 usec  
TE 292.2 K  
D1 2.00000000 sec  
d11 0.03000000 sec  
DELTA 1.89999998 sec  
TDO 1

===== CHANNEL f1 =====  
NUC1 13C  
P1 8.00 usec  
PL1 0.00 dB  
SFO1 125.7703643 MHz

===== CHANNEL f2 =====  
CPDPRG2 waltz16  
NUC2 1H  
PCPD2 80.00 usec  
PL2 -6.00 dB  
PL12 12.74 dB  
PL13 15.74 dB  
SFO2 500.1320005 MHz

F2 - Processing parameters  
SI 32768  
SF 125.7578519 MHz  
WDW EM  
SSB 0  
LB 1.00 Hz  
GB 0  
PC 1.40

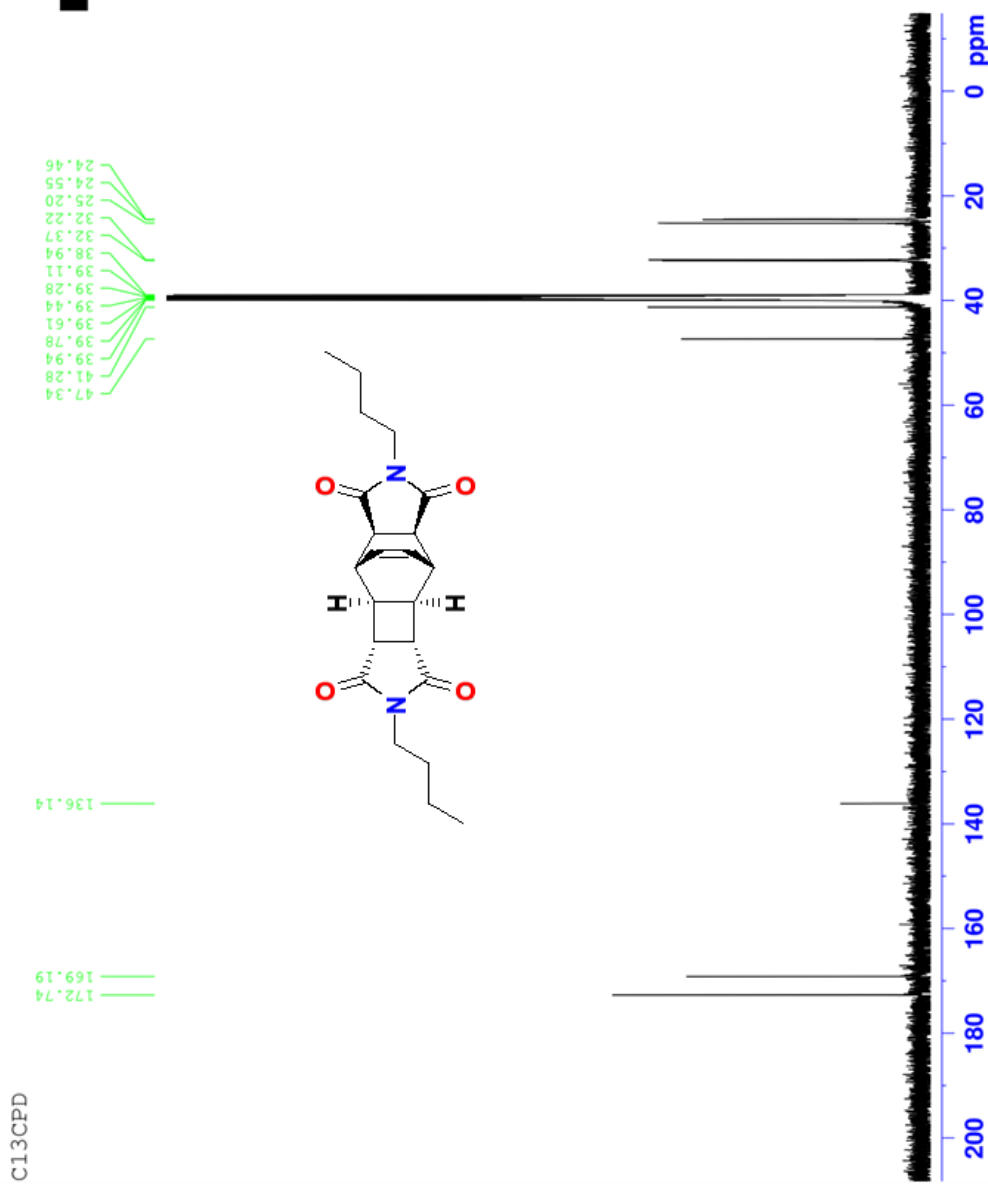
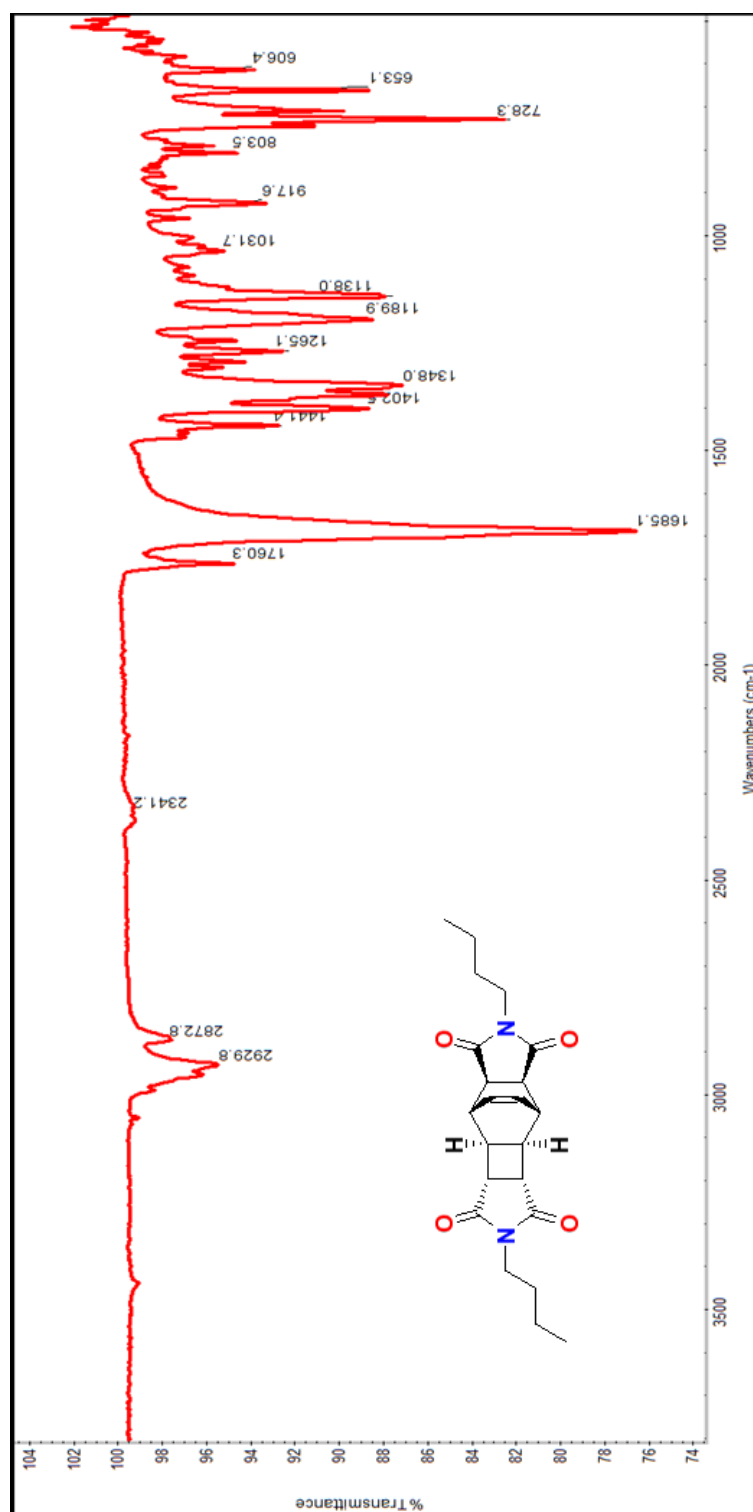
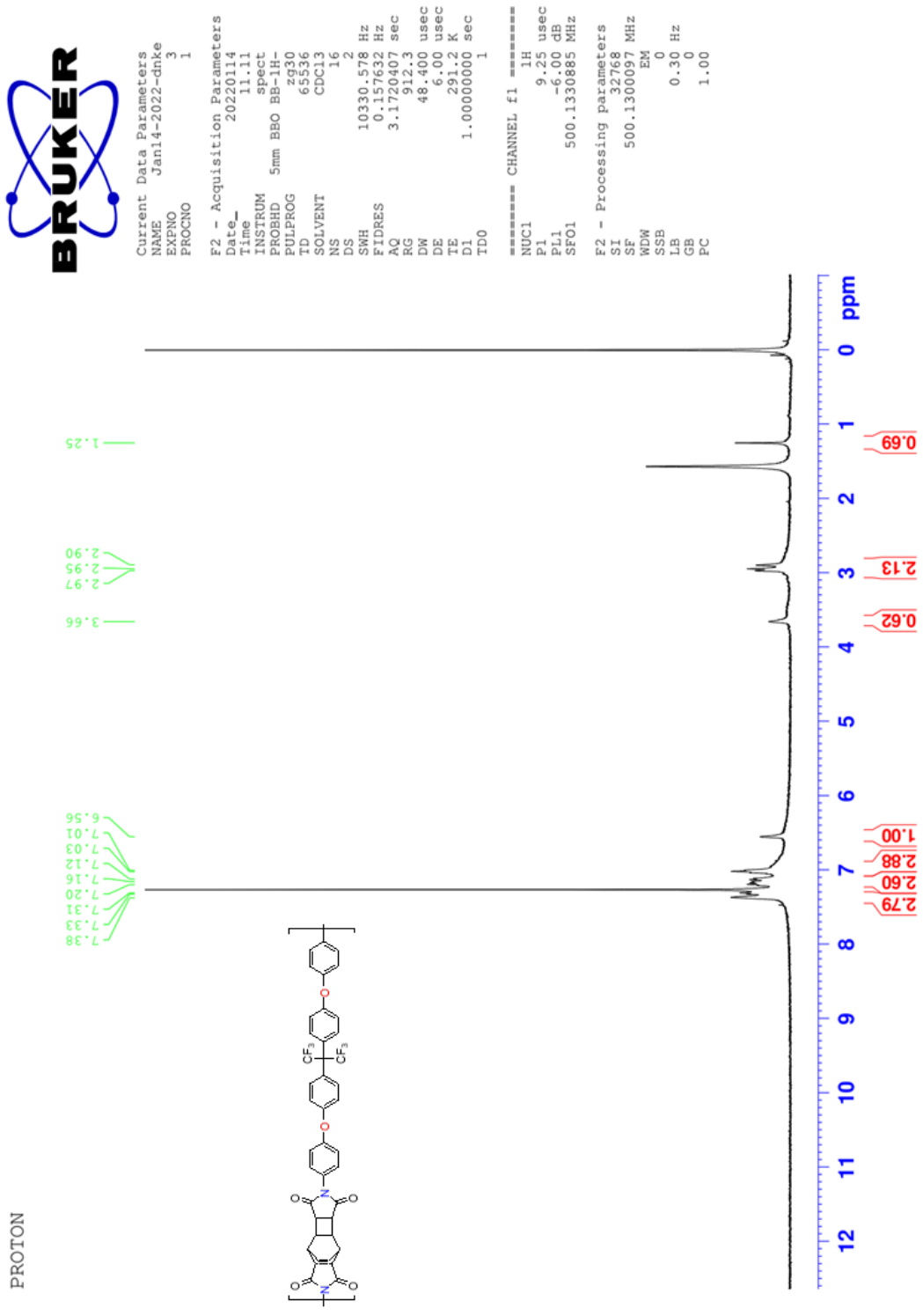


Figure 96: <sup>13</sup>C NMR spectrum of CBDIM-2 in DMSO-d<sub>6</sub> at room temperature



**Figure 97:** FT-IR NMR spectrum of CBDIM-2



**Figure 98:**  $^1\text{H}$  NMR spectrum of Polyimide-I in  $\text{CDCl}_3/\text{TFA}$  at room temperature

C13CPD



Current Data Parameters  
NAME Jan19-2022-drke  
EXPNO 16  
PROCNO 1

F2 - Acquisition Parameters  
Date\_ 20220120  
Time 15.58  
INSTRUM spect  
PROBHD 5mm BBO BB-1H-  
PULPROG zgpg30  
TD 65536  
SOLVENT CDCl3  
NS 3000  
DS 4  
SWH 30030.029 Hz  
FIDRES 0.458222 Hz  
AQ 1.0912410 sec  
RG 16384  
DW 16.650 usec  
DE 6.00 usec  
TE 290.2 K  
D1 2.00000000 sec  
d11 0.03000000 sec  
DELTA 1.89999998 sec  
TD0 1

===== CHANNEL f1 =====  
NUC1 13C  
P1 8.00 usec  
PL1 0.00 dB  
SFO1 125.7703643 MHz

===== CHANNEL f2 =====  
CPDPRG2 waltz16  
NUC2 1H  
PCPD2 80.00 usec  
PL2 -6.00 dB  
PL12 12.74 dB  
PL13 15.74 dB  
SFO2 500.1320005 MHz

F2 - Processing parameters  
SI 32768  
SE 125.7577818 MHz  
WDW EM  
SSB 0  
LB 1.00 Hz  
GB 0  
FC 1.40

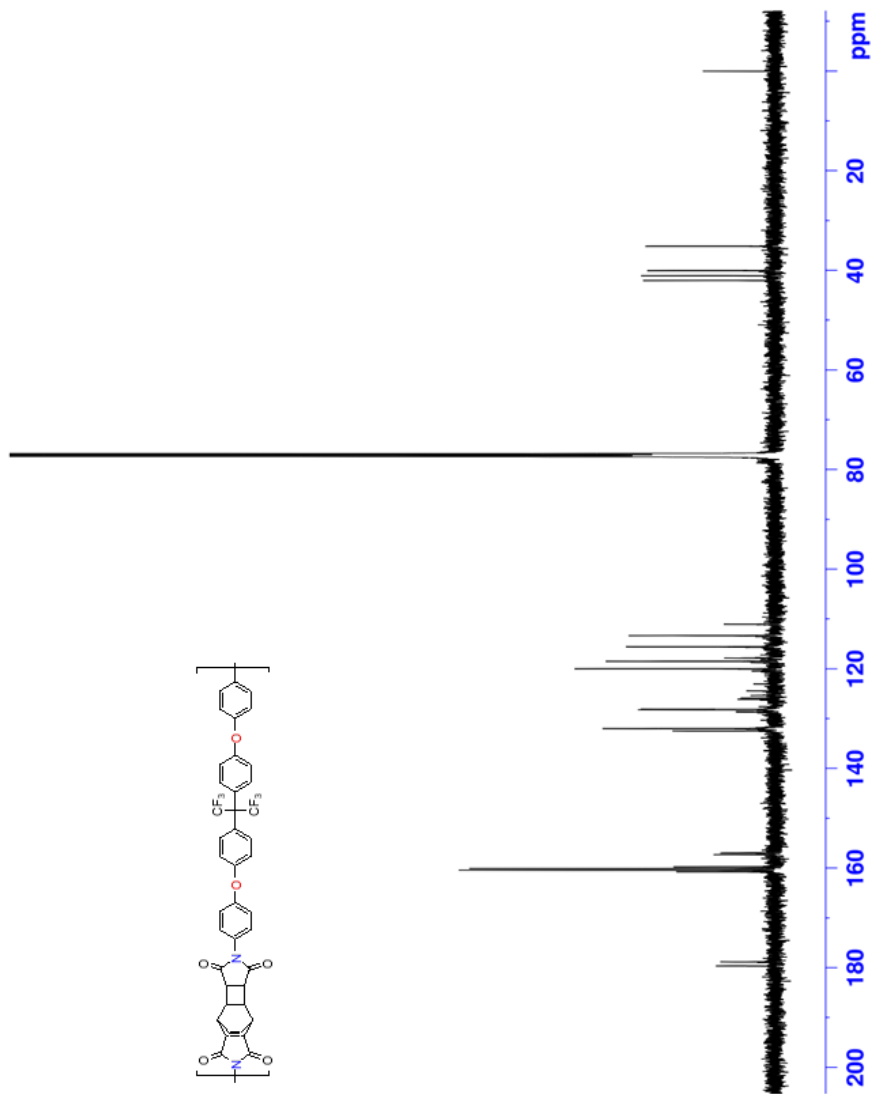
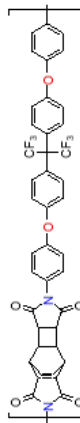
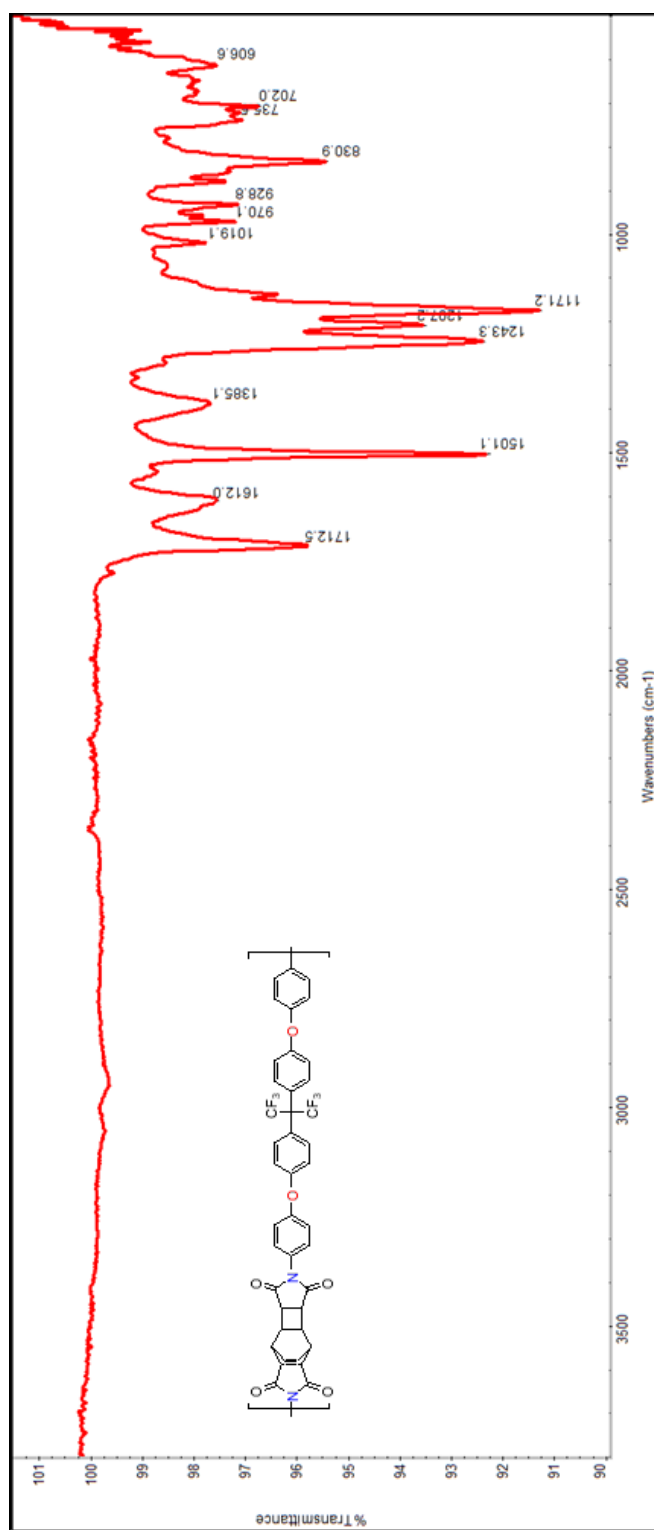
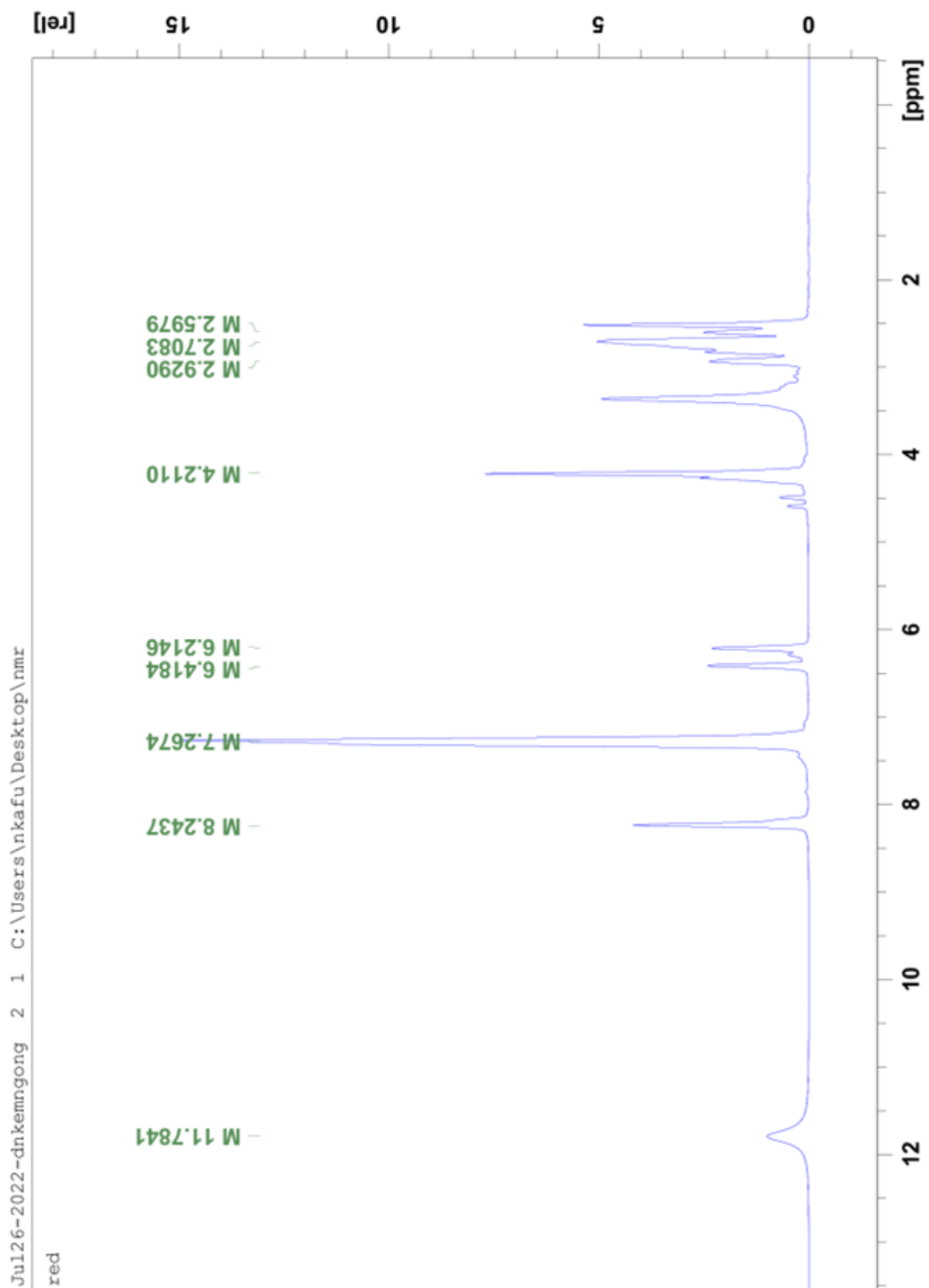


Figure 99:  $^{13}\text{C}$  NMR spectrum of Polyimide-I in  $\text{CDCl}_3/\text{TFA}$  at room temperature



**Figure 100:** FT-IR spectrum of Polyimide-I



**Figure 101:**  $^1\text{H}$  NMR spectrum of CBDAxx-1 in  $\text{DMSO-d}_6$  at room temperature



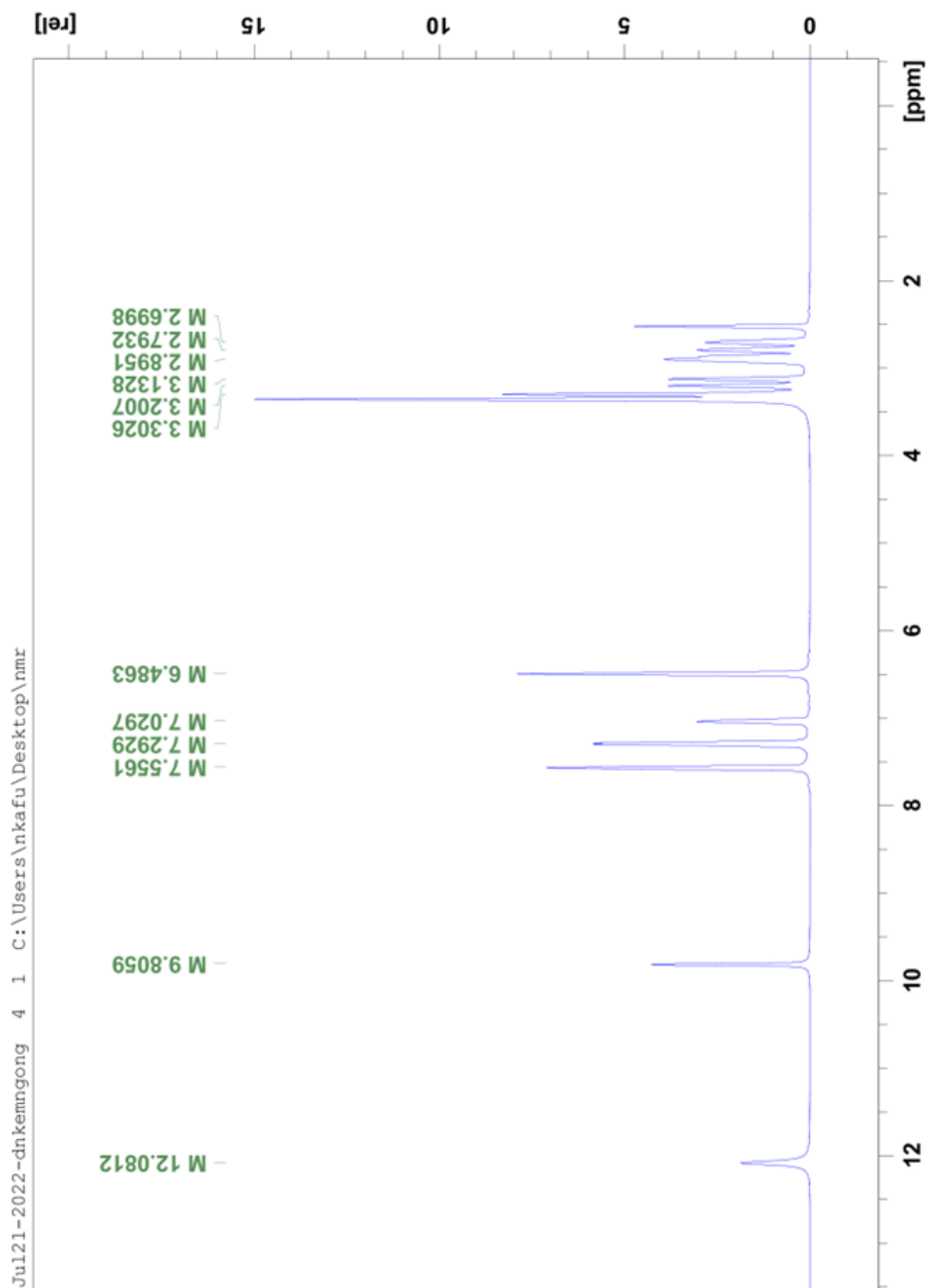


**Figure 102:**  $^1\text{H}$  NMR spectrum of CBDAxx-2 in  $\text{DMSO-d}_6$  at room temperature



Furone  
PROTON

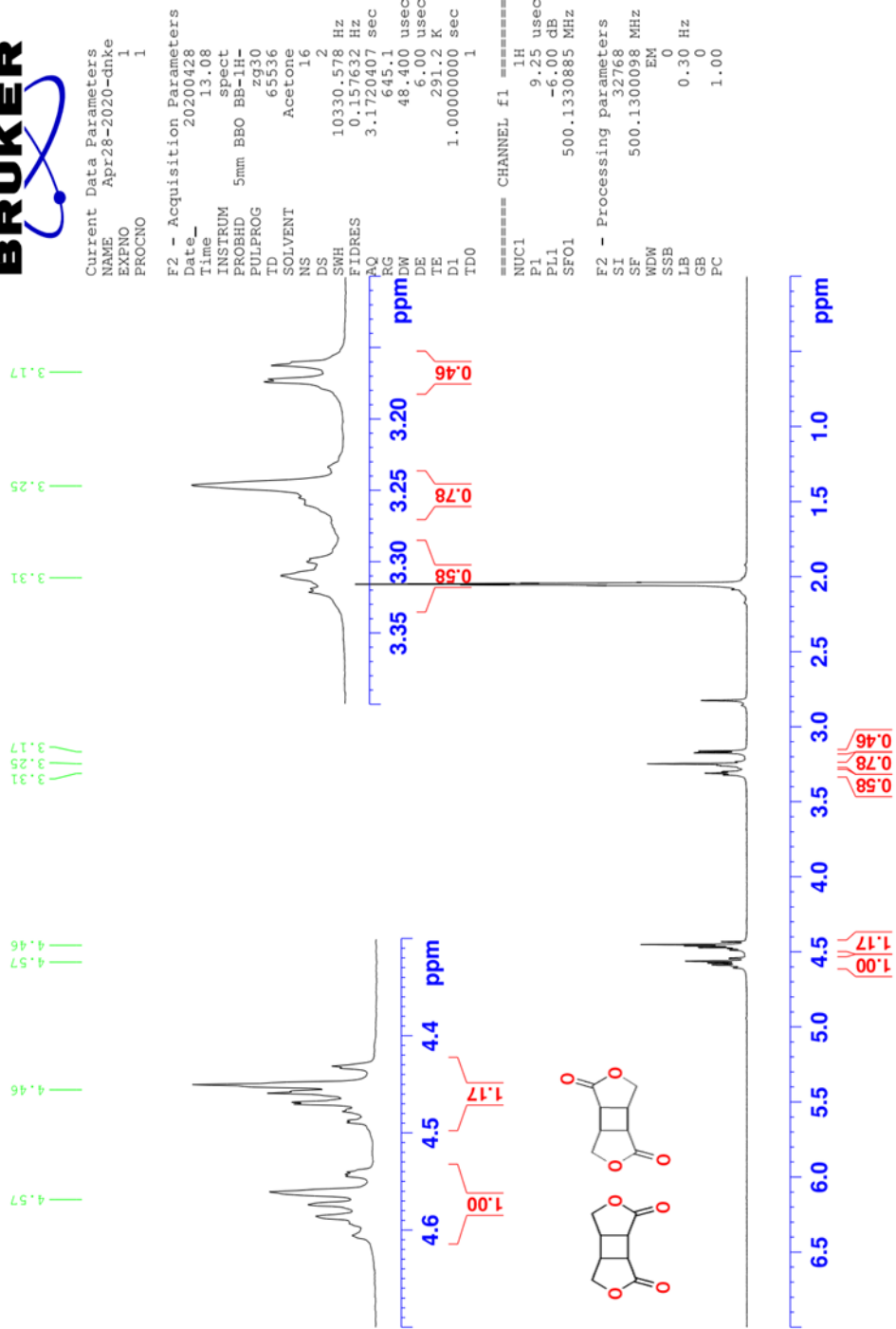
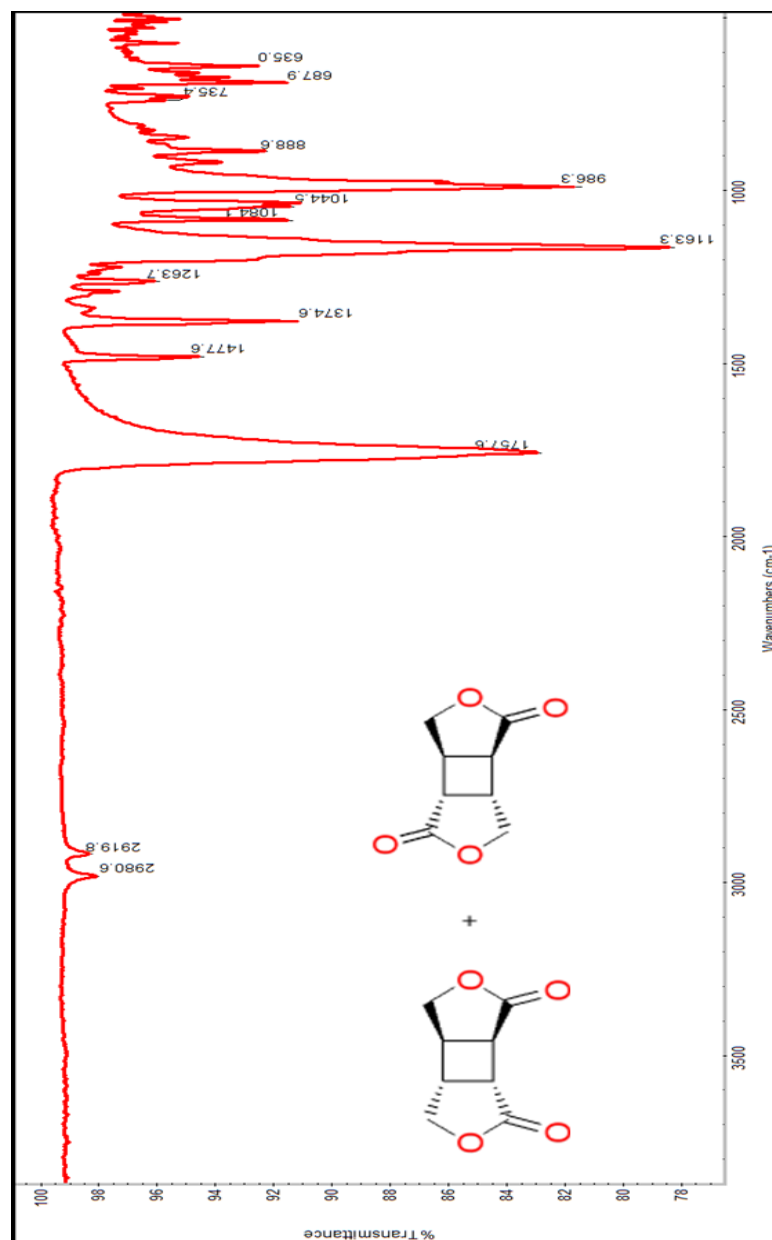
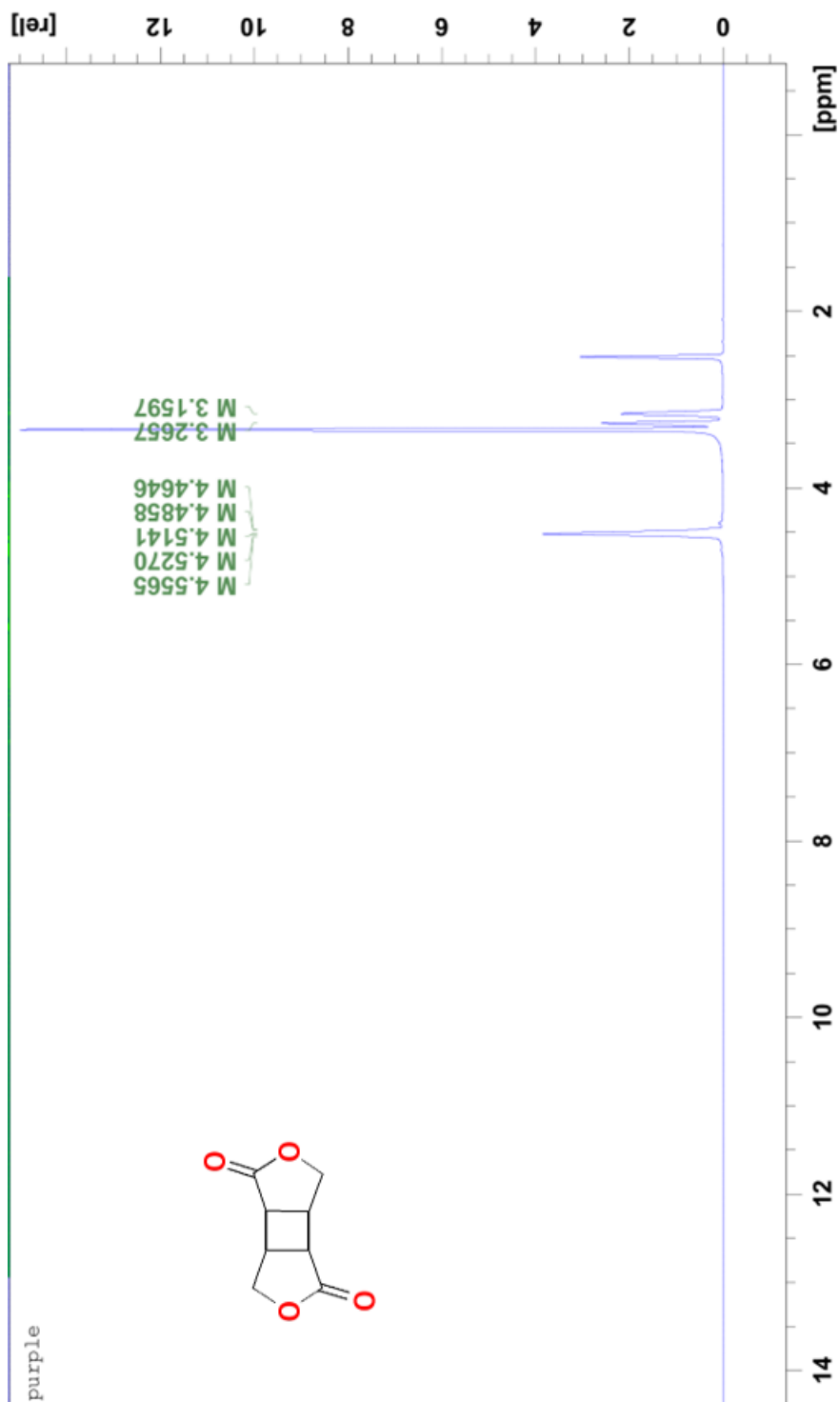


Figure 103:  $^1\text{H}$  NMR spectrum of mixture of CBDL-1&2 in  $\text{DMSO-d}_6$  at r.t.

**Figure 104:**  $^{13}\text{C}$  NMR spectrum of mixture of CBDL-1&2 in  $\text{DSMO-d}_6$  at r.t.



**Figure 105:** FT-IR NMR spectrum of mixture of CBDL-1&2 in  $\text{DSMO-d}_6$  at r.t.



**Figure 106:** <sup>1</sup>H NMR spectrum of CBDL-1 in DMSO-d<sub>6</sub> at room temperature

**Figure 107:**  $^{13}\text{C}$  NMR spectrum of CBDL-1 in  $\text{DSMO-d}_6$  at room temperature

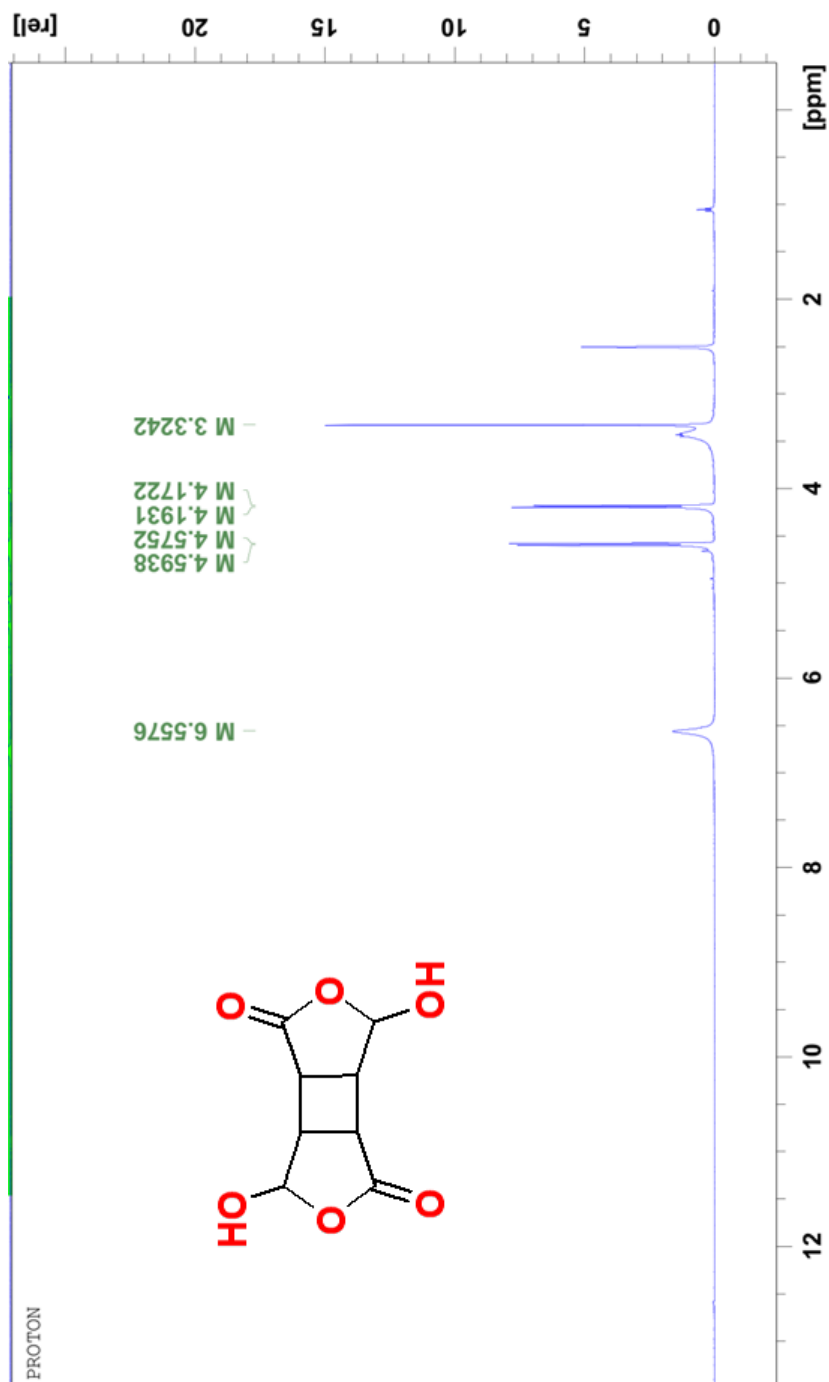


**Figure 108:**  $^1\text{H}$  NMR spectrum of CBDL-3 in  $\text{DSMO-d}_6$  at room temperature

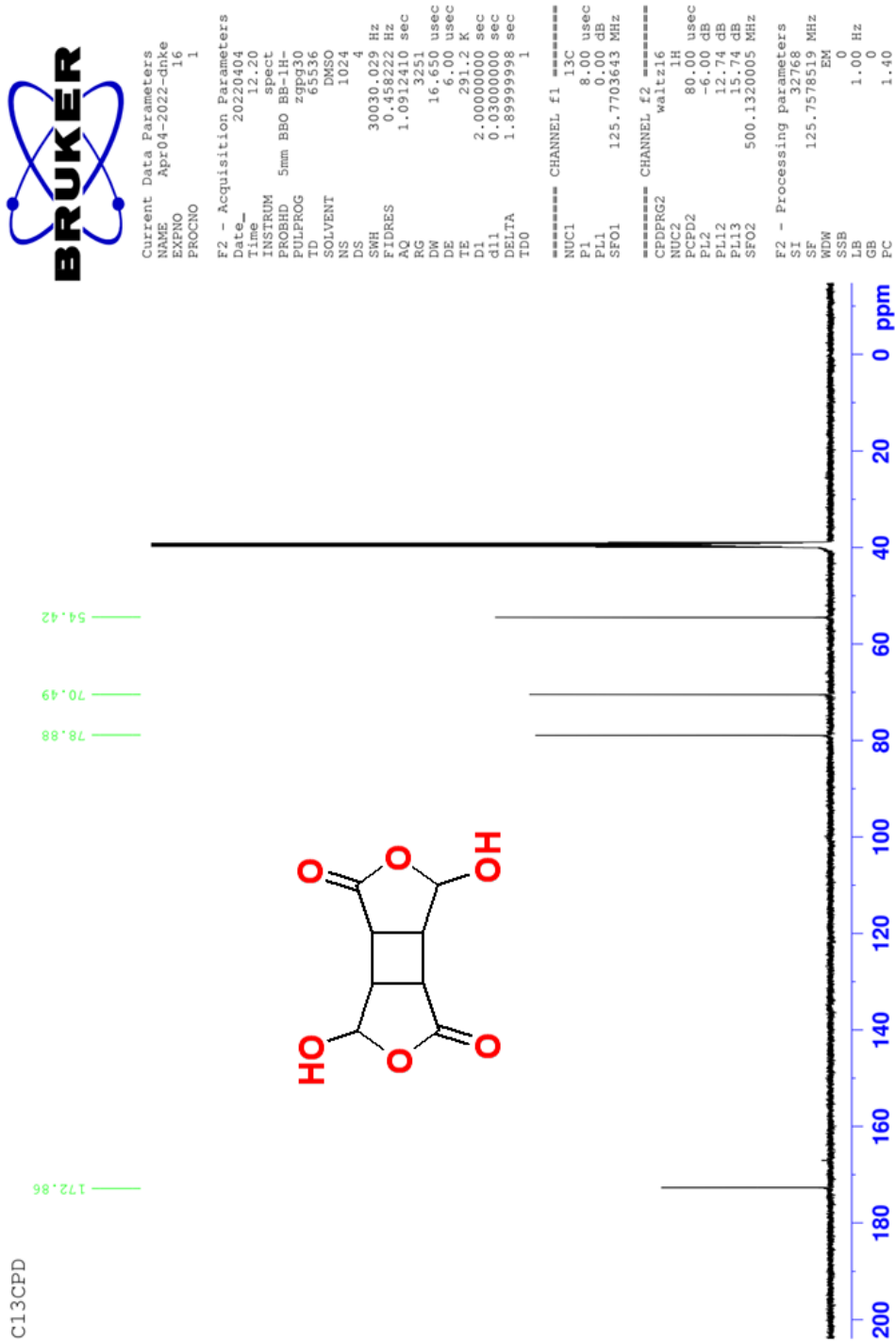
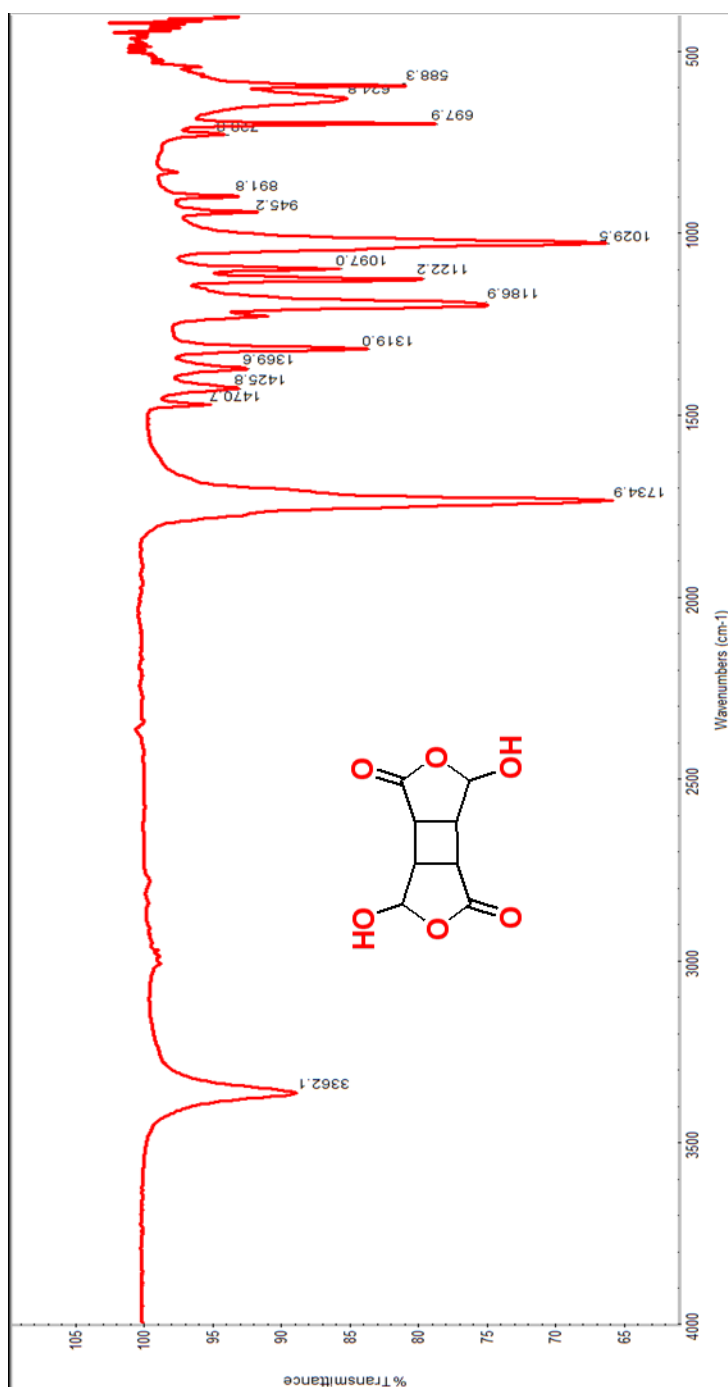
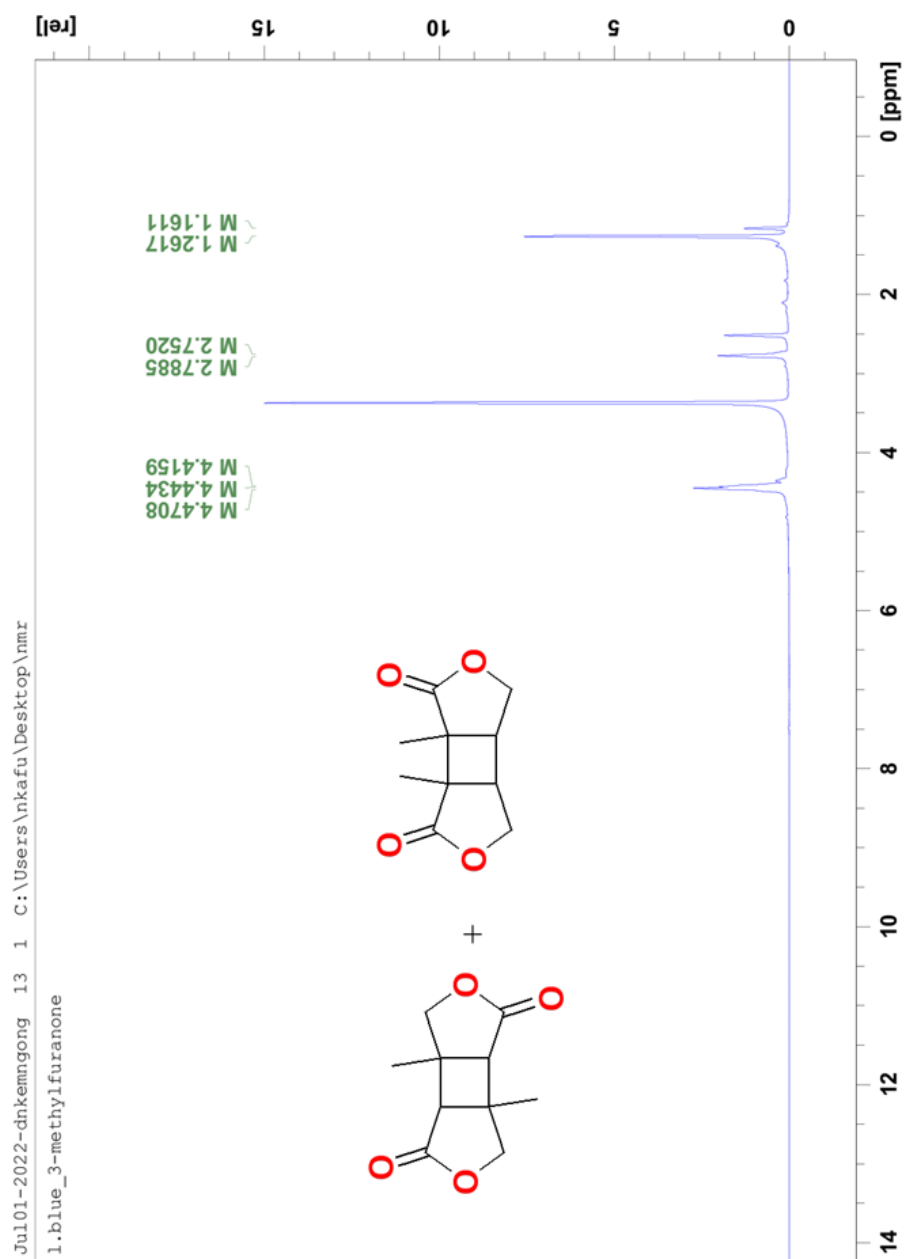


Figure 109:  $^{13}\text{C}$  NMR spectrum of CBDL-3 in  $\text{DMSO-d}_6$  at room temperature



**Figure 110:** FT-IR NMR spectrum of CBDL-3



**Figure 111:**  $^1\text{H}$  NMR spectrum of CBDL-4&5 in  $\text{DMSO-d}_6$  at room temperature



## **Appendix C**

### **High Resolution Mass Spectrometry Data of Synthesized Compounds**

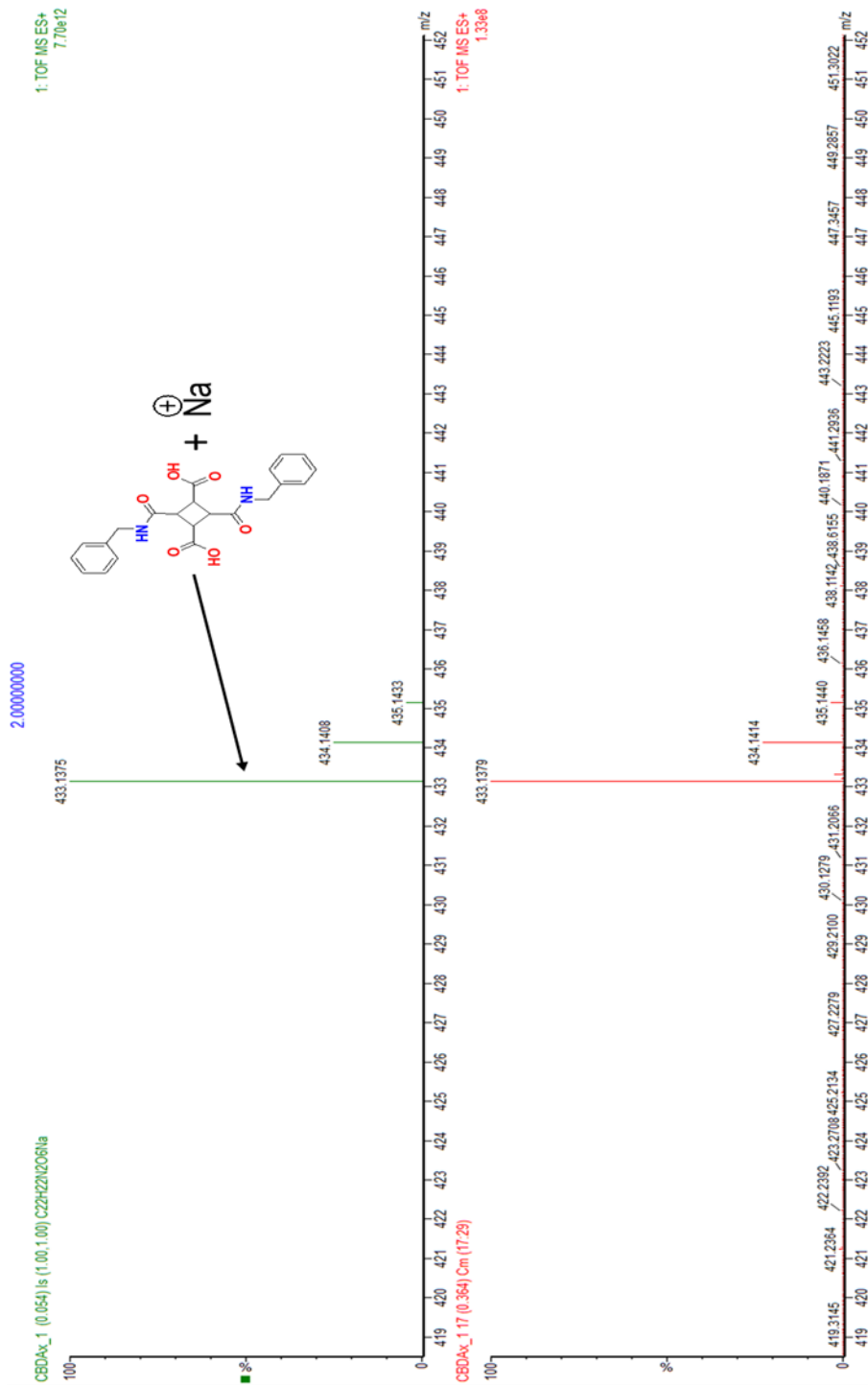


**Figure 112:** HRMS spectrum of CBDAx-1

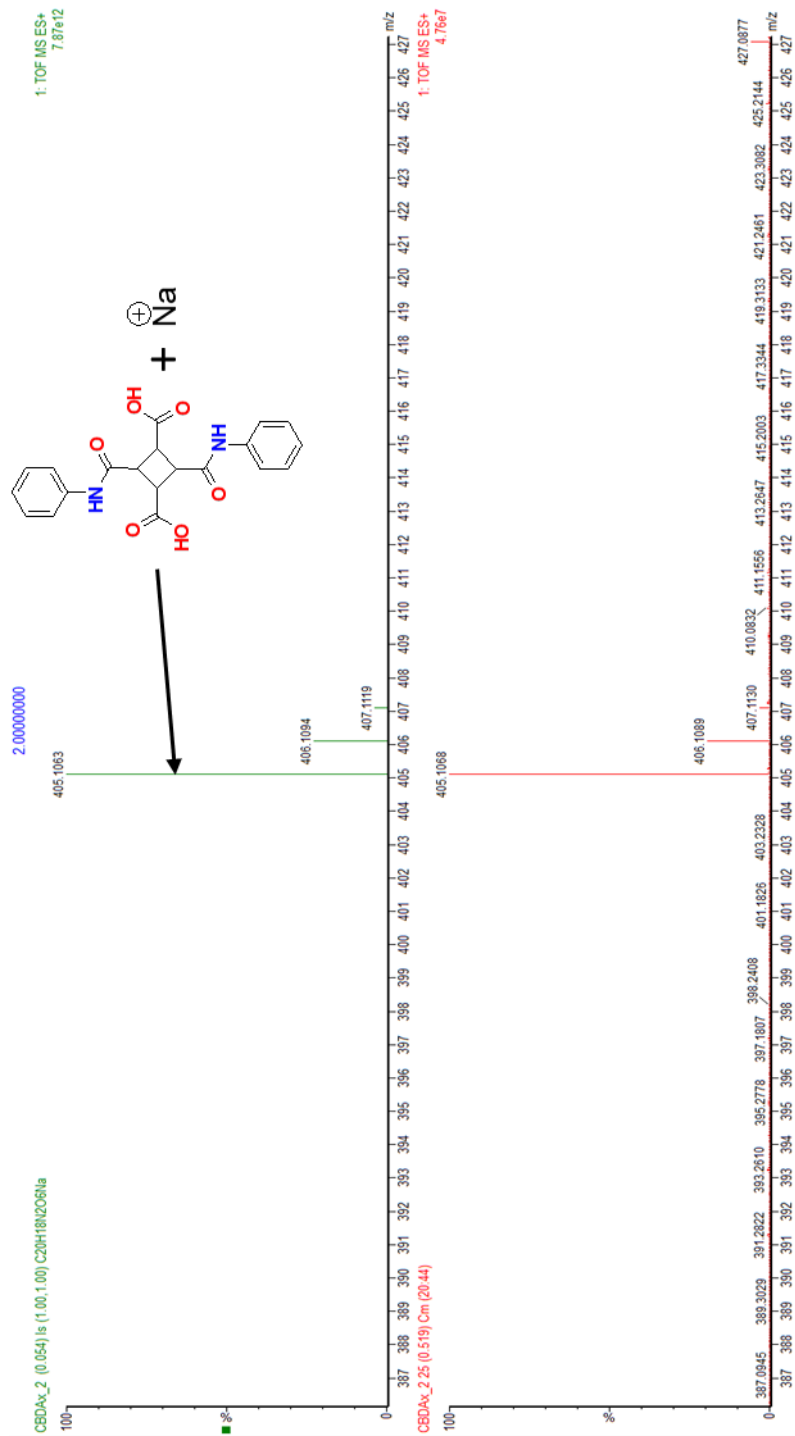


**Figure 113:** HRMS spectrum of CBDAx-2.

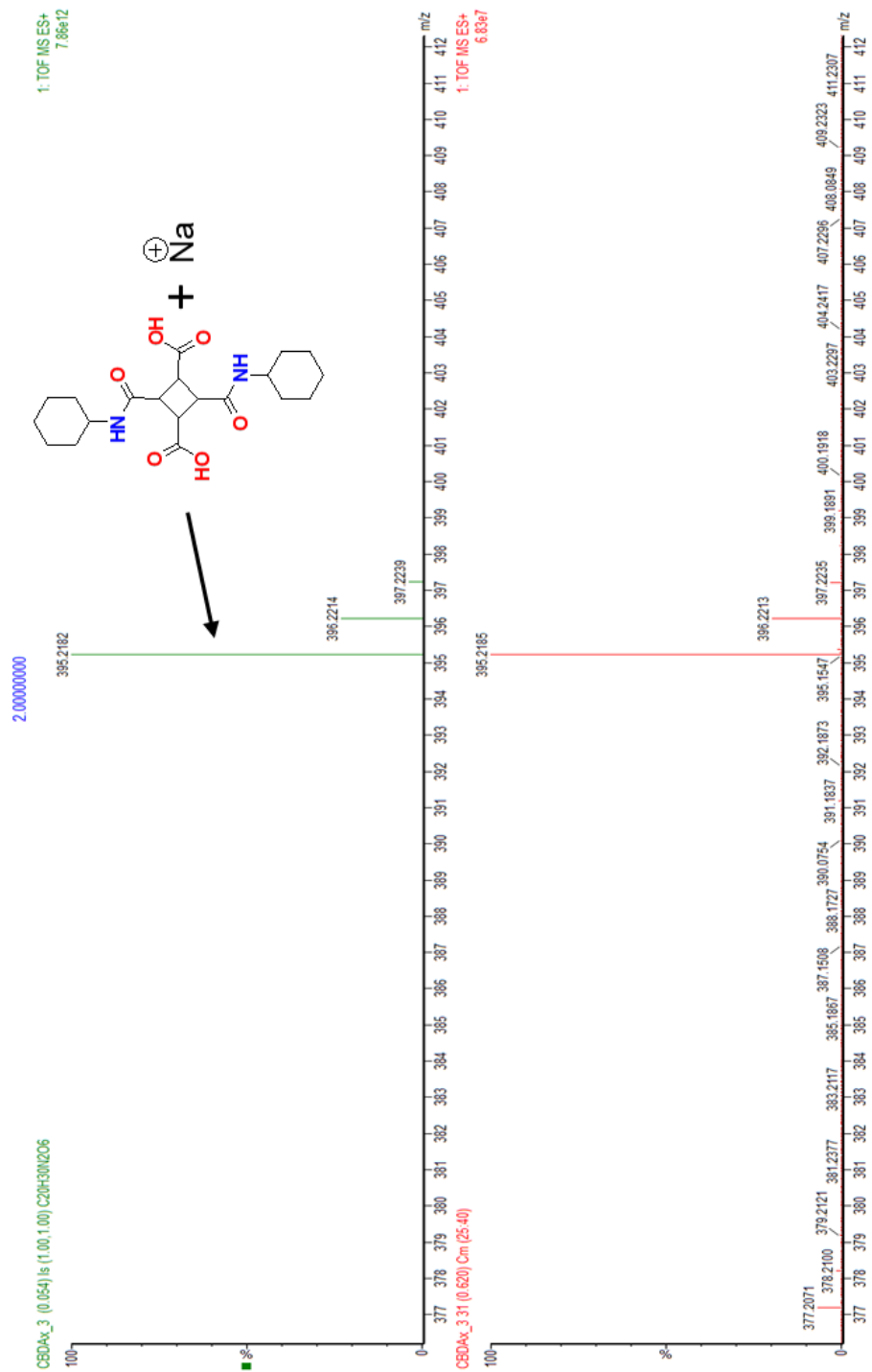


**Figure 114:** HRMS spectrum of CBDAx-3.

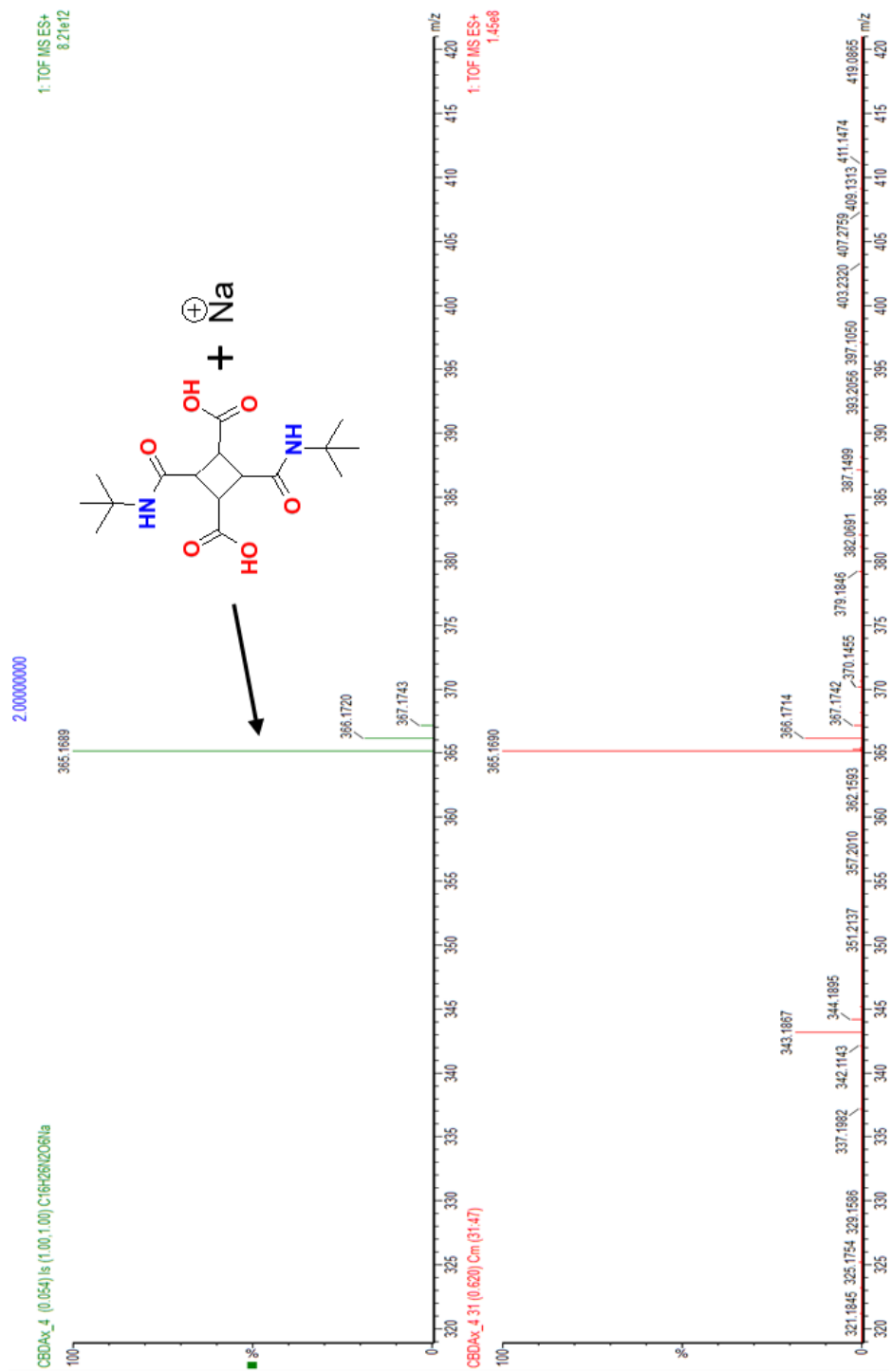


**Figure 115:** HRMS spectrum of CBDAx-4.

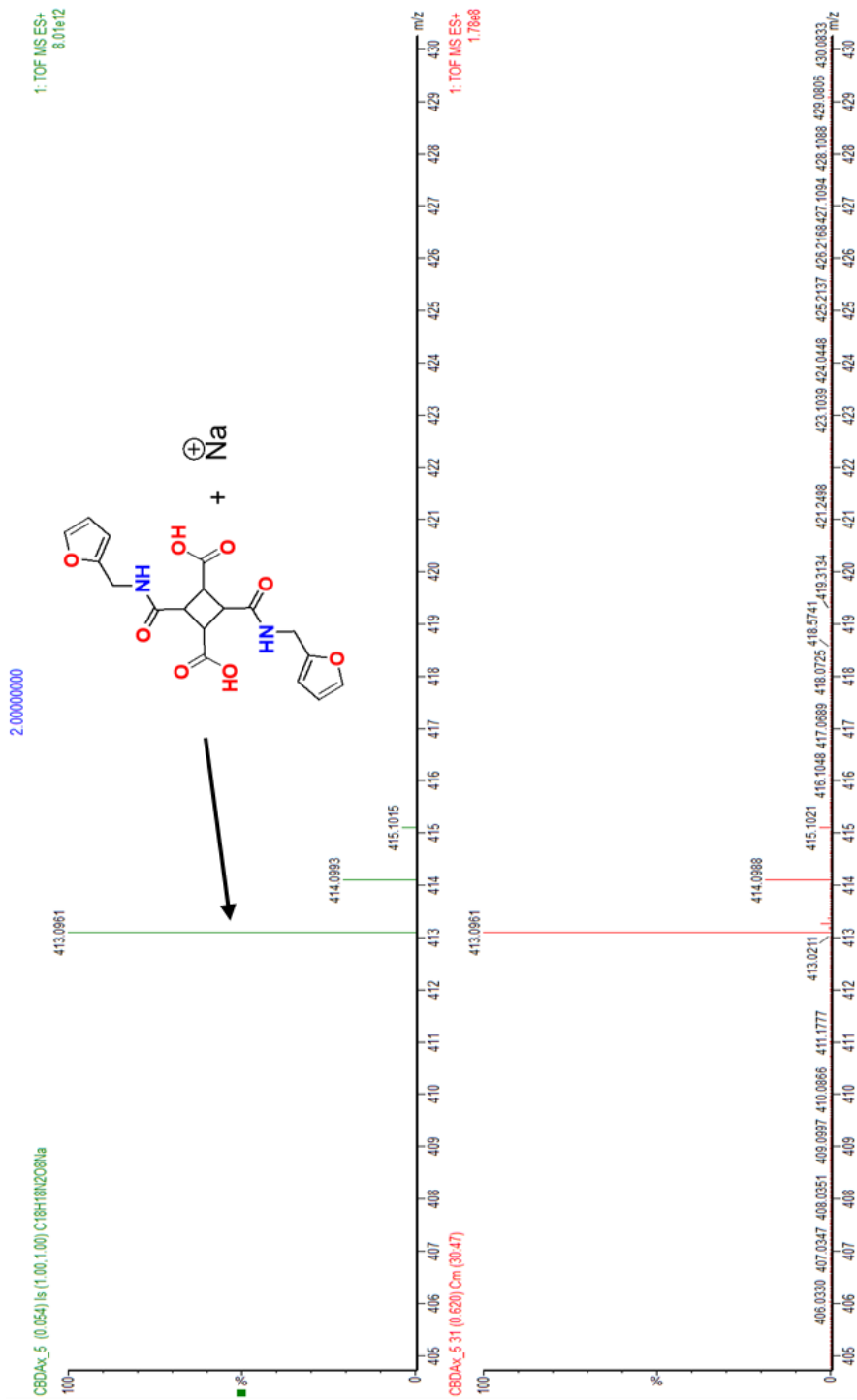


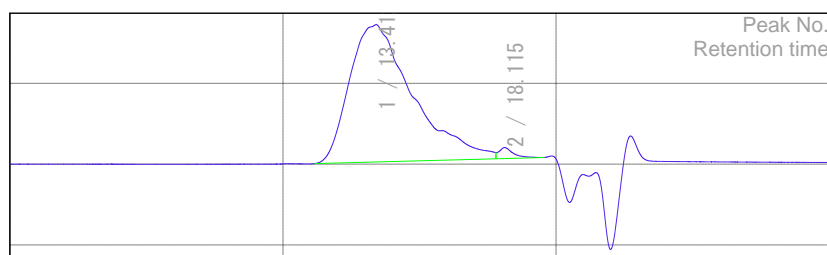
**Figure 116:** HRMS spectrum of CBDAx-5.

## Appendix D

### Selected GPC traces

Header

Title		Data acquisition date and time	2022/04/27 16:35:20
Sample name	UND-Dominic-CBDAN-2-CF3 Polymer	Calculation date and time	2022/04/27 16:47:21
Database name	4-27-2021 Column1 UND Dominic sample	Acquisition time [min]	0.000 - 30.000
Data name	RSLT0002	Sampling interval [msec]	100
Method name	STD PS for SuperH3000(less than 20,000 ) Column1 April2022	Cup number	36
Channel	RI	Calculation type	Molecular Weight



Result of molecular weight calculation (RI)

Peak 1 Base Peak

	[min]	[mV]	[mol]	Mn	
Peak start		0.374		Mw	2,858
	11.160		23,973	Mz	5,127
Peak top	13.412	86.410	5,282	Mz+1	7,232
Peak end	17.797	7.228	332		9,056

		Mv	5,127
Height [mV]	85.024	Mp	5,244
[eta]	5127.24483	Mz+1/Mw	1.766

**Figure 117:** GPC chromatogram report of polyimide I (P-1).



## REFERENCES

- (1) Ramamurthy, V.; Sivaguru, J. Supramolecular Photochemistry as a Potential Synthetic Tool: Photocycloaddition. *Chemical Reviews* **2016**, *116* (17), 9914-9993. DOI: 10.1021/acs.chemrev.6b00040.
  - (2) Schmidt, G. M. J. Photodimerization in the solid state. *Pure and Applied Chemistry* **1960**, *27* (4), 31.
  - (3) Kaupp, G. Solid-state reactions, dynamics in molecular crystals. *Current Opinion in Solid State and Materials Science* **2002**, *6* (2), 131-138. DOI: [https://doi.org/10.1016/S1359-0286\(02\)00041-4](https://doi.org/10.1016/S1359-0286(02)00041-4).
  - (4) Turro, N. J.; Ramamurthy, V.; Cherry, W.; Farneth, W. The effect of wavelength on organic photoreactions in solution. Reactions from upper excited states. *Chemical Reviews* **1978**, *78* (2), 125-145. DOI: 10.1021/cr60312a003.
  - (5) Yates, J. L. R.; Sparkes, H. A. 4-Bromo-trans-cinnamic acid: structural characterisation and crystallographic investigation into the solid state [2 + 2] cycloaddition reaction and temperature induced phase transition. *CrystEngComm* **2013**, *15* (18), 3547-3553. DOI: 10.1039/C3CE40300A.
  - (6) Mei, X.; Liu, S.; Wolf, C. Template-Controlled Face-to-Face Stacking of Olefinic and Aromatic Carboxylic Acids in the Solid State. *Organic Letters* **2007**, *9* (14), 2729-2732. DOI: 10.1021/ol071039c.
  - (7) Griffin, G. W.; Basinski, J. E.; Velluro, A. F. Photodimerization of maleic and fumaric acid derivatives. *Tetrahedron Letters* **1960**, *1* (24), 13-16. DOI: [https://doi.org/10.1016/S0040-4039\(01\)99280-9](https://doi.org/10.1016/S0040-4039(01)99280-9).
  - (8) Wu, T.; Branda, N. R. Using low-energy near infrared light and upconverting nanoparticles to trigger photoreactions within supramolecular assemblies. *Chemical Communications* **2016**, *52* (56), 8636-8644. DOI: 10.1039/C6CC03864F.
- Shimizu, N.; Shigemitsu, H.; Kida, T.; Bach, T.; Mori, T. Visible Light-Induced Regio- and Enantiodifferentiating [2 + 2] Photocycloaddition of 1,4-Naphthoquinones Mediated by Oppositely Coordinating 1,3,2-Oxazaborolidine Chiral Lewis Acid. *The Journal of Organic Chemistry* **2022**. DOI: 10.1021/acs.joc.2c00730.

- Pfund, B.; Steffen, D. M.; Schreier, M. R.; Bertrams, M. S.; Ye, C.; Börjesson, K.; Wenger, O. S.; Kerzig, C. UV Light Generation and Challenging Photoreactions Enabled by Upconversion in Water. *J Am Chem Soc* **2020**, *142* (23), 10468-10476. DOI: 10.1021/jacs.0c02835
- Hölz, K.; Lietard, J.; Somoza, M. M. High-Power 365 nm UV LED Mercury Arc Lamp Replacement for Photochemistry and Chemical Photolithography. *ACS Sustainable Chemistry & Engineering* **2017**, *5* (1), 828-834. DOI: 10.1021/acssuschemeng.6b02175.
- (9) Yoon, T. P.; Ischay, M. A.; Du, J. Visible light photocatalysis as a greener approach to photochemical synthesis. *Nature Chemistry* **2010**, *2* (7), 527-532. DOI: 10.1038/nchem.687.
- (10) Randazzo, K.; Wang, Z.; Wang, Z. D.; Butz, J.; Chu, Q. R. Lighting the Way to Greener Chemistry: Incandescent Floodlights as a Facile UV Light Source for Classic and Cutting-Edge Photoreactions. *ACS Sustainable Chemistry & Engineering* **2016**, *4* (9), 5053-5059. DOI: 10.1021/acssuschemeng.6b01506.
- (11) Rath, B. B.; Vittal, J. J. Photoreactive Crystals Exhibiting [2 + 2] Photocycloaddition Reaction and Dynamic Effects. *Accounts of Chemical Research* **2022**, *55* (10), 1445-1455. DOI: 10.1021/acs.accounts.2c00107.
- Sonoda, Y. Solid-State [2+2] Photodimerization and Photopolymerization of  $\alpha,\omega$ -Diarylpolyene Monomers: Effective Utilization of Noncovalent Intermolecular Interactions in Crystals. *Molecules* **2011**, *16* (1). DOI: 10.3390/molecules16010119.
- Ha, S.; Lee, Y.; Kwak, Y.; Mishra, A.; Yu, E.; Ryou, B.; Park, C.-M. Alkyne–Alkene [2 + 2] cycloaddition based on visible light photocatalysis. *Nature Communications* **2020**, *11* (1), 2509. DOI: 10.1038/s41467-020-16283-9.
- (12) Day, G. M.; Trask, A. V.; Motherwell, W. D. S.; Jones, W. Investigating the latent polymorphism of maleic acid. *Chemical Communications* **2006**, (1), 54-56. DOI: 10.1039/B513442K.
- (13) Brown, C. J. The crystal structure of fumaric acid. *Acta crystallographica* **1966**, *21* (1), 1-5. DOI: 10.1107/S0365110X66002226.

- (14) Carpenter, J. H. Applications of Maleic and Fumaric Acids and Their Salts in the Textile Industry. *Journal of Industrial & Engineering Chemistry* **1921**, *13* (5), 410-413. DOI: 10.1021/ie50137a014.
- (15) Wojcieszak, R.; Santarelli, F.; Paul, S.; Dumeignil, F.; Cavani, F.; Gonçalves, R. V. Recent developments in maleic acid synthesis from bio-based chemicals. *Sustainable Chemical Processes* **2015**, *3* (1), 9. DOI: 10.1186/s40508-015-0034-5.
- (16) Das, R. K.; Lonappan, L.; Brar, S. K.; Verma, M. Bio-conversion of apple pomace into fumaric acid in a rotating drum type solid-state bench scale fermenter and study of the different underlying mechanisms. *RSC Advances* **2015**, *5* (126), 104472-104479. DOI: 10.1039/C5RA22898K.
- (17) Araji, N.; Madjinza, D. D.; Chatel, G.; Moores, A.; Jérôme, F.; De Oliveira Vigier, K. Synthesis of maleic and fumaric acids from furfural in the presence of betaine hydrochloride and hydrogen peroxide. *Green Chemistry* **2017**, *19* (1), 98-101. DOI: 10.1039/C6GC02620F.
- (18) Lou, Y.; Marinkovic, S.; Estrine, B.; Qiang, W.; Enderlin, G. Oxidation of Furfural and Furan Derivatives to Maleic Acid in the Presence of a Simple Catalyst System Based on Acetic Acid and TS-1 and Hydrogen Peroxide. *ACS omega* **2020**, *5* (6), 2561-2568. DOI: 10.1021/acsomega.9b02141 PubMed.
- (19) Yang, T.; Li, W.; Liu, Q.; Su, M.; Zhang, T.; Ma, J. Synthesis of maleic acid from biomass-derived furfural in the presence of KBr/graphitic carbon nitride (g-C<sub>3</sub>N<sub>4</sub>) catalyst and hydrogen peroxide. *Bioresources* **2019**, *14* (3), 5025-5044. DOI: 10.15376/biores.14.3.5025-5044.
- (20) Shinde, S. H.; Hengne, A.; Rode, C. V. Chapter 1 - Lignocellulose-derived platform molecules: An introduction. In *Biomass, Biofuels, Biochemicals*, Saravanamurugan, S., Pandey, A., Li, H., Riisager, A. Eds.; Elsevier, 2020; pp 1-31.
- (21) Shi, S.; Guo, H.; Yin, G. Synthesis of maleic acid from renewable resources: Catalytic oxidation of furfural in liquid media with dioxygen. *Catalysis communications* **2011**, *12* (8), 731-733. DOI: 10.1016/j.catcom.2010.12.033.
- (22) Yu, Q.; Bai, R.; Wang, F.; Zhang, Q.; Sun, Y.; Zhang, Y.; Qin, L.; Wang, Z.; Yuan, Z. A sustainable system for maleic acid synthesis from biomass-derived sugar. *Journal*

*of chemical technology and biotechnology (1986)* **2019**, 95 (3), 751-757. DOI: 10.1002/jctb.6260.

(23) Thiagarajan, S.; Franciolus, D.; Bisselink, R. J. M.; Ewing, T. A.; Boeriu, C. G.; van Haveren, J. Selective Production of Maleic Acid from Furfural via a Cascade Approach Combining Photochemistry and Electro- or Biochemistry. *ACS sustainable chemistry & engineering* **2020**, 8 (29), 10626-10632. DOI: 10.1021/acssuschemeng.0c02833.

(24) Agirre, I.; Gandarias, I.; Granados, M. L.; Arias, P. L. Process design and techno-economic analysis of gas and aqueous phase maleic anhydride production from biomass-derived furfural. *Biomass conversion and biorefinery* **2019**, 10 (4), 1021-1033. DOI: 10.1007/s13399-019-00462-w.

(25) Yedur, S. K.; Dulebohn, J.; Werpy, T.; Berglund, K. A. Synthesis and Testing of Catalysts for the Production of Maleic Anhydride from a Fermentation Feedstock. *Industrial & engineering chemistry research* **1996**, 35 (3), 663-671. DOI: 10.1021/ie950414e.

(26) Zhang, M.; Colby, R. H.; Milner, S. T.; Chung, T. C. M.; Huang, T.; deGroot, W. Synthesis and Characterization of Maleic Anhydride Grafted Polypropylene with a Well-Defined Molecular Structure. *Macromolecules* **2013**, 46 (11), 4313-4323. DOI: 10.1021/ma4006632.

(27) Li, X.; Zhang, Y. The conversion of 5-hydroxymethyl furfural (HMF) to maleic anhydride with vanadium-based heterogeneous catalysts. *Green Chemistry* **2016**, 18 (3), 643-647. DOI: 10.1039/C5GC01794G.

(28) Suhas H. Shinde, A. H. a. C. V. R. *Lignocellulose-derived platform molecules: An introduction*; Elsevier, 2020.

(29) Chatzidimitriou, A.; Bond, J. Q. Oxidation of levulinic acid for the production of maleic anhydride: breathing new life into biochemicals. *Green Chemistry* **2015**, 17 (8), 4367-4376. DOI: 10.1039/C5GC01000D.

(30) Watson, J. *Fumaric Acid Market To Reach USD 974.4 Million By 2027*. GLOBE NEWSWIRE, May 05, 2020. (accessed 2022).

- (31) Martin-Dominguez, V.; Estevez, J.; Ojembarrena, F.; Santos, V.; Ladero, M. Fumaric Acid Production: A Biorefinery Perspective. *Fermentation (Basel)* **2018**, *4* (2), 33. DOI: 10.3390/fermentation4020033.
- (32) Xu, G.; Zou, W.; Chen, X.; Xu, N.; Liu, L.; Chen, J. Fumaric Acid Production in *Saccharomyces cerevisiae* by In Silico Aided Metabolic Engineering. *Plos One* **2012**, *7* (12), e52086. DOI: 10.1371/journal.pone.0052086.
- (33) Swart, R. M.; le Roux, F.; Naude, A.; de Jongh, N. W.; Nicol, W. Fumarate production with *Rhizopus oryzae*: utilising the Crabtree effect to minimise ethanol by-product formation. *Biotechnology for Biofuels* **2020**, *13* (1), 22. DOI: 10.1186/s13068-020-1664-8.
- (34) Sebastian, J.; Hegde, K.; Kumar, P.; Rouissi, T.; Brar, S. K. Bioproduction of fumaric acid: an insight into microbial strain improvement strategies. *Crit Rev Biotechnol* **2019**, *39* (6), 817-834. DOI: 10.1080/07388551.2019.1620677.
- Di Lorenzo, R. D.; Serra, I.; Porro, D.; Branduardi, P. State of the Art on the Microbial Production of Industrially Relevant Organic Acids. *Catalysts* **2022**, *12* (2). DOI: 10.3390/catal12020234.
- (35) Margulis, T. N. Structure of a planar cyclobutane. Cis,trans,cis-1,2,3,4-cyclobutanetetracarboxylic acid tetramethyl ester. *Journal of the American Chemical Society* **1971**, *93* (9), 2193-2195. DOI: 10.1021/ja00738a017.
- (36) Reid, E. B.; Sack, M. Synthetic Approaches to 1,2,3,4-Cyclobutanetetracarboxylic Acid. *Journal of the American Chemical Society* **1951**, *73* (5), 1985-1988. DOI: 10.1021/ja01149a027.
- (37) Ibarra, I. A.; Yang, S.; Lin, X.; Blake, A. J.; Rizkallah, P. J.; Nowell, H.; Allan, D. R.; Champness, N. R.; Hubberstey, P.; Schröder, M. Highly porous and robust scandium-based metal–organic frameworks for hydrogen storage. *Chemical communications (Cambridge, England)* **2011**, *47* (29), 8304-8306. DOI: 10.1039/c1cc11168j.
- (38) Wang, Z.; Miller, B.; Mabin, M.; Shahni, R.; Wang, Z. D.; Ugrinov, A.; Chu, Q. R. Cyclobutane-1,3-Diacid (CBDA): A Semi-Rigid Building Block Prepared by [2+2]

Photocyclization for Polymeric Materials. *Scientific reports* **2017**, 7 (1), 13704-13707. DOI: 10.1038/s41598-017-13983-z.

(39) Wang, Z. D.; Elliott, Q.; Wang, Z.; Setien, R. A.; Puttkammer, J.; Ugrinov, A.; Lee, J.; Webster, D. C.; Chu, Q. R. Furfural-Derived Diacid Prepared by Photoreaction for Sustainable Materials Synthesis. *ACS sustainable chemistry & engineering* **2018**, 6 (7), 8136-8141. DOI: 10.1021/acssuschemeng.8b02415.

(40) Wang, Z.; Miller, B.; Butz, J.; Randazzo, K.; Wang, Z. D.; Chu, Q. R. Polyladderane Constructed from a Gemini Monomer through Photoreaction. *Angewandte Chemie (International ed.)* **2017**, 56 (40), 12155-12159. DOI: 10.1002/anie.201705937.

(41) Amjaour, H.; Wang, Z.; Mabin, M.; Puttkammer, J.; Busch, S.; Chu, Q. R. Scalable preparation and property investigation of a -cyclobutane-1,2-dicarboxylic acid from  $\beta$ -cinnamic acid. *Chemical communications (Cambridge, England)* **2019**, 55 (2), 214-217. DOI: 10.1039/c8cc08017h.

(42) Shahni, R. K.; Mabin, M.; Wang, Z.; Shaik, M.; Ugrinov, A.; Chu, Q. R. Synthesis and characterization of BPA-free polyesters by incorporating a semi-rigid cyclobutanediol monomer. *Polymer Chemistry* **2020**, 11 (37), 6081-6090. DOI: 10.1039/D0PY01098G.

(43) Thuéry, P. Metal-organic frameworks built from alkali metal ions (Li<sup>+</sup>-Cs<sup>+</sup>) and 1,2,3,4-cyclobutanetetracarboxylic acid. *CrystEngComm* **2014**, 16 (9), 1724-1734. DOI: 10.1039/C3CE41565A.

(44) Braga, D.; Benedi, O.; Maini, L.; Grepioni, F. Organometallic crystal engineering with multidentate building blocks and template guest size effect. Supra-anionic organic frameworks obtained from cyclobutane-1,2,3,4-tetracarboxylic and trans-acotinic acids †. *Journal of the Chemical Society, Dalton Transactions* **1999**, (15), 2611-2618. DOI: 10.1039/A902258I.

(45) Shibano, Y.; Umeyama, T.; Matano, Y.; Imahori, H. Electron-Donating Perylene Tetracarboxylic Acids for Dye-Sensitized Solar Cells. *Organic letters* **2007**, 9 (10), 1971-1974. DOI: 10.1021/ol070556s.

- (46) Shahni, R. K.; Amjaour, H.; Krupinsky, B.; Reagen, S.; Wang, Z. D.; Wu, X.; Nkemngong, D.; Zhao, J. X.; Ugrinov, A.; Robertson, J.; et al. Biomass-derived rctt-3,4-di-2-furanyl-1,2-cyclobutanedicarboxylic acid: a polytopic ligand for synthesizing green metal-organic materials. *Journal of Coordination Chemistry* **2021**, *74* (1-3), 226-240. DOI: 10.1080/00958972.2021.1878500.
- (47) Lin, X.; Telepeni, I. r.; Blake, A. J.; Dailly, A.; Brown, C. M.; Simmons, J. M.; Zoppi, M.; Walker, G. S.; Thomas, K. M.; Mays, T. J.; et al. High capacity hydrogen adsorption in Cu(II) tetracarboxylate framework materials: the role of pore size, ligand functionalization, and exposed metal sites. *Journal of the American Chemical Society* **2009**, *131* (6), 12.
- (48) Rajashekar, Y.; Tonsing, N.; Shantibala, T.; Manjunath, J. R. 2, 3-Dimethylmaleic anhydride (3, 4-Dimethyl-2, 5-furandione): A plant derived insecticidal molecule from *Colocasia esculenta* var. *esculenta* (L.) Schott. *Scientific Reports* **2016**, *6* (1), 20546. DOI: 10.1038/srep20546.
- (49) Moshood, T. D.; Nawanir, G.; Mahmud, F.; Mohamad, F.; Ahmad, M. H.; AbdulGhani, A. Sustainability of biodegradable plastics: New problem or solution to solve the global plastic pollution? *Current Research in Green and Sustainable Chemistry* **2022**, *5*, 100273. DOI: <https://doi.org/10.1016/j.crgsc.2022.100273>.
- Rosenboom, J.-G.; Langer, R.; Traverso, G. Bioplastics for a circular economy. *Nature Reviews Materials* **2022**, *7* (2), 117-137. DOI: 10.1038/s41578-021-00407-8.
- (50) Products, N. R. C. U. C. o. B. I. *Biobased Industrial Products: Priorities for Research and Commercialization*; Washington (DC), 2000. <https://www.ncbi.nlm.nih.gov/books/NBK232955/>.
- (51) Isikgor, F.; Becer, C. R. Lignocellulosic biomass: a sustainable platform for the production of bio-based chemicals and polymers. **2016**. DOI: 10.1039/C5PY00263J.
- (52) Cordes, E. E.; Jones, D. O. B.; Schlacher, T. A.; Amon, D. J.; Bernardino, A. F.; Brooke, S.; Carney, R.; DeLeo, D. M.; Dunlop, K. M.; Escobar-Briones, E. G.; et al. Environmental Impacts of the Deep-Water Oil and Gas Industry: A Review to Guide Management Strategies. *Frontiers in Environmental Science* **2016**, *4*, Review.

- (53) Ferreira-Filipe, D. A.; Paço, A.; Duarte, A. C.; Rocha-Santos, T.; Patrício Silva, A. L. Are Biobased Plastics Green Alternatives?-A Critical Review. *International journal of environmental research and public health* **2021**, *18* (15), 7729. DOI: 10.3390/ijerph18157729 PubMed.
- (54) Timmons, D.; Harris, J. M.; Roach, B. *The Economics of Renewable Energy*; Tufts University, 2014. DOI: 10.5517/ccdc.csd.cc29dlz9.
- (55) Horie, T.; Sumino, M.; Tanaka, T.; Matsushita, Y.; Ichimura, T.; Yoshida, J.-i. Photodimerization of Maleic Anhydride in a Microreactor Without Clogging. *Organic process research & development* **2010**, *14* (2), 405-410. DOI: 10.1021/op900306z.
- (56) Bozell, J. J.; Petersen, G. R. Technology development for the production of biobased products from biorefinery carbohydrates—the US Department of Energy’s “Top 10” revisited. *Green Chemistry* **2010**, *12* (4), 539-554. DOI: 10.1039/B922014C.
- (57) Li, X.; Jia, P.; Wang, T. Furfural: A Promising Platform Compound for Sustainable Production of C4 and C5 Chemicals. *ACS catalysis* **2016**, *6* (11), 7621-7640. DOI: 10.1021/acscatal.6b01838.
- (58) Alba-Rubio, A. C.; Fierro, J. L. G.; León-Reina, L.; Mariscal, R.; Dumesic, J. A.; López Granados, M. Oxidation of furfural in aqueous H<sub>2</sub>O<sub>2</sub> catalysed by titanium silicalite: Deactivation processes and role of extraframework Ti oxides. *Applied catalysis. B, Environmental* **2017**, *202*, 269-280. DOI: 10.1016/j.apcatb.2016.09.025.
- (59) Alonso-Fagúndez, N.; Granados, M. L.; Mariscal, R.; Ojeda, M. Selective Conversion of Furfural to Maleic Anhydride and Furan with VO<sub>x</sub>/Al<sub>2</sub>O<sub>3</sub> Catalysts. *ChemSusChem* **2012**, *5* (10), 1984-1990. DOI: 10.1002/cssc.201200167.
- (60) Roa Engel, C. A.; Straathof, A. J. J.; Zijlmans, T. W.; van Gulik, W. M.; van der Wielen, L. A. M. Fumaric acid production by fermentation. *Applied microbiology and biotechnology* **2008**, *78* (3), 379-389. DOI: 10.1007/s00253-007-1341-x.
- (61) Gartner, T. E.; Jayaraman, A. Modeling and Simulations of Polymers: A Roadmap. *Macromolecules* **2019**, *52* (3), 755-786. DOI: 10.1021/acs.macromol.8b01836.
- Kamaly, N.; Yameen, B.; Wu, J.; Farokhzad, O. C. Degradable Controlled-Release Polymers and Polymeric Nanoparticles: Mechanisms of Controlling Drug Release.



*Chemical reviews* **2016**, *116* (4), 2602-2663. DOI: 10.1021/acs.chemrev.5b00346 PubMed.

(62) Stempfle, F.; Ortmann, P.; Mecking, S. Long-Chain Aliphatic Polymers To Bridge the Gap between Semicrystalline Polyolefins and Traditional Polycondensates. *Chemical Reviews* **2016**, *116* (7), 4597-4641. DOI: 10.1021/acs.chemrev.5b00705.

(63) Clark, E. J. Molecular and Microstructural Factors Affecting Mechanical Properties of Polymeric Cover Plate Materials. Washington (DC), 1985.

(64) Cotton, F. A.; Frenz, B. A. Conformations of cyclobutane. *Tetrahedron* **1974**, *30* (12), 1587–1594. DOI: [http://dx.doi.org/10.1016/S0040-4020\(01\)90681-7](http://dx.doi.org/10.1016/S0040-4020(01)90681-7).

(65) Lu, Y. C.; Liu, Z. C.; J., Z. Y. CCDC 1559784: Experimental Crystal Structure Determination. 2020.

(66) Carey, F. A. S., Richard J. *Advanced Organic Chemistry, Part A: Structure and Mechanisms*; Springer, 2007.

(67) Rappoport, Z.; Liebman, J. F. *The Chemistry of Cyclobutanes*; Wiley, 2005.

(68) Brown, W. H. I., Brent L. Anslyn, Eric Foote, C. *Organic Chemistry* Finch, Mary, 2014.

(69) Cheng, Y.; Fan, W.; Wang, L.; Liu, Y.; Yang, S.; Shi, Y.; Liu, S.; Zheng, L.; Cao, Q. Fast photostimulus-responsive ultralong room-temperature phosphorescence behaviour of benzoic acid derivatives@boric acid. *Journal of Materials Chemistry C* **2022**, *10* (22), 8806-8814. DOI: 10.1039/D2TC00804A. Yi, C.; Wenwen, F.; Longjie, W.; Yanxiong, L.; Shaoxiong, Y.; Yonggang, S.; Shixi, L.; Liyan, Z.; Qiue, C. CCDC 2127281: Experimental Crystal Structure Determination. 2022.

(70) Barton, L. M.; Edwards, J. T.; Johnson, E. C.; Bukowski, E. J.; Sausa, R. C.; Byrd, E. F. C.; Orlicki, J. A.; Sabatini, J. J.; Baran, P. S. Impact of Stereo- and Regiochemistry on Energetic Materials. *Journal of the American Chemical Society* **2019**, *141* (32), 12531-12535. DOI: 10.1021/jacs.9b06961.

(71) Author links open overlay panel Nakanishi, F.; Hasegawa, M.; Takahashi, H. Aliphatic poly(amido acids) and polyimides with cyclobutane ring in the main chain. *Polymer* **1973**, *14* (9), 4.

- (72) Hasegawa, M.; Horiuchi, M.; Kumakura, K.; Koyama, J. Colorless polyimides with low coefficient of thermal expansion derived from alkyl-substituted cyclobutanetetracarboxylic dianhydrides. *Polymer international* **2014**, *63* (3), 486-500. DOI: 10.1002/pi.4532.
- (73) Hasegawa, M. Development of Solution-Processable, Optically Transparent Polyimides with Ultra-Low Linear Coefficients of Thermal Expansion. *Polymers* **2017**, *9* (12), 520. DOI: 10.3390/polym9100520.
- (74) Hasegawa, M. Development of Solution-Processable, Optically Transparent Polyimides with Ultra-Low Linear Coefficients of Thermal Expansion. *Polymers* **2017**, *9* (10), 520 - 551.
- (75) Lee, Y. J.; Kim, Y. W.; Ha, J. D.; OH, J. M.; Yi, M. H. Synthesis and characterization of novel polyimides with 1-octadecyl side chains for liquid crystal alignment layers. *Polymers for advanced technologies* **2007**, *18* (3), 226-234. DOI: 10.1002/pat.862.
- (76) Biradha, K.; Ramanan, A.; Vittal, J. J. Coordination Polymers Versus Metal–Organic Frameworks. *Crystal growth & design* **2009**, *9* (7), 2969-2970. DOI: 10.1021/cg801381p.
- (77) Choi, S. M.; Kim, K. J.; Choi, K. Y.; Yi, M. H. Synthesis and characterization of negative-type photosensitive polyimides based on cyclobutane-1,2,3,4-tetracarboxylic dianhydride. *Journal of applied polymer science* **2005**, *96* (6), 2300-2308. DOI: 10.1002/app.21288.
- (78) Choi, S. M.; Ahn, T.; Kim, J. S.; Yi, M. Synthesis and characterization of photocrosslinkable poly(amic acid ester)s with 2-hydroxy-4-oxo-hept-5-enyl side chain. *Polymers for advanced technologies* **2010**, *21* (6), 418-423. DOI: 10.1002/pat.1445.
- (79) Hyun, M. H. Development of HPLC Chiral Stationary Phases Based on (+)-(18-Crown-6)-2,3,11,12-tetracarboxylic Acid and Their Applications. *Chirality* **2015**, *27* (9), 576-588. DOI: 10.1002/chir.22484 From NLM.
- (80) Lee, W.; Bang, E.; Yun, J.-H.; Paik, M.-J.; Lee, W. Enantiodiscrimination Using a Chiral Crown Ether as a Chiral Solvating Agent Using NMR Spectroscopy. *Natural*

*Product Communications* **2019**, *14* (5), 1934578X19849191. DOI: 10.1177/1934578X19849191.

(81) Pinggen, D.; Zimmerer, J.; Klinkenberg, N.; Mecking, S. Microalgae lipids as a feedstock for the production of benzene. *Green Chemistry* **2018**, *20* (8), 1874-1878. DOI: 10.1039/C8GC00423D.

(82) Niziolek, A. M.; Onel, O.; Guzman, Y. A.; Floudas, C. A. Biomass-Based Production of Benzene, Toluene, and Xylenes via Methanol: Process Synthesis and Deterministic Global Optimization. *Energy & Fuels* **2016**, *30* (6), 4970-4998. DOI: 10.1021/acs.energyfuels.6b00619.

Meng, Q.; Yan, J.; Wu, R.; Liu, H.; Sun, Y.; Wu, N.; Xiang, J.; Zheng, L.; Zhang, J.; Han, B. Sustainable production of benzene from lignin. *Nature Communications* **2021**, *12* (1), 4534. DOI: 10.1038/s41467-021-24780-8.

(83) Zhuang, Y.; Seong, J. G.; Lee, Y. M. Polyimides containing aliphatic/alicyclic segments in the main chains. *Progress in Polymer Science* **2019**, *92*, 35-88. DOI: <https://doi.org/10.1016/j.progpolymsci.2019.01.004>.

Yi, L.; Huang, W.; Yan, D. Polyimides with side groups: Synthesis and effects of side groups on their properties. *Journal of Polymer Science Part A: Polymer Chemistry* **2017**, *55* (4), 533-559, <https://doi.org/10.1002/pola.28409>. DOI: <https://doi.org/10.1002/pola.28409>.

(84) Li, T.; Huang, H.; Wang, L.; Chen, Y. High performance polyimides with good solubility and optical transparency formed by the introduction of alkyl and naphthalene groups into diamine monomers. *RSC Advances* **2017**, *7* (65), 40996-41003, 10.1039/C7RA07142F. DOI: 10.1039/C7RA07142F.

Tapaswi, P. K.; Choi, M.-C.; Jung, Y. S.; Cho, H. J.; Seo, D. J.; Ha, C.-S. Synthesis and characterization of fully aliphatic polyimides from an aliphatic dianhydride with piperazine spacer for enhanced solubility, transparency, and low dielectric constant. *Journal of Polymer Science Part A: Polymer Chemistry* **2014**, *52* (16), 2316-2328. DOI: <https://doi.org/10.1002/pola.27242>.

(85) Wang, X.; Zhang, Y.; Shi, Z.; Lu, T.; Wang, Q.; Li, B. Multifunctional Zr-MOF Based on Bisimidazole Tetracarboxylic Acid for pH Sensing and Photoreduction of

Cr(VI). *ACS Applied Materials & Interfaces* **2021**, *13* (45), 54217-54226. DOI: 10.1021/acsami.1c18130. Alawisi, H.; Li, B.; He, Y.; Arman, H. D.; Asiri, A. M.; Wang, H.; Chen, B. A Microporous Metal–Organic Framework Constructed from a New Tetracarboxylic Acid for Selective Gas Separation. *Crystal Growth & Design* **2014**, *14* (5), 2522-2526. DOI: 10.1021/cg500235j.

(86) Shi, C.; Zhou, X.; Liu, D.; Li, L.; Xu, M.; Sakiyama, H.; Muddassir, M.; Wang, J. A new 3D high connection Cu-based MOF introducing a flexible tetracarboxylic acid linker: Photocatalytic dye degradation. *Polyhedron* **2021**, *208*, 115441. DOI: <https://doi.org/10.1016/j.poly.2021.115441>.

Qiu, Q.; Wang, T.; Jing, L.; Huang, K.; Qin, D. Tetra-carboxylic acid based metal-organic framework as a high-performance bifunctional electrocatalyst for HER and OER. *International Journal of Hydrogen Energy* **2020**, *45* (19), 11077-11088. DOI: <https://doi.org/10.1016/j.ijhydene.2020.02.033>.

(87) Al-Qaradawi, S. Y.; Blakemore, D. C.; Gilbert, A. Sunlight-initiated cycloaddition reactions of the benzene ring. *Journal of Chemical Sciences* **1993**, *105* (6), 555-562. DOI: 10.1007/BF03040826.

(88) Bradshaw, J. S. The Preparation and Structure of Alkylbenzene—Maleic Anhydride Photoadducts. *Journal of organic chemistry* **1966**, *31* (12), 3974-3976. DOI: 10.1021/jo01350a021.

(89) Bryce-Smith, D. Photoaddition and photoisomerization reactions of the benzene ring. *Pure and applied chemistry* **1968**, *16* (1), 47-64. DOI: 10.1351/pac196816010047.

(90) Grovenstein, E.; Rao, D. V.; Taylor, J. W. The Structure and Stereochemistry of the Photochemical Adduct of Benzene with Maleic Anhydride<sup>1</sup>. *Journal of the American Chemical Society* **1961**, *83* (7), 1705-1711. DOI: 10.1021/ja01468a036.

(91) Bouas-Laurent, H.; Castellan, A.; Desvergne, J.-P. From anthracene photodimerization to jaw photochromic materials and photocrowns. *Pure and Applied Chemistry* **1980**, *52* (12), 2633-2648. DOI: doi:10.1351/pac198052122633.

(92) Poplata, S.; Tröster, A.; Zou, Y.-Q.; Bach, T. Recent Advances in the Synthesis of Cyclobutanes by Olefin [2 + 2] Photocycloaddition Reactions. *Chemical Reviews* **2016**, *116* (17), 9748-9815. DOI: 10.1021/acs.chemrev.5b00723.

- (93) Bryce-Smith, D.; Lodge, J. E. 514. Liquid-phase photolysis. Part V. Mechanism of the photo-addition of maleic anhydride to benzene. *Journal of the Chemical Society (Resumed)* **1962**, (0), 2675-2680. DOI: 10.1039/JR9620002675.
- (94) Gilbert, A. Photoaddition and Photocyclization Processes of Aromatic Compounds. In *Synthetic Organic Photochemistry*, Horspool, W. M. Ed.; Springer US, 1984; pp 1-60.
- (95) Hardham, W. M.; Hammond, G. S. Mechanisms of photochemical reactions in solution. XLIII. Addition of maleic anhydride to benzene. *Journal of the American Chemical Society* **1967**, 89 (13), 3200-3205. DOI: 10.1021/ja00989a021.
- (96) Liu, Q.; Wu, L.-Z. Recent advances in visible-light-driven organic reactions. *National Science Review* **2017**, 4 (3), 359-380. DOI: 10.1093/nsr/nwx039 (accessed 12/16/2020).
- (97) Wu, Y.-L.; Yang, R.-R.; Yan, Y.-T.; Yang, G.-P.; Liang, H.-H.; He, L.-Z.; Su, X.-L.; He, X.-H.; Ma, Z.-S.; Wang, Y.-Y. Ultra-high adsorption selectivity and affinity for CO<sub>2</sub> over CH<sub>4</sub>, and luminescent properties of three new solvents induced Zn(II)-based metal-organic frameworks (MOFs). *Journal of solid state chemistry* **2021**, 297, 122054. DOI: 10.1016/j.jssc.2021.122054.
- (98) Suzuki, H.; Abe, T.; Takaishi, K.; Narita, M.; Hamada, F. The synthesis and X-ray structure of 1,2,3,4-cyclobutane tetracarboxylic dianhydride and the preparation of a new type of polyimide showing excellent transparency and heat resistance. *Journal of polymer science. Part A, Polymer chemistry* **2000**, 38 (1), 108-116. DOI: 10.1002/(SICI)1099-0518(20000101)38:1<108::AID-POLA14>3.0.CO;2-G.
- (99) Wang, Y.-N.; Wang, S.-D.; Chen, Q.-Q.; Lv, J.-H.; Xu, Z. Two new compounds assembled by 2, 3, 3',4'-biphenyl tetracarboxylic acid: Luminescent properties for detection of acetylacetone. *Journal of Solid State Chemistry* **2021**, 298, 122094. DOI: <https://doi.org/10.1016/j.jssc.2021.122094>.
- (100) Zhang, S.; Ma, J.; Zhang, X.; Duan, E.; Cheng, P. Assembly of Metal–Organic Frameworks Based on 3,3',5,5'-Azobenzene-tetracarboxylic Acid: Photoluminescences, Magnetic Properties, and Gas Separations. *Inorganic chemistry* **2015**, 54 (2), 586-595. DOI: 10.1021/ic502488c.

- (101) Gao, X.; Geng, R.; Su, F. Three Co/Ni(II)-MOFs with dinuclear metal units constructed by biphenyl-3,3',5,5'-tetracarboxylic acid and N-donor ligands: Synthesis, structures, and magnetic properties. *Journal of solid state chemistry* **2021**, 293. DOI: 10.1016/j.jssc.2020.121706.
- (102) Bello, L.; Quintero, M.; Mora, A. J.; González, T.; Escalona, A.; Añez, R.; Ávila, E. E.; Briceño, A. Study of temperature and ligand flexibility effects on coordination polymer formation from cyclobutanetetracarboxylic acid. *CrystEngComm* **2015**, 17 (31), 5921-5931. DOI: 10.1039/C5CE00646E.
- (103) Köppen, M.; Meyer, V.; Ångström, J.; Inge, A. K.; Stock, N. Solvent-Dependent Formation of Three New Bi-Metal–Organic Frameworks Using a Tetracarboxylic Acid. *Crystal Growth & Design* **2018**, 18 (7), 4060-4067. DOI: 10.1021/acs.cgd.8b00439.
- (104) Amimoto, K.; Kawato, T. Photochromism of organic compounds in the crystal state. *Journal of Photochemistry and Photobiology C: Photochemistry Reviews* **2005**, 6 (4), 207-226. DOI: <https://doi.org/10.1016/j.jphotochemrev.2005.12.002>.
- (105) Chu, E. W.; Karr, J. R. Environmental Impact: Concept, Consequences, Measurement. *Reference Module in Life Sciences* **2017**, B978-970-912-809633-809638.802380-809633. DOI: 10.1016/B978-0-12-809633-8.02380-3 PMC.
- (106) Kirsch, S. Running out? Rethinking resource depletion. *The extractive industries and society* **2020**, 7 (3), 838-840. DOI: 10.1016/j.exis.2020.06.002 PubMed.
- (107) Jensen, M. H.; Riisager, A. Chapter 5 - Advances in the synthesis and application of 2,5-furandicarboxylic acid. In *Biomass, Biofuels, Biochemicals*, Saravanamurugan, S., Pandey, A., Li, H., Riisager, A. Eds.; Elsevier, 2020; pp 135-170.
- (108) Rathod, P. V.; Jadhav, V. H. Efficient Method for Synthesis of 2,5-Furandicarboxylic Acid from 5-Hydroxymethylfurfural and Fructose Using Pd/CC Catalyst under Aqueous Conditions. *ACS Sustainable Chemistry & Engineering* **2018**, 6 (5), 5766-5771. DOI: 10.1021/acssuschemeng.7b03124.
- (109) Xiao, Q.; Huang, Q.; Ho, C.-T. Occurrence, Formation, Stability, and Interaction of 4-Hydroxy-2,5-dimethyl-3(2H)-furanone. *ACS Food Science & Technology* **2021**, 1 (3), 292-303. DOI: 10.1021/acsfoodscitech.1c00011.

- (110) Hauck, T.; Brühlmann, F.; Schwab, W. Formation of 4-Hydroxy-2,5-Dimethyl-3[2H]-Furanone by *Zygosaccharomyces rouxii*: Identification of an Intermediate. *Applied and Environmental Microbiology* **2003**, *69* (7), 3911-3918. DOI: 10.1128/AEM.69.7.3911-3918.2003.
- (111) Lönn-Stensrud, J.; Landin, M. A.; Benneche, T.; Petersen, F. C.; Scheie, A. A. Furanones, potential agents for preventing *Staphylococcus epidermidis* biofilm infections? *Journal of Antimicrobial Chemotherapy* **2009**, *63* (2), 309-316. DOI: 10.1093/jac/dkn501 (accessed 4/22/2022).
- (112) Kuehl, R.; Al-Bataineh, S.; Gordon, O.; Luginbuehl, R.; Otto, M.; Textor, M.; Landmann, R. Furanone at Subinhibitory Concentrations Enhances Staphylococcal Biofilm Formation by luxS Repression. *Antimicrobial Agents and Chemotherapy* **2009**, *53* (10), 4159-4166. DOI: 10.1128/AAC.01704-08.
- (113) Husain, A.; Khan, S. A.; Iram, F.; Iqbal, M. A.; Asif, M. Insights into the chemistry and therapeutic potential of furanones: A versatile pharmacophore. *European Journal of Medicinal Chemistry* **2019**, *171*, 66-92. DOI: <https://doi.org/10.1016/j.ejmech.2019.03.021>.
- (114) Sharafutdinov, I. S.; Trizna, E. Y.; Baidamshina, D. R.; Ryzhikova, M. N.; Sibgatullina, R. R.; Khabibrakhmanova, A. M.; Latypova, L. Z.; Kurbangalieva, A. R.; Rozhina, E. V.; Klinger-Strobel, M.; et al. Antimicrobial Effects of Sulfonyl Derivative of 2(5H)-Furanone against Planktonic and Biofilm Associated Methicillin-Resistant and -Susceptible *Staphylococcus aureus*. *Frontiers in Microbiology* **2017**, *8*, Original Research.
- (115) Omanakuttan, V. K.; John, J.; Hopf, H. Synthesis of 3(2H)-Furanones: A Review. *European Journal of Organic Chemistry* **2021**, *2021* (2), 163-201. DOI: <https://doi.org/10.1002/ejoc.202001005>.
- (116) FERINGA, B. PHOTOOXIDATION OF FURANS. *Recueil des Travaux Chimiques des Pays-Bas-Journal of the Royal Netherlands Chemical Society*, **1987**, *106* (9), 469-488.
- (117) Shaik, M.; Peterson, J.; Du, G. Cyclic and Linear Polyhydroxybutyrate from Ring-Opening Polymerization of  $\beta$ -Butyrolactone with Amido-Oxazolinone Zinc

Catalysts. *Macromolecules* **2019**, *52* (1), 157-166. DOI: 10.1021/acs.macromol.8b02096.

(118) Badovskaya, L. A.; Poskonin, V. V.; Tyukhteneva, Z. I.; Kozhina, N. D. 2(5H)-Furanone and 5-Hydroxy-2(5H)-furanone: Reactions and Syntheses Based on Them. *Russian Journal of General Chemistry* **2021**, *91* (2), 133-153. DOI: 10.1134/S1070363221020018.

(119) Omar, R.; Shaik, M.; Griggs, C.; Jensen, J. D.; Boyd, R.; Oncel, N.; Webster, D. C.; Du, G. Star-shaped Poly(hydroxybutyrate)s from bio-based polyol cores via zinc catalyzed ring-opening polymerization of  $\beta$ -Butyrolactone. *European Polymer Journal* **2021**, *160*, 110756. DOI: <https://doi.org/10.1016/j.eurpolymj.2021.110756>.

(120) Gassama, A.; Ernenwein, C.; Hoffmann, N. Synthesis of surfactants from furfural derived 2[5H]-furanone and fatty amines. *Green Chemistry* **2010**, *12* (5), 859-865, 10.1039/B924187F. DOI: 10.1039/B924187F.

(121) Richard, C.; Hoffmann, N. Chapter 4 Direct Photolysis Processes. In *Surface Water Photochemistry*, The Royal Society of Chemistry, 2016; pp 61-75.

(122) Desvals, A.; Fortino, M.; Lefebvre, C.; Rogier, J.; Michelin, C.; Alioui, S.; Rousset, E.; Pedone, A.; Lemercier, G.; Hoffmann, N. Synthesis and characterization of polymethine dyes carrying thiobarbituric and carboxylic acid moieties. *New Journal of Chemistry* **2022**, *46* (19), 8971-8980. DOI: 10.1039/D2NJ00684G.

Harakat, D.; Pesch, J.; Marinković, S.; Hoffmann, N. Thiocarbonyl compounds as regulating reagent in the radical addition of tertiary amines with alkenes using photoelectron transfer conditions. *Organic & Biomolecular Chemistry* **2006**, *4* (7), 1202-1205. DOI: 10.1039/B600220J.

(123) Gassama, A.; Ernenwein, C.; Youssef, A.; Agach, M.; Riguet, E.; Marinković, S.; Estrine, B.; Hoffmann, N. Sulfonated surfactants obtained from furfural. *Green Chemistry* **2013**, *15* (6), 1558-1566. DOI: 10.1039/C3GC00062A.

Shvydkiv, O.; Yavorsky, A.; Tan, S. B.; Nolan, K.; Hoffmann, N.; Youssef, A.; Oelgemöller, M. Microphotochemistry: a reactor comparison study using the photosensitized addition of isopropanol to furanones as a model reaction.



*Photochemical & Photobiological Sciences* **2011**, *10* (9), 1399-1404, 10.1039/C1PP05024A. DOI: 10.1039/C1PP05024A.

Shvydkiv, O.; Yavorsky, A.; Nolan, K.; Youssef, A.; Riguet, E.; Hoffmann, N.; Oelgemöller, M. Photosensitized addition of isopropanol to furanones in a 365 nm UV-LED microchip. *Photochemical & Photobiological Sciences* **2010**, *9* (12), 1601-1603. DOI: 10.1039/C0PP00223B.

(124) Bhat, N. S.; Kumar, R.; Jana, A.; Mal, S. S.; Dutta, S. Selective oxidation of biomass-derived furfural to 2(5H)-furanone using trifluoroacetic acid as the catalyst and hydrogen peroxide as a green oxidant. *Biomass Conversion and Biorefinery* **2021**. DOI: 10.1007/s13399-021-01297-0.

(125) Yu, X.; Liu, H.; Wang, Q.; Jia, W.; Wang, H.; Li, W.; Zheng, J.; Sun, Y.; Tang, X.; Zeng, X.; et al. Selective Oxidation of Furfural to 2(5H)-Furanone and Maleic Acid over CuMoO<sub>4</sub>. *ACS sustainable chemistry & engineering* **2021**, *9* (39), 13176-13187. DOI: 10.1021/acssuschemeng.1c03420.

(126) Lee, G. C. M.; Syage, E. T.; Harcourt, D. A.; Holmes, J. M.; Garst, M. E. Singlet oxygen oxidation of substituted furans to 5-hydroxy-2(5H)-furanone. *The Journal of Organic Chemistry* **1991**, *56* (25), 7007-7014. DOI: 10.1021/jo00025a012.

(127) Jakovlev, M. M.; Poskonin, V. V. Method of producing 5-hydroxy-2(5h)-furanone. Russian Federation 2011.